

# **Biosynthesis and transport of flavonol sophorosides in *Arabidopsis thaliana* anthers**

Dissertation

zur Erlangung des  
Doktorgrades der Naturwissenschaften (Dr. rer. nat.)

der

Naturwissenschaftlichen Fakultät I – Biowissenschaften –

der Martin-Luther-Universität  
Halle-Wittenberg,

vorgelegt

von Herrn Stephan Grunewald

geb. am 10.05.1989 in Berlin

Gutachter:

1. PD. Dr. Thomas Vogt
2. Prof. Dr. Ingo Heilmann
3. Prof. Dr. Enrico Martinoia

Verteidigungsdatum: 18.01.2021



## Table of contents

<b>List of abbreviations</b> .....	<b>V</b>
<b>List of tables</b> .....	<b>VII</b>
<b>List of figures</b> .....	<b>VIII</b>
<b>1 Introduction</b> .....	<b>1</b>
1.1 The role of transport in plant secondary metabolism .....	1
1.2 Transporters of specialized metabolites .....	2
1.2.1 ABC-transporters .....	2
1.2.2 MATE-transporters .....	3
1.2.3 The nitrate/peptide family (NPF-transporters) .....	4
1.3 Flavonoids: highly diverse compounds .....	5
1.4 Biosynthesis of flavonol-3- <i>O</i> -sophorosides in <i>A. thaliana</i> .....	6
1.5 Flavonoid glycosylation .....	8
1.5.1 Biological relevance of flavonoid glycosylation.....	8
1.5.2 Plant glycosyltransferases .....	9
1.5.3 Flavonol sophorosides.....	9
1.6 Tapetum and pollen – A special relationship .....	10
1.6.1 Angiosperm pollen development.....	10
1.6.2 A special cell layer: the tapetum .....	11
1.6.3 Composition of the pollen wall .....	13
1.7 Flavonoid transport in plants .....	14
1.8 Aim of this investigation.....	17
<b>2 Materials and methods</b> .....	<b>18</b>
2.1 Materials.....	18
2.1.1 Chemicals and biochemical reagents .....	18
2.1.2 Media.....	18
2.1.3 Vectors.....	18
2.1.4 Bacterial strains .....	19
2.1.5 Preparation of electrocompetent cells .....	20
2.1.6 Plants and growth conditions.....	20
2.1.7 Isolation of T-DNA insertion lines.....	20
2.2 Molecular methods .....	21

2.2.1	Isolation of genomic DNA.....	21
2.2.2	Isolation of plasmid DNA.....	21
2.2.3	Polymerase chain reaction (PCR) .....	21
2.2.4	Agarose gel electrophoresis.....	22
2.2.5	RNA extraction and cDNA synthesis.....	22
2.2.6	Quantitative real-time polymerase chain reaction (qRT-PCR).....	23
2.2.7	Classical cloning for recombinant protein expression .....	24
2.2.8	Golden Gate Cloning.....	25
2.2.9	Restriction analysis.....	28
2.2.11	Site-directed mutagenesis.....	29
2.2.12	Sequencing and <i>in silico</i> analysis.....	29
2.2.13	Transformation of electrocompetent cells .....	30
2.2.14	Generation of transgenic Arabidopsis lines .....	30
2.3	Microscopic methods.....	31
2.3.1	Subcellular localization.....	31
2.3.2	Transient expression in <i>N. benthamiana</i> leaves .....	31
2.3.3	Isolation of protoplasts .....	32
2.3.4	Transformation of protoplasts .....	33
2.3.5	Promotor-GFP localization .....	33
2.3.6	Immunolabelling of anther cross-sections.....	34
2.3.7	Transmission electron microscopy (TEM) .....	35
2.4	Protein biochemical methods.....	35
2.4.1	Protein concentration determination .....	35
2.4.2	SDS-PAGE.....	35
2.4.3	Immunoblot analysis .....	36
2.4.4	Heterologous expression and partially purification of glycosyltransferases .....	37
2.4.5	Standard flavonol glycosyltransferase assays .....	38
2.4.6	Preparation of <sup>14</sup> C-labelled flavonol glucosides .....	38
2.4.7	Transporter uptake assays with <sup>14</sup> C-labelled flavonol glucosides.....	39
2.5	Analytical methods.....	40
2.5.1	Harvesting of pollen material from Arabidopsis .....	40
2.5.2	Preparation of pollen and anther extracts.....	40
2.5.3	High performance thin-layer chromatography .....	40
2.5.4	High performance liquid chromatography.....	41
2.5.5	Gas chromatography-mass spectrometry.....	41

---

2.6	Biological assays .....	41
2.6.1	Pollen viability assay.....	41
2.6.2	<i>In vitro</i> pollen germination assay .....	42
<b>3</b>	<b>Results .....</b>	<b>43</b>
3.1	The flavonoid glycosyltransferases UGT78D2 and UGT79B6.....	43
3.3	Transport and biosynthesis of flavonol sophorosides.....	45
3.3.1	<i>UGT79B6</i> is highly expressed in tapetal cells .....	45
3.3.2	Identification of a NPF-protein as putative flavonol glycoside transporter .....	46
3.4	Tissue-specific localization of the <i>FST1</i> transporter .....	50
3.4.1	Anther specificity of the <i>FST1</i> candidate.....	50
3.4.2	Anther- and flavonoid-specific <i>cis</i> -regulatory elements in the <i>FST1</i> promotor .....	51
3.4.3	Tapetum-specific expression of the <i>FST1</i> candidate .....	54
3.4.4	Complementation of <i>fst1</i> by <i>FST1</i> expression.....	55
3.4.5	Subcellular localization of the <i>FST1</i> transporter .....	56
3.4.6	<i>FST1</i> is functional in the plasma membrane of tapetal cells.....	57
3.5	TEM of <i>fst1</i> pollen development.....	59
3.6	No decreased <i>fst1</i> pollen fitness .....	62
3.7	Functional characterization of the <i>FST1</i> transporter .....	63
3.8	Phylogenetic analysis .....	66
3.9	Localization and biological relevance of phenylpropanoids .....	68
3.9.1	Subcellular localization of the <i>UGT79B6</i> .....	68
3.9.2	Generation of a 'phenylpropanoid-free' pollen coat mutant .....	70
3.9.3	Morphological appearance of the <i>78d2</i> x <i>sht</i> mutant.....	72
3.9.4	<i>78d2</i> x <i>sht</i> pollen development revealed no ultrastructural variances .....	73
3.9.5	Preliminary assays with <i>78d2</i> x <i>sht</i> mutant pollen.....	75
<b>4</b>	<b>Discussion .....</b>	<b>77</b>
4.1	Transport of pollen-specific flavonol glycosides in Arabidopsis .....	77
4.1.1	Identification of a tapetal flavonoid glycoside transporter.....	77
4.1.2	<i>FST1</i> -depending transport of flavonol sophorosides .....	78
4.1.3	Regulatory aspects of flavonol-3- <i>O</i> -sophoroside biosynthesis .....	79
4.2	Unsolved HCAA transport to the tryphine .....	79
4.3	The NPF-candidates in the current literature .....	80
4.3.1	NPF-transporters and specialized metabolites .....	80
4.3.2	<i>FST1</i> is neither a glucosinolate transporter nor a nitrogen exporter.....	81

4.4	Putative transport mechanism.....	82
4.4.1	Initial aspects about the origin of substrate specificity .....	82
4.4.2	Conserved motifs.....	84
4.4.3	Putative relationship between pH and flavonoid transport .....	85
4.5	New insights in the tapetal biosynthesis of flavonol glycosides .....	89
4.6	Physiological aspects of pollen-specific flavonol glycosides .....	91
4.6.1	Flavonol glycosides and pollen tube germination.....	91
4.6.2	UV-stress and pollen flavonoids.....	92
4.6.3	Heat stress and pollen flavonoids .....	93
4.6.4	Are pollen-specific flavonoid glycosides involved in biotic interactions? .....	94
4.7	Future aspects for applied research.....	95
<b>5</b>	<b>Summary.....</b>	<b>96</b>
<b>6</b>	<b>Zusammenfassung .....</b>	<b>97</b>
<b>7</b>	<b>References .....</b>	<b>98</b>
<b>8</b>	<b>Appendix.....</b>	<b>116</b>
	<b><i>Lebenslauf</i>.....</b>	<b>IX</b>
	<b><i>List of publications</i> .....</b>	<b>IX</b>
	<b><i>Danksagung</i> .....</b>	<b>X</b>
	<b><i>Eidesstattliche Erklärung</i>.....</b>	<b>XII</b>

## List of abbreviations

ABC	ATP-binding cassette
APS	ammonium peroxydisulfate
ATP	adenosine triphosphate
AU	absorbance units
BLAST	Basic Local Alignment Search Tool
bp	base pair
Bq	Becquerel
cDNA	complementary DNA
CDS	coding sequence
CHS	chalcone synthase
C <sub>i</sub>	Curie
Col	Columbia
conc.	concentration
Cq	quantification cycle
CYP	cytochrome P450 monooxygenase
DMSO	dimethylsulfoxide
DNA	deoxyribonucleic acid
DNase	deoxyribonuclease
dNTP	deoxyribonucleoside triphosphate
DTX	detoxification efflux carrier
EDTA	ethylenediaminetetraacetic acid
ER	Endoplasmic reticulum
et al.	<i>et aliter</i>
FDA	fluorescein diacetate
FST1	FLAVONOL SOPHOROSIDE TRANSPORTER 1
F <sub>2</sub>	second filial generation
GC	gas chromatography
gDNA	genomic DNA
GFP	green fluorescent protein
GGT	glycoside glycosyltransferase
GSH	glutathione
GST	glutathione S-transferase
GUS	β-glucuronidase
HCAA	hydroxycinnamic acid amide
HPLC	high performance liquid chromatography
HPTLC	high performance thin layer chromatography
HRP	horseradish peroxidase
IPB	Leibniz Institute of Plant Biochemistry
IPTG	isopropyl β-D-thiogalactopyranoside
kb	kilo base pair
kDa	kilo dalton
KPi	potassium phosphate buffer
K-3-GG	kaempferol-3-O-sophoroside
LB primer	left border primer of the T-DNA insertion
LB medium	lysogeny broth medium
LP	left genomic primer
LTP	lipid transfer protein
MATE	multiple drug and toxic compound extrusion protein

## List of abbreviations

---

MCS	multiple cloning site
MDR	multiple drug resistance
MES	2-( <i>N</i> -morpholino)ethanesulfonic acid
MS	mass spectrometry
NASC	Nottingham Arabidopsis Stock Centre
n.d.	not detectable
NPF	NRT1/PTR family
NRT1	nitrate transporter 1
n.s.	no significance
OD <sub>600</sub>	optical density at 600 nm
PAGE	polyacrylamide gel electrophoresis
PBS	phosphate-buffered saline
PCR	polymerase chain reaction
PDA	photodiode array
PDR	pleiotropic drug resistance
PEG	polyethylene glycol
PP2A	protein phosphatase 2A
PTR	peptide transporter
PVDF	polyvinylidene difluoride
Q-3-G	quercetin-3- <i>O</i> -glucoside
Q-3-GG	quercetin-3- <i>O</i> -sophoroside
qRT-PCR	quantitative real-time-PCR
RNA	ribonucleic acid
ROS	reactive oxygen species
RP	right genomic primer
RP <sub>18</sub>	reversed-phase C18
RT	retention time
SCB	sodium cacodylate buffer
SDS	sodium dodecyl sulfate
SHT	spermidine hydroxycinnamoyl transferase
SOC-medium	super optimal broth with catabolite repression
TAIR	The Arabidopsis Information Resource
TB-medium	Terrific broth medium
TBE	Tris-borate-EDTA buffer
TCA	trichloroacetic acid
T-DNA	transfer-DNA
TEM	transmission electron microscopy
TEMED	<i>N,N,N',N'</i> -Tetramethylethane-1,2-diamine
TFA	trifluoroacetic acid
T <sub>m</sub>	melting temperature
T <sub>1/2</sub>	first/second filial generation of transformt lines
TSM1	tapetum-specific methyltransferase 1
U	unit
UDP-glucose	uridine diphosphate glucose
UGT	uridine phosphate depending glycosyltransferase
UV	ultraviolet
v/v	volume per volume
WT	wild-type
w/v	weight per volume
X-Gal	5-bromo-4-chloro-3-indolyl- $\beta$ - <i>D</i> -galactopyranoside
YT medium	yeast extract trypton medium



## List of tables

<b>Table 2-1</b> Vectors used for heterologous protein expression.....	19
<b>Table 2-2</b> <i>E. coli</i> strains used in this work. ....	19
<b>Table 2-3</b> Standard PCR programs. ....	22
<b>Table 2-4</b> Primers used for qRT-PCR. ....	24
<b>Table 2-5</b> Primers used for conventional cloning. ....	25
<b>Table 2-6</b> Golden Gate cloning vectors.. ....	28
<b>Table 2-7</b> Overview of primers used for site-directed mutagenesis.....	29
<b>Table 2-8</b> Preparation of polyacrylamide gels. ....	36
<b>Table 3-1</b> Quantification of flavonol-3- <i>O</i> -sophorosides on <i>fst1</i> pollen.. ....	50
<b>Table 3-2</b> Quantification of flavonol-3- <i>O</i> -sophorosides in <i>fst1</i> anthers. ....	50
<b>Table 3-3</b> Predicted <i>cis</i> -acting motifs of the <i>FST1</i> promotor identified by PLACE.. ....	53
<b>Table 3-4</b> Quantification of flavonol-3- <i>O</i> -sophorosides on <i>78d2</i> x <i>sht</i> pollen.....	72
<b>Table 8-1</b> Overview of the examined T-DNA insertion lines obtained from NASC. ....	116
<b>Table 8-2</b> Primers used for conformation of the T-DNA-insertion lines. ....	116
<b>Table 8-3</b> Golden Gate cloning primers.. ....	122
<b>Table 8-4</b> Solvent gradients for HPLC-analysis.....	125

## List of figures

<b>Figure 1-1</b>	The general flavonoid structure.....	5
<b>Figure 1-2</b>	Flavonoid biosynthesis in <i>A. thaliana</i> . ....	7
<b>Figure 1-3</b>	Chronology of male gametophyte development.....	10
<b>Figure 1-4</b>	Overview of the anther cell layers in Arabidopsis. ....	12
<b>Figure 1-5</b>	Stratification of the pollen wall in Arabidopsis.....	13
<b>Figure 2-1</b>	Schematic overview of Golden Gate cloning. ....	27
<b>Figure 3-1</b>	Partial purification of UGT79B6 <sub>opt</sub> and UGT78D2. ....	43
<b>Figure 3-2</b>	Enzymatic activity of UGT79B6 <sub>opt</sub> and UGT78D2. ....	44
<b>Figure 3-3</b>	The transcription of <i>UGT79B6</i> is restricted to the tapetum. ....	46
<b>Figure 3-4</b>	The <i>npf2.8</i> line ( <i>fst1</i> ) exhibits a changed flavonoid profile. ....	48
<b>Figure 3-5</b>	HPLC-MS profiles of pollen extracts from various mutant lines. ....	49
<b>Figure 3-6</b>	Organ-specific transcription profiles of <i>FST1</i> and <i>TT12</i> . ....	51
<b>Figure 3-7</b>	The <i>FST1</i> promotor shows tapetal-specific expression. ....	54
<b>Figure 3-8</b>	A copy of the <i>FST1</i> wild-type gene complements the <i>fst1</i> chemotype. ....	55
<b>Figure 3-9</b>	Plasma membrane localization of FST1-GFP in epidermal leaf cells. ....	57
<b>Figure 3-10</b>	FST1 is functional in the plasma membrane of tapetal cells. ....	58
<b>Figure 3-11</b>	Development of wild-type and <i>fst1</i> mutant pollen observed by TEM. ....	61
<b>Figure 3-12</b>	<i>In vitro</i> pollen assays of wild-type and <i>fst1</i> mutant.....	63
<b>Figure 3-13</b>	FST1 mediates flavonol glycoside transport in <i>E. coli</i> .....	64
<b>Figure 3-14</b>	A changed EXXEK-motif did not affect the FST1 transporter activity. ....	65
<b>Figure 3-15</b>	FST1 defines a new clade within the NPF-family. ....	67
<b>Figure 3-16</b>	Localization of the UGT79B6 to the ER. ....	69
<b>Figure 3-17</b>	Reduced phenylpropanoid levels of <i>78d2 x sht</i> pollen. ....	71
<b>Figure 3-18</b>	Morphological appearance of <i>78d2 x sht</i> in the green house. ....	72
<b>Figure 3-19</b>	Colouration of wild-type, <i>78d2 x sht</i> , <i>sht</i> , and <i>78d2</i> mutant pollen. ....	73
<b>Figure 3-20</b>	Pollen development of the <i>78d2 x sht</i> mutant. ....	74
<b>Figure 3-21</b>	Classical pollen assays of wild-type and <i>78d2 x sht</i> mutant pollen. ....	75
<b>Figure 4-1</b>	The candidate FST1 (NPF2.8) in the current literature. ....	82
<b>Figure 4-2</b>	Crystal structure of NPF6.3 (NRT1.1). ....	84
<b>Figure 4-3</b>	<i>In vitro</i> transport of flavonol glycosides in presence of CCCP. ....	87
<b>Figure 4-4</b>	Currently identified transporters involved in Arabidopsis pollen coat formation. ....	90
<b>Figure 8-1</b>	Verification of the <i>fst1</i> knockout line. ....	118
<b>Figure 8-2</b>	Scheme of the <i>At5g28470</i> allele encoding FST1.....	119
<b>Figure 8-3</b>	Quality of isolated plant RNA preparations. ....	119
<b>Figure 8-4</b>	<i>UGT79B6</i> codon-optimized sequence for <i>E. coli</i> .....	120
<b>Figure 8-5</b>	Golden Gate constructs for <i>in planta</i> approaches.....	121
<b>Figure 8-6</b>	Control of the individual pAGV931 complementation lines.....	123
<b>Figure 8-7</b>	Additional controls for the subcellular localization studies.....	124
<b>Figure 8-8</b>	Calibration curve for quantification of flavonol glycosides. ....	126
<b>Figure 8-9</b>	GC-MS analysis of Arabidopsis pollen hexane extracts. ....	126
<b>Figure 8-10</b>	UV-/Vis-absorbance spectra from the HPLC-MS profiles. ....	127
<b>Figure 8-11</b>	<i>FST1</i> expression by the Arabidopsis eFP browser.....	127
<b>Figure 8-12</b>	Appearance of the <i>fst1</i> mutant line.....	128
<b>Figure 8-13</b>	Protein sequence alignment of NPF-family members. ....	129

# 1 Introduction

## 1.1 The role of transport in plant secondary metabolism

Plants have evolved an enormous repertoire of structurally diverse chemical compounds, which are not directly involved in central metabolism. These compounds traditionally termed as 'secondary' compounds are specialized metabolites involved in the interaction of sessile plants and their environment (Edreva et al., 2008). This coexistence resulted in the large number of over 200,000 structures of plant secondary metabolites reflecting the astounding adaptability of terrestrial plants to their surrounding environment (Dixon and Strack, 2003; Weng et al., 2012). Secondary metabolites are subdivided into several groups according to their biosynthesis and structural properties (Yazaki, 2005; Edreva et al., 2008) and include terpenoids, alkaloids, phenylpropanoids, and polyketids. Their biosynthetic routes are universally shared by all plant species, whereby some of them are presented in all taxonomic groups, whereas others exist only in single species (Weng et al., 2012). These specialized compounds fulfil various physiological functions. They are directly involved in plant defence as toxic compounds like glucosinolates, cyanogenic glucosides, alkaloids or astringent tannins. They can act as signal molecules like apigenin and luteolin which induce the expression of Nod-factors in root-nodule formation in the interaction between legumes and *Rhizobium* bacteria (Begum et al., 2001). Others support plant reproduction as effective attractants including scent volatiles like benzenoids and terpenoids or vivid pigments like anthocyanins, carotenoids and betalains (Tanaka et al., 2008). For volatile attractants, the interaction between scent benzenoids nocturnally produced by *Petunia axillaris* and the nocturnal pollinator *Manduca sexta* is a well elucidated example (Hoballah et al., 2005; Klahre et al., 2011). Moreover, specific phenolics serve as structural building blocks forming biopolymers like lignin and suberin (Vogt, 2010).

To deploy the whole potential of these specialized compounds, secondary metabolism highly depends on transport processes across biological membranes. Specialized metabolites accumulate in specific cells, tissues and within subcellular organelles to achieve their biological function (Yazaki, 2005). Beside modification (e.g. by glycosylation) (Vogt and Jones, 2000), excretion and sequestration, compartmentalisation allows plant cells to accumulate specialized compounds in high concentrations and preventing self-toxicity (Tissier et al., 2017). Cytotoxic alkaloids like berberine and nicotine are specifically synthesized in roots and long-distance transported into the rhizome or leaves, respectively (Yazaki, 2005). This suggests a precisely regulated and organized cellular and subcellular localization. Most Plants have evolved dedicated organs or tissues as secretory structures for the production and storage of specialized metabolites. A prominent example are glandular trichomes which produce mainly volatile organic compounds (VOCs) that are excreted and stored in extracellular cavities in large amounts (Tissier et al., 2017). It has often been discussed that the transport of lipophilic and readily volatile compounds like VOCs and especially terpenoids is mediated by simple emission also termed 'natural fumigation' (Hoballah et al., 2005; Boachon et al., 2019). Nevertheless, in the case of *Nicotiana spec.* and *Artemisia annua*, the transport of the sesqui- and diterpenoids: sclareol, cembrene, and  $\beta$ -

caryophyllene, which are stored in glandular trichomes, depends on membrane transporters (Jasiński et al., 2001; Pierman et al., 2017; Fu et al., 2017). Other specialized organs and tissues are situated inside, like laticifers, resin ducts, secretory cavities, and oil glands (Tissier, 2018), and the tapetum of the male reproductive organs (Pacini and Hesse, 2005). Especially for the last-mentioned tapetum, several transporters have been found in the last years which are involved in pollen wall formation (Quilichini et al., 2010; Quilichini et al., 2014a) and transport of pollen coat compounds in *Arabidopsis* (Hsieh and Huang, 2007; Choi et al., 2014).

On the subcellular level the pivotal compartmentation of metabolites into the vacuole which may take 40% to 90% of the inner cell space constitutes the key-strategy of plants for storage of metabolites (Yazaki, 2005). Thereby, vacuoles are particular organelles that fulfil specialized functions in plant metabolism supported by a complex vacuolar transporter system (Martinoia et al., 2007). Vacuoles exhibit an enormous capability to enrich specialized compounds in large amounts. Saffron crocins, for example, glycosylated apocarotenoids of the stigma which are stored in vacuoles may reach up to 10% of the spice dry weight (Demurtas et al., 2019).

In conclusion, not only biosynthetic enzymes are required for the biosynthesis of specialized metabolites and their biological function, also efficient transport mechanisms are essential (Yazaki, 2005).

## 1.2 Transporters of specialized metabolites

The framework to organize the complexity of transport processes in secondary plant metabolism is set by membrane transporters (Haferkamp and Linka, 2012). Approximately, 5%-10% of the entire plant proteome represents membrane transporters (Haferkamp and Linka, 2012) reflecting the broad chemical diversity of plant metabolites. Three different types of multidrug transporter superfamilies have been implicated in plant secondary metabolite transport: the ATP-binding cassette (ABC) transporters, the multidrug and toxic compound extrusion (MATE) transporters and the major facilitator superfamily (MFS) (Yazaki, 2005; Nour-Eldin and Halkier, 2013; Takanashi et al., 2014). These superfamilies are widely spread in all living organisms including prokaryotes, fungi, animals, humans and plants (Kang et al., 2011; Shoji et al., 2014; Takanashi et al., 2014; Niño-González et al., 2019). All three transporter types are involved in energy-dependending transport and depend on a proton electrochemical gradient generated by a proton pump ATPase (Lefèvre and Boutry, 2018).

### 1.2.1 ABC-transporters

The ABC-transporter superfamily which constitutes one of the largest known protein families has diverse transport activities not only limited to specialized metabolites but also towards phytohormones, xenobiotics, metal ions and organic acids (Kang et al., 2011). ABC-transporters are ATP-driven primary transporters in contrast to transporters of the MATE and MFS superfamilies (Shoji et al., 2009). The ABC superfamily consists of eight subfamilies which are clarified by the renewed ABC naming system introduced by Verrier et al. (2008) from ABCA to ABCI, though the ABCH subfamily is not presented in plants. Their classification depends on their topology and phylogenetic relationships (Lefèvre and Boutry, 2018). ABC transporters consist of hydrophobic transmembrane domains and cytosolic nucleotide-binding domains involved in MgATP-binding and hydrolysis. They can be organised as half sized

and full-sized transporters, in which case they homodimerize or heterodimerize to be functional (Kang et al., 2011; Lefèvre and Boutry, 2018). The transmembrane domains are more divergent than the nucleotide-binding domains and assumed to be involved in recognition and channelling of the structural highly diverse substrates (Shoji, 2009). An impressive feature of this transporter family is their ability to build up steep concentration gradients across membranes implementing an accumulation of transported substrates in high amounts (Lefèvre and Boutry, 2018). Especially, members of the subfamilies B, C and G have been shown to be involved in various life processes associated with plant secondary metabolism. The CjABCB1 (CjMDR1), a member of the former named multidrug resistance transporters (MDR) (ABC subfamily B) was shown to be capable to transport the alkaloid berberine in *Coptis japonica* (Shitan et al., 2003). Members of the ABC subfamily C, also known as multidrug resistance-associated protein (MRP) transporters were initially thought to be responsible for general detoxification by transport of various xenobiotics (Kang et al., 2011), but have also been reported to transport diverse secondary compounds like flavonoids and crocins (Francisco et al., 2013; Behrens et al., 2019; Demurtas et al., 2019). Further, members of the classically termed pleiotropic drug resistance (PDR) transporters (ABC subfamily G) are involved in transport of defence-related plant compounds like the sclareol transferring NpABCG1 (NpPDR1) (Jasiński et al., 2001). MtABCG10 has recently been demonstrated to be involved in plant defence by transporting precursors of the phytoalexin medicarpin in roots (Banasiak et al., 2013; Baiña et al., 2017). But the ABC subfamily G is also well known to be important for pollen wall formation concerning the transport of lipophilic compounds like lipids, waxes, steroyl glycosides and polyketides to the pollen surface (Yadav et al., 2014; Choi et al., 2014; Quilichini et al., 2014a) as well as the formation of the hydrophobic biopolymer suberin (Landgraf et al., 2014; Yadav et al., 2014).

### 1.2.2 MATE-transporters

The second large group of secondary membrane transporters in plants is formed by the MATE superfamily. These transporters were originally described as exporters conferring drug resistance in bacteria (Omote et al., 2006). The first examined MATE transporter in *Arabidopsis* DTX1 (DETOXIFICATION 1) displayed a wide range of transport activities towards exogenous toxic compounds including heavy metals, ethidium bromide, norfloxacin and also berberine alkaloids (Li et al., 2002). Since then, MATE transporters were shown to transport diverse secondary metabolites (Omote et al., 2006). Several MATE transporters were reported to be involved in the long distance transport of nicotine (Shitan et al., 2009). Another MATE transporter from *Arabidopsis*, DTX18, extrudes hydroxycinnamic acid amides and was shown to confer a preventive pathogen defence against *Phytophthora infestans*, when heterologous expressed in the natural host *Solanum tuberosum* (Dobritzsch et al., 2016). Besides this transport of secondary compounds and detoxification, members of the MATE family contribute to other physiological functions in plants like aluminium tolerance and signalling pathways (Omote et al., 2006). The MATE transporter EDS5 (enhanced disease susceptibility 5) is required for the transport of the phytohormon salicylic acid from the plastid into the cytosol (Serrano et al., 2013). Plant MATE transporters consist of twelve transmembrane domains which are organized as transmembrane  $\alpha$ -helices (Omote et al., 2006). As secondary transporters they link  $H^+$  or  $Na^+$  electrochemical gradients to substrate transfers across membranes (Shoji, 2014). Based on phylogenetic analysis the MATE

superfamily is categorized into three large subfamilies which are subdivided into fourteen subgroups. Plant MATE transporters belong to the eukaryotic MATE subfamily 2B besides yeast and fungi (subfamily 2A), animals (subfamily 2C) and protozoan (subfamily 2D) (Omote et al., 2006). MATE proteins share approximately 40% sequence similarity without the conservation of an apparent consensus sequence (Omote et al., 2006; Shoji, 2014).

### 1.2.3 The nitrate/peptide family (NPF-transporters)

By their almost canonical role as secondary metabolite transporters ABC and MATE transporters are well-established. Though, in the last years an additional plant transporter family which composes to the major facilitator superfamily entered the specialized metabolites research community: the nitrate transporter 1/peptide transporter (NRT1/PTR) family, also named as NPF (NRT1/PTR-family) according to a recent nomenclature system (Léran et al., 2014; Corratgé-Faillie and Lacombe, 2017; Niño-González et al., 2019). One pivotal feature of the NPF transporters is their high number in plants in contrast to the low number in other organisms. The genome of *Arabidopsis* and rice encodes 53 and 80 NRT1/PTR family members, whereas the human and yeast genomes contain only six or a single member, respectively (Tsay et al., 2007). This high number in plants accompanied by broad substrate specificity finally contributed to the discussion about their specific function in higher plants (Tsay et al., 2007; Jørgensen et al., 2017; Niño-González et al., 2019). Its superordinate, the major facilitator superfamily (MFS) is the largest known superfamily of secondary carriers. Thereby, MFS acts initially in primary metabolite transport with a wide variety of substrates: inorganic and organic ions, drugs, sugars, nucleosides, amino acids, as well as peptides (Pao et al., 1998). The superfamily includes uniporters (facilitators) but mostly proton-coupled symporters and antiporters which are generally monomers. These monomers consist of two similar domains each formed by mostly six transmembrane  $\alpha$ -helices (Niño-González et al., 2019). The NPF members were originally well-described as nitrate and peptide transporters, whereby the nitrate transporters are not capable to translocate peptides and *vice versa* (Tsay et al., 2007). Their heterogeneous spectrum of physiological functions is not only restricted to nitrate and peptide transport. Especially members of the second subfamily, NPF2, are highly promiscuous. They translocate phytohormones and glucosinolates among eight NPF subfamilies (Niño-González et al., 2019). Some are associated to inorganic stress response and associated with nitrate excretion, salt stress and alleviation of chloride toxicity (Niño-González et al., 2019). Others form a clade of low-affinity nitrate transporters. NPF2.10 (GTR1) and NPF2.13 (GTR2) were however, also identified as high-affinity glucosinolate-specific transporters (Nour-Eldin et al., 2012). Other members of this clade transport glucosinolates but not exclusively. NPF2.9 prefers indole glucosinolates (Jørgensen et al., 2017) whereas NPF2.10 (GTR1) was also demonstrated to transport chemically dissimilar jasmonoyl-isoleucine and gibberellins (Saito et al., 2015), implementing an astonishing multifunctional transporter activity of the NPF2 subfamily, not limited to *Arabidopsis*.

### 1.3 Flavonoids: highly diverse compounds

Flavonoids are ubiquitous in all taxonomic groups of the plant kingdom (Buer et al., 2010). They are not only restricted to higher flowering plants, but are also present in algae, mosses, and ferns implicating that flavonoid metabolism arose very early in plant evolution (Markham and Porter, 1969; Goiris et al., 2014). Flavonoids are dispersed in all organs, but especially present in generative entities like flowers, pollen, and seeds (Wiermann and Vieth, 1983; Mo et al., 1992; Tanaka et al., 2008). They form a broad, heterogeneous class of structures including chalcones, anthocyanidines, proanthocyanidines, flavonols, isoflavones, flavones, and flavanones. Their enormous chemical diversity of about 9,000 reported molecules (Williams and Grayer, 2004) reflects their wide ranged biological functions in UV-light protection, vivid pigmentation, plant defence, allelopathy, reproduction, and auxin transport (Dixon and Paiva, 1995; Buer et al., 2010). Flavonoids, especially anthocyanines are considered as antioxidants and dihydroxylated B-ring-substituted flavonoids reveal also great activity as scavengers of reactive oxygen species (ROS) (Yamasaki et al., 1996; Acquaviva et al., 2003; Agati and Tattini, 2010). These health-promoting antioxidative properties make flavonoids important as dietary compounds for humans (Birt et al., 2001). Additionally, these small, natural compounds are of increasing pharmaceutical interest because of their potential anti-carcinogenic, anti-inflammatory, anti-fungal, or memory-promoting activities as well as a function in prevention of cardiovascular diseases (Birt et al., 2001; Maher et al., 2006; Jin et al., 2019).

Despite flavonoids may appear as a heterogeneous group, their general structure is derived from the flavan molecule (Figure 1-1 A). This basic aromatic ring system consists of two phenyl rings termed as A and B which are connected by a heterocyclic C-ring. The degree of oxidation of the C-ring, the hydroxylation pattern of the rings, and the substitution of the third position divides the flavonoids into different groups (Leopoldini et al., 2011). As a unique structural characteristic within the flavonoids, anthocyanidines contain a flavylum-cation in the heterocyclic C-ring (Figure 1-1 B). In particular, hydroxylation of the B-ring appears to be important for their antioxidative capacity (Agati and Tattini, 2010; Plaza et al., 2014).

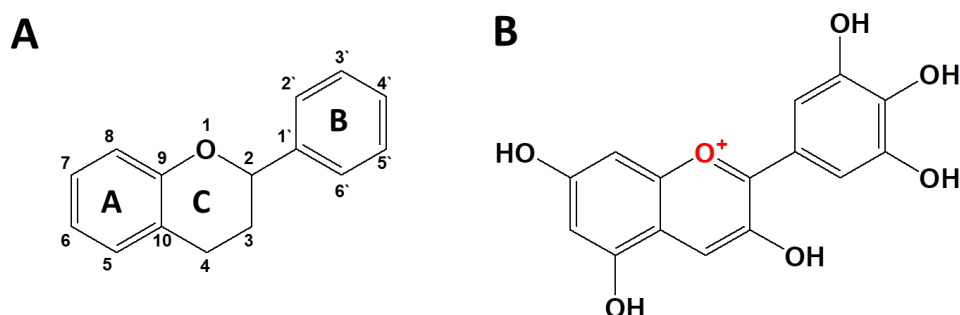


**Figure 1-1** The general flavonoid structure.

The basic flavan molecule (A) with indicated numbering system and nomenclature of the rings A, B, and C compared to (B) delphinidine as representative of the prominent anthocyanidines that contains a flavylum-cation (red marked).

## 1.4 Biosynthesis of flavonol-3-*O*-sophorosides in *A. thaliana*

Two metabolic pathways are involved in the general flavonoid biosynthesis (Figure 1-2). Firstly, the shikimate pathway contributing to the synthesis of the aromatic B-ring, derived from phenylalanine. Phenylalanine is deaminated by the phenylalanine ammonia lyase (PAL), the first enzyme in the phenylpropanoid pathway, to *trans*-cinnamic acid and further hydroxylated to *para*-coumaric acid by the cinnamate-4-hydroxylase (C4H) (Winkel-Shirley, 2001). PAL catalyses the committed step of the phenylpropanoid synthesis and links the primary to secondary metabolism. The hydroxycinnamic acid is then activated by the 4-coumarate: CoA-ligase to *para*-coumaroyl-CoA. The thioester activated *para*-coumaroyl-CoA is the central precursor of the large group of phenylpropanoids (Vogt, 2010). Secondly, the acetate-malonate pathway provides malonyl-CoA units as activated precursors for the aromatic rings A and C. Both pathways are joined by the key reaction of the chalcone synthase (CHS) that catalyses the aldol condensation of *para*-coumaroyl-CoA and three malonyl-CoA units resulting in the basic narigenin chalcone. Each malonyl-CoA molecule provides two carbonic atoms for the formation of the A-ring. The Arabidopsis CHS is encoded by a single gene and its corresponding knockout line devoid of endogenous flavonoids has often been used in studies regarding *in planta* flavonoid function (Ylstra et al., 1996; Yin et al., 2014). Next, the chalcone isomerizes to narigenin, a flavanone catalysed by the chalcone isomerase (CHI) closing the C-ring. Narigenin is the general precursor of flavonols, flavones, isoflavones, proanthocyanins, and anthocyanins (Yonekura-Sakakibara et al., 2019). Subsequently, hydroxylation and oxidation by the flavanone-3-hydroxylase (F3H) and flavonol synthase (FLS) generate the dihydrokaempferol and kaempferol, respectively. The B-ring can be further hydroxylated by the flavonoid-3'-hydroxylase (F3'H) and subsequently oxidized to quercetin by the FLS. Possible formation of myricetin, the third basic flavonol, is not detected in Arabidopsis due to the absence of the flavonoid-3', 5'-hydroxylase (F3'5'H) activity (Tohge et al., 2013). The two hydroxylases, F3'H and F3'5'H, belong to the cytochrome P450 monooxygenases. The flavonol core structures are generally further modified by glycosylation and/or methylation (Figure 1-2). In tapetal cells, kaempferol and quercetin are glucosylated at the 3-OH-position by the glycosyltransferase UGT78D2 producing kaempferol-3-*O*-glucoside and quercetin-3-*O*-glucoside, respectively (Lim et al., 2004; Yonekura-Sakakibara et al., 2014; Knoch et al., 2018). An UGT78D2-equivalent galactosyltransferase relevant for the formation of flavonol-3-*O*-diglycosides on the pollen surface of *Petunia* had already been described (Vogt and Taylor, 1995). These flavonol-3-*O*-glucosides are the substrates for the strictly tapetum-specific UGT79B6 which catalyses the final formation of the characteristic 1 → 2 inter-glycosidic linkage between the two glucose units (Yonekura-Sakakibara et al., 2014). The resulting quercetin- and kaempferol-3-*O*-sophoroside specifically accumulate on the Arabidopsis pollen surface. Beside this tapetum-specific flavonol sophoroside branch, dihydroflavonols are also substrates of the dihydroflavonol-4-reductase (DFR) that catalysed the preliminary reduction of the prominent ketone function at position 4 to a hydroxyl group. The resulting leucoanthocyanidin is afterwards stepwise converted into the coloured anthocyanidines by the anthocyan synthase (ANS) also termed as leucoanthocyanidin dioxygenase (LDOX) (Tanaka et al., 2008).



It is assumed that the essential enzymes of the flavonoid biosynthesis (PAL, CHS, and CHI) act in an enzymatic complex (Saslowky and Winkel-Shirley, 2001) which is discussed as a dynamic 'flavonoid metabolon' anchored to the ER-membrane (Burbulis and Winkel-Shirley, 1999; Dastmalchi et al., 2016). Such metabolons have been reported for various plant species and are hypothesized to be based on cytochrome P450 enzymes mediating specific protein-protein interactions with the membrane resulting in specific flavonoid metabolons (Nakayama et al., 2019). F3'H and F3'5'H are localized to the ER-membrane (Ralston and Yu, 2006) whereas the other flavonoid biosynthetic and decorating enzymes are discussed to be soluble in the cytoplasm or the vacuole (Miyahara et al., 2013; Sasaki et al., 2014; Sun et al., 2016; Nakayama et al., 2019). In Arabidopsis the chalcone synthase appears as the central hub of these protein-protein interactions (Nakayama et al., 2019).

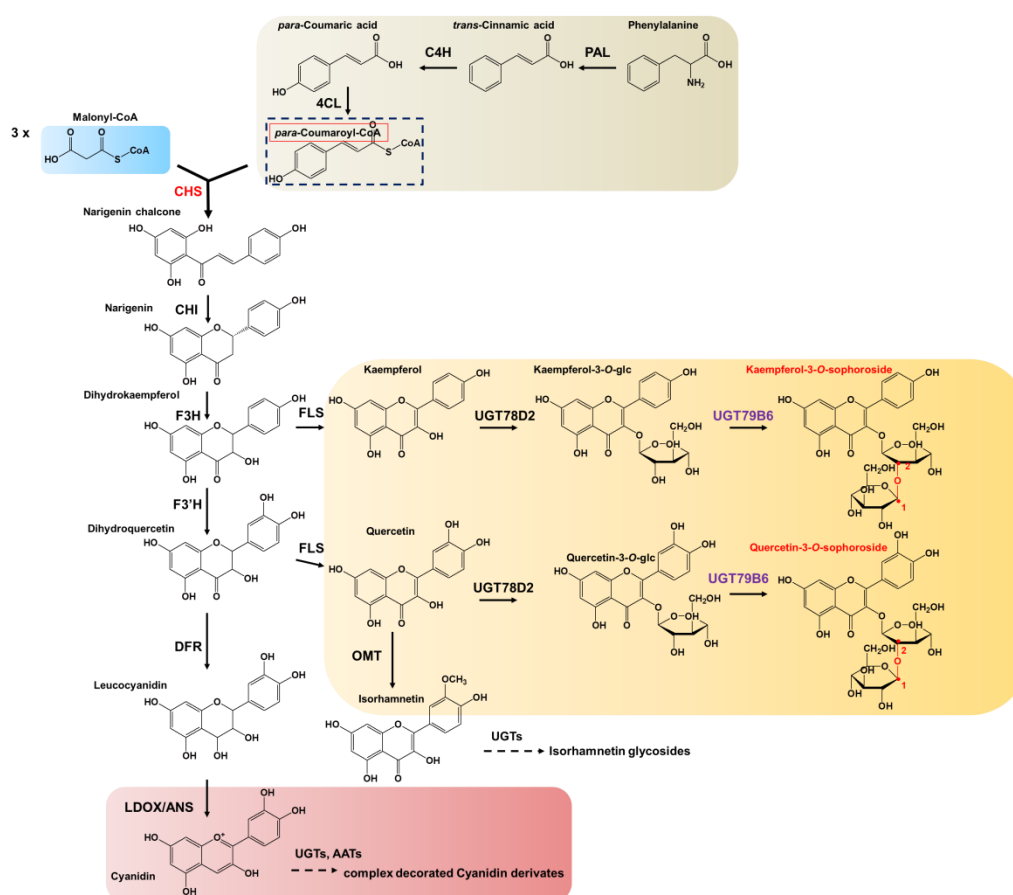


**Figure 1-2** Flavonoid biosynthesis in *A. thaliana*.

The general phenylpropanoid pathway (brown shaded) provides *para*-coumaroyl-CoA the central phenylpropanoid precursor (blue framed) and is joined by the chalcone synthase reaction with the acetate-malonate pathway that provides three units malonyl-CoA (blue shaded). Thereby, the chalcone synthase (red) catalyses the first committed step of the flavonoid biosynthesis. The flavonol-3-O-sophoroside formation catalysed by the UGT78D2 and the terminal UGT79B6 (purple) is limited to the tapetal cells (yellow shaded). The characteristic 1 → 2 inter-glycosidic linkage of the sophoroside is indicated in red. Dihydroflavonols are also converted to coloured cyanidin derived anthocyanins (red shaded). The parallel branch to dihydromyricetin leading to tri-hydroxylated anthocyanins does not occur in Arabidopsis and is not shown (Tohge et al., 2013). phenylalanine ammonia lyase (PAL), cinnamate 4-hydroxylase (C4H), 4-coumarate:CoA ligase (4CL), chalcone synthase (CHS), chalcone isomerase (CHI), flavanone 3-hydroxylase (F3H), flavonoid 3'-hydroxylase (F3'H), flavonol synthase (FLS), flavonoid O-methyltransferase (OMT), dihydroflavonol 4-reductase (DFR), leucoanthocyanidin dioxygenase/anthocyanin synthase (LDOX/ANS), anthocyanin acyltransferase (AAT) and the flavonoid glycosyltransferases: UGT78D2 (UGT78D2) and UGT79B6 (UGT79B6).

## 1.5 Flavonoid glycosylation

In plants flavonoids are usually decorated by a broad spectrum of modifications including hydroxylation, acylation, methylation, and glycosylation (Plaza et al., 2014). Flavonoids are commonly glycosylated in the final steps of their biosynthesis, prior to acylation (Vogt and Jones, 2000; Plaza et al., 2014). Complex glycosylation patterns drastically increase the number of flavonoid derivatives, directly reflecting their various biological roles in plants (Vogt and Jones, 2000). The largest numbers of glycosides for individual flavonols were reported for kaempferol with 257 and quercetin with 232 (Harborne and Baxter, 1999). Whereby, the glycosylation is favoured at the 3-OH and 7-OH position of the C- and A-ring, respectively (Harborne and Baxter, 1999; Yin et al., 2012).

### 1.5.1 Biological relevance of flavonoid glycosylation

Glycosylation affects the chemical properties of the molecules regarding the solubility and the stability which directly have an impact on their biological activity. Glycosylation decreases antioxidative capacity compared to the aglycone (Plaza et al., 2014), but results in an increased stability. This increased stability is crucial for the stabilization of the flavylum cation required for the formation of complex anthocyanin conjugates by further acylation with *trans*-cinnamic acid (Goto and Kondo, 1991). In the case of the highly decorated anthocyanin A11 in *Arabidopsis* leaves, glycosylation acts also as an anchor for building up further complex substitution patterns, which result in co-pigmentation required for stability (Miyahara et al., 2013; Kovinich et al., 2014; Sasaki et al., 2014).

Specific glycosylation may feedback inhibit the entry enzymes of the phenylpropanoid and flavonoid pathway. A double null mutation of *UGT78D1* and *UGT78D2*, which are required for the initial flavonol-3-*O*-glucosylation, blocks the transcription of the key enzymes CHS and PAL resulting in flavonoid biosynthesis levels of one third of the wild-type (Yin et al., 2012). Additionally, Yin et al. (2014) demonstrated that an excess of an incorrect flavonol glycosylation pattern causes an inhibition of the polar auxin transport in *Arabidopsis*. Such an incorrect glycosylation pattern can also affect various other phytohormones like abscisic acid, cytokines, and brassinosteroids (Vogt and Jones, 2000).

Besides the glycosylation pattern, specific linkage of two sugar moieties determines the properties of individual flavonoid glycosides. In naringenin-7-*O*-hesperidoside, substitution of the rhamnose residue to glucose of the 1→2 linkage results in the characteristic, bitter citrus flavour in grapefruit (Frydman et al., 2004). Conversely, the 1→6 inter-glycosidic linkage of naringenin-7-*O*-rutinosides which is found in non-bitter, sweet species like mandarins, is tasteless (Frydman et al., 2004). Whether this bitter flavour has repulsion effect on herbivores has not been fully elucidated (Del Río et al., 2004). For the flavanone diglycosides naringin and hesperidin highly enriched in the citrus peel of grapefruit and orange an antifungal activity against *Penicillium digitatum* was discussed by Ortuño et al. 2006. Transposition of neohesperidose from the 7-OH position (bitter taste) to the 4'-OH position decreases bitterness in case of the flavanone glycosides. Whereas, the 4'-OH substitution of the neohesperidin dihydrochalcone determines an intense sweet taste, 1,000 times sweeter than sucrose (Esaki et al., 1994).

### 1.5.2 Plant glycosyltransferases

The key players of these flavonoid glycosylations are plant glycosyltransferases of the family I. These enzymes catalyse the transfer of single sugar residues to a broad spectrum of small molecular weight natural compounds like phenylpropanoids, terpenoids, or phytohormones (Vogt and Jones, 2000). The glycosyltransferases depend on uridine diphosphate (UDP) activated sugar groups and therefore, are termed as uridine diphosphate depending glycosyltransferases (UGTs). The most common sugar-donor in plants is UDP-glucose besides UDP-xylose, UDP-galactose, UDP-rhamnose or UDP-mannose, whereby mono-, di- and triglycosides can be formed (Vogt and Jones, 2000). The catalysis mechanism of the UGTs is highly conserved and acts as a SN<sub>2</sub>-like reaction under retention or inversion of the anomeric C-atom (Osmani et al., 2009). The broad catalytical capability of UGTs to function in a regio-selective and stereo-specific manner contributes to the huge diversity of glycosylated secondary compounds and their potential application in pharmaceutical biotechnology (Lim, 2005). Although a high number of flavonoid aglycone glycosyltransferases have been characterized (Lim et al., 2004; Sun et al., 2016), just a handful of flavonoid-glycoside-glycosyltransferases have been reported for the generation of the specific 1 → 2 inter-glycosidic linkage found in flavonol sophorosides (Trapero et al., 2012; Yonekura-Sakakibara et al., 2014; Knoch et al., 2018).

### 1.5.3 Flavonol sophorosides

Flavonol sophorosides were reported for the first time in 1938 by Rabaté and Dussy. They reported the isolation of kaempferol sophoroside as a new heteroside from green fruits of the tree *Sophora japonica* (L.). The original root *sophoreae* was eponymously for these new flavonol diglycosides originally termed by the French authors as “*Sophoraflavonoloside*” and the referring 1 → 2 linked glucose – glucose disaccharide as sophoroside (Rabaté and Dussy, 1938; Freudenberg et al., 1951). In 1960s the quercetin-3-*O*-sophoroside was isolated from whole flowers of *Solanum tuberosum*, *Petunia hybrida*, and *Gossypium barbadense* as well as from pollen of *Alnus cordata* and both flavonol-3-*O*-sophorosides were firstly chemically synthesised (Wagner et al., 1968). Harborne (1963) described flavonoid sophorosides to be present in various organs of diverse plant species and its disaccharide as frequently associated in nature with these pigments. Anthocyanins are also known to be “sophoroyleated” (Harborne, 1963; Tatsuzawa et al., 2010).

The flavonol-3-*O*-sophorosides present a special class within the large range of flavonol diglycosides due to the rare 1 → 2 inter-glycosidic linkage of the sophoroside. In nature, flavonol sophorosides, usually derived from quercetin and kaempferol, are highly abundant on the surface of pollen grains from diverse plant species (Tomás-Barberán et al., 1989; Ferreres et al., 1989; Markham and Campos, 1996). They are considered to be pollen-specific and are part of the tryphine and are not covalently bound to the sporopollenin (Ferreres et al., 1989; Vogt and Taylor, 1995; Yonekura-Sakakibara et al., 2014; Knoch et al., 2018). Though, the glycosylation pattern has been described to be relative complex and species-specific (Tomás-Barberán et al., 1989), the unique 1 → 2 inter-glycosidic linkage between two sugar units on the third position of the C-ring appears to be a highly conserved motif in all angiosperm plants. On the pollen of maize (*Zea mays*) quercetin- and isorhamnetin-3-*O*-neohesperidosides are present (Ceska and Styles, 1984). Due to their high pollen and species specificity, they are proposed

as biochemical markers for the determination of the origin of bee pollen and honey, respectively (Ferrerres et al., 1989; Akbari et al., 2017). Their conserved glycosidic-linkage implicates an evolutionary conserved physiological function *in planta* (Markham and Campos, 1996; Ferreres et al., 1989). It is well-known that pollen-specific flavonol glycosides are essential for pollen tube germination and growth especially in diverse Solanaceae species (Mo et al., 1992; van der Meer et al., 1992; Ylstra et al., 1992). In *Petunia (Petunia hybrida)* pollen germination of a *chs* mutant lacking all endogenous flavonoids was induced by external supplement of kaempferol leading to the rescue of the pollen tube growth and the male sterile phenotype (Napoli et al., 1999). Beside, flavonol-3-*O*-sophorosides may have pharmaceutical relevance. Flavonol-3-*O*-sophorosides as well as –neohesperidosides are found in diverse traditional medicinal herbs like candle bush (*Cassia alata*), *Physalis angulata* or mountain ginseng (Palanichamy and Nagarajan, 1990; Ismail and Alam, 2001; Kim et al., 2012). Studies imply that kaempferol-3-*O*-sophoroside has anti-inflammatory (Kim et al., 2012) and analgesic activity (Palanichamy and Nagarajan, 1990).

## 1.6 Tapetum and pollen – A special relationship

### 1.6.1 Angiosperm pollen development

Pollen development is of crucial importance for reproduction in flowering plants and based on the unique interplay between the diploid and haploid generation (Blackmore et al., 2007). The development of the male gametophyte is divided into two successive phases presented in Figure 1-3.

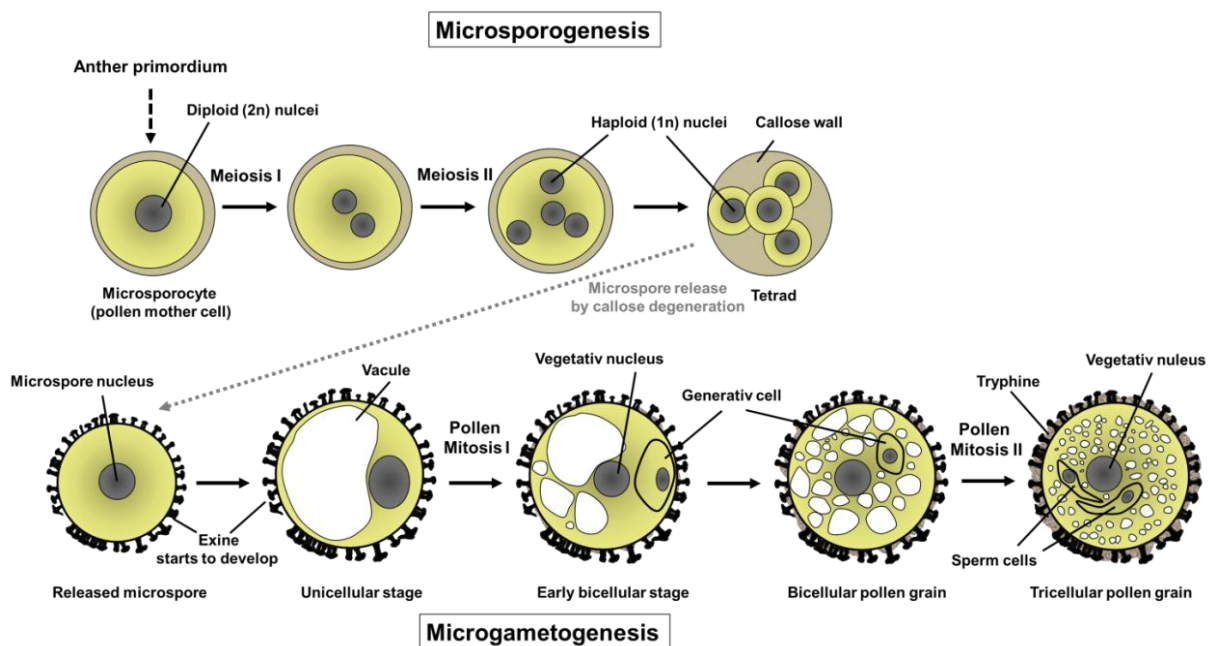


**Figure 1-3** Chronology of male gametophyte development.

Illustrated are the major cytological events of the pollen development pathway in *Arabidopsis* based on transmission electron microscopy studies and according to Twell et al. (1998).

The first phase, the microsporogenesis, starts with the microsporocyte also termed as pollen mother cell which is derived from the anther primordium, an undifferentiated cell-cluster. The diploid

microsporocyte is surrounded with a callose wall and is divided by meiosis into four haploid, unicellular microspores. These four microspores are connected to each other by the callose wall in a tetrad stage. At the end of microsporogenesis, the callose wall is degenerated and the single microspores are released and free in the locule fluid. After release of the unicellular microspore stage, the development of the outer pollen wall layer, the exine, is initiated. At this stage, the second phase takes up, the microgametogenesis. It starts with the polarisation of the microspore by the expansion of the microspore due to the expansion of the central vacuole accompanied by the movement of the nucleus close to the pollen wall. Critical for vital pollen maturation is the subsequent asymmetric division by the first pollen mitosis resulting in the formation of two unequally sized daughter cells (Twell et al., 1998). The large vegetative cell takes the majority of space and cytoplasm. The vegetative cell has dispersed nuclear chromatin and is excluded from further cell cycle; it stores high levels of metabolites essential for sustaining the later rapid pollen tube growth (Twell et al., 1998). In contrast, the generative cell is very small and completely enclosed by the vegetative cell, appearing as 'cell within the cell' and is closely pressed towards the periphery pollen wall. It contains condensed chromatin and migrates into the centre of the bicellular pollen where it undergoes the second pollen mitosis into two sperm cells, the male gametes. The microgametogenesis finally ends with the formation of usually tricellular pollen accompanied by the accumulation of the pollenkit completing the mature pollen wall deposition.

Later pollen tube growth critically depends on an apical plasma membrane domain enriched with the regulatory phospholipid phosphatidylinositol 4,5-bisphosphate (PtdIns(4,5)P<sub>2</sub>) (Ischebeck et al., 2008). It was recently demonstrated that this apical production of PtdIns(4,5)P<sub>2</sub> is linked with the mitogen activated protein kinase (MAPK)-mediated regulation (Hempel et al., 2017).

### **1.6.2 A special cell layer: the tapetum**

Stamen out of anthers and filament are the male reproductive organs of flowering plants. The anthers contain four locules where the male gametophytes (pollen grains) develop protected by several layers of sporophytic cells (Figure 1-4). The outermost layers, the epidermis and the endothecium contain large central vacuoles. Small middle layers sustain the tapetal cells which surrounds the developing microgametes contained within the locule. Each tissue is only one cell layer deep (Owen and Makaroff, 1995).

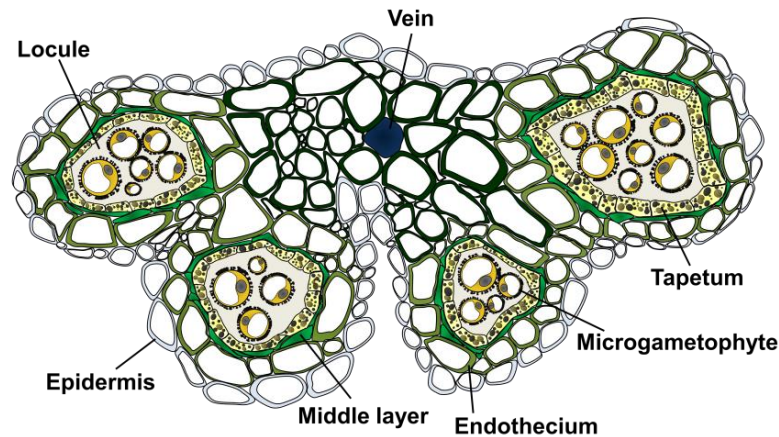


**Figure 1-4** Overview of the anther cell layers in Arabidopsis.

Illustrated is an anther cross-section before anther dehiscence. The developing male microgametophytes are at the late unicellular stage. The epidermis and the endothecium cells contain large, central vacuoles. The tapetal cell layer highly packaged with storage compounds, elaioplasts and tapetosomes is still intact. Connective cells connecting the single lobes within the anther are coloured dark green. The vascular strand tissue of the vein is just blue signified. (Scheme is self-drawn based on light- and fluorescence-microscopy studies).

The innermost cell layer the tapetum is a unique, highly specialized tissue which is universally present in land plants (Pacini et al., 1985). The tapetum is essential for male fertility. These 'altruistic' cells feed the developing microsporocytes in the premeiotic phase, produce the locule fluid and enzymes like callase and constituents of the outer pollen wall (exine) (Pacini et al., 1985; Muriga et al., 1991). Finally, during the late stages of pollen development the tapetal cells undergo programmed cell death resulting in the deposition of the pollenkit (Quilichini et al., 2014b). In spermatophytes, tapeta are classified into two main types: the secretory (parietal) type as it is present in Arabidopsis and an invasive type, the periplasmodial (amoeboid) tapetum (Pacini et al., 1985; Quilichini et al., 2014b). Whereas the amoeboid tapetum provides a direct nutrition of the microspores, the secretory tapetum requires transport to the microspores through the locule fluid (Quilichini et al., 2014a; Quilichini et al., 2014b). In Arabidopsis and other Brassicaceae these transport processes are facilitated by the loss of the tapetal cell wall during the time of microsporocyte meiosis (Muriga et al., 1991; Owen and Makaroff, 1995).

Tapetal cells are metabolic highly active, characterized by many ribosomes, high number of mitochondria, dispersed chromatin and a high density of storage compounds like lipid drops as well as two special subcellular organelles, elaioplasts and tapetosomes (Muriga et al., 1991; Wu et al., 1997; Hsieh and Huang, 2007). Tapetal elaioplasts are specialized plastids with reduced thylakoids which accumulate unusual sterol esters as major lipid components (Murphy, 2006). Tapetosomes are unique storage organelles, firstly characterized by Wu et al. (1997) which are formed at the cisterna of the endoplasmic reticulum. They contain highly significant amounts of lipids with a relatively high density of  $1.05 \text{ g cm}^{-3}$  (Piffanelli, 1998), but were also described by Hsieh and Huang (2005; 2007) to store flavonoids and oleosins.

### 1.6.3 Composition of the pollen wall

The formation of the angiosperm pollen demonstrates 'pinnacle of evolutionary progression towards gametophyte miniaturisation' (Scott, 1994) that apparently was an adaptation for the development of land plants (Quilichini et al., 2014b). The pollen wall ensures a prolonged survival of the reproductive cells and allows their safe and wide dispersal by protecting them against diverse terrestrial stresses like desiccation (Choi et al., 2014). Although pollen grains show an astonishing high diversity concerning their species-specific characteristics like size, shape and elaborate external morphology, they share a basic construction principle (Scott, 1994). The pollen wall is stratified in a concentric series of different layers (Figure 1-5).

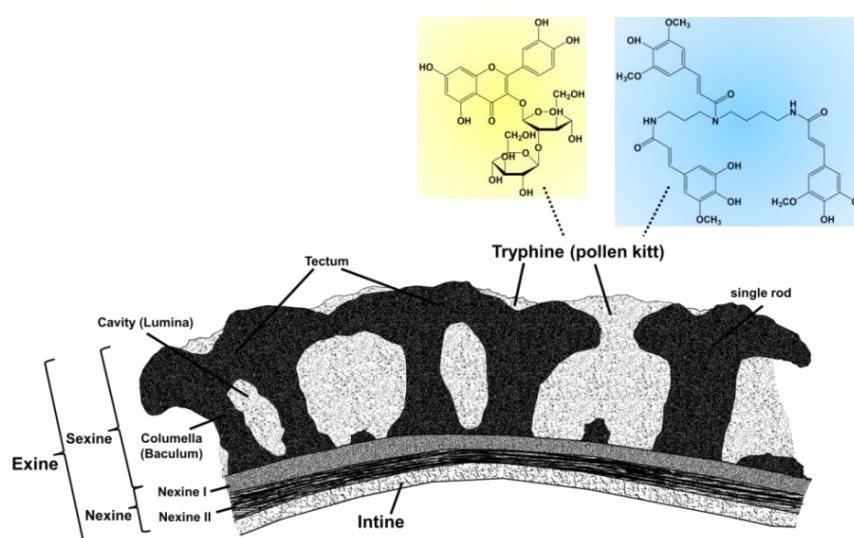


**Figure 1-5** Stratification of the pollen wall in *Arabidopsis*.

The terminology of the single layers used in this thesis differentiates two major cell layers: the outer exine and the inner intine. The exine consists of the nexine stratified in two distinct layers nexine I and II. This basis is ornamented by the upper sexine. The sexine presents rod-like structures: tectum sustained by the columella and unconnected rods with a simple head supported by a single columella named as baculum. The tryphine commonly termed as pollenkitt is deposited on the pollen surface and fills gaps and cavities (lumina) of the tectum. Phenylpropanoids constitute to the pollenkitt. Representative shown are the flavonol diglycoside quercetin-3-O-sophoroside (yellow shaded) and a *tris*-hydroxycinnamic acid-spermidin-conjugate (phenolamide) (blue shaded) as two major water-soluble phenylpropanoid class constituents. The illustration was self-drawn according to Scott (1994) and Blackmore et al. (2007).

Two main layers can be distinguished as the outer exine and the inner intine. The intine, directly adjacent to the plasma membrane, is generated from the inner side by the microspore and composed of pectin, cellulose, and hemicellulose. The intine appears as a light band by transmission electron microscopy (TEM) observation (Quilichini et al., 2014b). The thick exine is divided into the outer complex sculptured sexine and the simple inner nexine. The sexine consists of rod-like structures termed as baculae and columella which are vaulted by the tectum forming void-like structures including cavities (lumina). The surface of the tectum contains mostly in reticula pattern arranged germinal apertures (colpi) which are emergence sites of the germinating pollen tube (Scott, 1994). Striking supratpectal elements as found in other species are not present in *Arabidopsis* with its simple structured pollen wall (Blackmore et al., 2007). The supporting nexine is subdivided into nexine I and nexine II. Nexine I appears similar to the sexine, while nexine II has a characteristic laminated appearance (Scott, 1994). The major component of the exine layer is sporopollenin which is resistant to acetolysis and



temperatures about 300 °C (Scott, 1994). An open question is the exact chemical nature of this extreme robust biopolymer. Genetic approaches and biochemical data suggested that it includes phenolic and fatty acid derived compounds and tetraketide alpha-pyrone that a covalently coupled by ether and ester linkages (Kim et al., 2010; Quilichini et al., 2014a).

A heterogeneous mixture of compounds on the outer pollen wall forms the pollen coat. The pollen coat is easily extractable by non-polar organic solvents and consists of alkanes, carbohydrates, neutral-ester lipids, free fatty acids, long-chain wax esters, volatile lipids, terpenoids, flavonoids and phenolamides as well as proteins (Pacini and Hesse, 2005; Hsieh and Huang, 2005; Murphy, 2006; Quilichini et al., 2014a). Notably, flavonoids are estimated to be about 2% to 4% of the pollen dry weight and are associated in a facile manner (Wiermann and Vieth, 1983). Besides the flavonoids, a second group of phenylpropanoids, the hydroxycinnamic acid amides (HCAAs), are also conserved on the pollen of various plant species (Meurer et al., 1988). This extracellular matrix provides an isotropic media (Murphy, 2006) and seals the top of the tectum and is filled inside the cavities of the sexine (Quilichini et al., 2014b). In contrast to the sporopollenin precursors which are extruded during the early microspore phase, the different tryphine compounds are presumed to be dispensed short before or after tapetum degeneration (Hsieh and Huang, 2007; Quilichini et al., 2014a). Some scientists further differentiate the adhesive pollen coat material in the Brassicaceae specifically as tryphine, a mixture of hydrophilic and hydrophobic substances, and the hydrophobic pollenkitt (Pacini and Hesse, 2005). Nevertheless, both terms are equally used in literature.

According to its heterogeneous composition the tryphine fulfils of diverse biological functions. Preservation of the pollen grains against water loss by abundant hydrophobic compounds (Murphy, 2006; Choi et al., 2014), but also UV-light protection is suggested (Pacini and Hesse, 2005). Further, a protective role against bacteria and fungi, which can be transmitted by pollen, is discussed (Paul et al., 1992; Pacini and Hesse, 2005; Card et al., 2007). Noteworthy, the role of flavonoids as potential anti-fungal (Jin et al., 2019), has not been sufficiently clarified to date. The pollen coat is more than a protective shield; it carries specific self-incompatibility proteins and promotes outbreeding/pollen dispersal by facilitating adhesion of pollen grains to each other (clumping), pollinators, and the female, recipient stigma. It has been shown that some of the lipid compounds are necessary for initiative pollination (Jessen et al., 2011). Especially in case of the dry stigma of Brassicaceae, the tryphine is required during the pollen-stigma communication including the so called coat conversion, when the pollen coat material floats out of the exine cavities generating a moisture adhesion area (Murphy, 2006).

### **1.7 Flavonoid transport in plants**

Flavonoids have different sites of biosynthesis, storage and various target sites which make efficient transport mechanisms univocally essential for their physiological functions. Three different but not exclusive mechanisms for flavonoid transport processes in plants were reported (Zhao, 2015). These mechanisms include membrane transporters, glutathione-S-transferase (GST) mediated transport, and vesicle trafficking. Whereby, all three model routes are suggested to be linked and



collaborative (Zhao, 2015). Up to now, there are two membrane transporter families known to be involved in plant flavonoid transport: ABC- and MATE-transporters.

Several members of the ABC-transporter subfamily C were reported to be involved in transport of mainly anthocyanins (Kang et al., 2011; Zhao, 2015). Noteworthy, a member of the G-type subfamily has also been demonstrated to transport isoflavonoids (Banasiak et al., 2013) indicating that also other ABC subfamilies are capable to use flavonoids as substrates. Goodman et al. (2004) firstly indicated that two multiple drug resistance-associated proteins ZmMDR3 and ZmMDR4 are required for anthocyanin transport in *Zea mays*. Later, anthocyanin transport activity for *Vitis vinifera* ABCC1 was examined by yeast microsome assays (Francisco et al., 2013). Interestingly, it has also been shown that ABC C-type transporters that are apparently not related with flavonoid transport like the crocin transporters CsABCC4a and CsABCC2 might be capable to transport flavonoid glycosides (Demurtas et al., 2019). It should be noted, that these C-type transporters were originally considered to be glutathione-substrate-conjugate pumps involved in detoxification with a broad range of unrelated substrate types (Kang et al., 2011). Other GSH-conjugated phenylpropanoids like *trans*-cinnamic acid are also taken up by vacuolar transporters with a ten times higher velocity than non-glutathionated compounds (Walczak and Dean, 2000). In the case of anthocyanin and proanthocyanins transport, several reports led to the assumption that the ABC-C transport is assisted by GST linked transport (Zhao, 2015). The GST proteins TT19 (Kitamura et al., 2004) and AN9 (Mueller et al., 2000) are essential for anthocyanin and proanthocyanin accumulation in Arabidopsis and Petunia vacuoles. Furthermore, the transport of malvidin-3-*O*-glucoside by the VvABCC1 has been examined to be strictly depended on the presence of glutathione (Francisco et al., 2013). Initially, it was assumed that GST proteins would catalyse the formation of glutathione-conjugated flavonoid complex (Goodman et al., 2004). But so far such a complex has never been identified in plants (Mueller et al., 2000; Behrens et al., 2019). Actually, a physically interaction of the GST protein as a carrier to the substrate appears more likely (Zhao, 2015). A single report by Hsieh and Huang (2007) about the impact of the *tt19* mutation on the pollen coat flavonoid glycoside content is so far the only evidence for an equivalent GST-assisted flavonol glycoside export in anthers (Zhao, 2015).

An early indication about the role of MATE transporter in flavonoid transport resulted from the classical phenotype screening of the *transparent testa* mutants exhibiting altered seed colouration in Arabidopsis seeds (Debeaujon et al., 2001; Takanashi, et al., 2014). Thereby, the MATE transporter TT12 which is probably one of today's best characterized plant transporters was identified based on the altered flavonoid composition in *tt12* mutant seeds. The vacuolar Arabidopsis TT12 transporter was functionally characterized using microsomal vesicles from yeast to transport cyanidin-3-*O*-glucoside and epicatechin-3'-*O*-glucoside by Marinova et al. (2007). Since cyanidin-3-*O*-glucoside levels were not impacted by *tt12* mutation. TT12 is mainly considered to transport epicatechin-3'-*O*-glucoside as the native substrate (Takanashi et al., 2014). Later, several functional orthologues of *TT12* were described and shown to complement the *tt12* Arabidopsis mutant (Frank et al., 2011; Yang et al., 2016). Other members of the MATE transporter superfamily, like anthoMATE1 and anthoMATE3 were reported from grapevine (*Vitis vinifera*) (Gomez et al., 2009). Though, recent studies suggest a GST mediated transport mechanism as mentioned above in case of the ABCC transporters (Zhao, 2015;

Behrens et al., 2019), the MATE mediated transport is regarded to function GST-independently (Takanashi et al., 2014). Though, proteins essential for vesicle trafficking like Rab GTPases and SNAREs have not been described to be required for flavonoid transport (Shoji, 2014), there is new evidence for an intracellular flavonoid vesicle trafficking by the contribution of the trafficking factor GFS9 (TT9) in *Arabidopsis* (Ichino et al., 2014). There, the *tt9* mutation causes low flavonoid accumulation in seeds accompanied by membrane trafficking defects like mis-sorting of vacuolar proteins, aggregation of enlarged vesicles, and vacuolar fragmentation (Ichino et al., 2014).

For both transporter types glycosylation of the aglycone appears to be essential for flavonoid transport. Zhao et al. (2011) tested different flavonoid aglycones towards MtMATE2 without detection of transport activity. It has been discussed that the modification pattern of the transferred flavonoids determines the transporter type (Marinova et al., 2007). The VvABC-C1 homologous to the ZmMRP3 which is assumed to accept malonylated anthocyanidin derivatives (Goodman et al., 2004) exhibited no transport activity when delphinidin or epicatechin were tested in comparison to delphinidin-3-*O*-glucoside and the preferred malvedin-3-*O*-glucoside (Francisco et al., 2013). Acylation also appears *in vitro* as a chemical requirement for the vacuolar MATE-mediated transport by the anthoMATEs (Gomez et al., 2009). Nevertheless, *in planta* anthoMATE3 was examined to be capable of cyanidin-3-*O*-glucoside transport by partially complementation of the *pab1* mutant (Kitamura et al., 2016). Phylogenetic analysis implicates that MATE transporter involved in flavonoid accumulation are subdivided in two distinct clades according to their substrates proanthocyanin precursors or acylated anthocyanins (Takanashi et al., 2014).

The MATE transporter DTX35 termed as FLOWER FLAVONOID TRANSPORTER (FFT) by Thompson et al. (2010a) has been implicated in floral transport of flavonol glycosides in *A. thaliana*. The *dtx35* mutant exhibits changed flavonoid levels in buds and siliques (Thompson et al., 2010a). Furthermore, the DTX35 transporter has been shown to be specifically expressed in guard cells of various plant organs (Thompson et al., 2010a; Zhang et al., 2017). Interestingly, DTX35 as well as its homolog DTX33 were also characterized as turgor-regulating Cl<sup>-</sup> ion channels (Zhang et al., 2017). Profound data about the impact of DTX35 as flavonoid transporter was given by Kitamura et al. (2016) using the *Arabidopsis banyuls* (*ban*) mutant background that accumulates coloured anthocyanins instead of proanthocyanin precursors in the seed coat. They demonstrated that the *pale banyuls 1* (*pab1*) mutant which caused reduced anthocyanin levels in mature seeds is allelic to DTX35 and was rescued by a genomic copy of the DTX35 allele. Thereby, it was also measured that *pab1 ban* seeds contain lower levels of quercetin glycosides supporting the previous assumption by Thompson et al. (2010a) about a flavonol glycoside transport activity. But a clarifying *in vitro* transporter activity of DTX35 towards flavonoids has not been demonstrated yet.

In summary, although several transporters have been suggested for flavonol glycoside transport *in planta*, some accompanied by a distinct phenotype as in the case of the *tt12* mutant, the overall picture appears rather indistinct and still quite fragmentary.

## 1.8 Aim of this investigation

The accumulation of flavonol-3-*O*-sophorosides in large amounts on the surface of pollen grains is known for a long time (Pratviel-Sosa and Percheron, 1972). Together with hydroxycinnamic acid amides, these special metabolites are highly conserved in the pollenkit of angiosperms implementing a still unsolved essential physiological function of these phenylpropanoids for the male gametophyte (Fellenberg and Vogt, 2015). At the beginning of this work, UGT79B6 (*At5g54010*) was identified to catalyze the terminal biosynthetic step in tapetal flavonol-3-*O*-sophoroside formation by Yonekura-Sakakibara et al. (2014) and in parallel by us (unpublished). Successively, this raised questions about the unknown transport of these tapetum-derived tryphine constituents. Identification of UGT79B6 allowed for production of <sup>14</sup>C-labelled flavonol-3-*O*-sophorosides essential for *in vitro* transporter studies. In consequence, the major aim of this study was to evaluate the transport process of the flavonol-3-*O*-sophorosides from the tapetal cell to the outer pollen wall. Hence, the present investigation includes the following points:

- 1) We aimed to identify a flavonol glycoside-specific or non-specific (!) transporter by screening a series of ABC, MATE, and NPF2 candidate mutant lines from Arabidopsis for alteration in the phenolic profile of anthers and pollen. We wanted to know whether the transport is tapetum-specific and generate complementation lines but also stable *promFST1:GFP*-reporter lines. These lines combined with GFP-fusion constructs should allow monitoring the organ-specific expression and subcellular localization of the tapetal transporter.
- 2) Through radioactive uptake assays, based on synthesis of the transporter substrates and a microbial expression system, activity and substrate profile of the transporter should be established.
- 3) In order to illuminate the physiological function and relevance of the pollen-specific flavonoids and their transporter, classical assays as well as TEM-imaging of pollen grains should be performed.
- 4) In addition, a *78d2 x sht* knockout line should be generated to further elucidate the physiological function of tapetal phenylpropanoid biosynthesis.

Analysis and characterization of such a proposed flavonol sophoroside transporter *in planta* would increase our understanding about flavonoid transport processes and might help to uncover the conserved and enigmatic role of the transported metabolites on the outer pollen wall.

## 2 Materials and methods

### 2.1 Materials

#### 2.1.1 Chemicals and biochemical reagents

Chemicals used in this study were of analytical quality and were obtained from Carl Roth (Karlsruhe, Germany), Merck (Darmstadt, Germany), Serva (Heidelberg, Germany) and Duchefa (Haarlem, Netherlands). The flavonoid standards used for glycosyltransferase assays were obtained from Extrasynthese (Genay, France). Ascorbic acid as well as uridine diphosphate (UDP) glucose and quercetin were obtained from Merck (previously Sigma-Aldrich). The  $^{14}\text{C}$ -labelled UDP-glucose was acquired from Hartmann Analytik (300 mCi/mmol, Braunschweig, Germany).

Enzymes, vectors and antibodies were acquired from Thermo Scientific (Waltham, USA), Bio&Sell (Feucht, Germany), New England Biolabs (Ipswich, Massachusetts, USA), Qiagen (Hildesheim, Germany), Merck (Darmstadt, Germany), Roche Diagnostics (Risch, Schweiz) and Takara Bio Europe S.A.S. (Saint-Germain-en-Laye, Frankreich). All Primers were synthesised by Eurofins Genomics (Ebersberg, Germany). Kits used for molecular biology approaches are specified. All aqueous solutions, buffers, and media were prepared with distilled water provided by a Milli-Q-system (Millipore, Schwalbach, Germany).

#### 2.1.2 Media

Cultivation of the bacterial strains was performed with lysogeny broth (LB) medium liquid or solid as LB agar obtained from Duchefa. Antibiotics (ampicillin, carbenicillin, chloramphenicol, kanamycin, rifampicin, spectinomycin, tetracyclin; final conc.  $25\ \mu\text{g ml}^{-1}$  to  $100\ \mu\text{g ml}^{-1}$ ) were supplied as required. For Golden Gate cloning LB agar was prepared with X-Gal (5-bromo-4-chloro-3-indolyl- $\beta$ -D-galactoside) ( $50\ \mu\text{g ml}^{-1}$  final conc.) for blue-white colony screening.

For increased yield of cell material for heterologous protein expression bacterial strains were grown on Terrific Broth (TB) medium (Merck) supplied with 1% (v/v) glycerol. Bacterial strains cultivated for transporter studies were grown on yeast extract tryptone (YT) medium prepared as follows:  $8\ \text{g l}^{-1}$  tryptone;  $5\ \text{g l}^{-1}$  yeast extract ;  $2.5\ \text{g l}^{-1}$  NaCl.

In the final step of transformation Super Optimal Broth with Catabolite repression (SOC) medium was used for the cultivation of freshly transformed bacterial cells. The nutrient rich SOC medium included:  $20\ \text{g l}^{-1}$  tryptone;  $5\ \text{g l}^{-1}$  yeast extract;  $10\ \text{mM}$  NaCl;  $2.5\ \text{mM}$  KCl;  $10\ \text{mM}$   $\text{MgCl}_2$ ;  $10\ \text{mM}$   $\text{MgSO}_4$ ;  $20\ \text{mM}$  glucose. After preparation, all media were sterilized by autoclaving at  $121\ ^\circ\text{C}$  for at least 20 min.

#### 2.1.3 Vectors

An overview of all expression vectors used in this study is given in Table 2-1. Golden Gate vectors and newly generated constructs are separately given in Table 2-7. The vectors FST1 pET16b, UGT78D2 pQE70, and UGT79B6<sub>opt</sub> petDuet-1 were used as templates for site directed mutagenesis. The vector pETDuet-1 was chosen for recombinant expression of the UGT79B6<sub>opt</sub> to leave the possibility of co-

expression with other candidates (e.g. UGT78D2) cloned into the second multiple cloning site or inserted into compatible pET vectors (e.g. pRSFDuet-1) open.

**Table 2-1** Vectors used for heterologous protein expression. All listed expression vectors contain an ampicillin resistance marker gene. Multiple cloning site (MCS).

vector	short description	reference
pET16b	<i>E. coli</i> expression vector, provides N-terminal His-tag	Merck
pETDuet-1	<i>E. coli</i> co-expression vector with two MCS, N-term His-tag (MCSI) / C-term S-tag (MCSII)	Merck
pQE70	<i>E. coli</i> expression vector, provides C-terminal His-tag	Qiagen
FST1 pET16b	CDS of FST1 ( <i>At5g28470</i> ) inserted into pET16b for heterologous expression	Grunewald
UGT78D2 pQE70	CDS of UGT78D2 ( <i>At5g17050</i> ) cloned into pQE70 for heterologous expression	Grunewald
UGT79B6 <sub>opt</sub> pETDuet-1	codon optimized variant of UGT79B6 ( <i>At5g54010</i> ) cloned into pETDuet-1 for heterologous expression	Grunewald

#### 2.1.4 Bacterial strains

For cloning, plasmid preparation and the purpose of plasmid stock cultures the DH10B strain (Thermo Scientific) of *Escherichia coli* (*E. coli*) bacteria was used. The genotypes of all *E. coli* strains are shown in Table 2-2.

**Table 2-2** *E. coli* strains used in this work.

strain	genotype	reference
DH10B	F <sup>-</sup> <i>mcrA</i> Δ( <i>mrr hsdRMS mcrBC</i> ) φ80 <i>lacZ</i> ΔM15 Δ <i>lacX74 recA1 endA1 araD139</i> Δ( <i>ara, leu</i> )7697 <i>galU galK λ rpsL nupG</i> /pMON14272 / pMON7124	Thermo Scientific
Rosetta (DE3) pLys	F <sup>-</sup> <i>ompT hsdS<sub>B</sub>(r<sub>B</sub><sup>-</sup> m<sub>B</sub><sup>-</sup>) gal dcm</i> (DE3) pLysS pRARE (Cam <sup>R</sup> )	Merck
M15 [pRep4]	<i>Nal<sup>s</sup> str<sup>s</sup> rif<sup>s</sup> thi<sup>-</sup> lac<sup>-</sup> ara<sup>-</sup> gal<sup>+</sup> mtl<sup>-</sup></i> F <sup>-</sup> <i>recA<sup>+</sup> uvr<sup>+</sup> ion<sup>+</sup></i> [pREP4 KanR],	Qiagen

For heterologous protein expression in *E. coli*, the BL21 strain derivative Rosetta™ (DE3) pLys (Merck) were used. This bacterial strain contains the inducible T7 RNA polymerase system and is further modified to increase expression of eukaryotic target proteins. The Rosetta™ cells provide rarely used tRNAs to overcome limitations of the prokaryotic codon usage. For heterologous expression of the UGT78D2 the M15 [pRep4] *E. coli* strain was used, since the T5 RNA polymerase based pQE70 expression vector is incompatible with the T7 expression system. The *Agrobacterium tumefaciens* strain GV3101 provided by Dr. Sylvestre Marillonnet (IPB) was used for transformation of *Arabidopsis thaliana* and *Nicotiana benthamiana* plants.

### 2.1.5 Preparation of electrocompetent cells

A volume of 200 ml LB medium was inoculated with 2 ml *E. coli* pre-culture incubated overnight at 30 °C. The culture was incubated about 4 hours at 30 °C. After the culture reached an OD<sub>600</sub> about 0.5 the cells were collected by centrifugation at 4000 g, at 4 °C, for 15 min. The cell pellet were washed twice in a volume of 240 ml ice-cold 10% (v/v) glycerol and centrifuged at 4000 g, at 4 °C for 15 min. Afterwards the bacterial cells were dissolved in 1 ml 10% (v/v) ice-cold glycerol and cell aliquots of 50 µl were prepared and stored at -80 °C. Bacterial cells prepared by this protocol are stable for transformation about 8 months. Preparation of the *Agrobacterium* strain GV3101 for electroporation was kindly performed by Ramona Grützner (IPB, Halle).

### 2.1.6 Plants and growth conditions

The *Arabidopsis thaliana* plants used in this study were grown under long day conditions with a 16 hours photoperiod in a greenhouse provided with LED-lamps (R-SB-IPB002, RHENAC Green Tec AG, Hennef, Germany). The average temperatures were 24 °C during the day and 19 °C during the night. The greenhouse was fully conditioned and had humidity about 55% to 65%. All *Arabidopsis* plants were in the ecotype Columbia-0 background except the T-DNA insertion line *tt12-1* (W10067) that was in the ecotype Wassilewskija (Ws2). The insecticide Exemptor® (granulat with 10% thiacloprid, Everris, Nordhorn) was added to the soil. *N. benthamiana* plants which were used for the subcellular localization assays were also grown under long day conditions in a comparable fully acclimatized greenhouse.

### 2.1.7 Isolation of T-DNA insertion lines

All T-DNA insertion lines used in this thesis were obtained from the Nottingham Arabidopsis Stock Center (NASC, <http://arabidopsis.info>). Each Arabidopsis T-DNA insertion line was considered by the SALK Institute to be a homozygous line (Alonso et al., 2003). Nevertheless, the T-DNA insertion was verified for each line by PCR of genomic DNA using primers recommended by the SALK primer design tool (<http://signal.salk.edu/tdnaprimers.2.html>) for conformation of the homozygous lines. For the genotyping of each line, three primers were used, a LP and RP primer specific for the allele and the T-DNA-specific LB primer (specific against the left border T-DNA). To verify that the tested T-DNA insertion lines were deficient in transcript synthesis of each candidate gene a PCR from cDNA of young buds using full-length-specific primers for each mutant line was performed. The *COMT1* (*At5g54160*) and *UGT79B6* (*At5g54010*) encoding genes were used as controls. The individual lines and the primers for identification are given (Appendix, Tables 8-1 and 8-2). The used *tt12* mutant lines *tt12-1* (W10067) and *tt12-2* (GK797D03) were provided by NASC as isolated homozygous knockout lines and showed the characteristic transparent testa phenotype of the seed coat and were described before (Debeaujon et al., 2001; Kitamura et al., 2010). The *dtx33*-mutant line (SALK\_131275C) has also been reported as *dtx33-2* by Zhang et al. (2017). Additionally, the *chs* (*tt4*, *At5g13930*) point mutation line N85 in the *Landsberg erecta* ecotype was used in this thesis for comparison. For the generation of the *78d2 x sht* double knockout mutant line the *78d2* (*At5g17050*) T-DNA insertion line SALK\_049338C and the *sht* (*At2g19070*) T-DNA-line SALK\_055511C were crossed. Individual F<sub>2</sub> lines homozygous for each T-DNA insertion were similar isolated and tested by PCR for each particular knockout. The *78d2* T-DNA line was described before by Yin et al. (2014). The *sht* T-DNA insertion line was also investigated before by Grienberger et al. (2009), Fellenberg et al. (2009), and Fellenberg et al. (2012a). The genotyping and

the verification of the knockout as necessary controls for the isolation of a homozygous knockout line are representative shown for the main candidate, the *fst1* mutant line (SALK\_027288C) (Appendix Figure 8-1). A schematic overview of the *FST1* allele and the T-DNA-insertions of the lines SALK\_02788C and SALK\_113184C are given (Appendix Figure 8-2). The T-DNA Express: Arabidopsis Gene Mapping tool (<http://signal.salk.edu/cgi-bin/tdnaexpress>) can be used to check length and position of the T-DNA insertions of each individual line.

## 2.2 Molecular methods

If not stated otherwise, all kits were used according to the manufacturers instructions.

### 2.2.1 Isolation of genomic DNA

The isolation of gDNA from *Arabidopsis thaliana* wild-type was required for the Golden Gate cloning applications and the genotyping of the T-DNA insertions lines. Preparative isolation of high quality gDNA further used for cloning was performed with the DNeasy Plant Mini Kit (Qiagen, Hilden, Germany). Usually, 250 mg plant material from *Arabidopsis thaliana* (Col-0) wild-type buds frozen in liquid nitrogen and grinded by a CyroMill MM100 beadmill (Retsch, Haan, Germany) were used. The elution was performed with 100  $\mu$ l elution buffer. The concentration of the isolated gDNA was measured by the Nanodrop 1000 spectrophotometer (peqlab, Erlangen, Germany). The gDNA was stored at 4 °C.

For a fast and cheap screening of the T-DNA insertion lines a 'quick and dirty' protocol for the isolation of gDNA from small plant samples was used. With this method gDNA was successfully isolated from single inflorescences or parts of young leaves. First the plant material was solubilized by adding of 40  $\mu$ l NaOH (0.25 M) heating at 95 °C in a thermocycler for 30 s and mixed with 20  $\mu$ l detergent buffer (0.25% (v/v) Igepal® CA 630; 0.5 M Tris-HCl; pH 8.0). After this, the samples were neutralized by adding 40  $\mu$ l (0.25 M HCl) and again incubated in a thermocycler at 95 °C for 2 min. Finally, 2  $\mu$ l of the gDNA were used as template in PCR for genotyping.

### 2.2.2 Isolation of plasmid DNA

The NucleoSpin® Plasmid EasyPure kit from Macherey-Nagel (Düren, Germany) was used for extraction of plasmid DNA. The preparation was performed according to the manufactures instructions. For the transformation of protoplast used in the subcellular localization assays higher concentrations of plasmid DNA were necessary. To provide the required amounts of plasmid DNA, plasmid midi-preparations were performed using the QIAGEN Plasmid Midi Kit (Qiagen, Hilden, Germany). To increase the yield of plasmid DNA the bacterial cultures were grown in TB-medium (terrific broth; trypton 12 g l<sup>-1</sup>; yeast extract 24 g l<sup>-1</sup>; K<sub>2</sub>HPO<sub>4</sub> 9.4 g l<sup>-1</sup>; KH<sub>2</sub>PO<sub>4</sub> 2.2 g l<sup>-1</sup>; 0.8% (v/v) glycerol; Merck (Sigma-Aldrich)) and the elution buffer preheated at 70 °C and the elution volume reduced at 30  $\mu$ l or 50  $\mu$ l, respectively.

### 2.2.3 Polymerase chain reaction (PCR)

The Phusion high fidelity DNA polymerase (Finnzymes, Thermo Scientific) with proofreading activity was used for preparative DNA amplification subsequently used for cloning applications. For standard PCR applications (e.g. genotyping of the T-DNA lines) the ALLin™ Red Taq 2x Mastermix

(highQu, Kraichtal, Germany) was used. Reactions were performed. For genotyping of the transgenic Arabidopsis lines the reaction volume was decreased down to 30  $\mu$ l. The PCR programs are given in Table 2-3. All primer sequences were synthesised by Eurofins Genomics (Ebersberg, Germany). The reactions were performed in a thermocycler (C1000 Touch<sup>TM</sup> Thermal Cycler, Bio-Rad, Munich, Germany).

**Table 2-3** Standard PCR programs. The Phusion high fidelity DNA polymerase was used for preparative PCR for cloning applications of cDNA and gDNA. \*In case of the gDNA the initial denaturation time was increased up to 2 min to provide a complete separation of the template strands. The ALLin Red taq DNA polymerase was used for standard PCR. The  $T_m$  means primer melting temperature. The chosen elongation time depends on the template size.

steps	Phusion	ALLin Red taq
initial denaturation	98 °C, 30 s or 2 min*	95 °C, 1 min
1.denaturation	98 °C, 7 s	95 °C, 15 s
2. annealing	$T_m$ 50-65 °C, 30 s	$T_m$ 55-65 °C, 15 s
3. elongation	72 °C, 30 s kb <sup>-1</sup>	72 °C, 15 s kb <sup>-1</sup>
replication (1 to 3)	34 cycles	34 cycles
final extension	72 °C, 10 min	72 °C, 10 min
hold	4 °C, $\infty$	4 °C, $\infty$

#### 2.2.4 Agarose gel electrophoresis

An electrophoretic method for the separation of nucleic acids according to their fragment size is given by the agarose gel electrophoresis. Thereby the concentration of the agarose gel was generally chosen between 0.8% to 2% agarose (w/v) to provide a clear separation fragment lengths between 300 bp to 5 kb of DNA and RNA, respectively. The method was used for analysis of PCR products, plasmid restriction analysis and to confirm the integrity of isolated RNA. A 0.8% to 1.2% agarose solution was prepared with 1x TBE buffer (10x TBE stock solution: 121.1 g l<sup>-1</sup> Tris; 55 g l<sup>-1</sup> boric acid, 7.4 g l<sup>-1</sup> EDTA) and heated in a microwave. After shortly cooling 0.01% (v/v) ethidium bromide (Roth, Karlsruhe, Germany) was added to the solution. After polymerization of the agarose, the samples were loaded on the gel. To provide a better sample application the sample buffer (50% (v/v) glycerol; 0.2% EDTA; 0.1% (w/v) bromophenol blue) was added to the samples before. The fragment sizes of the nucleic acids were determined by a DNA ladder such as Hyperladder<sup>TM</sup> I (Bioline, Luckenwalde, Germany). The gel electrophoresis was performed from 50 V to 120 V with TBE as running buffer for at least one hour. Subsequently, gels were recorded using the FUSION FX7 gel documentation system (Vilbert Lourmet, Eberhardzell, Germany).

#### 2.2.5 RNA extraction and cDNA synthesis

Around 200 mg plant material of different green plant organs (open flowers, inflorescence, leaves, young siliques, stems) from Arabidopsis wild-type plants were collected and frozen in liquid nitrogen, stored at -80 °C and subsequently grinded with a Beadmill (CryoMill MM100, Retsch, Haan, Germany). The tiny Arabidopsis anthers and carpels were collected by dissection from young inflorescences under a stereomicroscope (Stemi DV4, Zeiss, Germany) using ultra-fine forceps. For one preparation, usually 500 anthers or 200 carpels were harvested and directly frozen in liquid nitrogen and stored at -80 °C.



Total RNA of the different plant organs was isolated with the NucleoSpin® RNA Plus Kit (Machery-Nagel). The total RNA from young anthers and carpels was extracted with the NucleoSpin® RNA Plus XS Kit for extra small tissue samples from Machery-Nagel. Impurities of gDNA were removed by the included NucleoSpin® gDNA removal columns. In case of the carpel RNA samples an additional DNase I (Thermo Scientific) digestion was performed to remove residual gDNA. The quantity and quality of extracted RNA was determined photometrically by the 260 nm /280 nm ratio using a NanoDrop1000 spectrophotometer (peqlab). The integrity of the isolated RNA was analysed by agarose gel electrophoresis (1.2% (w/v) agarose). The distinct appearance of 28S rRNA and 18S rRNA indicated an intact quality of the isolated RNA (Appendix, Figure 8-3).

The isolated RNA was transcript into cDNA with the Maxima H Minus First Strand cDNA Synthesis Kit (Thermo Scientific). To compare the relative transcription levels 250 ng RNA of each sample were used for cDNA synthesis. The resulting cDNA was used for quantitative Real time PCR (qRT-PCR). For cloning applications 3 µg RNA isolated from young inflorescences of Arabidopsis wild-type plants were transcribed into cDNA.

### 2.2.6 Quantitative real-time polymerase chain reaction (qRT-PCR)

The expression of the transporter candidate genes *FST1* (*At5g28470*) and *TT12* (*At3g59030*) were measured by qRT-PCR, which enables the relative quantification of the target gene compared to a reference gene. As internal reference gene the constitutively expressed 65 kDa subunit of the protein phosphatase 2A (PP2A, *At1g13320*) which was used previously, was chosen (Fellenberg et al., 2009). The fluorescence signal is recorded during every reaction cycle by nucleic acid intercalating fluorescence dyes, in this case the EvaGreen® Dye (Bio&Sell, Feucht, Germany) and its intensity is proportional to the amount of amplified PCR products. Thereby, an indirect conclusion about the initial amount of the target sequence (used as template) is allowed. Quantification cycle (Cq) values were used to determine the relative target abundance between the samples. The reactions were run on the CFX Connect™ Real-Time System (Bio-Rad, Munich, Germany). The resulting data was evaluated using the CFX Manager Software (Bio-Rad). The qRT-PCR was performed using the following protocol: denaturation (95 °C for 15 min), amplification (40 cycles of 95 °C for 15 s and 60 °C for 30 s), and melting curve (95 °C for 10 s, 65 °C heating up to 95 °C with a heating rate of 0.05 °C s<sup>-1</sup>). The relative expression levels were examined in three independent experiments and each reaction was performed as technical triplicate. The mean values of the Cq values from the technical triplicates were calculated and subsequently the Cq values were calculated by the difference of the target and reference Cq values:  $\Delta Cq = Cq_{\text{target gene}} - Cq_{\text{reference gene}}$ . The relative transcription rate was calculated by the formula:  $2^{-\Delta Cq}$ . The mean values of the biological replicates were used to determine the standard error.

All reactions were performed using the 5x EvaGreen® qPCR Mix II (Bio & Sell, Feucht, Germany) and a reaction volume of 10 µl. As template in the qRT-PCR cDNA reverse transcribed from 250 ng total RNA were diluted 1:5 and used at fixed quantities (150 ng cDNA per reaction). In parallel reactions with 1 µg isolated RNA as template were used as additional controls. Additionally, controls with water instead of a template were used to control the clean experimental sample preparation. The qPCR primers were designed to bind at an overlapping sequence of an exon-intron changeover to be highly

specific for the targeted cDNA and to exclude non-specific product formation from residual gDNA. Non-specific product formation could be excluded by the analysis of the individual melting curves. All used qPCR primers are listed (Table 2-4).

**Table 2-4** Primers used for qRT-PCR. Oligonucleotide sequences of the target genes *FST1* (*At5g28470*) and *TT12* (*At3g59030*) and the reference gene *PP2A* (*At1g13320*) used for qRT-PCR and their product sizes. The underlined sequences indicate the exon-intron changeover. The binding specificity was tested by BLAST search.

gene	sequence	product length
<i>FST1</i> ( <i>At5g28470</i> )	fw 5'- <u>GTCCGAGACAAAC</u> ACAGATTAAGG-3' rw 5'-CTGCTGCACACTACATAATCTCC-3'	117 bp
<i>TT12</i> ( <i>At3g59030</i> )	fw 5'- <u>TATCATG</u> TTAGGAATGGCGAGCGC-3' rw 5'-CCATGGCTCGTTGGCAGATTATT-3'	101 bp
<i>PP2A</i> ( <i>At1g13320</i> )	fw 5'- <u>AGACA</u> AGGTTCACTCAATCCGTG-3' rw 5'-CATTCAGGACCAAACCTTTCAGC-3'	75 bp

### 2.2.7 Classical cloning for recombinant protein expression

For functional characterization, the coding DNA sequence (CDS) of the *FST1* (*At5g28470*) transporter candidate was inserted into the prokaryotic expression vector pET16b. The associated glycosyltransferases *UGT78D2* (*At5g17050*) and *UGT79B6* (*At5g54019*) required for production of the <sup>14</sup>C-labelled substrates were cloned into pQE70 (Qiagen) and pETDuet-1 (Novagen) for heterologous expression in *E. coli*, respectively. The insertions of the CDS fragments were performed by classical cloning. In case of the *UGT79B6* the coding DNA sequences was codon optimized for the codon usage in *E. coli* by Eurofins Genomic for enhanced protein expression (Novy et al., 2001). The codon optimized sequence is given (Appendix, Figure 8-4) and was directly cloned into the expression vectors without a PCR step.

The preparative amplification of the target gene CDS by RT-PCR of cDNA from young Arabidopsis wild-type buds was performed using the Phusion high fidelity DNA polymerase (Finnzymes, Thermo Scientific). Primers were synthesised with overhangs including restrictions sites to generate vector compatible fragments after restriction digestion. The conventional cloning of the target genes and the primers are shown (Table 2-5). The amplified products were purified using the NucleoSpin® Gel and PCR Clean-up Kit (Machery-Nagel). In the case of the appearance of unspecific PCR fragments the Kit was also used for gel extraction. Both, purified PCR product and vector were digested with the suitable FastDigest™ restriction enzymes (Thermo Scientific) at 37 °C for at least 1 hour in a reaction volume of 50 µl. The restriction was stopped by adding 50 µl of water and the DNA was precipitated by adding 10 µl of sodium acetate (3 M; pH 4.9) and 275 µl cold 96% (v/v) ethanol. To improve precipitation, samples were quickly frozen in liquid nitrogen and thawed several times. Samples were subsequently centrifuged at 2,0817 g for 1 hour, at 4 °C. The supernatant was removed and the DNA pellet was washed with 300 µl 70% (v/v) ethanol and centrifuged at 2,0817 g, for 10 min, at 4 °C. Afterwards the supernatant was removed and the pellet was dried for 5 min to evaporate residual ethanol. Finally, the DNA was solved in nuclease-free water and the concentration was photometrically determined at 260 nm.

In the case of cloning the *FST1* (*At5g28470*) and the *UGT78D2* (*At5g17050*), only one restriction site of the multiple cloning site could be used. Therefore, it was necessary to dephosphorylate the restricted plasmids to avoid re-ligation. 5'-dephosphorylation was performed using the Shrimp Alkaline Phosphatase (SAP) (Thermo Scientific).

**Table 2-5** Primers used for conventional cloning. The used restriction enzymes are written in braces. The restriction sites contained in the primer overhangs are marked bold. The encoded start and the stop codon are indicated yellow and grey, respectively. According to the manual instructions of the QIAexpressionist (Qiagen) the start codon of the *UGT78D2* (*At5g17050*) was included into a *SphI* recognition site to be in frame and the stop codon was removed.

candidate	term	sequence
<i>FST1</i> ( <i>At5g28470</i> )	FST1pET16bfw	5'-CATGCA <b>CTCGAG</b> ATGGACGTCGAATCTTCATCACC-3' ( <i>XhoI</i> )
	FST1pET16brw	5'-TGCATG <b>CTCGAG</b> TTAGTGTCTTTTTGTTTTCAGTGGC-3' ( <i>XhoI</i> )
<i>UGT78D2</i> ( <i>At5g17050</i> )	78D2pQE70fw	5'-CATGCAG <b>CATG</b> CCCAAACCTCCGACCCAAC-3' ( <i>SphI</i> )
	78pQE70D2rw	5'-TGCAAT <b>G</b> CATGCAAATAATGTTTACAAC-3' ( <i>SphI</i> )
<i>UGT79B6<sub>opt</sub></i> ( <i>At5g54010</i> )	-	directly cloned without PCR using <i>EcoRI</i> and <i>HindIII</i>

DNA fragments were ligated into the vectors using the T4 DNA Ligase (Thermo Scientific) according to the manual. The reaction volume was 20 µl and the ligation was performed at 22 °C for at least 1h 30 min. The ratio of fragment and vector was 1:5. The ligase was inactivated by heating at 65 °C for 10 min. A volume of 2 µl ligation mix was used for the electrochemical transformation of bacterial cells. Colonies were screened by colony PCR. Resultant plasmids from positive clones were isolated and sequenced (Eurofins Genomic, Ebersberg, Germany) to verify the sequence identity and the orientation of insertion.

### 2.2.8 Golden Gate Cloning

The cloning of *FST1* complementation constructs, the subcellular localization constructs and promoter GFP reporter constructs were performed by using the Golden Gate modular cloning system developed by Dr. S. Marillonnet (IPB, Halle) (Engler et al., 2014). An advantage of this method is that the restriction and assembling of several DNA fragments can be performed in parallel in one reaction in one step with a high efficiency. The Golden Gate System uses the type II restriction endonucleases *BsaI* and *BpiI* and their ability to cut outside of their recognition sites. This allows DNA fragments flanked by overhangs including compatible restriction sites to be restricted and ligated in one reaction, because the type II recognition site will be removed after ligation avoiding re-restriction. Further it enables a specific orientated ligation for assembly of multiple DNA fragments directed by four additional compatible base pairs remaining after cleavage. The assembling of the complete target DNA sequence is performed in level 0 using *BsaI* sites. Further cloning steps into higher levels (level 1 (*BpiI*) and level 2 (*BsaI*)) are used to add different modular elements (e.g. GFP-reporter gene). A large toolbox of modular Golden Gate elements has been developed up to now (Engler et al., 2014). Prior to ligation all pre-existing *BsaI* and *BpiI* recognition sites inside the target DNA fragments must be removed by silent

point mutations. Therefore, an additional cloning level (level -1) for individual fragments was usually necessary. The vector maps of the finally generated *FST1* level 2 constructs are representative shown (Appendix, Figure 8-5). The cloned DNA fragments were confirmed by sequencing (Eurofins Genomics) in level -1 and level 0, respectively. A restriction analysis of the generated plasmids was performed after each cloning step representative shown for the construct pAGV891 (Appendix, Figure 8-5 D). Golden Gate primers and constructs are listed (Appendix Table 8-3 and Table 2-7, respectively). A schematic overview for the cloning of the UGT79B6 subcellular localization construct pAGV561 (level 1) is shown in Figure 2-1.

The backbones of the Golden Gate vectors contain a selection marker depending on the level: kanamycin (level -1 and level 2), spectinomycin (level 0), and carbenicillin (level 1). A LacZ reporter gene unit inside the destination vector enables blue-white selection of positive colonies. The final level 1 and level 2 constructs are binary vectors suitable for the replication in *E. coli* and *A. tumefaciens* and used as shuttle vectors for plant transformation. The stable replication of the plasmids is provided in *E. coli* by the pUC origin of replication (ori) and by the pVS1 ori in *A. tumefaciens*. They contain a coding sequence module placed between the T-DNA right border (TB) and left border (LB) which will be undirected inserted as transfer DNA fragment (T-DNA) into the plant genome. The level 1 constructs designed for the subcellular localization use the Cauliflower mosaic virus 35S promoter. For fluorescence-based localization studies the green fluorescence protein (GFP) was used as reporter gene. Transcript termination of the gene of interest was mediated by an octopine synthase terminator (*tOcs*) and the putative *FST1* terminator, respectively. The expression of the level 2 constructs is driven by the putative promoters of *FST1* (2245 bp) and *UGT79B6* (928 bp). Additionally, a putative *TSM1* promoter (559 bp) and a putative *SHT* promoter (858 bp) were used for the production of a tapetum-specific positive control. They contain an optimized variant of the *BAR* gene that mediates resistance against glufosinate, the active agent of the BASTA® herbicide used for selection of positive transformants. The expression of the *BAR* gene is controlled by the bacterial nopaline synthase promoter (*pNos*) and terminator (*tNos*).

For generation of the *FST1* complementation constructs pAGV931 and pAGV1043 the *FST1* (*At5g28470*) full-length genomic DNA fragment of 2550 bp was cloned under the control of a putative 2245 bp *FST1* promoter and a 719 bp *FST1* terminator. Additionally, the pAGV1043 construct encodes the *FST1* gene fused to a GFP reporter gene. Notably, the full-length gDNA fragment of *FST1* (*At5g28470*) was finally used to generate the pAGV993 construct acting in the subcellular localization assays. Thereby, the original stop codon was removed by PCR using the subcfst6 primer. A primary generated construct using just the *FST1* CDS fused to the GFP reporter gene did not work. The activities of the *UGT79B6*, *SHT*, and *TSM1* promoter-GFP-reporter constructs were cloned before and firstly tested in this study.

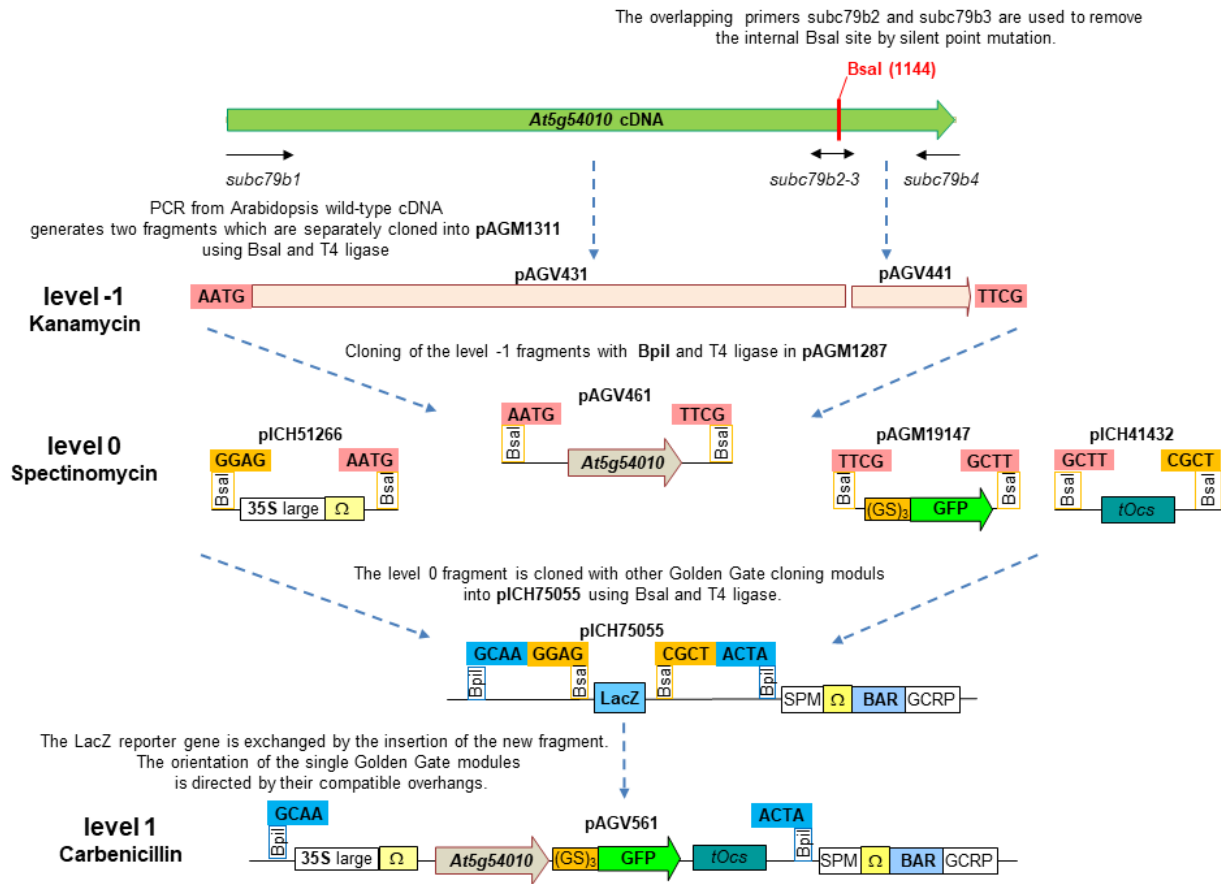


**Figure 2-1** Schematic overview of Golden Gate cloning.

The cloning of the pAGV561 level 1 construct is representative shown. First two PCR fragments are amplified from *A. thaliana* wild-type cDNA from young buds. The primers *subc79b1-4* add *Bsal* sites and compatible 4 base pairs overhangs are shown in Appendix Table 8-3). The overlapping primers *subc79b2* and *subc79b3* are used to create a base pairs exchange introducing a silent point mutation to remove an endogenous *Bsal* site. Each PCR product is cloned in the universal level -1 vector pAGM1311 containing a kanamycin resistance. The level -1 constructs pAGV431 and pAGV441 are cloned together into the level 0 destination vector pAGM1287 (spectinomycin resistance) using the *Bpil* sites (provided by pAGM1311) and the AATG and TTCG overhang, respectively. The resulting level 0 constructs pAGV461 contains the complete UGT79B6 (*At5g54010*) CDS. Subsequently, pAGV461 is cloned together with the modular Golden Gate constructs pICH51266 (35S promoter), pAGM19147 (GFP reporter gene with linker) and pICH41432 (octopine synthase terminator) into the level 1 destination vector pICH75055 containing a carbenicillin resistance. Thereby, the single units are ligated in a specific direction based on their complementary overhangs generating the level 1 construct pAGV561 finally used for subcellular localization. The new fragment is flanked by two *Bpil* sites provided by pICH75055 allowing more cloning applications into level 2. For fast colony screening the Golden Gate destination vectors contain a LacZ reporter gene for blue-white selection.

**Table 2-6** Golden Gate cloning vectors. Listed are all used modular cloning vectors kindly provided by Sylvestre Marillonnet (IPB, Halle) and the final, newly generated Golden Gate constructs. \*For the cloning of the pAGV993 construct full-length gDNA of *FST1* (*At5g28470*) was used.

vector	short description
pAGM1311	universal level -1 cloning vector
pICH41295	cloning of promotor fragments into level 0
pICH75055	backbone vector, cloning of fragments into level 1
pICH41531	contains the GFP reporter gene for level 1 cloning
pICH41432	provides <i>Ocs</i> terminator for level 1 cloning
pICH45066	backbone vector, cloning of promotor fragments into level 2
pICH43201	introduces <i>BAR</i> gene and <i>Nos</i> promotor/terminator into level 2
pICH41744	provides short linker DNA fragment for level 2 cloning
pICH41308	level 0 cloning vector for complementation construct
pAGM1287	level 0 cloning vector without stop codon for subcellular localization
pAGM37443	level 2 cloning vector for complementation construct
pICH51266	contains the 35S promotor for subcellular localization (GFP C-terminal)
pAGM19147	provides GFP reporter gene with (GS) <sub>3</sub> linker for subcellular localization (GFP C-terminal)
pAGM16831	contains 35S promotor for subcellular localization (GFP N-terminal)
pAGM19123	contains GFP reporter gene with (GS) <sub>3</sub> linker for subcellular localization (GFP N-terminal)
pAGM16841	provides stop codon with <i>Ocs</i> terminator for subcellular localization (GFP N-terminal)
pICH75044	backbone vector for subcellular localization (GFP N-terminal)
pAGM14122	GFP positiv control for subcellular localization, level 1
pAGV72	<i>UGT79B6</i> promotor GFP reporter construct, level 2
pAGV82	<i>SHT</i> promotor GFP reporter construct, level 2
pAGV92	<i>TSM1</i> promotor GFP reporter construct, level 2
pAGV561	prom35S: <i>UGT79B6-GFP:tOcs</i> for subcellular localization, level 1
pAGV581	prom35S: <i>GFP-UGT79B6:tOcs</i> for subcellular localization, level 1
pAGV993*	prom35S: <i>FST1-GFP:tOcs</i> for subcellular localization, level 1
pAGV891	<i>FST1</i> promotor GFP reporter construct, level 2
pAGV931	<i>FST1</i> complementation construct, level 2
pAGV1043	prom <i>FST1:FST1-GFP:tFST1</i> for complementation

### 2.2.9 Restriction analysis

The digestion of generated plasmids by endonucleases and the subsequently analysis of the restricted DNA by agarose gel electrophoresis were used to control the correct cloning and amplification of DNA fragments. According to the manual instructions the FastDigest™ restriction enzymes from Thermo Scientific were used for this approach. The digestion of 0.5 µg to 1 µg DNA was performed in 20 µl reaction volume with 0.5 µl restriction enzyme. For preparative application, the amounts of DNA and the sample volume were increased to 5 µg DNA and 50 µl, respectively. For the Golden Gate cloning method, the restriction enzymes *BsaI* and *BpiI* (isoschizomer of *BbsI*) from Fermentas/Thermo Scientific were used.

### 2.2.11 Site-directed mutagenesis

The generation of the amino acid exchange variants were performed by an optimized method for site-directed mutagenesis described by Edelheit et al. (2009). The plasmid FST1 pet16b was used as templates for introduction of the individual mutations. Two parallel PCR reactions are performed using a degenerated single primer, resulting in two single stranded transcripts with complementary sequence. Both reactions are mixed, heated at 95 °C, and stepwise annealed to 37 °C to initiate new double strand formation. The third step consists of a *DpnI* digestion leading to the specific restriction of methylated plasmids initial used as templates (only the isolated template-plasmids isolated from *E. coli* are methylated, not the *in vitro* transcribed daughter-plasmids). The samples were incubated with 5 µl *DpnI* (10 U/µl) (Thermo Scientific) overnight at 37 °C for a complete restriction to remove non-mutated plasmids. Finally, 2 µl of the mutagenesis mix were used for transformation of electrocompetent cells. Introduction of the single mutations was confirmed by sequencing (Eurofins Genomics) of the generated plasmids. All sequences of mutagenesis primers used for this thesis are listed in Table 2-7. The amino acid exchanges E31A, F33R and F33D in the FST1 (*At5g28470*) candidate were chosen based on a publication by Jørgensen et al. (2015) about the highly conserved EXXEK-motif in the POT/PTR-subfamily.

**Table 2-7** Overview of primers used for site-directed mutagenesis. The mutated codon is marked bold and the exchanged base pairs are red indicated.

candidate	term	sequence
FST1 ( <i>At5g28470</i> )	E31Afw	5'-GTACATTATTGCAAAC <b>CG</b> CTCTTTTGAGAAGCTGG-3'
	E31Arw	5'-CCAGCTTCTCAAAGAC <b>CG</b> GTTTGCAATAATGTAC-3'
	F33Rfw	5'-GCAAACGAGTCT <b>CG</b> TGAGAAGCTGGCCTC-3'
	F33Rrw	5'-GAGGCCAGCTTCTCA <b>CG</b> AGACTCGTTTGC-3'
	F33Dfw	5'-GCAAACGAGTCT <b>GAT</b> GAGAAGCTGGCCTC-3'
	F33Drw	5'-GAGGCCAGCTTCTCA <b>ATC</b> AGACTCGTTTGC-3'

### 2.2.12 Sequencing and *in silico* analysis

The sequence identity of all cloned DNA-fragments used for conventional cloning and Golden Gate cloning in level -1 or level 0 were confirmed by sequencing. The sequencing was performed by Eurofins Genomics (Ebersberg, Germany). The sequencing results were evaluated with the Vector NTI Advance® 11.5.2 program (Invitrogen, part of life technologies). Sequence database query and analysis were performed with the BLAST search program using the GenBank webpage (<http://www.ncbi.nlm.nih.gov/BLAST/>) (Altschul et al., 1997) and The Arabidopsis information resource (TAIR) webpage (<https://www.arabidopsis.org/>). The schematic overview of the T-DNA insertion lines *fst1* (SALK\_027288C) and the 'knockabout'-line (SALK\_113184C) was drawn with the Exon-Intron Graphic Maker (<http://wormweb.org/exonintron>). Identification of specific plant *cis*-acting elements inside the putative promotor sequences was performed with the New PLACE program (<https://www.dna.affrc.go.jp/PLACE/?action=newplace>) (Higo et al., 1999). Phylogenetic analysis and sequence alignments of a series of protein sequences were performed by using MegAlign (DNA Star, Madison, Wisconsin, USA). For the dendrogram a bootstrap analysis was performed with 1000

replicates. Orthologous proteins of FST1 in maize and various Solanaceae species were also searched in the Maize Genetics and Genomics Database (<https://maizegdb.org/>) and the Sol Genomics Network database (<https://solgenomics.net/>).

The co-expression analysis between putative transporter candidates and the UGT79B6 (*At5g54010*) and other annotated pollen and anther-specific genes was performed with the Genevestigator software (<https://genevestigator.com/gv/>) (Zimmermann et al., 2004) using the standard parameters. Transporter candidates were also analysed by the ARAMENNON plant membrane protein database from the University of Cologne (<http://aramemnon.uni-koeln.de/>) (Schwacke et al., 2003) and the ATTED-II co-expression database (<http://atted.jp/>) (Obayashi et al., 2018). For *in silico* prediction of the subcellular localization of the target proteins UGT79B6 and FST1 the SUBA (<http://suba.live/>) (Hooper et al., 2017) was used.

### 2.2.13 Transformation of electrocompetent cells

For electroporation, an aliquot of 50  $\mu$ l electrocompetent cells were thawed on ice for 5 min and mixed with 2  $\mu$ l ligation mix. Then the transformation mix was transferred into a pre-cooled electroporation cuvette (Eurogentec, Seraing, Belgium). A current pulse was carried out with the Micropulser<sup>®</sup> (Bio-Rad, Munich, Germany) at the parameters Ec2 (2.5 kV; 1 current pulse; < 1 ms). Next, 300  $\mu$ l SOC media were added, and the sample was incubated at 37 °C for at least 45 min, at 900 rpm in a thermomixer (Eppendorf, Wesseling-Berzdorf, Germany). A volume of 50  $\mu$ l to 150  $\mu$ l was plated on LB agar plates prepared with the corresponding antibiotic and incubated overnight at 37 °C. Positive colonies were identified by colony PCR and restriction analysis of the isolated plasmid DNA.

Transformation of the agrobacteria used for the generation of transgenic *Arabidopsis* plants and transient protein expression in *N. benthamiana* leaves was performed using a slightly different protocol. Golden Gate level constructs were transformed into agrobacteria strain GV3101 cells by electroporation using the current pulse parameter Ar2 (2.2 kV; 1 current pulse; 2.5 ms). Subsequently, 1 ml LB media was added and the cells were incubated for 4 h, at 900 rpm, at 28 °C in a thermomixer. Then the sample was shortly centrifuged at 500 g, 1 min, at room temperature and 900  $\mu$ l of the supernatant were removed. The cell pellet was resuspended in the residual 100  $\mu$ l and completely plated on a LB agar plate containing the corresponding antibiotic and rifampicin (50  $\mu$ g/ml). The plates were incubated over two days at 28 °C.

### 2.2.14 Generation of transgenic *Arabidopsis* lines

Stable transgenic *Arabidopsis thaliana* lines were generated by a slightly modified protocol based on the floral dip method described by Clough and Bent (1998).

The binary Golden Gate level 2 vectors pAGV931, pAGV931, and pAGV1043 were transformed into the Agrobacterium strain GV3101. A volume of 200 ml LB medium containing kanamycin (final conc. 50  $\mu$ g ml<sup>-1</sup>) and rifampicin (final conc. 50  $\mu$ g ml<sup>-1</sup>) was inoculated by 4 ml start culture of the appropriate strain and grown about 24 hours at 28 °C. The cultures were harvested by centrifugation by 5,000 g, at room temperature, for 10 min. Afterwards the cell pellets were resuspended with transformation buffer containing 5% (w/v) sucrose and 0.05% (v/v) Silwet L-77 (GE Advanced Materials



Silicons). In parallel the OD<sub>600</sub> of the bacterial cell suspensions were spectrophotometric measured and adjusted to 0.8. Eventually, about three weeks old *Arabidopsis* plants which started blossom were carefully dipped into the bacterial solution. To prevent unintentional spreading inside the greenhouse the plants were completely covered with a plastic bag and the work area was disinfected. The plants were shaded overnight in a box and bound on the next day. For the complementation approach the constructs pAGV931 and pAGV1043 were transformed into the *fst1* T-DNA-insertion line (SALK\_027288C). The binary vectors pAGV72 and pAGV891 were transformed into the *Arabidopsis thaliana* (Col-0) wild-type background for the promotor activity localization studies. Plants of the T<sub>1</sub>-generation were screened by BASTA selection. Additionally, the transcription of the FST1 complementation construct pAGV931 was verified by RT-PCR using cDNA of young buds from individual T1 plants (Appendix, Figure 8-6).

## 2.3 Microscopic methods

### 2.3.1 Subcellular localization

The subcellular localization of the UGT79B6 (*At5g54010*) was examined in mesophyll protoplasts of *Nicotiana benthamiana* using the Golden Gate level 1 constructs pAGV561 and pAGV581 encoding UGT79B6 fused to a C-terminal and N-terminal GFP reporter protein, respectively.

To clarify the subcellular localization of the FST1 (*At5g28470*) the transporter protein was transiently expressed in *N. benthamiana* leaves using the pAGV993 construct. The binary vector contains the full-length genomic *FST1* sequence without stop codon C-terminal fused to a GFP reporter gene. Thereby, the localization in leaves was chosen to observe the movement of the plasmalemma during plasmolysis.

In the subcellular localization studies the construct pAGM14122 encoding free GFP was used as a positive control. Further, the plasmamembran marker CD1007 and the mCherry marker CD959 for the endoplasmic reticulum (ER) were used for co-localization studies. Both mCherry tagged markers are from the multi-coloured *in vivo* organelle marker set from Nelson et al. (2007) and courtesy of Prof. Dr. Bettina Hause (IPB, Halle).

### 2.3.2 Transient expression in *N. benthamiana* leaves

Four-week-old, well developed *N. benthamiana* plants were chosen for transient expression of the subcellular localization constructs. Three well expanded, young leaves were selected for infiltration. The residual leaves were removed from the plants. For *Agrobacterium* mediated transformation an infiltration mixture was freshly prepared as follows: First 4 ml TB medium cultures of *Agrobacterium* strain GV3101 containing the referred constructs were grown overnight at 28 °C. On the next day the cultures were adjusted to an OD<sub>600</sub> of 0.2 with dissolving buffer containing 10 mM MES (pH 5.5) and 10 mM MgSO<sub>4</sub> in a volume of 2 ml for infiltration. The *Agrobacterium* infiltration mixture was then gently infiltrated into the leaf bottom side using a syringe. Three days after infiltration the infiltrated spots were outrivaled using a cork borer. Then the leaf discs were infiltrated with water using a big syringe. Epidermal leaf cells were studied under a confocal laser scanning microscope (LSM780, Zeiss, Jena, Germany). The fluorescence of GFP and chlorophyll A was excited at 488 nm using an argon laser.

The fluorescence of the mCherry tagged organelle markers were excited at 561 nm. Fluorescence signals were recorded at 497 nm to 551 nm for GFP, 589 nm to 650 nm for mCherry and 652 nm to 717 nm for chlorophyll A autofluorescence. Images obtained from the three spectral settings were overlaid.

In case of the plasmolysis assays the infiltrated leaf discs were shortly transferred into saline solutions (2 M to 5 M NaCl). The characteristic movement of the plasmalemma and the formation of the 'Hechtian strands' in the hypertonic medium was observed and visualized by recording a time series with an image rate of 1 image 50 s<sup>-1</sup> over 16 min.

Besides the subcellular localization studies the transient expression in *N. benthamiana* leaves was also used for expression analysis of the target proteins UGT79B6 and FST1 by immunoblot analysis (Appendix, Figure 8-7).

Additionally, the subcellular localization of the FST1 candidate was also studied in young anthers (3.4.6). Inflorescences of different stages from transgenic pAGV1043 complementation lines expressing a C-terminal GFP tagged FST1 transporter protein were collected. Anthers were isolated and the GFP signal was as well observed by confocal laser scanning microscopy (LSM700, Zeiss, Jena) using spectral settings for GFP (excitation: 488 nm; emission 520 nm). For an improved visualization of the anther cells the autofluorescence of chlorophyll A was also imaged.

### 2.3.3 Isolation of protoplasts

Mesophyll protoplasts were isolated from four-week-old *N. benthamiana* plants. Small but well-expanded young leaves from the shoot tip were chosen for the isolation. The margin and the midnerve of the freshly harvested leaves were carefully removed with a fresh razor blade and they were cut into small 0.5 mm – 4 mm strips. An enzyme solution used for vacuum infiltration was prepared as follows: 1.5% (w/v) cellulase R-10 (Yakult Pharmaceutical, Tokyo, Japan), 0.4% (w/v) macerozyme® R-10 (Yakult Pharmaceutical, Tokyo, Japan), 400 mM mannitol, 20 mM MES (pH 5.7), 20 mM KCl were warmed up in a water bath at 55 °C for 5 min. The enzyme solution was cooled to room temperature before 10 mM CaCl<sub>2</sub> and 0.1% (w/v) bovine serum albumin (BSA) were added. Then the enzyme solution was filtered with filter paper (80 g m<sup>2</sup>, Grade 6, Sartorius, Göttingen, Germany). The leaf pieces were put in a small petri dish and completely submerged in the enzyme mixture and vacuum infiltrated for 30 min using a vacuum exsiccator and a water jet pump. Subsequently, the preparation was incubated for 4 hours at 21 °C in the dark. During incubation, the plant tissue is decomposed to single cells by the cellulose, pectinase, and hemicellulase activity in the enzyme mixture. After digestion, the mesophyll protoplasts were released from the leaf tissue by gently agitating at 150 rpm for 30 min in the dark. The suspension was filtrated through a 100 µm nylon mesh to remove undigested tissue debris and collected in a sterile Cellstar® 12 ml cell culture tube (Greiner Bio-One, Monroe, North Carolina, USA). The flow-through was centrifuged at 200 g at 4 °C for 1 min and the supernatant was carefully removed. The pelleted protoplasts were gently resuspended in 2 ml W5-solution containing 2 mM MES (pH 5.7), 154 mM NaCl, 125 mM CaCl<sub>2</sub> and 5 mM KCl. Since the digested cell wall protoplasts are very sensitive towards mechanical stress, samples were just agitated gently and the protoplasts were just

pipetted with cut pipet tips. Then the protoplast samples were shaded and incubated on ice for 40 min. At this step the quality of the isolated protoplasts were checked under a light microscope and their concentration was determined using a Fuchs-Rosenthal counting chamber. In parallel the protoplasts were pelleted by gravity and the pellet was washed a second time with 2 ml W5-solution. Again, the supernatant was removed, and the protoplast concentration was adjusted with MMG-solution to  $0.1$  to  $0.35 \times 10^5$  cells  $\text{ml}^{-1}$ . The MMG-solution consisted of 4 mM MES (pH 5.7), 400 mM mannitol, 15 mM  $\text{MgCl}_2$ . The protoplast suspension was kept shaded and on ice.

#### 2.3.4 Transformation of protoplasts

After fresh preparation of the protoplasts a modified PEG-mediated transformation protocol (Yoo et al., 2007) was used. The method uses a PEG-solution which should be freshly prepared at least 1 hour before transfection. It contains 200 mM mannitol, 100 mM  $\text{CaCl}_2$  and 40% (w/v) PEG4000. The PEG-solution is heated at 55 °C for 10 min in a water bath and then stored at room temperature.

Plasmid DNA for protoplast transformation was prepared by Plasmid Midi preparation for higher yields as described before (2.2.2.). For each sample 10  $\mu\text{g}$  plasmid DNA of each construct were put on the bottom of a new culture tube. A ratio of 5  $\mu\text{g}$  to 10  $\mu\text{g}$  of each plasmid DNA per  $1 \times 10^4$  protoplasts is considered as optimal for transformation. Then 200  $\mu\text{l}$  of the protoplast solution were added to the DNA and carefully shaken. Afterwards 220  $\mu\text{l}$  of the PEG-solution was added. Then the sample was gently mixed and incubated for 5 min before 880  $\mu\text{l}$  W5-solution were added. The samples were centrifuged at 200 g for 1 min at 4 °C. Then a critical step followed where the PEG containing supernatant was completely removed. The protoplast pellets were resuspended in 200  $\mu\text{l}$  W1-solution containing 4 mM MES (pH 5.7), 500 mM mannitol and 20 mM KCl. The protoplast samples were incubated at room temperature in a nearly horizontal position overnight in the dark. On the next morning, the transformed protoplasts were examined under a confocal laser scanning microscope (LSM780, Zeiss, Jena, Germany) using similar settings as described above (2.3.2). First signals can be detected after about 7 hours in case of free GFP or mCherry by fluorescence microscopy.

#### 2.3.5 Promotor-GFP localization

For examination of the tissue-specific promoter activity the GFP reporter gene was driven under the control of a putative 2245 bp *FST1* promoter encoded in the pAGV891 level 2 construct. Previously, the putative *FST1* promoter sequence was *in silico* analysed for the presence of anther and pollen-specific *cis*-acting elements using the New PLACE program (Higo et al., 1999) (<https://www.dna.affrc.go.jp/PLACE/?action=newplace>).

The binary vector was introduced into *A. thaliana* wild-type plants by Agrobacterium mediated transformation as described before (2.2.14). Young anthers from five independent transgenic lines of the T<sub>1</sub> generation were collected using fine forceps and transferred into a confocal dish and submerged into water. The tissue-specific expression of the GFP signal was observed by confocal laser scanning microscopy using a LSM780 (Zeiss, Jena, Germany). The microscope settings were as follows: excitation by an argon diode laser at 488 nm, recording of the emission at 497 nm to 542 nm for the GFP signal and at 651 nm to 717 nm for the autofluorescence of chlorophyll A. Images obtained with the two

spectral settings were overlaid together with the transmission image to distinct the individual tissue structures.

### 2.3.6 Immunolabelling of anther cross-sections

Besides the *FST1* promotor activity, the tapetum-specific expression of the *UGT79B6*, *TSM1*, and *SHT* promotor was also analysed for comparison. Transgenic lines were previously generated (Grunewald and Vogt, unpublished data). The GFP signal of the examined anthers from the T<sub>1</sub> generation was strong. Hence, it was decided to perform immunolocalization of anther cross-sections for a clear visualisation of the tapetum located *UGT79B6* promotor activity (Figure 3-3).

Young inflorescences were gently dissected from individual transgenic pAGV72 plants and fixed in 1x PBS buffer containing 4% (v/v) paraformaldehyde, 0.1% Triton X-100. The PBS buffer is prepared as 4 x stock solution as follows: 0.8 g l<sup>-1</sup> KCl; 0.8 g l<sup>-1</sup> KH<sub>2</sub>PO<sub>4</sub>; 5 g l<sup>-1</sup> Na<sub>2</sub>HPO<sub>4</sub>; 32 g NaCl. The freshly collected inflorescences were submerged into the fixation-PBS solution and vacuum infiltrated for 2 hours using a vacuum desiccator. Afterwards the samples were washed three times for 10 min with 1x PBS buffer. During all washing and incubation steps, tissue preparations were slowly rotated for complete infiltration using a rotator (Agarscientific, Stansted, UK). Then the samples were dehydrated using an ethanol series: 10% (v/v) ethanol for 30 min, 30%, and 50% (v/v) ethanol for 1 hour, 70% (v/v) over night at 4 °C. On the next day the ethanol series was continued with 90% (v/v) ethanol, 96% (v/v) ethanol for 1 hour at room temperature. Finally, the samples were incubated in absolute ethanol for 30 min at 55 °C. Polyethylene glycol (PEG1500) was carefully melted in a microwave and warmed at about 80 °C on a stirring hot plate. Subsequently, the samples were stepwise infiltrated by an increasing PEG gradient. The samples were incubated for 1 hour at 50 °C in a PEG1500: ethanol mixture in a ratio of 1:3, 1:1, and 3:1. Twice the samples were transferred into pure PEG1500 and incubated for 1 hour at 50 °C. Finally, the inflorescences were bubble-free imbedded into warm (not hot!) PEG1500 using an embedding mould.

Section series of 1 to 2 µm cutting thickness were prepared using a rotary microtome. Then the sections were transferred with a 45% (v/v) PEG6000 solution on Poly-Lysine coated object slides. The samples were incubated in 1x PBS buffer for 10 min to dissolve the PEG. Next, free aldehyde groups were blocked with 1x PBS including 0.1 M NH<sub>4</sub>Cl for 5 min. The samples were washed in 1x PBS buffer for 10 min followed by incubation for 30 min in 1x PBS buffer containing 5% (w/v) BSA to avoid unspecific antibody binding. The preparations were incubated with the first antibody (AS184175, mouse, Agrisera, Vännäs, Sweden) over night at 4 °C. Thereby, the first antibody is specific against GFP and was diluted 1:100 with 1x PBS buffer containing 5% (w/v) BSA. After 12 hours the samples are washed three times for 10 min with 1x PBS buffer containing 0.1% (w/v) BSA and once with 1x PBS buffer including 1% (w/v) BSA for 10 min. Afterwards the samples were incubated in a humid chamber with the second AlexaFluor® 488 labelled antibody (goat, Invitrogen) specific against rabbit IgG (1:500 diluted) in the dark for 1 hour at 37 °C. After incubation, the samples were washed four times with 1x PBS buffer for 10 min. For staining of cell nuclei the samples were incubated in 1x PBS containing 1 µg ml<sup>-1</sup> 4', 6-diamidino-2-phenylindole (DAPI) for 15 min. The preparations were washed twice using 1x PBS buffer for 10 min. Finally, the samples were embedded with Citifluor™ AF1 Glycerol/PBS anti-

fading reagent and air bubble-free covered. The cover glass was fixed with nail polish. For fluorescence microscopy the samples DAPI was excited by 365 nm and emission was detected at 420 nm. Alexa Fluor 488 was excited by 490 nm and emission was detected at 520 nm.

### 2.3.7 Transmission electron microscopy (TEM)

Freshly isolated anthers for electron microscopy were fixed with 3% (v/v) glutaraldehyde (Sigma) in 0.1 M sodium cacodylate buffer (SCB) (pH 7.2) for 4 hours. Samples were washed in SCB, postfixed for 1 hour with 1% (w/v) osmiumtetroxide (Carl Roth) solved in SCB and stepwise dehydrated by an ethanol series. The preparations were embedded in epoxy resin according to Spurr (1969). Subsequently, ultrathin sections (80 nm) were observed with an EM 900 (Carl Zeiss Microscopy, Jena, Germany) transmission electron microscope (acceleration voltage 80 kV). Images of the electron micrographs were recorded with a slow scan camera (Variospeed SSCCD camera SM-1k-120, TRS, Moorenweis, Germany). Additionally, the material fixed and embedded for transmission electron microscopy was also used for light microscopy. Semithin sections (1  $\mu\text{m}$ ) were made with an ultramicrotome S (Leica, Wetzlar, Germany) and stained with 1% (w/v) toluidine blue. Images were taken with an Axioskop 20 light microscope (Carl Zeiss Microscopy, Jena, Germany) equipped with an AxioCam MRC camera. The preparation for the histological and ultrastructural investigations and the electron microscopy were performed in cooperation by Simone Frass and Dr. Gerd Hause (Biozentrum, MLU, Halle).

## 2.4 Protein biochemical methods

### 2.4.1 Protein concentration determination

Protein concentration was photometrically measured with Coomassie Brilliant Blue-G250 (Serva, Heidelberg, Germany) at 595 nm (Bradford, 1976). For the determination of the protein concentration a volume of 10  $\mu\text{l}$  sample were incubated for 5 min at room temperature with 990  $\mu\text{l}$  Bradford solution prepared as follows: 0.065% (w/v) Coomassie G-250 solved in 5% (v/v) methanol and 10% (v/v) phosphoric acid. The extinction of the samples was measured according to a blank at 595 nm using a spectral photometer (DU<sup>®</sup>530 UV/VIS, Beckman Coulter, Krefeld, Germany). The protein concentration was calculated based on bovine serum albumin (BSA) as a reference. Protein concentration of partially purified enzymes with known amino acid sequence was further determined based on calculated extinction coefficients at 280 nm calculated by the ExPasy ProtParam tool (<https://web.expasy.org/prot-param/>).

### 2.4.2 SDS-PAGE

For the electrophoretic separation of proteins, the discontinuous, denatured sodium dodecyl sulfate–polyacrylamide gel electrophoresis (SDS-PAGE) was used (Laemmli, 1970). The preparation of the gels is shown in Table 2-8. Separation gels with 14% (v/v) acrylamide concentration were used for protein analysis. Protein samples were mixed with 10  $\mu\text{l}$  protein sample loading buffer (62.5 mM Tris-HCl, (pH 6.8); 10% (v/v) glycerol; 2% (w/v) SDS; 0.05% (v/v) 2-mercaptoethanol; 0.025% (w/v) bromophenol blue) and denatured at 65 °C for 10 min. The electrophoresis was performed by constant 25 mA per gel. The 1x electrophoresis buffer was diluted from a 10x stock buffer containing: 30 g l<sup>-1</sup> Tris-HCl; 144 g l<sup>-1</sup> glycine; 10 g l<sup>-1</sup> SDS. After electrophoresis the gels were either stained with Coomassie

blue or blotted for immunoblotting analysis. For Coomassie Blue staining, a solution was prepared as follows: 200 mg SERVA Blue G, 40 ml acetic acid, 200 ml ethanol, and 40 ml water. As destaining solution 10% (v/v) acetic acid were used. The prestained pEqGOLD protein marker V (VWR, Vienna, Austria) was used to determine the individual molecular protein size.

**Table 2-8** Preparation of polyacrylamide gels.

solution	stacking gel	separation gel
1.5 M Tris-HCl (pH 8.8)	-	2.5 ml
0.5 M Tris-HCl (pH 6.8)	1.2 ml	-
Acrylamide/Bisacrylamide (37.5:1)	0.8 ml	4.7 ml
bidest. Water	3.0 ml	2.8 ml
TEMED	7.5 $\mu$ l	7.5 $\mu$ l
10% (w/v) APS	37.5 $\mu$ l	75 $\mu$ l
0.05% (v/v) bromophenol blue	150 $\mu$ l	-

### 2.4.3 Immunoblot analysis

For immunoblot analysis the electrophoretic separated proteins were transferred ('blotted') from the gel to a polyvinylidene difluoride (PVDF) membrane using a wet blot technique. For this, the Mini Transfer-Blot® Electrophoretic Transfer Cell (Bio-Rad) was used according to the manufacturers instructions. For blotting the following solutions were prepared: transfer buffer (25 mM Tris; 192 mM glycine (pH 8.3); 20% (v/v) methanol), 10x PBS buffer (2 g l<sup>-1</sup> KCl; 2 g l<sup>-1</sup> KH<sub>2</sub>PO<sub>4</sub>; 11.5 g l<sup>-1</sup> Na<sub>2</sub>HPO<sub>4</sub>; 80 g l<sup>-1</sup> NaCl), PBST buffer (0.1% (v/v) tween dissolved in 1x PBS buffer), blocking solution (5% (w/v) non-fat dry milk solved in PBST buffer). Before blotting the membrane was soaked with methanol for 'activation', which increases the protein binding capacity of the PVDF membrane. The protein gel, the filter papers, the sponge, and the activated PVDF membrane were equilibrated for 10 min with transfer buffer. Then the membrane was gently put on the protein gel without air bubbles and the blotting electrophoresis chamber was assembled. The protein transfer was run for 1 hour 30 min at constant 30 V and 400 mA, respectively. After transfer the protein gel was stained with Coomassie Blue to control the blotting efficiency. The following incubations steps were performed while gently shaking. The membrane was blocked for 30 min with blocking solution at room temperature. The first antibody was directly added to the membrane (1: 10,000 dilution) and incubated in the cold room at 15 °C overnight. For the immuno detection of the His-tagged proteins only one monoclonal ant-His<sub>6</sub>-epitope-specific antibody conjugated to the horseradish peroxidase (HRP) (mouse, Roche Diagnostics, Mannheim, Germany) was required. On the next day, the membrane was washed with PBST buffer and 1x PBS buffer three times for 10 min at room temperature. Afterwards enhanced chemiluminescence (ECL) detection was performed using the ECL™ Primer Western Blotting Detection Reagents (RPN2232, GE Healthcare, Munich, Germany). Images of the analysed immunoblots were recorded and documented by the Fusion FX (Vilber Lourmat, Munich, Germany) provided with a CCD camera.

Expression of the GFP tagged UGT79B6 and FST1 used in the subcellular localization studies was also verified by immunoblot analysis. Infiltrated leaf spots from *N. benthamiana* leaves used for

transient expression of the Golden Gate constructs pAGV561 (UGT79B6-GFP), pAGV993 (FST1-GFP) and pAGM14112 (GFP control) were dissected, frozen in liquid nitrogen and grinded using a bead mill (CryoMill MM100, Retsch, Haan, Germany). The freshly grinded plant material was directly solved in denaturation buffer containing: 25 mM Tris-HCl (pH 8.0), 150 mM NaCl, 1% (v/v) IGEPAL® CA-630, 0.1% (v/v) Triton X-100, 0.1% (w/v) SDS, and 1% (v/v) Serva protease inhibitor mix P. The detergents provided in the buffer were especially required for effective denaturation of transmembrane and membrane associated proteins. Approaches to denature the target proteins just with protein sample buffer as recommended for soluble proteins failed. The samples were constantly vortexed for 15 min at room temperature. The protein concentration was determined by Bradford method. Samples containing 10 µg proteins were mixed with protein loading buffer (2.4.2) and heated at 95 °C for 10 min. The samples were further used for immunoblotting.

For the immunoblot detection of GFP tagged proteins a primary antibody specific against GFP (JL-8, mouse (IgG2a) Living Colors® A.v., Clontech) (working dilution of 1: 5,000) and an anti-mouse-specific HRP conjugated secondary antibody for ECL detection (L0315, goat (IgG-HRP (Cruz-Marker): sc-2031), Santa Cruz Biotechnology, Dallas, Texas, USA) (working dilution of 1: 5,000) were used.

#### 2.4.4 Heterologous expression and partially purification of glycosyltransferases

Enzymatic synthesis of the <sup>14</sup>C-labelled flavonol glycosides was performed by using the flavonol-specific glycosyltransferases UGT78D2 (*At5g17050*) and UGT79B6 (*At5g54010*) which were heterologously expressed in *E. coli*.

For functional protein expression the *E. coli* strains Rosetta (DE3) pLys transformed with the UGT79B6<sub>opt</sub> pETDuet-1 plasmid and M15 [rep4] transformed with the UGT78D2 pQE70 plasmid were used. To increase the UGT79B6 expression rates a codon optimized variant of the *At5g54010* coding sequence was expressed to overcome low bacterial expression level of the UGT79B6. Different expression conditions were optimized for the both glycosyltransferases. Thereby, it was recognized that lower expression temperatures and early induction reduce inclusion body formation and increase the soluble amount of the target proteins. Therefore, the cultivation temperature was constantly held at 25 °C (UGT79B6) and 30 °C (UGT78D2), respectively.

The expression strains were cultivated in 1.2 litre TB medium containing a final concentration of 50 µg ml<sup>-1</sup> ampicillin. Cultures were grown until the OD<sub>600</sub> reached 0.4. Protein expression was induced by addition of isopropyl-β-D-thiogalactopyranoside (IPTG) to the culture at a final concentration of 1 mM. The cultures were further cultivated for 16 hours by shaking at 230 rpm and constant temperature. Bacterial cells were harvested by centrifugation at 10,000 g and 4 °C for 15 min and stored at -80 °C. Cell pellets were suspended in KPi buffer containing 50 mM potassium phosphate (KPi) (pH 7.5) and 10% (v/v) glycerol and lysozyme (10 mg ml<sup>-1</sup>, Serva) in a 1: 1,000 ratio and 1 ml per 20 g pellet His-tag protease inhibitor cocktail (P8849, Sigma) were added and incubated on ice for 20 min. After lysozyme digestion the bacterial cells were disrupted by ultrasonication using a SONOPULS ultrasonic sonotrode HD2070 (Ti6A/4V) (Bandelin, Berlin, Germany). Disrupted cells were centrifuged at 12,000 g at 4 °C for 15 min. Afterwards nucleic acids inside the crude extract were removed by precipitation with 4% (w/v)

protamine sulphate solution in a 1: 30 ratio and twice centrifuged at 12,000 g at 4 °C for 15 min. The viscosity of the crude extract was reduced by this step. The clear supernatant containing the crude protein extract was loaded for purification on a 5 ml Protino® Ni-NTA Column (Marchery-Nagel, Dürren, Germany) using a peristaltic pump. The Ni-NTA column was equilibrated with KPi buffer. Two wash steps with each 25 ml were performed using KPi buffer containing 15 mM imidazole and 30 mM imidazole, respectively. The partially purified protein was eluted in 5 ml fractions with KPi buffer containing 240 mM imidazole. Sample protein concentrations of all fractions were measured using the Bradford method described above (2.4.1). Measured protein concentrations of the partially purified enzymes were 0.5 µg µl<sup>-1</sup> (UGT78D2) and 0.32 µg µl<sup>-1</sup> (UGT79B6). All fractions of the purification were monitored for proteins by SDS-PAGE and immunoblot analysis (Figure 3-1). All protein fractions were investigated for UGT activity by a standard UGT-assay using quercetin (UGT78D2) or quercetin-3-*O*-glucoside (UGT79B6) as substrate. Finally, the partially purified enzymes were desalted with a Sephadex G-25M PD-10 Column (GE Healthcare, UK) and used for preparative assays.

#### 2.4.5 Standard flavonol glycosyltransferase assays

Enzymatic activity of the recombinant UGTs was measured with a standard enzyme assay including flavonoid substrate (sugar acceptor, final conc. 20 µM), UDP-glucose (sugar donor, final conc. 1 mM), ascorbic acid (final conc. 200 µM), and KPi (pH 7.5) buffer. Working concentrations of flavonoid substrates were dissolved in 25% (v/v) dimethyl sulfoxide (DMSO). The enzyme assays were performed at 37 °C in 50 µl reaction volume. The reactions were stopped by protein precipitation with 10 µl 10% (v/v) trichloroacetic acid (TCA) solution. After removal of the precipitated protein by centrifugation (20,817 g, 4 °C, 5 min) the reaction products were analysed by reversed phase liquid chromatography on a Nucleoshell RP<sub>18</sub> column. The HPLC-gradient of the HPLC-programme MS\_Qshell\_QDA\_5cm\_12min\_79B6 standardly used for the analysis of the UGT assays is included in Appendix (Table 8-4).

#### 2.4.6 Preparation of <sup>14</sup>C-labelled flavonol glucosides

The recombinant glycosyltransferases were used for the radiolabelling of flavonol glucosides in preparative assays. The assays were scaled up to a reaction volume of 5 ml and prepared with 10 mM KPi buffer (pH 7.5) without glycerol and final concentrations of 200 µM ascorbic acid, 100 µM unlabelled UDP-glucose and a final concentration of 50 µM of the individual flavonol sugar acceptor quercetin (UGT78D2) or quercetin-3-*O*-glucoside and kaempferol-3-*O*-glucoside (in the case of UGT79B6), respectively. 92.5 kBq <sup>14</sup>C-labelled UDP-glucose (0.1 mCi ml<sup>-1</sup>, 300 mCi mmol<sup>-1</sup>, Hartmann Analytik) was added to the assay. The reactions were started by application of 270 µg (UGT79B6<sub>opt</sub>) and/or 400 µg (UGT78D2) partially purified proteins. Preparative reactions were run for 16 hours at 30 °C while gently shaking at 750 rpm using a thermomixer (Thermomixer Comfort, Eppendorf). An equivalent cold reaction was setup in parallel to monitor the product formation by HPLC-MS.

Purification of <sup>14</sup>C-labelled products was performed by solid phase extraction (SPE) using amphiphilic Oasis® HLB3cc columns (Waters, Eschborn, Germany). The matrix was activated with 3 ml methanol and equilibrated with 4 ml KPi buffer (50 mM, without glycerol; pH 7.5). The reactions were not terminated but directly loaded on the SPE column followed by three wash steps including twice 1



ml KPi buffer and once 500  $\mu$ l 20% (v/v) methanol. After that the column was eluted with 500  $\mu$ l methanol. Due to the dead volume of the column tip the first 100  $\mu$ l were discarded the flavonol glucosides eluted in the residual 400  $\mu$ l methanol. A wash step followed with 500  $\mu$ l methanol. To determine incorporation 1% sample volume of each fraction was dissolved in 4 ml scintillation cocktail (Ultima Gold MV, Perkin Elmer) and analysed by liquid scintillation counting where the radioactive  $\beta$ -decay was recorded for 1 min. The total and specific radioactivities of the purified  $^{14}\text{C}$ -labelled flavonol glycoside samples were calculated. Specific activities of the  $^{14}\text{C}$ -labelled quercetin- and kaempferol-3-*O*-sophoroside were 130 MBq/mmol and 190 MBq/mmol, respectively. UGT78D2 was used to produce  $^{14}\text{C}$ -labelled quercetin-3-*O*-glucoside with a specific activity of 71 MBq/mmol. As a control for non-radioactive approaches, the unlabelled reactions were processed in parallel and non-labelled fractions were monitored by HPLC-MS. The produced  $^{14}\text{C}$ -labelled flavonol glycoside standards were stable and stored at -20 °C. The radioactivity of all fractions was measured using the Hidex 300 SL scintillation counter (Hidex, Mainz, Germany).

#### 2.4.7 Transporter uptake assays with $^{14}\text{C}$ -labelled flavonol glucosides

For investigation of the transport activity of the FST1 candidate, radioactive uptake assays were performed. For this, the full-length FST1 (*At5g28470*) coding DNA sequence was expressed in *E. coli* Rosetta II (DE3) pLys cells using the FST1 pET16b plasmid.

50 ml YT medium supplemented with ampicillin (200  $\mu\text{g ml}^{-1}$ ) and chloramphenicol (25  $\mu\text{g ml}^{-1}$ ) was inoculated with 500  $\mu$ l pre-culture and cultivated under aerobic conditions at constant 37 °C. Bacterial cell cultures were grown until  $\text{OD}_{600}$  0.5, the cells were induced by adding 0.8 mM IPTG, and FST1 was heterologous expressed for one hour. Afterwards, a volume of 25 ml culture was pelleted by centrifugation at 5,000 g, 4 °C and 5 min. *E. coli* cells were directly suspended in potassium phosphate buffer (50 mM  $\text{KH}_2\text{PO}_4$ , pH 7.0). Thereby the  $\text{OD}_{600}$  was adjusted to 5. A second non-induced culture was grown and processed in parallel as non-induction control. For the preparation of the transport medium (TM) 128  $\mu$ l  $^{14}\text{C}$ -labelled substrate equivalent to 12.7 kBq were added into potassium phosphate buffer (pH 7.0) to a working concentration of 20  $\mu\text{M}$ .

Single reactions were started by adding 100  $\mu$ l cells to 100  $\mu$ l TM buffer, obtaining a final concentration of 10  $\mu\text{M}$  for the flavonol glycoside substrate in the uptake assays. Uptakes of the radioactive compounds were measured at several time points up to 30 min. The uptake assays were performed at 30 °C while gently shaking. Induced and non-induced cells were measured as replicates for each trial. To stop the transport samples were pipetted on a mixed cellulose ester (MCE) membrane filter (0.45  $\mu\text{m}$  pore, MCE045025BL, Hahnemühle, Dassel, Germany). External substrate was removed by vacuum filtration and the MCE filters were washed three times with 4 ml potassium phosphate buffer. Subsequently, the MCE filters were dissolved in scintillation cocktail. Accumulated radioactivity in the cell samples on the MCE filters was measured by liquid scintillation counting by a Beckman LSC6500. FST1 transporter studies were performed in cooperation with Dr. Ilka Haferkamp (TU Kaiserslautern).

## 2.5 Analytical methods

### 2.5.1 Harvesting of pollen material from *Arabidopsis*

The collection of high amounts of mature pollen grains from *Arabidopsis* was performed by the vacuum-cleaner method as published by Johnson-Brousseau and McCormick, 2004. The pollen material was harvested from open flowers of five to six weeks old plants in the greenhouse. Two nylon meshes with a pore size of 40  $\mu\text{m}$  and 11  $\mu\text{m}$  (Neolab, Heidelberg, Germany) were used. Highly purified pollen grains were obtained on the 11  $\mu\text{m}$  nylon filter (Figure 3-19). Pollen material were either used directly for pollen germination assays or stored at  $-80\text{ }^{\circ}\text{C}$  for analytical purposes.

### 2.5.2 Preparation of pollen and anther extracts

Pollen material from wild-type and transgenic plants were harvested by the vacuum-cleaner method (Johnson-Brousseau and McCormick, 2004). Freshly collected pollen from five to six weeks old *Arabidopsis* plants was degreased with hexane in a ratio of 10 mg pollen to 500  $\mu\text{l}$  hexane. The suspension was centrifuged at  $4\text{ }^{\circ}\text{C}$ , 15 min, 20,817 g. The hexane supernatant was removed from the pollen pellet and further used for gas chromatography-mass spectrometry (GC-MS) analysis. After the hexane wash the pollen material was completely dried at  $30\text{ }^{\circ}\text{C}$  for 15 min to evaporate the remaining solvent and resuspended in 90% (v/v) methanol with a ratio of 10 mg pollen to 200  $\mu\text{l}$  90% (v/v) methanol. The samples were incubated in a sonication bath (Transsonic 460 Elma, Germany) for 15 min at 35 kHz. Subsequently, the samples were centrifuged to separate the residual pollen material from the extract for 15 min at 20,817 g and  $4\text{ }^{\circ}\text{C}$ . Afterwards the methanolic extracts were analysed by high performance liquid chromatography-mass spectroscopy (HPLC-MS) and high performance thin layer chromatography (HPTLC) analysis.

For the analysis of the phenylpropanoid pattern from *Arabidopsis* wild-type and *fst1* deficient anthers at least 200 intact anthers were collected of each line by dissection from the inflorescence under a stereomicroscope (Stemi DV4, Zeiss). Anthers were directly suspended in 90% (v/v) methanol in a ratio of 1  $\mu\text{l}$  per anther and solubilized for 15 min at 35 kHz by ultrasonication. Then, samples were centrifuged for 15 min at 20,817 g and  $4\text{ }^{\circ}\text{C}$ . The supernatant was further analysed by HPLC-MS using the programme MS\_5cm\_QDA\_Transp354\_14min (Appendix Table 8-4).

### 2.5.3 High performance thin-layer chromatography

For HPTLC analysis 20  $\mu\text{l}$  of the methanolic pollen extracts from wild-type and T-DNA insertion lines were loaded on a precoated silica NanoAdamant UV254 thin-layer chromatography plate (Macherey-Nagel) (stationary phase) with a 20 cm x 10 cm size. The TLC-plates were prewashed with 100% methanol and dried overnight before use. For comparison 10  $\mu\text{l}$  of the standards quercetin-3-*O*-glucoside (0.5 M) and quercetin-3-*O*-sophoroside (0.5 M) were spotted on the TLC-plate. A solvent system of ethylacetate, formic acid, acetic acid, and water was used as mobile phase in a volume ratio of 100: 11: 11: 27 in a closed glass tank. Separated compounds were detected first under UV light at 254 nm and 366 nm before derivatization. The derivatization of the phenylpropanoid pattern was performed by staining with 1% (w/v) 2-aminoethyl diphenylborate (DPBA) solved in 100% methanol and dried. The pattern of the fluorescent compounds was detected at 366 nm with the CAMAG TLC visualizer

system (CAMAG, Berlin, Germany) and documented with the winCats-Planar Chromatography Manager (CAMAG).

#### 2.5.4 High performance liquid chromatography

The phenylpropanoid profiles of methanolic extracts from degreased pollen and anthers of *Arabidopsis* wild-type and transgenic lines were analysed by HPLC-MS. The pollen extracts were diluted 1:5 in 90% (v/v) methanol and analysed at a flow rate of 0.6 ml min<sup>-1</sup> using a 5 cm RP<sub>18</sub> Nucleoshell column (Macherey-Nagel) and a Waters e2695 separation module (Eschborn, Germany). As mobile phase the solvents 0.1% (v/v) formic acid (solvent A) and acetonitrile (solvent B) were used. The UV-absorbance of the analysed compounds were detected by the Waters 2998 PDA detector at 354 nm and simultaneously, between 220 nm to 550 nm. The injected sample volume was 10 µl. Eluted compounds were also detected by an Acquity QDA Detector (Waters) in a range from m/z 150 Da to 800 Da using the negative scan mode and 15 V cone voltage for ionization. HPLC-analysis of the methanolic anther extracts was performed by using a 25 cm Nucleosil 100-5 8C column (Macherey-Nagel). Identification of individual compounds was based on their characteristic UV-absorbance, m/z ratio, retention time, and available standards: quercetin-3-*O*-glucoside, kaempferol-3-*O*-glucoside, rutin, quercetin- and kaempferol-3-*O*-sophoroside (produced from quercetin-3-*O*-glucoside by UGT79B6). UGT activity assays and substrate preparations were examined using similar parameters. HPLC-programmes and solvent gradients are listed (Appendix, Table 8-4). The solvent gradient of the programme MS\_5cm\_QDA\_Transp354\_14min for the analysis of the pollen extracts was also used to determine the flavonol glycoside standard curve (Appendix, Figure 8-8).

#### 2.5.5 Gas chromatography-mass spectrometry

Lipophilic pollen surface metabolites in hexane extract of washed pollen material was analysed by gas chromatography-mass spectrometry (GC-MS) by Dr. Thomas Vogt (IPB) (Appendix, Figure 8-9). 1 µl of the hexane pollen surface extracts was injected and analysed by a Trace GC Ultra gas chromatograph (Thermo Scientific) connected to an ATAS Optic 3 injector and an ISQ single quadrupole mass spectrometer (Thermo Scientific). The chromatographic separation of the pollen surface extracts was performed on a ZB-5ms capillary column (30 m x 0.32 mm, Phenomenex, Aschaffenburg, Germany) using splitless injection. An injection volume of 1µl was used. The injection temperature gradient increased from 60 °C to 250 °C within 10 °C s<sup>-1</sup> and the flow rate of helium was 1 ml min<sup>-1</sup>. The gradient of the GC oven temperature was as follows: 50 °C for 1 min, 50 °C to 300 °C with 7 °C min<sup>-1</sup>, 300 °C to 330 °C with 20 °C min<sup>-1</sup> and 330 °C for 5 min. Mass spectrometry was performed at 70 eV, in a full scan mode from 50 to 450 m/z. The Xcalibur software (Thermo Scientific) was used to analyse the data based on a NIST (National Institute of Standards and Technology, Gaithersburg, Maryland, USA) database for identification.

## 2.6 Biological assays

### 2.6.1 Pollen viability assay

The pollen viability rate was assayed using the fluorescein diacetate (FDA) staining method developed by Heslop-Harrison and Heslop-Harrison (1970). The FDA was dissolved in acetone as stock

solution at 5 mg ml<sup>-1</sup> and stored at -20 °C. Pollen grains were dissected from anthers of five to six weeks old Arabidopsis plants and directly suspended in a staining solution containing 10% sucrose and 0.1 mg ml. The pollen grains were examined under a Nikon AZ100 microscope (Zeiss, Jena, Germany). The total number of pollen was counted in the bright field and the living pollen grains stained by FDA, were counted separately. The green fluorescence of the fluorescein was excited at 490 nm and detected at 520 nm. The pollen viability rate was determined in three independent trials. For each experiment at least 600 pollen grains were counted. The number of living pollen is shown as percentage of the total number of pollen.

### 2.6.2 *In vitro* pollen germination assay

Pollen material freshly harvested from five to six weeks old Arabidopsis plants by the vacuum cleaner method (Johnson-Brousseau and McCormick, 2004) was used to determine the pollen germination rate. The germination medium was prepared according to Li et al. (1999) containing 18% sucrose, 0.01% boric acid, 1mM MgSO<sub>4</sub>, 1mM CaCl<sub>2</sub>, 1 mM Ca(NO<sub>3</sub>)<sub>2</sub> and 0.8% low melt agar (Roth), pH 7.0. After carefully heating the medium, the agar was slowly cooled down and the collected pollen was dispensed in the agar medium on an object slide and incubated for 6 hours in the dark in a humid chamber at room temperature. The total number of mature pollen grains and of germinating pollen was counted under a microscope (Axio Imager.Z2, Zeiss); at least 300 pollen grains were counted for each sample per trial. Additionally, the length of 30 pollen tubes was measured for wild-type and *fst1* line to determine the average tube length using the ZEN 2.5 (blue edition) imaging software (Zeiss, Jena, Germany).

To examine the susceptibility of wild-type, *fst1*, and *78d2 x sht* pollen to UV-irradiation, freshly harvested pollen from 5-week-old Arabidopsis plants grown under identical greenhouse conditions was used. Directly after harvesting the pollen was exposed for zero, one or two hours to strong UV-irradiation provided by a Philips Xenon HPR400 lamp at a distance of 60 cm. The light intensity at this position was measured by a Yeti Specbos 1211UV (JETI, Jena, Germany) with a total intensity between 315 nm and 780 nm of 532 μmol m<sup>-2</sup> s<sup>-1</sup>, and between 315 nm and 340 nm with 17.8 μmol m<sup>-2</sup> s<sup>-1</sup>. At least 200 pollen grains were counted from each pool of wild-type, *fst1*, and *78d2 x sht* pollen. At least four replicates were analysed each.

### 3 Results

#### 3.1 The flavonoid glycosyltransferases UGT78D2 and UGT79B6

The availability of suitable substrates for the complete functional characterization of transporter activity and substrate specificity is a general limitation in transporter studies (Larsen et al., 2017). In case of the studied flavonol glycoside transporter activity the production of  $^{14}\text{C}$ -labelled flavonol-3-*O*-glycosides was essential for the subsequent work and synthesis of transporter substrates, which were not commercially available. Radioactive labelling was chosen because of its high sensitivity and its workability using  $^{14}\text{C}$ -labelled UDP-glucose in the UGT catalysed reaction. At this point the glycosyltransferases UGT78D2 (*At5g17050*) and UGT79B6 (*At5g54010*) were of high value for this project. Both enzymes were recently characterized (Lim et al., 2004; Yonekura-Sakakibara et al., 2014).

The UGT78D2 and the UGT79B6 were heterologously expressed in *E. coli* with a His-tag at the C- or N-terminus, respectively. In the case of the poorly expressed UGT79B6 the expression could be optimized using a codon optimized variant adapted to the *E. coli* codon usage (Appendix Figure 8-4). Expression rates of both proteins were optimized by growth at low temperatures to avoid the formation of inclusion bodies (see 2.4.4). To confirm the purification, representative fractions of the metal-affinity chromatography purification were analysed by SDS-PAGE (Figure 3-1).

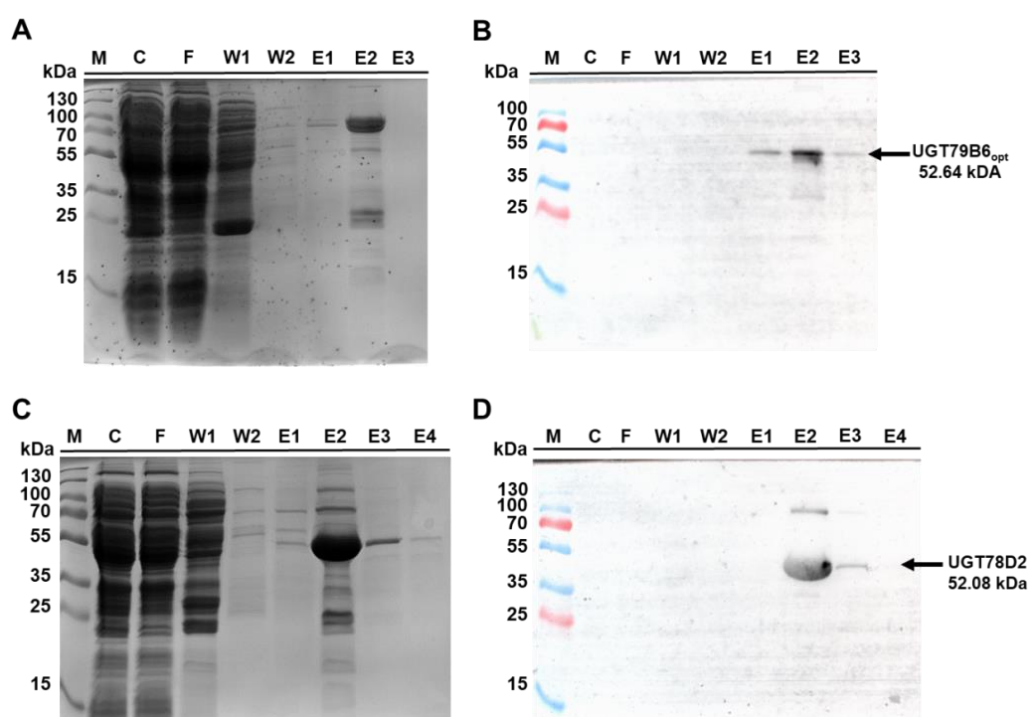


**Figure 3-1** Partial purification of UGT79B6<sub>opt</sub> and UGT78D2.

Recombinant UGTs were expressed in *E. coli* and partially purified by metal affinity chromatography. **(A)** SDS-PAGE and **(B)** corresponding immunoblot of the UGT79B6<sub>opt</sub>; **(C)** SDS-PAGE and **(D)** corresponding immunoblot of the UGT78D2. Protein ladder (M) and the individual fractions: crude protein extract (C), flow through (F), first wash fraction (W1), second wash fraction (W2), first elution (E1), second (E2), third elution (E3), and fourth elution (E4). For the immunolabelling a monoclonal anti-His-antibody conjugated to horse radish peroxidase was used.

The SDS-PAGE analysis showed expression and partial purification of both glycosyltransferases. Especially, in the case of the poorly expressed UGT79B6 several other proteins were still present (Figure 3-1 A). In comparison, the UGT78D2 was the major protein in the elution fractions E2 and E3 (Figure 3-1 C). The presents of the purified His-tagged proteins were tested by western blot analysis (Figure 3-1 B and 3-1 D). For the codon optimized UGT79B6 a distinct signal was detectable in the immuno blot in the case of the elution fractions (Figure 3-1 B). In parallel, all fractions were standard tested for glycosyltransferase activity. Representative reverse phase chromatograms of the UGT enzyme assays are presented in Figure 3-2. Partially purified enzymes were desalted and further used for the radioactive labelling of flavonol glycosides as described before (2.4.6). HPLC-MS profiles of the solid phase extraction elution fractions revealed that no side products were contained (Inserts Figure 3-2 A and B).

In summary, both glycosyltransferases were expressed and partially purified. The recombinant UGTs were stable and active giving the opportunity for production of  $^{14}\text{C}$ -labelled flavonol glycosides (2.4.6) for the following transporter studies (3.7).

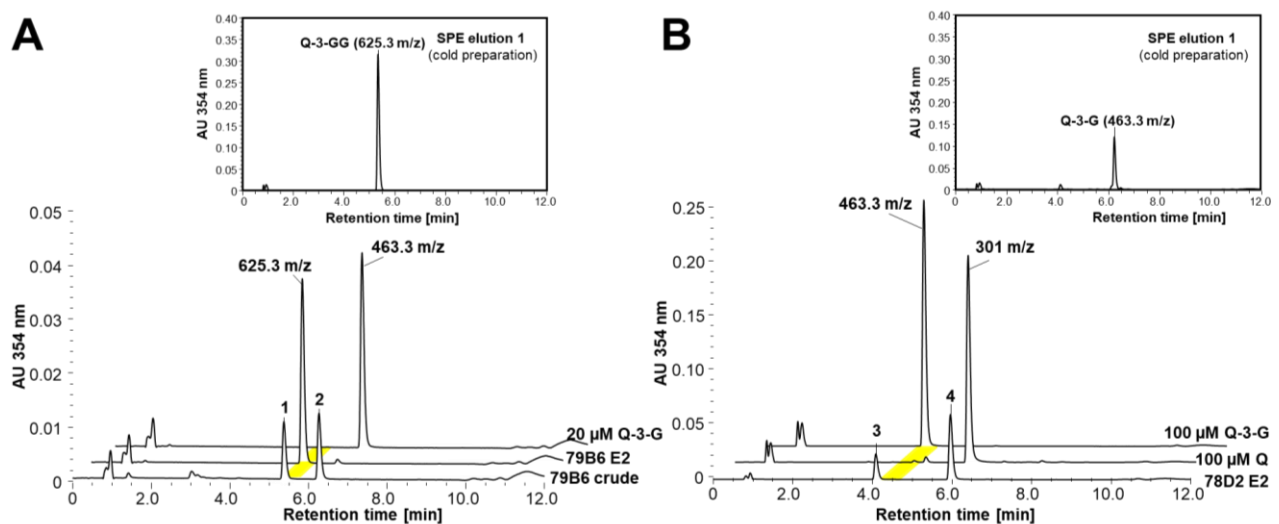


**Figure 3-2** Enzymatic activity of UGT79B6<sub>opt</sub> and UGT78D2.

(A) UGT79B6 enzyme assays. Shown are the assays (0.6 µg protein, 20 µM quercetin-3-*O*-glucoside, 2 min, 37 °C) of the protein crude extract (79B6 crude) and the partially purified UGT79B6 (79B6 E2) compared the 20 µM quercetin-3-*O*-glucoside (20 µM Q-3-G, 463.3 m/z) standard. (1) Product peak of quercetin-3-*O*-sophoroside (625.3 m/z) (yellow-highlighted). (2) Substrate peak of quercetin-3-*O*-glucoside (463.3 m/z). (B) UGT78D2 enzyme assay. Shown are a representative assay (0.42 µg protein, 40 µM quercetin, 2 min, 37 °C) with the partially purified enzyme (78D2 E2) compared to the 100 µM standards of quercetin (Q, 301 m/z) and quercetin-3-*O*-glucoside (Q-3-G, 463.1 m/z). (3) Product peak of quercetin-3-*O*-glucoside (463.3 m/z) (yellow-highlighted). (2) Substrate peak of quercetin (301 m/z). (In (B) the slightly different HPLC-program MS\_QDA\_5cm\_12min\_78D2\_V287A was used). Main elution fractions of quercetin-3-*O*-sophoroside (Q-3-GG) and quercetin-3-*O*-glucoside (Q-3-G) from the solid phase extraction (SPE) of the cold control preparations are shown in the inserts. Detection was performed at 354 nm.

### 3.3 Transport and biosynthesis of flavonol sophorosides

#### 3.3.1 *UGT79B6* is highly expressed in tapetal cells

The *UGT79B6* (*At5g54010*) was characterized as the terminal key enzyme in the biosynthesis of flavonol-3-*O*-sophorosides by Yonekura-Sakakibara et al. (2014). To identify the specific expression of the *UGT79B6* and thereby the location of the flavonol-3-*O*-sophorosides, a promoter *UGT79B6:GFP* reporter construct (pAGV72) was produced. It comprises a 928 bp fragment upstream of the *UGT79B6* translation start site, was fused to a *GFP* reporter gene, and was used for the generation of stable *Arabidopsis* reporter lines. Transgenic plants of the T<sub>1</sub> generation were examined for a GFP-signal by fluorescence microscopy and immuno staining (Figure 3-3). In several independent pAGV72 lines a GFP-signal was detected and was restricted to young anthers (Figure 3-3 A). (The GFP-signal was not detected in the filament.) Remarkably, the GFP-fluorescence was very strong at the pollen sacs and appeared to decrease at the anther tip. Anthers of stable transformed pAGV82 lines expressing GFP under the control of a putative *SHT* promoter (858 bp) exhibited an adequate anther-specific GFP fluorescence (Figure 3-3 B). In young anthers of the wild-type control the GFP-signal was not detected (Figure 3-3 C). This indicates that the observed fluorescence signal was not emitted by the anther wall or pollen grain autofluorescence. Due to the strong fluorescence signal an immuno-localization based on the exogenous GFP expression was performed (Figures 3-3 D, E, and F). Cross-sections of young inflorescences from the T<sub>2</sub> generation were immuno-stained. Immuno-staining of wild-type cross-sections verified that the yellow autofluorescence of the pollen coat and the tapetal cells were probably caused by the high amounts of phenolic compounds (Figure 3-3 D). In contrast, immuno-stained cross-sections of the pAGV72 plants revealed a GFP-signal exclusively located in the tapetal cell layer (Figure 3-3 E). The GFP-fluorescence distinctly surrounded the locule space (Figure 3-3 E and F). The epidermis and the endothecium appeared unstained. As comparison for a tapetal expression and positive control for the immuno staining anther sections of the stable promoter *TSM1:GFP*-reporter line (pAGV92) were in parallel examined. Thereby, a 559 bp sized *TSM1* promoter was used. This positive control, based on expression of the tapetal-specific methyltransferase 1 (Fellenberg et al., 2008) confirmed an identical tapetum-specific GFP signal as observed for the *UGT79B6* promoter (Figure 3-3 F).

The *UGT79B6* promoter activity appeared in a spatially specific manner and clearly confirms the tapetal cell layer as the source tissue for flavonol-3-*O*-sophoroside biosynthesis. This result independently confirms the tapetum-specific *UGT79B6* expression observed by Yonekura-Sakakibara et al. (2014) using a 2 kb promoter fragment. But in contrast to their work no *UGT79B6* promoter activity was identified in the microspores which might be due to the different promoter sizes. The functional 928 bp *UGT79B6* promoter was further used as comparison for the identification of a putative *FST1* promoter fragment.

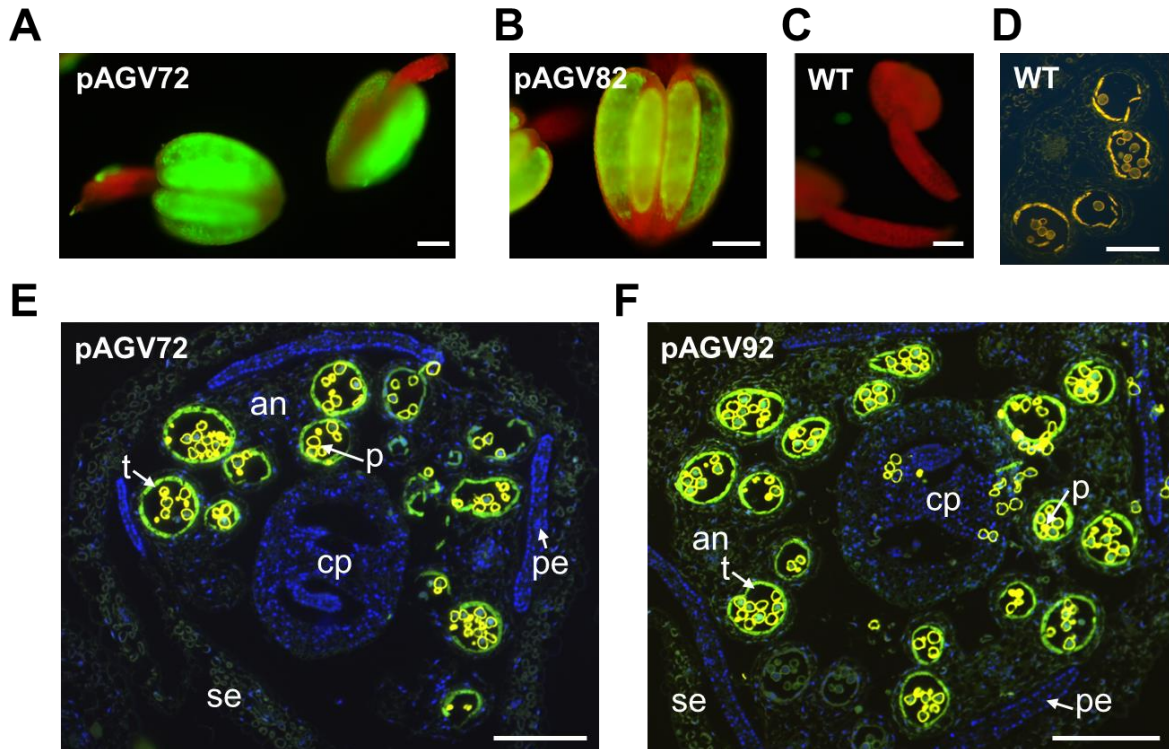


**Figure 3-3** The transcription of *UGT79B6* is restricted to the tapetum.

Anthers isolated from inflorescences of stable transformed *Arabidopsis* plants expressing (A) the prom*UGT79B6*:*GFP* reporter gene construct (pAGV72) compared to (B) stable prom*SHT*:*GFP* reporter (pAGV82) lines and (C) wild-type anthers imaged by fluorescence microscopy. Bars = 100  $\mu$ m. (D, E, and F) Immuno-stained cross-sections of young inflorescences for indirect visualization of the promoter activity. (D) Yellow autofluorescence of phenylpropanoids on the pollen coat and the tapetal cells in the wild-type immuno-control. Bar = 50  $\mu$ m. (E and F) Bright GFP fluorescence was exclusively restricted to the tapetum (t) of the prom*UGT79B6*:*GFP* reporter line pAGV72 and not found in carpel (cp), petals (pe) or sepals (se). Pollen grains (p) showed yellow autofluorescence. Bar = 100  $\mu$ m. The *TSM1* promoter activity in the prom*TSM1*:*GFP* reporter lines stable transformed with pAV92 were used as tapetum-specific control. Bar = 100  $\mu$ m. Sections of 2  $\mu$ m thickness were immunolabelled with a primary anti-GFP antibody and visualized by a secondary Alexa Fluor 488 conjugated antibody. The nuclei were counterstained by DAPI. Bar = 100  $\mu$ m.

### 3.3.2 Identification of a NPF-protein as putative flavonol glycoside transporter

The identification of transporters with defined substrate specificity is 'notoriously challenging' (Larsen et al., 2017) and a general problem in this field. The identification approach was based on the assumptions (i) that the translocation of tryphine forming compounds is an active process, distinct from the programmed tapetal cell death and (ii) that a putative transporter candidate gene would notably be co-expressed with the tapetum-specific key enzyme of the flavonol-3-*O*-sophoroside formation, the *UGT79B6* (*At5g54010*) (Yonekura-Sakakibara et al., 2014) (Figure 3-3). In the case of the flavonol-3-*O*-sophorosides the tapetum-specific biosynthesis was of some advantage to exclude spatially unspecific expressed candidates. In the classical model *A. thaliana*, co-expression analyses are not limited to experimental approaches but also rely on a large community and deposition of hundreds of datasets in open platforms (Larsen et al., 2017). An intensive screening of free available microarray data sets of TRAVA and the BAR eFP browser (Klepekova et al., 2016), Genevestigator (Zimmermann et al., 2004), ATTED-II (Obayashi et al., 2018), as well as the ARAMENON database (Schwacke et al., 2003) were performed to identify promising candidate genes.



As no exclusively flavonol-glycoside-specific transporter has been characterized up to now, the initial search was combined with previous reports that highlighted the ABC and MATE transporter superfamilies as potential candidates for flavonoid and/or hydroxycinnamic acid amides (HCAA) transport (Quilichini et al., 2014a; Dobritsch et al., 2016; Marinova et al., 2007). In total, two ABC family members (*ABCG17* and *ABCG18*) and five different MATE transporters termed as detoxification proteins (DTX) (*DTX27*, *DTX29*, *DTX33*, *DTX34*, and *DTX36*) were identified. Additionally, the MATE transporter TT12 (*At3g59030*) and the glutathione-S-transferase TT19 (*At5g17220*) were included as putative candidates based on the report of Hsieh and Huang (2007). Beside these candidates, two NPF transporter genes (*NPF2.8* and *NPF7.1*) from the heterogeneous NRT1/PTR superfamily were also identified. Despite their weak co-expression with the *UGT79B6*, the NRT1/PTR family members were suggested to be promising candidates due to their annotation as anther-specific by TRAVA (<http://travadb.org/>) and the BAR eFP browser (<http://bar.utoronto.ca/>) (Klepikova et al., 2016). Several members of the NPF subfamily were known for transport activity towards specialized plant metabolites like glucosinolates (Nour-Eldin et al., 2012). The identification was combined with a classical forward genetic screen using Arabidopsis T-DNA-insertion lines obtained from the Arabidopsis Stock Centre. Such phenotype-driven screens have often been used for identification of transporter or also exine associated genes (Kang et al., 2011; Tal et al., 2016; Dobritsa et al., 2011).

To test the preliminary identified candidates a chemotype-driven screen was performed suspecting that a null mutation in a tapetal exporter would result in a changed tryphine composition. Fifteen ordered Arabidopsis T-DNA insertion lines were genotyped and confirmed to be knockout lines by PCR and RT-PCR, respectively. This is just representative shown for the positive knockout line SALK\_027288C and the excluded 'knock about' line SALK\_113184C (Appendix Figure 8-1). The TAIR accessions of all candidate genes and the individual lines are given (Appendix Table 8-1). Pollen was harvested from wild-type and verified knockout lines. The tryphine material from the pollen coat was extracted with methanol and analysed by HPTLC and HPLC-MS (Figure 3-4 and 3-5). Each spot corresponds to 1 mg extracted pollen material. In extracts of the wild-type pollen both flavonol-3-*O*-sophorosides as well as the HCAAs are present. In comparison to the wild-type the levels of both phenylpropanoids were unchanged for nearly all tested knockout lines. Only *npf2.8* which is following termed as FLAVONOL SOPHOROSIDE TRANSPORTER 1 (FST1) revealed a strong reduction for both flavonol glycosides. This observation indicates FST1 as putative flavonol glycoside transporter candidate for subsequent characterization. The reduction of the flavonol-3-*O*-sophorosides was furthermore not accompanied by a reduction of the HCAAs, suggesting that the knockout has a distinct effect on flavonoids. Notably, the accumulation of the phenolamides was not affected in any other transporter knockout line. Therefore, a transporter independent translocation of these compounds to the exine layer could be assumed. Contradictory to the reported role of the TT12 transporter for tapetal flavonoid transport by Hsieh and Huang (2007), no effect on the flavonol-3-*O*-sophorosides was observed in case of the two independent knockout lines *tt12-1* and *tt12-2*. The TT19 candidate which was also suggested by Hsieh and Hunag (2007) was tested later by HPTLC using the confirmed line *tt19-8*, but revealed as well no changed profile compared to the wild-type.

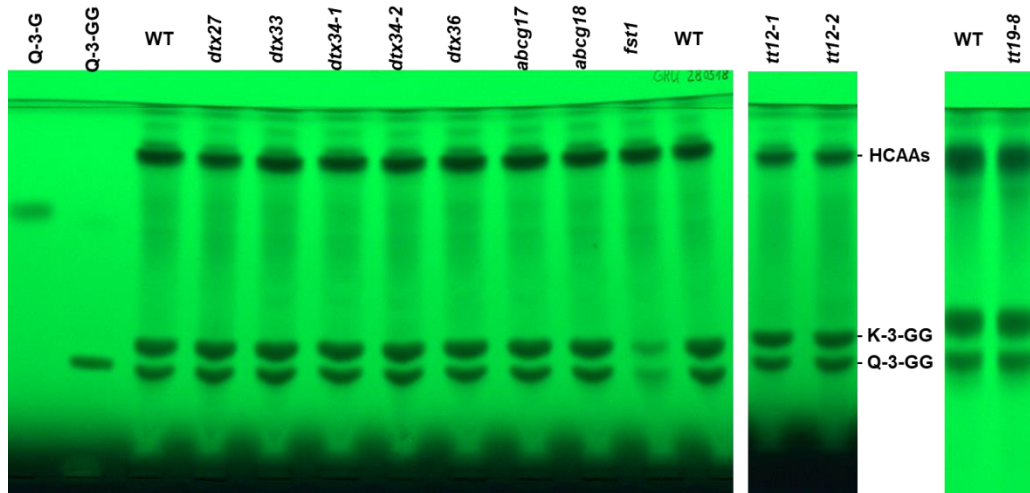


**Figure 3-4** The *npf2.8* line (*fst1*) exhibits a changed flavonoid profile.

Methanolic extracts of the pollen coat material from Arabidopsis wild-type (WT) and T-DNA lines – *dtx27* (*At5g65380*), *dtx33* (*At1g47530*), *dtx34-1* and *dtx34-2* (two independent *At4g00350* T-DNA lines), *dtx36* (*At1g11670*), *abcg17* (*At3g55100*), *abcg18* (*At3g55110*), *fst1* (*At5g28470*) were analysed by HPTLC. The lines *tt12-1* and *tt12-2* (two independent *At3g59030* T-DNA lines) as well as *tt19-8* (*At5g17220*) were analysed before on a separate plate. The image presents the phenylpropanoid pattern before DPBA staining at illumination by 254 nm for a better visual comparison of the contained amounts. Standards are quercetin (Q), quercetin-3-*O*-glucoside (Q-3-G) and quercetin-3-*O*-sophoroside (Q-3-GG). Indicated are the spots of the hydroxycinnamic acid amides (HCAAs) and both sophorosides, Q-3-GG and kaempferol-3-*O*-sophoroside (K-3-GG).

Using the more qualitative HPLC-MS analysis, phenylpropanoid profiles of the pollen extracts were further examined (Figure 3-5). Thereby the strong reduction of the flavonol-3-*O*-sophorosides on pollen of the *fst1* mutant was clearly confirmed (Figure 3-5 A compared to 3-5 B). In contrast, the second NPF candidate knockout line *npf7.1* did not exhibit any effect on the phenylpropanoid pattern (Figure 3-5 C). The HPLC-MS profiles of all other candidates (Figure 3-5 D to H) complied with the HPTLC analysis and revealed no variance in their phenylpropanoid pattern. The major peaks of the phenylpropanoids were identified by their characteristic UV-absorbance spectra and according to their *m/z* (Appendix Figure 8-10). Furthermore, a quercetin-3-*O*-sophoroside standard was used to confirm the correct flavonol glycoside pattern.

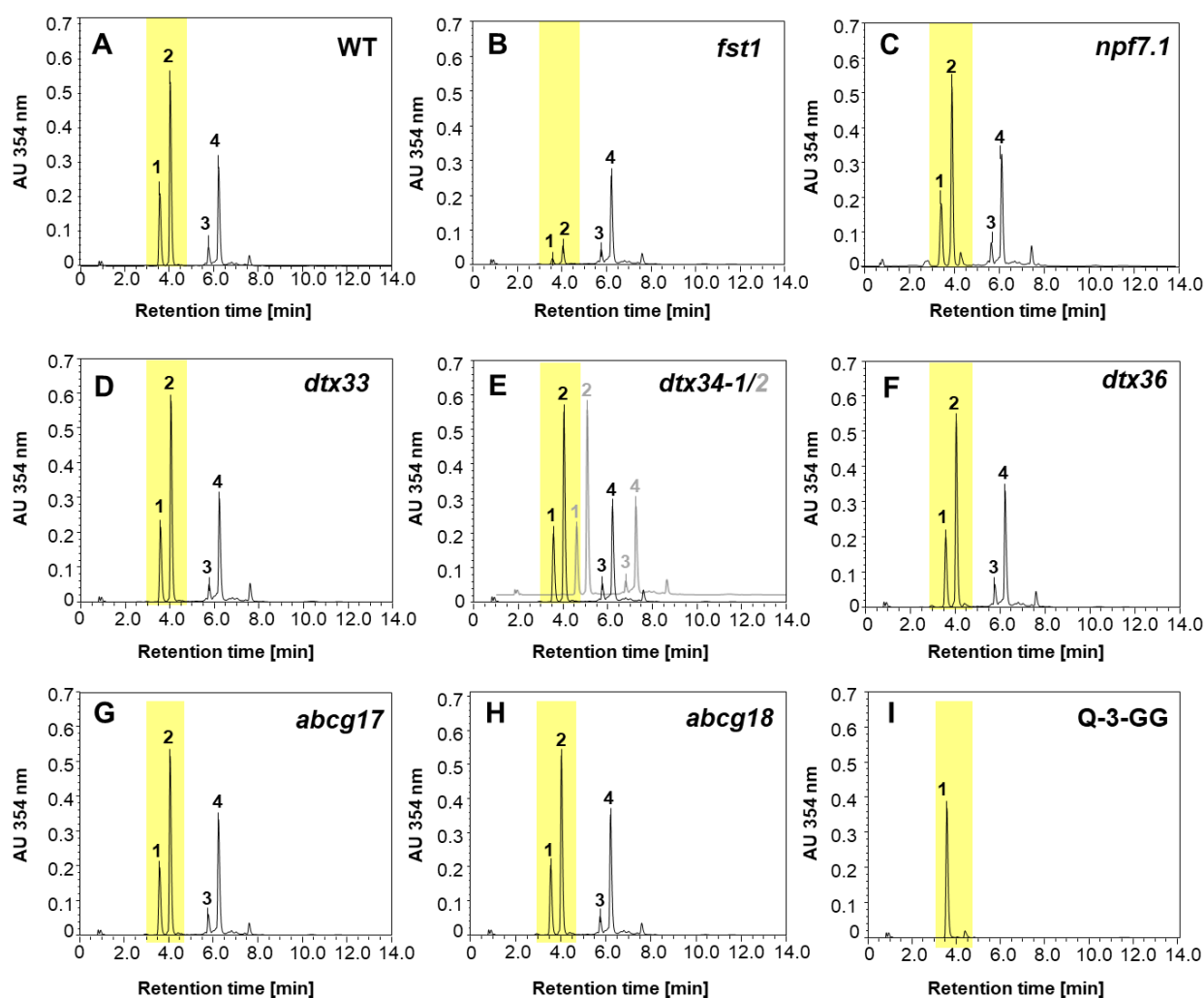


**Figure 3-5** HPLC-MS profiles of pollen extracts from various mutant lines.

Comparison of the methanolic pollen extracts from (A) the wild-type (WT) and (B to H) the knockout lines: *fst1* (*At5g28470*), *npf7.1* (*At5g19640*), *dtx33* (*At1g47530*), *dtx34-1* and *dtx34-2* (two independent *At4g00350* T-DNA lines), *dtx36* (*At1g11670*), *abcg17* (*At3g55100*), *abcg18* (*At3g55110*) as well as *tt12-1* and *tt12-2* (two independent *At3g59030* T-DNA lines) recorded by 354 nm. (I) Quercetin-3-*O*-sophoroside standard (Q-3-GG) (100  $\mu$ M) was used for identification. The hydrophilic flavonoldiglucosides eluted earlier from the reversed phase column than the more hydrophobic phenolamides and are highlighted in yellow. Indicated peaks are (1) quercetin-3-*O*-sophoroside (625.3 m/z), (2) kaempferol-3-*O*-sophoroside (609.3 m/z) and (3 and 4) two major hydroxycinnamic amide acids with 720.4 m/z and 734.4 m/z, respectively.

For quantification and reproducibility of the *fst1* chemotype, the flavonol glycoside levels of the *fst1* mutant and wild-type were determined by a standard curve (Table 3-1). The curve was based on quercetin- and kaempferol-3-*O*-glucoside, which have similar UV-absorbance at 354 nm (Appendix Figure 8-8). For the wild-type, the mean values of 383 pmol/mg (quercetin-3-*O*-sophoroside) and 845 pmol/mg (kaempferol-3-*O*-sophoroside) were measured. In extracts from the *fst1* pollen coat, the amounts of quercetin-3-*O*-sophoroside and kaempferol-3-*O*-sophoroside were strongly reduced to 41 pmol/mg and 93 pmol/mg, respectively.

To test, if the *fst1* mutation is accompanied by a storage effect like it was observed in case of the glucosinolate transporters (Nour-Eldin et al., 2012) or may have a feedback inhibition effect, the levels of the flavonol-3-*O*-sophorosides in *fst1* anthers were compared to the wild-type (Table 3-2). Notably,

no significant change of the flavonol glycoside levels was observed. So it can be noted, that there was no indication for a feedback inhibition. But it should be mentioned that due to the impracticality to separate the tapetum (source) from the pollen (sink) a clear storage effect is challenging to investigate.

**Table 3-1** Quantification of flavonol-3-*O*-sophorosides on *fst1* pollen. Quantities of quercetin- and kaempferol-3-*O*-sophoroside were quantified based on UV<sub>354nm</sub> –absorption of quercetin- and kaempferol-3-*O*-glucoside. Presented are the mean values  $\pm$  standard derivation of three biological replicates (n = 3).

compound	wild-type [pmol/mg pollen]	<i>fst1</i> [pmol/mg pollen]
Quercetin-3- <i>O</i> -sophoroside	383 $\pm$ 38	41 $\pm$ 7
Kaempferol-3- <i>O</i> -sophoroside	845 $\pm$ 51	93 $\pm$ 6

**Table 3-2** Quantification of flavonol-3-*O*-sophorosides in *fst1* anthers. Quantities of quercetin- and kaempferol-3-*O*-sophoroside were measured based on UV<sub>354nm</sub>-absorption of quercetin- and kaempferol-3-*O*-glucoside. Quantities are referred to one anther. Shown are the mean values  $\pm$  standard derivation of three biological replicates (n = 3). At least 200 anthers were collected per trial.

compound	wild-type [pmol/anther]	<i>fst1</i> [pmol/anther]
Quercetin-3- <i>O</i> -sophoroside	5 $\pm$ 1	6 $\pm$ 0
Kaempferol-3- <i>O</i> -sophoroside	14 $\pm$ 2	13 $\pm$ 1

### 3.4 Tissue-specific localization of the *FST1* transporter

#### 3.4.1 Anther specificity of the *FST1* candidate

The selection of *At5g28470* encoding *FST1* as putative candidate was initially based on the *in silico* data given by the Arabidopsis information resource (TAIR) (<https://www.arabidopsis.org/>), the Genevestigator software (<https://genevestigator.com/>) and the ARAMENNON database (<http://aramemnon.uni-koeln.de/>). These datasets suggested a specific expression of *FST1* in Arabidopsis anthers. To verify these *in silico* studies a quantitative Real-time PCR approach was performed using RNA extracted from various floral organs at early flower stages.

The relative expression levels of *At5g28470* are increased in young inflorescences and especially highest in early stage anthers (Figure 3-6). Notably, nearly no expression could be observed in other floral organs like the female carpel and leaves indicating a very specific expression for the *FST1* candidate. These findings are consistent with TRAVA (<http://travadb.org/>) and the BAR eFP browser (<http://bar.utoronto.ca/>) (Klepikova et al., 2016) which point to a specific expression in anthers mainly during the flower stages 6-8 and 9-11 (Appendix, Figure 8-11). After post-anthesis the expression levels are decreased. The data clearly substantiate the observation that *At5g28470* is specifically expressed in young anthers correlating with early stages of the pollen development.

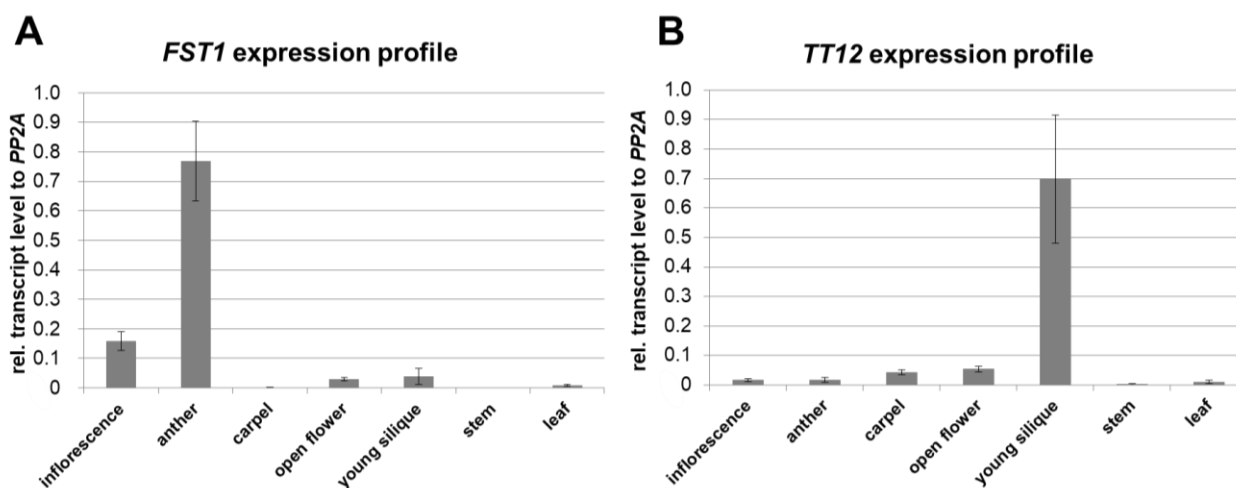


**Figure 3-6** Organ-specific transcription profiles of *FST1* and *TT12*.

(A) Transcription profile of *At5g28470* encoding *FST1* in floral organs of *Arabidopsis* wild-type analysed by quantitative Real-time PCR. The highest expression rate of *FST1* was observed in anthers. (B) Transcription profile of *At3g59030* encoding *TT12* in floral organs of *Arabidopsis* wild-type. The highest expression rate of *TT12* was observed in young siliques. No significant expression of *TT12* was observed in anthers. *PP2A* (*At1g13320*) was used as a reference gene. Shown data are mean relative expression values  $\pm$  standard error of three independent experiments in triplicate ( $n = 3$ ).

Additionally, the expression pattern of the *TT12* (*At3g59030*) candidate was tested for comparison, since it was published that *TT12* affected the deposition of flavonoids on pollen grains (Hsieh and Huang, 2007). In contrast to *FST1* (*At5g28470*), transcripts of *TT12* (*At3g59030*) were absent in anthers (Figure 3-6 B). A low detection may be caused by impurities due to difficulties in anther harvesting. *TT12* transcripts were high in female organs and open flowers. *TT12* showed the highest expression rates in young siliques correlating with the reported expression in the endothelium and developing seeds (Marinova et al, 2007). Together with the unchanged flavonol-3-*O*-sophoroside levels on *tt12* pollen compared to wild-type, the low *TT12* expression levels corroborate that *TT12* is not involved in the transport of flavonol sophorosides to the pollen surface.

### 3.4.2 Anther- and flavonoid-specific *cis*-regulatory elements in the *FST1* promoter

In preparation of the *in planta* *FST1* expression approach (3.4.3), a 2245 bp fragment upstream of the *FST1* start codon was chosen as putative *FST1* promoter. Upon an *in silico* analysis using the Signal Scan software of the New PLACE Database (Higo et al., 1999) several putative DNA *cis*-regulatory elements of this fragment were detected. A selection of the most relevant *cis*-acting elements is given (Table 3-3). The tapetum-specific *UGT79B6* promoter (928 bp) was analysed for comparison and shared *cis*-regulatory elements are indicated.

An anther and tapetum-specific activity of the putative *FST1* promoter was suggested by the presence of the SITEIIATCYTC motif which is known from tapetum-specific promoters (Welchen and Gonzales, 2005). The SITEIIATCYTC *cis*-regulatory motif is also present in the *UGT79B6* promoter indicating a putative tapetum restricted activity of this promoter element. In contrast to the 928 bp sized *UGT79B6* promoter the SITEIIATCYTC motifs in the *FST1* promoter are more distant at position -1944 and -1438 from the start codon. Additionally, pollen-specific elements like the POLLEN1LELAT52 and GTGANTG10 *cis*-acting motifs were detected ten times in both promoters. The 6 bp consensus motif

AGGTCA of the QELEMENTZM13 (position -966) was demonstrated in maize and Arabidopsis enhancing the activity of the pollen-specific ZM13 promoter (Hamilton et al., 1998).

MYB-binding *cis*-regulatory elements are found in the promoter of *FST1* and *UGT79B6*, including the *cis*-regulatory elements MYB1AT, MYBST1, MYBCOREATCYCB1, MYB2CONSENSUAT and MYBCORE. Additionally, the MYCCONSENSUAT motif was found in the *FST1* promoter region. MYB1AT and MYBST1 *cis*-acting motifs are identified close to the *FST1* transcription start suggesting these elements as part of the *FST1* core promoter. MYB1AT is the recognition site of the Arabidopsis MYB2 and MYC2 transcription factors (Abe et al., 2003). The MYBCORE motif is the DNA-binding element of the MYB.Ph3 factor required for the flavonoid biosynthesis in Petunia petals (Solano et al., 1995). The direct overlap at position -1790 of the three *cis*-acting motifs MYBCORE, MYB2CONSENSUAT, and MYCCONSENSUAT mark this region as putative essential for *FST1* transcription activation. Two MYB associated binding motifs reported to activate phenylpropanoid metabolism are MYBPZM and EBOXBN-NAPA. The EBOXBN-NAPA *cis*-regulatory motif is associated with the flavonoid biosynthesis and contains the bHLH factor consensus binding site CANNTG which is essential for activation of the chalcone synthase promoter (Hartmann et al., 2005). MYBPZM is recognized by the MYB homologous *P* gene, activating the *A1* gene transcription required for the 3-deoxy flavonoid and phlobaphene biosynthesis in maize (Grotewold et al., 1994). A putative role in the translocation of phenylpropanoid derived compounds was further indicated by the PALBOXAPC and the TATABOXPAL. These motifs are *cis*-acting elements of the *PAL* promoter in parsley and rice, respectively (Logemann et al., 1995; Zhu et al., 2002). Furthermore, the *cis*-regulatory elements GAREAT1 and GARE10SREP-1 which are associated with the plant gibberellin response were identified.

The TATABOX4 and the GATABOX *cis*-regulatory motifs close to the transcription start could be part of the *FST1* core promoter and responsible for the basal transcription initiation. The GATABOX is a gibberellin as well as light responsive element (Teakle et al., 2002) and is repeated ten times within the first 1000 bp of the *FST1* promoter. Another light responsive *cis*-regulatory element which occurred several times inside the putative core-region is GT1CONSENSUS (Terzaghi and Cashmore, 1995).

In summary, the sequence analysis of the *FST1* promoter revealed anther-/pollen-specific as well as phenylpropanoid/flavonoid related *cis*-acting elements. These findings imply a putative function of *FST1* in tapetal flavonoid metabolism and transport and contribute to the observed flavonoid glycoside deficient *fst1* pollen chemotype and the anther-specific *FST1* expression.

**Table 3-3** Predicted *cis*-acting motifs of the *FST1* promotor identified by PLACE. \*indicates *cis*-regulatory DNA motifs which were also identified in the *UGT79B6* promotor region. Overlapping positions between two or more motifs are bold printed. Identical positions which are shared by several motifs are highlighted with colours (purple, red and green).

<i>cis</i> -regulatory element	motif	position (strand)	reference
SITEIIATCYTC*	TGGGCY	-1944(+), -1438(+)	Welchen and Gonzales, 2005
POLLEN1LELAT52*	AGAAA	-1897(-), -1855(-), -1777(-), -1748(-), -1351(-), -1283(+), -1165(-), -1134(-), -1002(+), -812(+), -703(-), -685(+), -488(+), -482(+), -440(+), -424(+), -345(+), -329(-), -306(-)	Bate and Twell, 1998
GTGANTG10*	GTGA	-2144(-), -2079(+), -2072(-), -1716(+), -1482(-), -1475(-), -1428(-), -1401(+), -1363(+), -1106(-), -1037(+), -963(-), -92(+)	Rogers et al., 2001
QELEMENTZMZM13	AGGTCA	-966(+)	Hamilton et al., 1998
MYBCORE*	CNGTTR	<b>-1790(-)</b> , -955(+)	Lüscher and Eisenman, 1990
MYCONSENSUAT	CANNTG	<b>-1920(-)</b> , <b>-1920(+)</b> , <b>-1790(-)</b> , <b>-1790(+)</b> , <b>-1446(-)</b>	Abe et al., 2003
MYBST1*	YACT	-1937(+), -595(-), -471(+), -141(-)	Baranowskij et al., 1994
MYB1AT*	WAACCA	-1983(-), -1574(-), -1525(-), -796(-)	Abe et al., 2003
MYB2CONSENSUAT*	YAACKG	<b>-1790(+)</b>	Abe et al., 2003
MYBCOREATCYCB1	AACGG	-223(+)	Planchais et al., 2002
PALBOXAPC	CCGTCC	-2040(+)	Logemann et al., 1995
MYBPZM	CCWACC	-1493(-), -1461(+)	Grotewold et al., 1994
EBOXBNNAPA	CANNTG	<b>-1920(-)</b> , <b>-1920(+)</b> , <b>-1446(-)</b>	Hartmann et al., 2005
TATABOXSPAL	TATTTAA	-725(+), -582(+), -295(-)	Zhu et al., 2002
IBOXCORE*	GATAA	<b>-783(-)</b> , <b>-633(-)</b> , <b>-566(-)</b> , -273(-), <b>-249(-)</b> , <b>-189(+)</b>	Terzaghi and Cashmore, 1995
GAREAT*	TAACAAR	-1176(-), -1124(-), -1014(+), -158(+)	Ogawa et al., 2003
TATABOX4	TATATAA	-366(-), -365(+), -53(+)	Grace et al., 2004
GATABOX	GATA	-2068(-), -1936(+), -1926(-), -1413(-), -1211(-), -1196(+), -782(-), -639(-), -632(-), -595(-), -565(-), -470(+), -339(+), -272(-), -254(+), -248(-), -189(+), -42(-)	Teakle et al., 2002
GT1CONSENSUS	GRWAAW	-1876(-), -1779(-), -1380(-), -1282(+), -1048(-), -1001(+), -944(+), -891(+), -890(+), -849(-), -824(-), <b>-784(-)</b> , -705(-), <b>-634(-)</b> , <b>-567(-)</b> , -439(+), -423(+), -308(-), -254(+), <b>-250(-)</b> , <b>-189(+)</b> , -83(-), -82(-), -31(-), -25(-)	Terzaghi and Cashmore, 1995

n).

### 3.4.3 Tapetum-specific expression of the *FST1* candidate

The expression of the *UGT79B6* (*At5g54010*), the terminal key enzyme in flavonol-3-*O*-sophoroside formation is tapetum specific (3.3.1). If *FST1* contributes to the translocation of flavonoids to the pollen surface, a tapetal expression of the candidate gene seems to be indispensable. This assumption was proven by a promoter-GFP assay. A prom*FST1*:GFP reporter construct was produced using the putative 2245 bp *FST1* promoter. Stable transformed *Arabidopsis* reporter lines were analysed regarding *FST1* promoter activity (Figure 3-7).

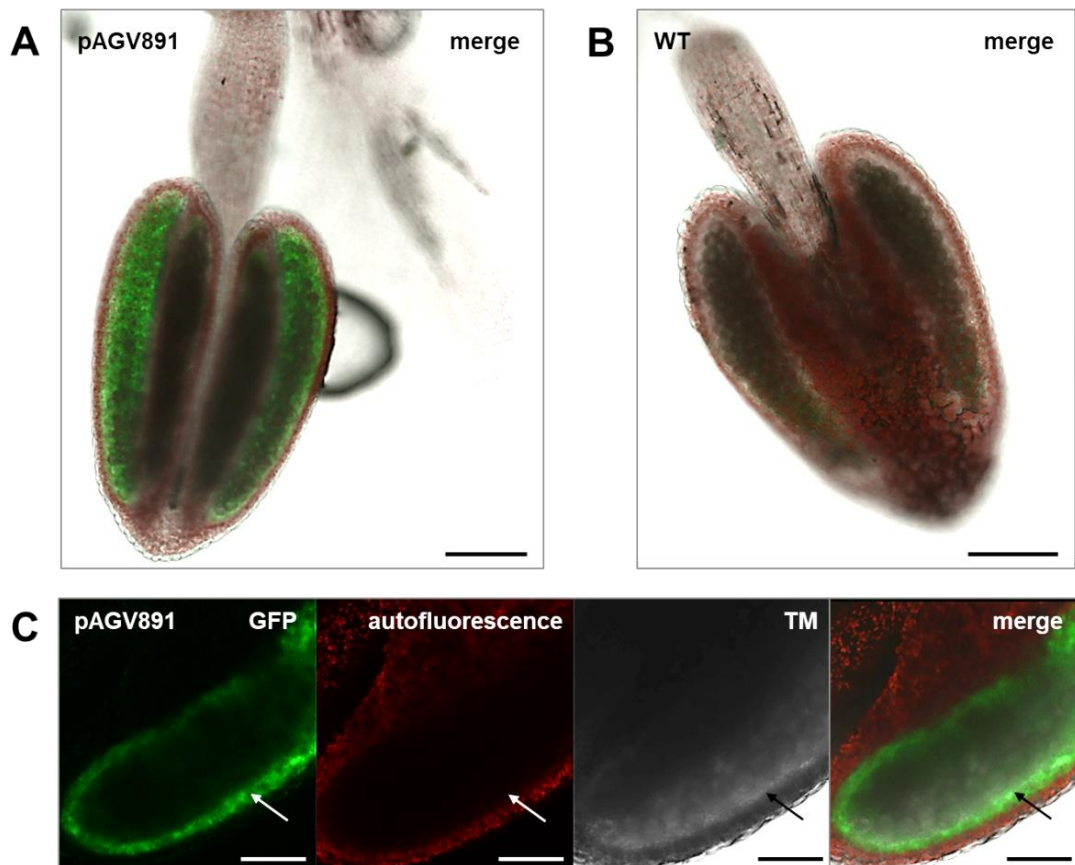


**Figure 3-7** The *FST1* promoter shows tapetal-specific expression.

Representative confocal fluorescence images of isolated anthers from stable transformed *Arabidopsis* prom-*FST1*:GFP reporter lines (**A**) expressing the Golden Gate construct pAGV891 in comparison to (**B**) the wild-type. Bars = 100  $\mu$ m. (**C**) Detailed confocal image of the tapetum-specific GFP signal in pAGV891 anthers. The GFP signal is located to the innermost surrounding tissue of the pollen sacs, the tapetum (indicated by an arrow) and not to the pollen grains. The autofluorescence of the plastids located in the outer anther wall is shown in red for a better visualisation of the anther structure. Bar = 20  $\mu$ m. Shown are the GFP-channel (GFP), the autofluorescence of the outer anther wall (autofluorescence), the transmission image (TM) and the merged image of all three channels (merge). Anthers from five independent transgenic T<sub>1</sub>-lines were analysed by CLSM (n = 5).

In transgenic lines of the T<sub>1</sub> generation a GFP signal was exclusively found in the anthers. The GFP-fluorescence signal is located to the surrounding cell layer of the locule space containing the pollen grains inside the anthers (Figure 3-7 A). The green fluorescence signal is visible in the innermost cell layer of the anthers, the tapetum and is not co-localized with the autofluorescence occurring in the endothecium (Figure 3-7 C). In *Arabidopsis* wild-type plants the GFP-fluorescence was not observed (Figure 3-7 B). This result is consistent with the *FST1* qRT-PCR data (3.4.1) and verifies a tapetum-specific co-expression with the *UGT79B6*.



### 3.4.4 Complementation of *fst1* by *FST1* expression

To validate that the observed *fst1* pollen chemotype is caused by the non-expressed *FST1* transporter and not due unknown background mutations. The *FST1* gene (2.55 kb) was put under the control of its natural, tapetum-specific promoter. The generated Golden Gate construct pAGV931 (Appendix Figure 8-5 A) encoded *FST1* and was stably transformed into the *fst1* mutant line. Transformed plants of the first generation transcribed the artificial inserted *FST1* wild-type copy (Appendix Figure 8-6) and were single events. Positive tested individual lines were used for seed propagation. Methanolic pollen extracts of several independent lines from the T<sub>2</sub> generation were analysed by HPLC-MS (Figure 3-8). For all tested *FST1:fst1* complementation lines the flavonol sophoroside levels on the pollen surface were significantly higher than in the *fst1* mutant. Several *FST1:fst1* lines presented flavonol sophorosides levels comparable to the wild-type (shown are 931-1 and 931-10). Single *FST1:fst1* lines differed slightly to each other in their flavonol sophoroside levels indicating that each line is a unique event (e.g. line 931-8 and 931-1 in Figure 3-8). Accumulation of the HCAAs on the pollen surface was not affected suggesting that the biosynthesis of both pollen-specific phenylpropanoid classes is independent of each other. The here identified *FST1* (*At5g28470*) is essential for the composition of flavonol sophorosides on the pollen exine.

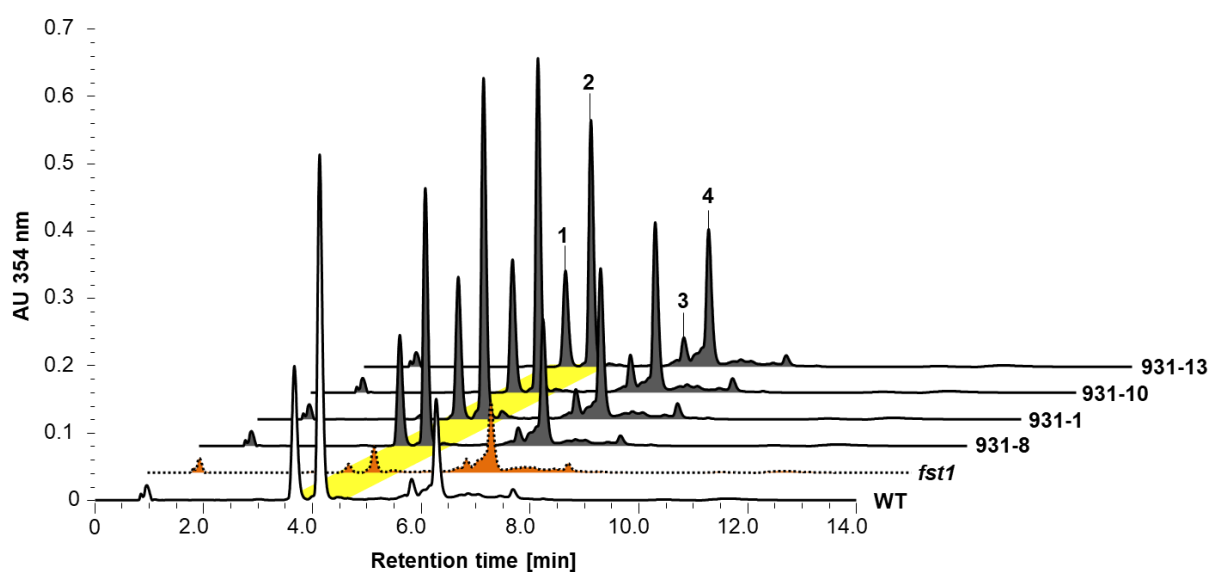


**Figure 3-8** A copy of the *FST1* wild-type gene complements the *fst1* chemotype.

Phenylpropanoid composition of methanolic pollen extracts from *Arabidopsis* wild-type (WT) (white-filled in front), *fst1* mutant (SALK\_027288C, orange-filled, dotted line) (*fst1*) and four independent *FST1:fst1* complementation lines (931-1, 931-8, 931-10 and 931-13). The specific flavonol-3-*O*-sophorosides are highlighted in yellow. Peak numbers are: quercetin-3-*O*-sophoroside (625.3 m/z) (1) and kaempferol-3-*O*-sophoroside (609.3 m/z) (2) and two major HCAAs (3 and 4) which are obviously unchanged in all lines (16 independent lines, n = 16).

### 3.4.5 Subcellular localization of the FST1 transporter

Flavonoid transporters mainly acting in anthocyanin metabolism are usually reported to be localized to the tonoplast (Goodman et al., 2004; Marinova et al., 2007; Francisco et al., 2013; Yang et al., 2016). Localization to the tonoplast was also highly predicted for FST1 by the subcellular localization database for Arabidopsis proteins (SUBA, <http://suba.live/>). The subcellular localization of FST1 was investigated using the *prom35S:FST1-GFP* reporter construct pAGV993 that was transiently expressed in *N. benthamiana* leaves. Interestingly, a construct only containing the *FST1* coding sequence did not function, therefore the full-length genomic *FST1* sequence was used. Live cell images of transformed epidermal leaf cells exhibited a GFP-signal localized to the plasmalemma (Figure 3-9). To distinctly confirm the plasmalemma localization of FST1 a double labelling experiment was performed by combined expression with the plasma membrane marker CD3-1007. The marker CD3-1007 encodes the Arabidopsis plasma membrane intrinsic protein 2A (PIP2A, *At3g53420*) fused to mCherry (Nelson et al., 2007). The GFP-signal of FST1-GFP located in the plasmalemma appeared typically very thin and smooth compared to the strong and diffuse fluorescence of the GFP-control (pAGM14112) as a typical cytosolic protein (Figures 3-9 A and B, respectively). Characteristically, the plasma membrane signal forms a single layer uniform labelling along the cell surface (Figures 3-9 A and C) without entering the interior cell or transvacuolar strands (Figure 3-9 B). A clear distinction between the plasmalemma and the tonoplast membrane appears sometimes 'tricky' because both organelles are close together and show a similar labelling along the cell (Nelson et al., 2007). Therefore, the localization of FST1 was further detailed visualized to explicitly validate the plasmalemma localization (Figures 3-9 C, D, and E). The hypothetical plasmalemma localization was further examined by plasmolysis. When the epidermal cells were exposed to a reduced turgor in a hypertonic milieu, the partial detachment of the plasma membrane from the cell wall could be observed (Figure 3-9 D). During the plasmolysis the characteristic formation of the hechtian strands was observed (Figure 3-9 E). Despite the detachment, the fluorescence signals of the FST1-GFP fusion protein and CD3-1007 remained consistent inside the plasmolysed cells (Figures 3-9 D and E). In a concave plasmolysis the plasmalemma was stretched from the cell wall and is only attached along the plasmodesmata to the neighbouring cells. These data consolidate that the membrane transporter protein FST1 is indeed localized in the plasmalemma, which is consistent with most reports of the NPF-gene family members (Nour-Eldin et al., 2012; Niño-González et al., 2019). Expression of the FST1-GFP fusion protein was additionally controlled by immunoblot analysis (Appendix Figure 8-7).

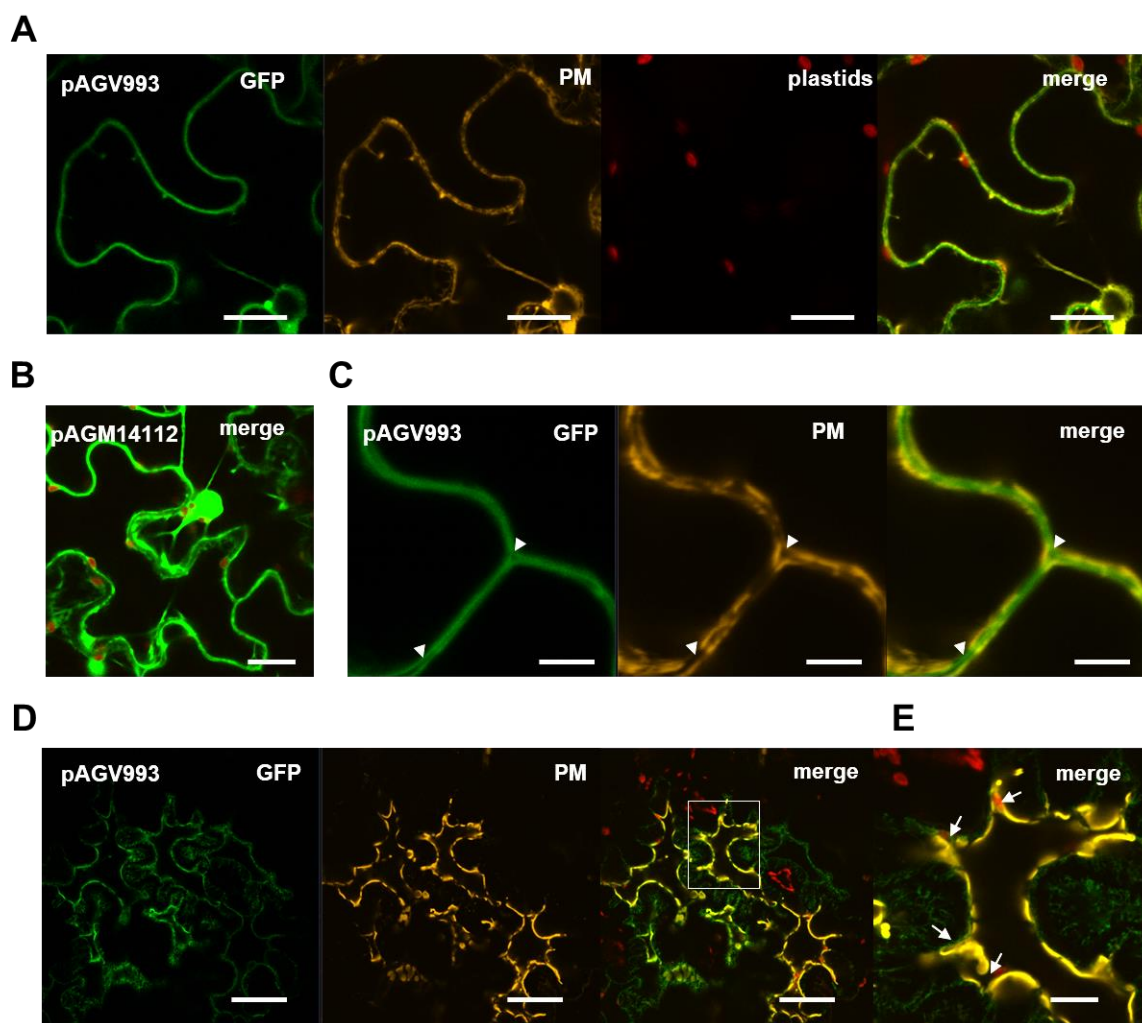


**Figure 3-9** Plasma membrane localization of FST1-GFP in epidermal leaf cells.

Confocal fluorescence images of GFP fluorescence in epidermal cells of *N. benthamiana* leaves expressing (A) pAGV993 encoding *prom35S:FST1-GFP* and (B) pAGM14112 the GFP-control as a typical soluble protein. Bars = 200  $\mu$ m. Shown are the GFP-channel (GFP), the mCherry fluorescence of the plasma membrane marker CD3-1007 (PM), the autofluorescence of chlorophyll A (plastids) and the merged images (merged). (C) Enlarged image of epidermal cells, the arrowheads indicate plasma membrane localization, the cell wall appears as a dark interspace. Bars = 5  $\mu$ m. (D) Plasmolysis of the epidermal leaf cells in hypertonic media after 10 minutes. Bars = 50  $\mu$ m. (E) Detail image of a single plasmolysed cell, which shows the characteristic formation of the hechtian strands (indicated by arrows). Bar = 10  $\mu$ m.

### 3.4.6 FST1 is functional in the plasma membrane of tapetal cells

Previous reports suggest that a transporter involved in tapetal flavonoid transport could be localized and may co-migrated within vesicles derived from the endoplasmic reticulum, termed as tapetosomes (Hsieh and Huang, 2007; Li et al., 2012; Zhao, 2015). To validate that FST1 is functional in the tapetal plasma membrane, the localization and the complementation approach were combined (Figure 3-10).

Golden Gate cloning was used to generate a second complementation construct termed pAGV1043 which was stable transformed into the *fst1* background. The construct pAGV1043 encodes the C-terminal GFP labelled FST1 driven by the *FST1* promoter (Appendix Figure 8-5 B). The natural stop codon of the 2.55 kb *FST1* wild-type allele was removed. Stable transformed pAGV1043 plants of the T<sub>1</sub> generation were examined by fluorescence microscopy. Several independent lines exhibited a GFP-signal situated in the anthers and were further used for seed propagation. Methanolic pollen extracts from positive

pAGV1043 lines of the T<sub>2</sub> generation were analysed by HPLC-MS (Figure 3-10 A). As in the case of the untagged pAGV931 lines the flavonol sophoroside levels in all tested pAGV1043 complementation lines were significantly higher than in the *fst1* mutant. Again, the accumulation of the HCAAs on the pollen coat was not changed as observed before for the pAGV931 complementation lines (Figure 3-8).

The subcellular localization inside the anthers of positive pAGV1043 rescue lines was further observed in more detail by confocal laser scanning microscopy. The GFP-signal was localized in the tapetal cell layer. On the subcellular level the GFP-signal was situated in the plasmalemma of the tapetal cells (Figure 3-10 B). The signal was smooth and formed a thin layer around the cell. Transvacuolar strands as in case of a free soluble protein were not noticed. No reticular signal pattern or vesicle-like structures as expected for ER-derived tapetosomes were observed. Surprisingly, a weak GFP-signal was detected to be co-localized with the eliaoplast autofluorescence. In transient localisation studies in epidermal leaf cells such (co-)localization was never detected. As control, plastids from leaf material of the transgenic lines revealed no GFP-signal suggesting an anther-specific feature.

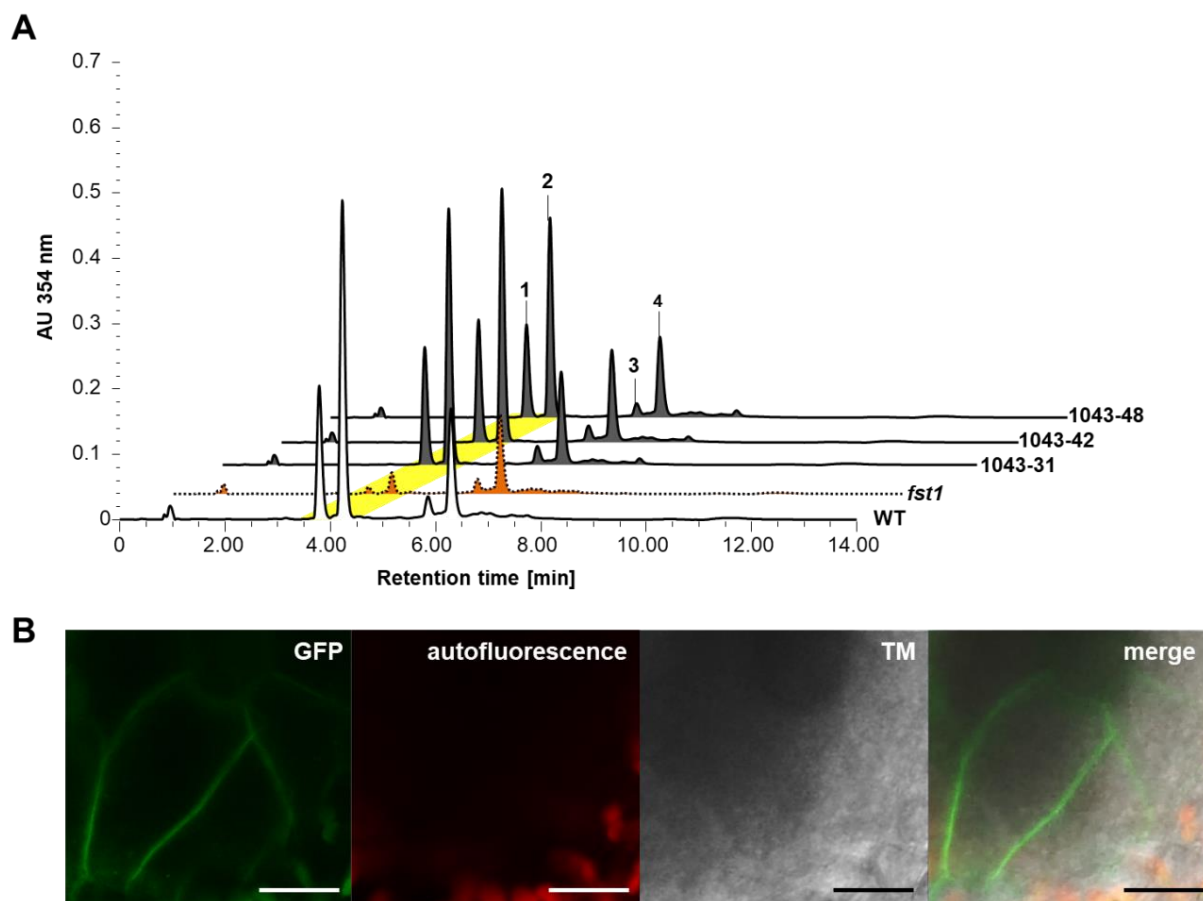


**Figure 3-10** FST1 is functional in the plasma membrane of tapetal cells.

(A) Methanolic pollen extracts from *A. thaliana* wild-type (WT) (white-filled in front), the *fst1* mutant (*fst1*) (SALK\_027288C, orange-filled, dotted line) and three independent pAGV1043 complementation lines (1043-31, 1043-42, and 1043-48). Both flavonol-3-*O*-sophorosides are highlighted in yellow. Peak numbers are: quercetin-3-*O*-sophoroside (625.3 m/z) (1) kaempferol-3-*O*-sophoroside (609.3 m/z) (2) and two major HCAAs (3 and 4). Representative confocal fluorescence images of an enlarged tapetal cell (B) from a stable pAGV1043 line encoding prom-FST1:FST1-GFP. Bar = 10 μm. The GFP-channel (GFP), the autofluorescence of the anther wall (autofluorescence), the transmission image (TM) and the merged images of all three channels (merge) are shown. Three independent lines were tested (n = 3).

The live imaged plasmalemma localization of FST1-GFP inside the tapetal cells is consistent with the previous results of the subcellular localization in epidermal leaf cells (3.4.5). The fact that the *fst1* chemotype can be complemented by FST1-GFP situated in the plasmalemma suggests that this is the functional localization of the FST1 transporter in Arabidopsis tapetal cells. A possible localization in the elaioplast envelope should carefully be confirmed by further controls. Additionally, this complementation approach suggested that GFP neither inhibited transporter function nor its localization.

### 3.5 TEM of *fst1* pollen development

Former transporter mutants involved in the exine formation were usually accompanied by ultrastructural abnormalities in the sporopollenin secreting tapetum like inclusions or incomplete pollen coat formation (Choi et al., 2014; Quilichini et al., 2014a). Based on the observed reduction of the flavonol sophoroside content in *fst1* pollen extracts, the mutant was further analysed for the appearance of such morphological changes. The direct observation of the tapetum and pollen is challenging caused by their deeply embedded localization inside the anthers. In recent reports transmission electron microscopy has been confirmed as a valuable technique for the direct imaging of these hardly accessible tissues (Choi et al., 2014; Quilichini et al., 2014a). To investigate, if the *fst1* mutation results in ultrastructural alterations in sporopollenin formation, the *fst1* mutant was examined for morphological changes in the tapetal cell layer and microspore development.

Transmission electron microscopy images of *fst1* mutant and wild-type plants exhibited no obvious variations during the observed microgametogenesis (Figure 3-11). In the *fst1* mutant, the central locule space and the anther wall were normally developed as compared to wild-type (Figures 3-11 A and E). In *fst1* and wild-type the developing pollen grains were freely distributed inside the locular liquid without any striking abnormalities in shape or exine formation. The tapetal cell layer was intact and continuously coating the locule space. Hardly to identify, thin middle layer cells appeared next to the tapetum. The endothecium cell layer appeared as normal highly vacuolated as well as the outermost cell layers, the epidermis. In the tapetum where the FST1 transporter is expressed (3.4.3) no ultrastructural anomalies were observed (Figures 3-11 B and F). No subcellular changes could be identified inside the whole tapetal cell structure. As normal the tapetal cells contained many smaller vacuoles for storage instead of one central vacuole. In contrast, tapetal mutants like the *ms1* mutant (*MALE STERILITY1*) incomplete in sporopollenin formation are accompanied by a highly vacuolated tapetum or early degeneration (Yang et al., 2007) and also devoid of flavonol sophorosides on the pollen surface (Yonekura-Sakakibara et al., 2014). The tapetum cell layer appeared darker as compared to the outermost anther wall due to the dense cytosol. The tapetal cells were packed with various storage organelles as elaioplasts, lipid drops, and starch grains. These observations indicate that the tapetal cells of both lines are functional and metabolically highly active. The presence of ER-derived vesicles termed as tapetosomes inside the tapetum was observed (Inserts Figures 3-11 B and F). No ultrastructural alterations of the ER or the tapetosomes were identified. The presence of small orbicules in the locule was observed for the wild-type as well as for the *fst1* mutant (Figures 3-11 B and F). This observation supports the concept of an orbicule independent flavonoid glycoside translocation. The microgametogenesis was compared between wild-type and *fst1*

mutant from the early bicellular stage marked by an asymmetric cell division after the first pollen mitosis (Figures 3-11 C and G) to the mature tricellular stage (Figures 3-11 D and H). No abnormalities were observed in *fst1* microspores. It indicates no effect on the earlier microsporogenesis, the microspore release, and the following microgametogenesis of the *fst1* mutation (Figures 3-11 C, D, G, and H). Early microgametogenesis (Figures 3-11 C and G) was accompanied by the formation of the exine which was completely formed at the tricellular stage (Figures 3-11 D and H). In comparison to the wild-type, the *fst1* exine exhibited a normally constructed sexine and baculae pattern filled with tryphine (Inserts Figures 3-11 D and H). Concerning that flavonol sophorosides are part of the tryphine, it was surprising that within the *fst1* tryphine no changes were visible (Insert Figure 3-11 H).

In summary, the TEM analysis indicated that the tapetal FST1 transporter has no visible influence on the formation of mature pollen grains or the morphological structure of the tapetal cells. In addition, pollen colour and growths of the *fst1* mutant plants were identical to *A. thaliana* wild-type (Appendix Figure 8-12).

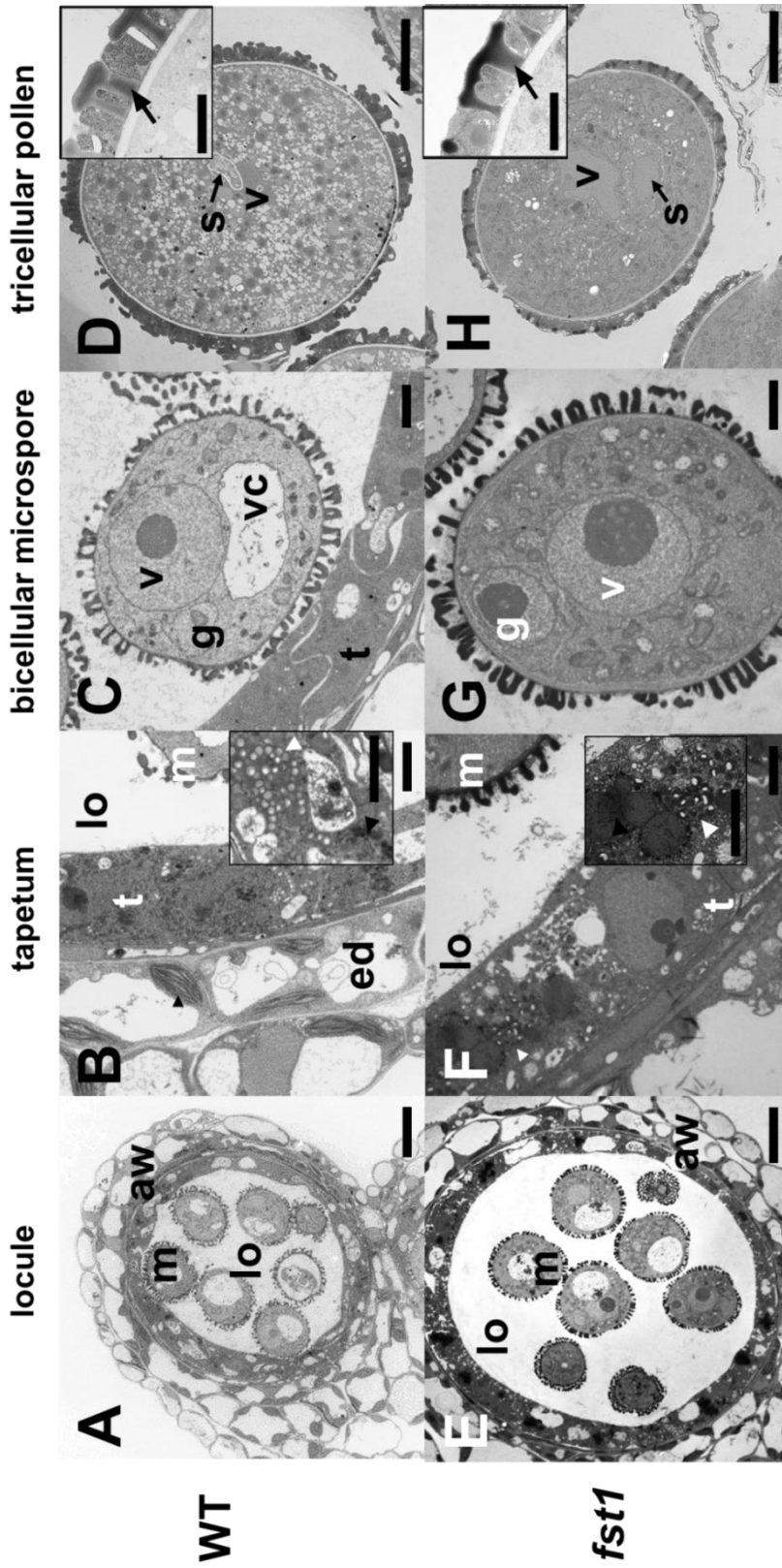


**Figure 3-11** Development of wild-type and *fst1* mutant pollen observed by TEM. No obvious morphological contrasts in the microspore development of *A. thaliana* wild-type (**A to D**) and *fst1* mutant plants (**E to H**) were observed by TEM. (**A and E**) Locular spaces (lo) with microspores (m) at the bicellular stage surrounded by the anther wall (aw). Bars = 10  $\mu$ m. (**B and F**) the tapetum (t) and the highly vacuolated endothecium (ed) cell layer during early microspore development. Chloroplasts and tapetosomes indicated by a white and black arrow head, respectively. Bars = 2  $\mu$ m. (**C and G**) Bicellular microspores after first mitosis, containing a vegetative (v) and a generative cell (g) which is strictly located in the endothecium. Bars = 2  $\mu$ m. (**D and H**) Mature, tricellular pollen grains, the central vacuole is completely decreased and the vegetative cell (v) is in a central position. Generative sperm cells are indicated by an arrow. Bars = 2  $\mu$ m. Inserts in (**D**) and (**H**) show baculae (arrows) filled with the tryphine. Bars = 1  $\mu$ m

### 3.6 No decreased *fst1* pollen fitness

To investigate whether the strongly reduced flavonol sophorosides levels cause a reduced male-fertility, *in vitro* germination rate of *fst1* pollen was determined (Figure 3-12 A). No differences were observed in morphology or dynamics of the pollen tube growth between the wild-type and the *fst1* deficient line. The mean values of the pollen tube length with a high variable standard derivation was  $262 \mu\text{m} \pm 136 \mu\text{m}$  for wild-type and  $241 \mu\text{m} \pm 140 \mu\text{m}$  for *fst1* pollen tubes. After 8 hours the *in vitro* germination rate of wild-type and *fst1* mutant line was similar with about 44% and 43%, respectively (Figure 3-12 A). It should be mentioned that *in vitro* pollen germination does not entirely simulate the *in vivo* germination where a pollen tube germination rate above 60% is reached after 30 minutes (Mayfield and Preuss, 2000). These results are consistent with the findings of Yonekura-Sakakibara et al. (2014) who reported no effect on the male fertility of a flavonol-3-*O*-sophoroside lacking *ugt79b6* Tilling line. Earlier reports already demonstrated that in case of Arabidopsis, pollen development and fertility seem to be independent of flavonoids (Burbulis et al., 1996; Ylstra et al., 1996).

Defects in the formation of the pollen coat have often been reported to result in reduced pollen viability like an increased sensibility to drought stress in case of the *abcg9* and *abcg31* transporter mutants (Choi et al., 2014). A putative flower flavonoid transporter (FFT, *At4g25640*) was postulated by Thompson et al. (2010a) to influence the pollen viability in Arabidopsis. To test, if the *fst1* pollen viability is reduced, a classical pollen viability assay was performed according to Heslop-Harrison and Heslop-Harrison, 1970 (Figure 3-12 B). The relative pollen viability of the wild-type was about 77% and about 68% for the *fst1* mutant line. The slight reduction of the *fst1* pollen viability showed just a weak significance ( $p\text{-value} = 0.018$ ). These results obviously indicate that the pollen fitness in Arabidopsis is, if at all, only slightly affected by the *fst1* mutation despite the high reduction of flavonol-3-*O*-sophorosides on the pollen coat.

The flavonoids which highly accumulate on the pollen surface of diverse plant species absorb UV-light in two ranges of 250 nm to 280 nm and 350 nm to 380 nm. Therefore, flavonoids are commonly considered to have a photoprotective function for the haploidic pollen. Hsieh and Huang (2007) described a reduced germination of pollen from the flavonoid-deficient mutants *tt4* (*chs*) and *tt12* germinating under UV-light stress. Therefore, wild-type and *fst1* pollen were exposed for zero, one, and two hours to extremely high UV-radiation, emitted by a Xenon-lamp ( $262 \mu\text{mol m}^{-2} \text{s}^{-1}$ , in a range from 300 nm to 400 nm) and the *in vitro* pollen germination was measured after two hours. Although the work of Hsieh and Huang (2007) suggested a reduced pollen tube germination rate under UV-stress, in our case no altered pollen germination was observed upon UV-radiation in the *fst1* mutant (Figure 3-12 C). This observation may lead to the assumption that flavonol sophorosides are not the major UV-protectants of pollen grains. But it should be mentioned that there were still low amounts of flavonol sophorosides present on the *fst1* pollen surface.



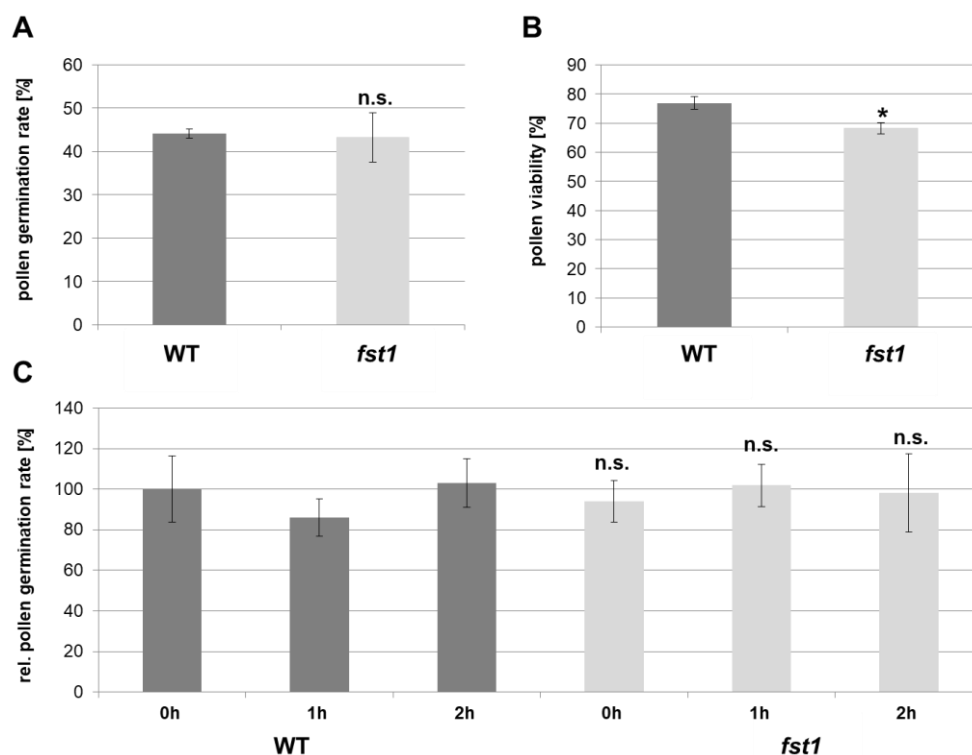


**Figure 3-12** *In vitro* pollen assays of wild-type and *fst1* mutant.

(A) The *in vitro* germination rate of wild-type (WT) and *fst1* mutant pollen (*fst1*). The pollen tube formation was observed after 8 hours. At least 300 pollen grains were counted for each trial. Three independent experiments were performed ( $n = 3$ ). (B) Comparison of the relative pollen viability between wild-type and *fst1* pollen grains examined by FDA-staining. Four replicates were analysed and 600 pollen grains were counted per trial ( $n = 4$ ). (C) Relative pollen germination with UV-treatment for zero, one and two hours. Percentage of pollen germination is shown and wild-type set to 100%. Four independent trials ( $n = 4$ ) were measured and at least 200 pollen grains were counted per trial. Shown are the relative mean values  $\pm$  standard errors. Significance analysis was performed by *students t*-test comparing wild-type with *fst1* (in C per time point) (\* indicates  $p$ -value  $< 0.05$  and ns means no significance).

### 3.7 Functional characterization of the FST1 transporter

To demonstrate the direct flavonol-3-*O*-sophoroside transport activity of FST1, uptake assays were performed in collaboration with Dr. Ilka Haferkamp. For this purpose FST1 was heterologously expressed in *E. coli* and  $^{14}\text{C}$ -labelled flavonol glycosides were tested as substrates.

The eukaryotic FST1 transporter protein was heterologously expressed in *E. coli* Rosetta 2 cells using the IPTG inducible pET16b vector system. After one hour of protein synthesis, uptake activity towards the  $^{14}\text{C}$ -labelled flavonol glycosides was determined in a time course. Non-induced cells were used as control as well as induced empty vector cells to exclude that IPTG-induction itself affects the bacterial cells (Figure 3-13 A).

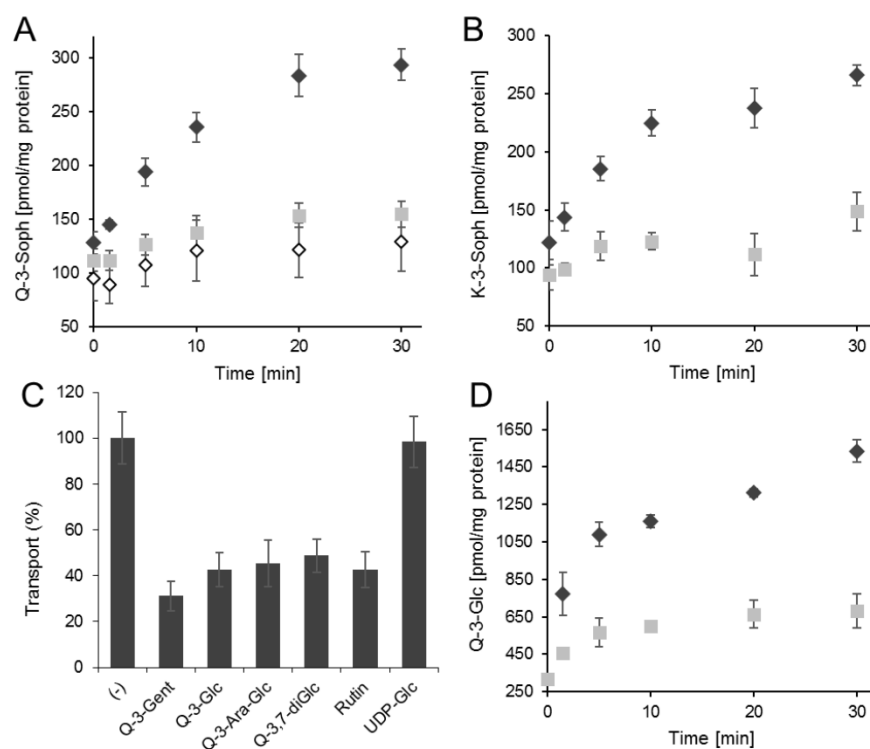


**Figure 3-13** FST1 mediates flavonol glycoside transport in *E. coli*.

Rosetta 2 cells expressing FST1 exhibited time-dependent uptake of  $^{14}\text{C}$ -labelled (A) quercetin-3-*O*-sophoroside (Q-3-Soph) and (B) kaempferol-3-*O*-sophoroside (K-3-Soph), respectively (each final conc.  $10\mu\text{M}$ ). The transported amounts of  $^{14}\text{C}$ -labelled flavonol glycosides were referred to the total amount of membrane protein (pmol/mg protein). Indication: IPTG induced cells (black rhombs), non-induced cells (grey squares) and empty vector control (white rhombs). (C) Investigation of a preferred flavonol glycoside specificity by *cis*-inhibitory uptake assays with transport medium containing final  $10\mu\text{M}$   $^{14}\text{C}$ -labelled quercetin-3-*O*-sophoroside without effector (-) and with ten times excess ( $100\mu\text{M}$ ) of unlabelled flavonol glycosides. Tested effectors were quercetin-3-*O*-gentioidoside (Q-3-Gent), quercetin-3-*O*-glucoside (Q-3-Glc), quercetin-3-*O*-arabinoglucoside (Q-3-Ara-Glc), quercetin-3,7-*O*-diglucoside (Q-3,7-diGlc), quercetin-3-*O*-rhamnosido-glucoside (Rutin) and UDP-glucose as additional control. Shown are the relative transport activities referred to the unsupplemented  $^{14}\text{C}$ -quercetin-3-*O*-sophoroside uptake. (D) Time-dependent uptake of  $^{14}\text{C}$ -labelled quercetin-3-*O*-glucoside (Q-3-Glc) (final conc.  $10\mu\text{M}$ ) by induced cells. In each data set mean values of at least three independent trials are represented. Standard errors are indicated. (Modified from Grunewald et al., 2020).

When the uptake activity was compared to both controls, a time-dependent uptake of the  $^{14}\text{C}$ -flavonol-3-*O*-sophorosides was observed in induced cells (Figures 3-13 A and B). Thereby, a saturation of the transport activity was recognized after 30 minutes. No substrate preference was notable between both tested flavonol-3-*O*-sophorosides. The uptake was reduced by a ten times excess of various unlabelled flavonol glycosides, as tested by *cis*-inhibition assays (Figure 3-13 C). In contrast UDP-glucose was not able to affect the transport, clearly indicating that the observed uptake is not initiated by an endogenous response of *E. coli* towards glycosylated molecules. This confirms that no  $^{14}\text{C}$ -UDP-glucose perhaps residual from the flavonol glycoside  $^{14}\text{C}$ -labelling was transported. Furthermore, it proves that even in high excess UDP-glucose acts not as a substrate of FST1 and intact glycosides were translocated.

Different flavonol glycosides were tested for the influence of the glycosylation pattern on the substrate specificity. Apparently, no preferred glycosylation pattern could be identified. The monoglucoside quercetin-3-*O*-glucoside was taken up with even higher activity compared to the diglucosides

(Figure 3-13 D). Several flavonoid glycosides were able to compete for the transport activity, when added in excess in a similar way (Figure 3-13 C). Similar competition was detected between quercetin-3-*O*-rhamnosido-glucoside (rutin) (1→6 *rha-glc*), quercetin-3-*O*-gentiobioside (1→6 *glc-glc*) and quercetin-3-*O*-arabinoglucoside (1→6 *ara-glc*). Even the quercetin-3,7-*O*-diglucoside, where the glucose residues are at the 7-OH-position of the A-ring showed similar inhibitory effects. In conclusion, the transporter assays demonstrated that FST1 accepts several closely related flavonol glycosides and has no specificity towards the 1→2 glucose-glucose-linkage of the sophorosides.

The alignment of the phylogenetic analysis (3.8) revealed that the EXXEK-motif which is required for substrate binding and transport activity of the GTR2 (Jørgensen et al., 2015) is present in FST1 and its putative orthologues (Figure 3-14 A). Notably, Phe was frequently included as second non-determined amino acid (X) within the EXXEK-motif of the FST1- and GTR2-subgroup, respectively. To test their influence, the residues Glu (position 31) and Phe (position 33) were exchanged by site-directed mutagenesis to Ala and Asp, respectively. The mutated FST1 variants were tested in a second transporter study (Figure 3-14 B) regarding their activity towards <sup>14</sup>C-labelled quercetin-3-*O*-sophoroside. But strikingly, no significantly reduced or enhanced transporter activities were found.

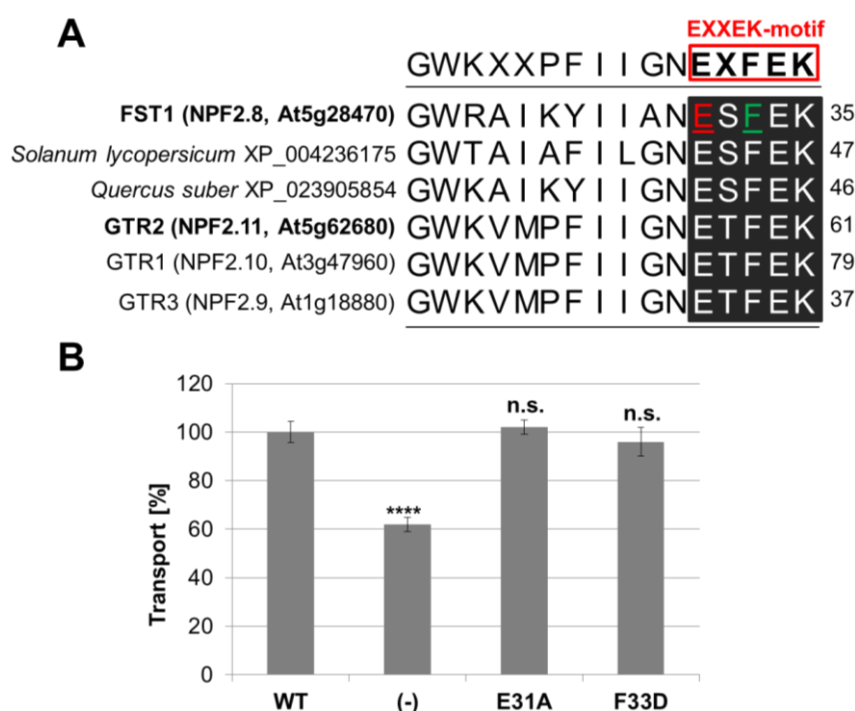


**Figure 3-14** A changed EXXEK-motif did not affect the FST1 transporter activity.

(A) EXXEK-motif (red-indicated) of FST1 (bold), two FST1 orthologues from *S. lycopersicum* (XP\_004236175) and *Q. suber* (XP\_023905854), and the glucosinolate transporters GTR1 (NPF2.10), GTR2 (NPF2.11, bold) and GTR3 (NPF2.9). Exchanged amino acid positions of glutamate (red) and phenylalanine (green) within the FST1 EXXEK-motif are underlined. (B) Uptake rates of the FST1 wild-type variant (WT) and the FST1 amino acid exchange variants E31A (E31A) and F33D (F33D). Only the non-induced control (-) showed decreased transport activity. The transport rate of radiolabelled substrate was determined and the FST1 wild-type variant set to 100%. Four independent trials ( $n = 4$ ) were measured using a final concentration of 10  $\mu$ M <sup>14</sup>C-labelled quercetin-3-*O*-sophoroside. Shown are the relative mean values  $\pm$  standard errors. Significance analysis was performed by *students t*-test comparing each FST1 variant to wild-type (\*\*\*\* indicates  $p$ -value < 0.0001 and n.s. means no significance).

### 3.8 Phylogenetic analysis

FST1 is categorized as a member of the heterogeneous NRT1/PTR family within the major facilitator superfamily (Patil et al., 2019; Jørgensen et al., 2017). The transporter protein consists of 559 amino acids.

The amino acid sequence of FST1 (*At5g28470*) was subjected to the NCBI protein BLAST software and relevant orthologues with high sequence similarities were selected for phylogenetic analysis. For investigation of the evolved substrate specificity, the GTR1 (*At3g47960*) and GTR2 (*At5g62680*) NRT1/NPF family members which are well-established as glucosinolate transporters (Nour-Eldin et al., 2012; Jørgensen et al., 2017) were included. As an out-group, the as “most studied” (Li et al., 2010) declared dual-nitrate transporter NRT1.1 (*At1g12110*) expressed in lateral roots and guard cells was integrated (Okamoto et al., 2003). Moreover, NRT1.1 was crystallized by two independent studies (Parker and Newstead, 2014; Sun et al., 2014). FST1 shares about 27% amino acid sequence homology to NRT1.1. Protein sequences were aligned using the ClustalW alignment mode of the MegAlign software and a bootstrapped cladogram was generated (Figure 3-15). The phylogenetic tree clusters into two clades followed indicated as clade I and clade II (indicated as brackets on the right side). FST1 and putative FST1 orthologues are members of clade I. The second clearly distinct clade II contains of GTR1, GTR2 and appropriate orthologues, like glucosinolate transporters. The strict separation of FST1 from the GTR1/GTR2 group seems contra dictionary to the first categorization by Jørgensen et al. (2017) and the presumed glucosinolate transporter capability of the NPF group including FST1. Additionally, FST1 had no glucosinolate transporter activity in oocyte assays (Jørgensen et al., 2017) and its protein sequence was just about 38% homologous to the GTR1 and GTR2 glucosinolate transporters.

Orthologous proteins with at least 30% sequence identity to the FST1 candidate were identified by the NCBI BLAST in nearly all plant species. A selection of relevant candidates from eight different plant families (Brassicaceae, Cleomaceae, Rosaceae, Fagaceae, Fabaceae, Solanaceae, Salicaceae and Poaceae) is presented in the cladogram. FST1 homologous from evolutionary distant angiosperms like *Coffea arabica* (Rubiaceae), *Olea europea* (Oleaceae), *Cucumis melo* (Cucurbitaceae) or *Theobroma cacao* (Malvaceae) with amino acid sequence identities over 50% were also identified in the NCBI database. Representatives of all pollination types - anemophilous angiosperms, dicots (Salicaceae, Fagaceae) as well as monocots (Poaceae), various types of entomophilous plants (*Malus domestica*, *Nicotiana tabacum*) and self-pollinators (*Glycine max*, *Capsicum anuum*) are represented.

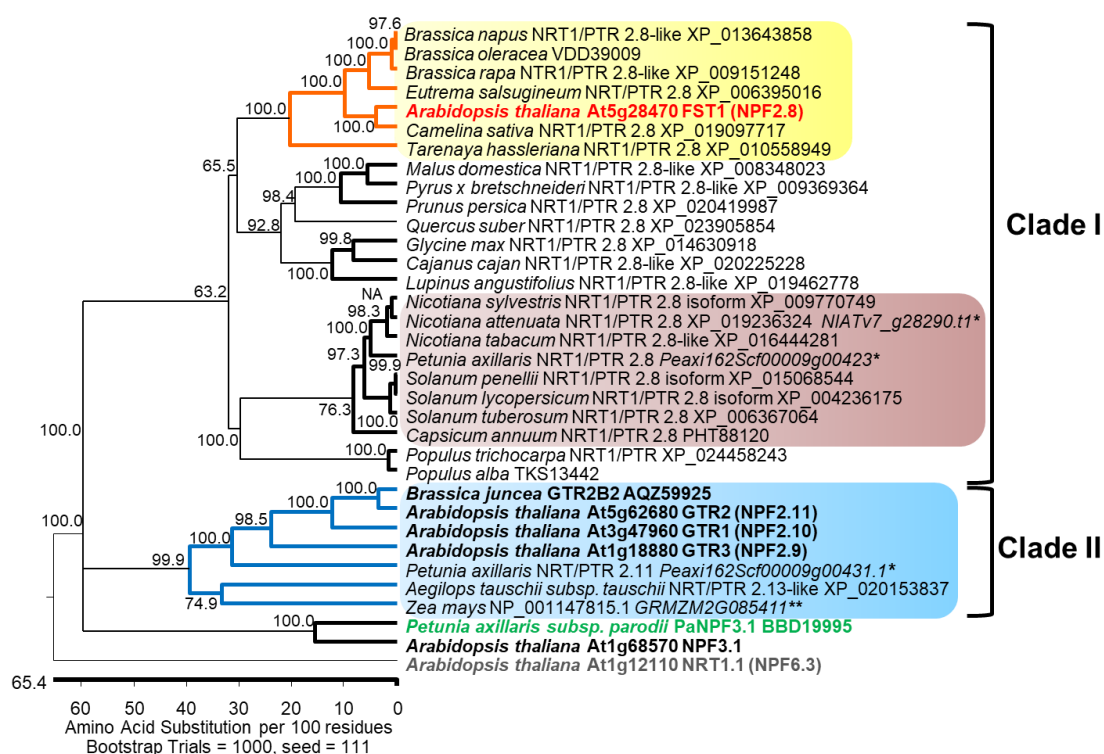


**Figure 3-15** FST1 defines a new clade within the NPF-family.

Orthologous proteins of FST1 were selected by high sequence similarity included in a bootstrapped phylogenetic tree generated by using the MegAlign software. The percentages of the bootstrap-values are shown at each branch. NA means that no value was available. The bootstrap analysis was repeated in 1000 trials. The scaling indicates the amino acid exchanges per 100 residues. Yellow highlighted are the FST1 orthologues from the Brassicaceae including FST1 (*At5g28470*) (red, bold). A purple background indicates the large subgroup of FST1 (NPF 2.8) orthologues from Solanaceae species. Both subgroups are included in clade I which is distinctly separated from clade II including the subgroup of the glycosinolate transporters marked in blue. Each subclade is characterized by > 50% sequence identity. Functionally well characterized candidates are printed black bold. The *Petunia* orthologue PaNPF3.1 (green, bold) is suggested by Amano et al. (2018) as a putative gibberellin transporter. The high affinity nitrate transporter NRT1.1 (*At1g12110*) (grey, bold) crystallized by Parker and Newstead (2014) was included as outgroup. NCBI reference sequence accessions or TAIR gene loci accessions are specified for each candidate. If the protein sequences were not contained in the NCBI database, the gene loci accessions are presented that were obtained from the Sol Genomics Network (<https://solgenomics.net/>) and the Maize Genetics and Genomics Database (<https://maizegdb.org/>), respectively (indicated by \* and \*\*).

A broad subgroup of Solanaceae NRT1/NPF 2.8 orthologues was found, which exhibited sequence similarities of about 50% like the NRT1/NPF 2.8 orthologue from potato (*Solanum tuberosum*, 57%), tomato (*Solanum lycopersicum*, 56%), tobacco (*Nicotiana tabacum*, 56%) or chili pepper (*Capsicum annuum*, 55%). Similar high sequence identities were found for putative orthologous candidates from other plant families like apple (*Malus domestica*, 58%) or pecan nuts (*Cajanus cajan*, 58%). The wide distribution suggests a putative biological function of the transported compounds, not exclusively for a specific pollination type. In contrast, protein sequences from the two monocotyledon candidates, maize (*Zea mays*) and *Aegilops tauschii* display a maximum sequence identity of 38% and 40%. In contrast, the homology to GTR2 was about 52%. In the Maize Genetics and Genomics Database (<https://maizegdb.org/>) no candidates with higher sequence similarity to FST1 were found. Whether the different mostly amoeboid tapetum type of monocots has an influence on the putative conservation is speculative. Concerning this, a completely different mechanism for the storage and translocation of proteins and flavonoids in the maize tapetum was postulated by Li et al. (2012).

Consistent with the verified anther-specific *FST1* expression, several orthologues of the Solanaceae family were suggested by ePlant (<http://bar.utoronto.ca/eplant/>) and the *Nicotiana attenuata* DataHUB (<http://nadh.ice.mpg.de/NaDH/>) to be expressed in the male reproductive organs. This again emphasizes the conserved activity of FST1 and its putative role in plant reproduction given the fact that biological function of flavonols was among others firstly described for the pollen fertility in Solanaceae species (Mo et al., 1992; Ylstra et al., 1992). In the case of the poplar orthologues expression was annotated for the male and female ‘catkins’ ([http://bar.utoronto.ca/eplant\\_poplar/](http://bar.utoronto.ca/eplant_poplar/)). The putative FST1 orthologue from *Z. mays* (*GRMZM2g085411*) is also indicated to be specifically expressed in anthers and ‘tassels’ by the ePlant viewer ([http://bar.utoronto.ca/eplant\\_maize/](http://bar.utoronto.ca/eplant_maize/)).

It is tempting to speculate about an association of a conserved role of the FST1 candidate, the transported flavonols, and plant reproduction in higher plants, specifically *Petunia* (Mo et al., 1992). However, a sequence like the Arabidopsis gibberellin importer NPF3.1 from *Petunia axillaris* with just 37% homology was the closest candidate in the NCBI database. PaNPF3.1 was shown to be expressed in the whole flower including stamen, but especially in limbs (Amano et al., 2018). Together with the Arabidopsis NPF3.1, PaNPF3.1 forms the core of an own, distinct clade (Figure 3-15) excluding PaNPF3.1 as a FST1 orthologue. Two homologs from *P. axillaris* with higher protein sequence identities of about 55% and 39% were identified as NTR1/PTR family members with similarity to FST1 and GTR2, respectively, in the Sol Genomics Network database (<https://solgenomics.net/>). Both candidates clustered well into the appropriate clade I or clade II of Figure 3-15. This illustrates that the generated phylogenetic tree is reliable.

### 3.9 Localization and biological relevance of phenylpropanoids

Besides efforts to elucidate the transport mechanism of flavonol sophorosides, subcellular localization of the tapetum-specific UGT79B6 and the generation of ‘phenylpropanoid-free’ pollen were of interest to reveal further biological functions of phenylpropanoids.

#### 3.9.1 Subcellular localization of the UGT79B6

In contrast to the most mammalian UGTs which are situated in the endoplasmic reticulum or the Golgi apparatus, plant UGTs are considered as-soluble enzymes (Li et al., 2015; Sun et al., 2016). Contradictory to a former postulated membrane association (Vogt and Taylor, 1995), the localization of UGT79B31, an orthologous 1 → 2 glycoside-galactosyltransferase from *Petunia hybrida* was recently reported to be cytosolic (Knoch et al., 2018).

By TAIR (<https://www.arabidopsis.org/>), UGT79B6 is described as an intracellular membrane/organelle-bounded protein located in chloroplasts, but inconsistent with the lack of plastidic transit peptides, S-acylation, or N-terminal myristoylation sites as determined by ChloroP ([www.cbs.dtu.dk/services/ChloroP/](http://www.cbs.dtu.dk/services/ChloroP/)), SwissPalm (<https://swisspalm.org/proteins>), and Myristoylator (<https://web.expasy.org/myristoylator/>). *In silico* prediction by SUBA (<https://suba.live/>) was also not convincing and suggested an extracellular or plasma membrane bound localization. To determine the

subcellular localization of the UGT79B6 (*At5g54010*), the construct pAGV561 was expressed in *N. benthamiana* leaf protoplasts (Figure 3-16).

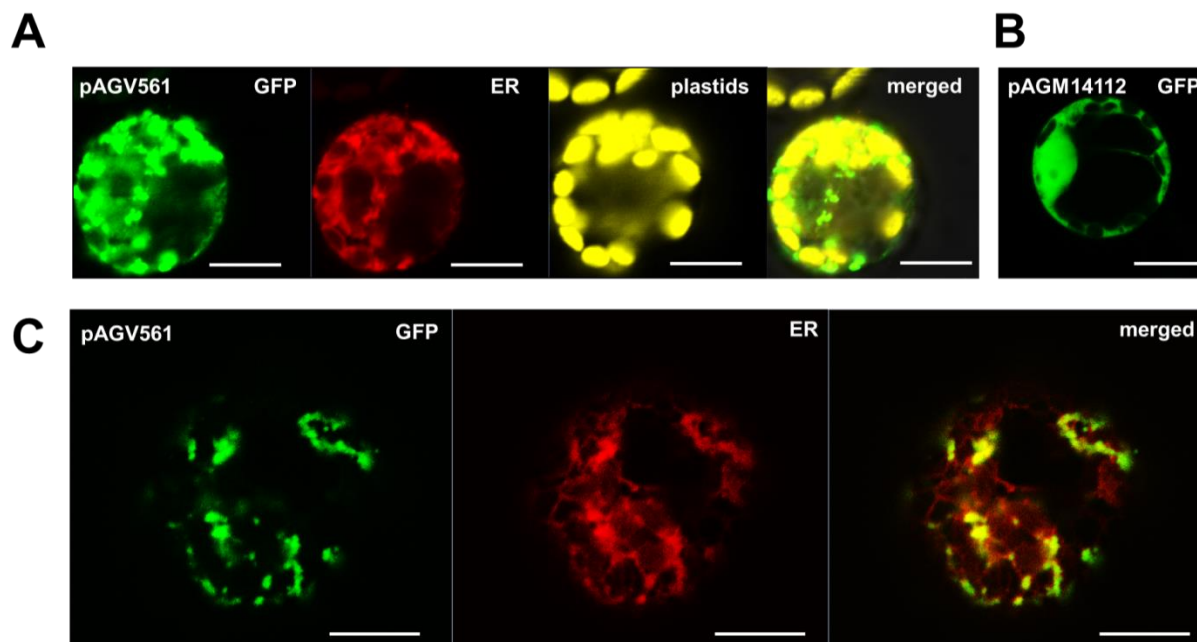


**Figure 3-16** Localization of the UGT79B6 to the ER.

Representative confocal fluorescence images of *N. benthamiana* mesophyll protoplasts expressing pAGV561 encoding prom35S:UGT79B6-GFP. **(A)** A protoplast co-expressing pAGV561 and the mCherry-tagged ER-organelle marker CD3-959. The focus is placed inside the protoplast on the cortical ER. Bars = 10  $\mu$ m. **(B)** For comparison the construct pAGM14112 was used as positive control to express free GFP. Bar = 10  $\mu$ m. **(C)** To clearly image the ER-associated GFP-signal an array scan was performed which increased the resolution of the fine reticular ER pattern. The autofluorescence of the plastids was removed for a better visualization of the signal. Bars = 10  $\mu$ m. Pictured are the GFP-channel (GFP), a channel for the mCherry fluorescence of the ER-marker (ER), the autofluorescence of chlorophyll A (plastids, yellow coloured), and the merged image (merge).

The GFP-reporter protein was fused to the C-terminus of the UGT79B6. Surprisingly, the GFP-fluorescence of UGT79B6-GFP (pAGV561) showed a spotted appearance indicating a putative ER-localization (Figure 3-16 A) and was un-typical for a soluble protein (Figure 3-16 B). The observed GFP-signals were not randomly situated rather it seemed to be associated to the ER-signal (Figure 3-16 A). To make a more precise statement, protoplasts were co-transformed with the mCherry labelled ER-marker CD3-959 (Nelson et al., 2007). For a better visualisation of the ER-signal the images were focussed near to the cortical cytoplasm as advised by Nelson et al. (2007). To show the co-localization and the reticulate pattern in more detail, an array-scan was performed and the autofluorescence of the plastids was dismissed (Figure 3-16 C). The clearly discernible structure of the UGT79B6-GFP seems to be directly attached to the fine branched ER-network revealing a (partial) co-localization with the endoplasmic reticulum. The labelled endoplasmic reticulum forms an extensive network inside the cell of fine tubular and sheet-like elements (Figure 3-16 C). The structure of the observed GFP-fluorescence signal did not correspond to the typical morphology of punctate organelles like mitochondria or peroxisomes (Nelson et al., 2007). Localization to the Golgi apparatus was also excluded. A signal of the Golgi apparatus would appear randomly distributed throughout the cortical cytoplasm and would also occur in

transvacuolar strands (Nebenführ et al., 1999). Additionally, signals of the Golgi stacks are typically smaller spots and lines forming disc-like structures or rings (Nebenführ et al., 1999).

Expression of the full-length fusion protein was confirmed by immunoblot analysis (Appendix Figure 8-7 A). The blotted UGT79B6-GFP fusion protein showed a lower molecular mass than expected. This might be caused by truncation of the UGT79B6-GFP due to the strong 35S-promotor driven ectopic overexpression, incomplete denaturation or lipidation. Additionally, the construct pAGV561 was also tested in Arabidopsis leaf protoplasts to exclude species effects (Appendix Figure 8-7 B). A construct encoding UGT79B6 fused to an N-terminal GFP reporter (pAGV581) exhibited a similar retiform stippled GFP-signal that was not co-localized to cytosolic mCherry (Appendix Figure 8-7 C).

In summary, the current results suggest that the UGT79B6 could be associated with the ER consistent with an attachment to a transient ER-associated flavonoid metabolon (Burbulis and Winkel-Shirley, 1999; Dastmalchi et al., 2016).

### **3.9.2 Generation of a 'phenylpropanoid-free' pollen coat mutant**

Despite the well-established biosynthesis of anther-specific phenylpropanoids there is a great lack of understanding about their function *in planta*. As a first approach to reveal the biological function of the two major phenylpropanoids in Arabidopsis pollen, the flavonol-3-*O*-sophorosides and the hydroxycinnamic amide acids, the null mutants *78d2* and *sht* were crossed. Former studies identified the glycosyltransferase UGT78D2 (*At5g17050*) as limiting for the first step in sophoroside biosynthesis and the presence of flavonol-3-*O*-sophorosides on the pollen surface (unpublished data, Grunewald and Vogt). A flavonol-dependent feedback repression and strongly reduced flavonoid levels were described for *78d1* x *78d2* double knockout lines impaired in the two major flavonol-3-*O*-glycosyltransferases in Arabidopsis (Yin et al, 2012). *UGT78D2* is flower and anther specifically expressed compared to the ubiquitous *UGT78D1* (*At1g30530*). The spermidine hydroxycinnamoyl transferase (SHT, *At2g19070*) was characterized to catalyze the essential step in HCAA biosynthesis (Grienenberger et al., 2009; Fellenberg et al., 2009). In conclusion, a *78d2* x *sht* double mutant should produce "phenylpropanoid-free" pollen, which would be a valuable tool for the functional characterization of these compounds on the pollen coat.

Methanolic pollen extracts from wild-type and the newly generated *78d2* x *sht* double mutant as well as the two single mutants *78d2* and *sht* were analysed by HPTLC and HPLC-MS (Figure 3-17). The phenylpropanoid composition of each line is shown by the TLC-images (Figures 3-17 A and B). For a better visualization, the compounds were stained by DPBA and illuminated at 366 nm, clearly indicating quercetin-3-*O*-sophoroside (yellow), kaempferol-3-*O*-sophoroside (green), and the HCAs (blue). In wild-type, both phenylpropanoid classes are present in pollen extracts (Figure 3-17 C).



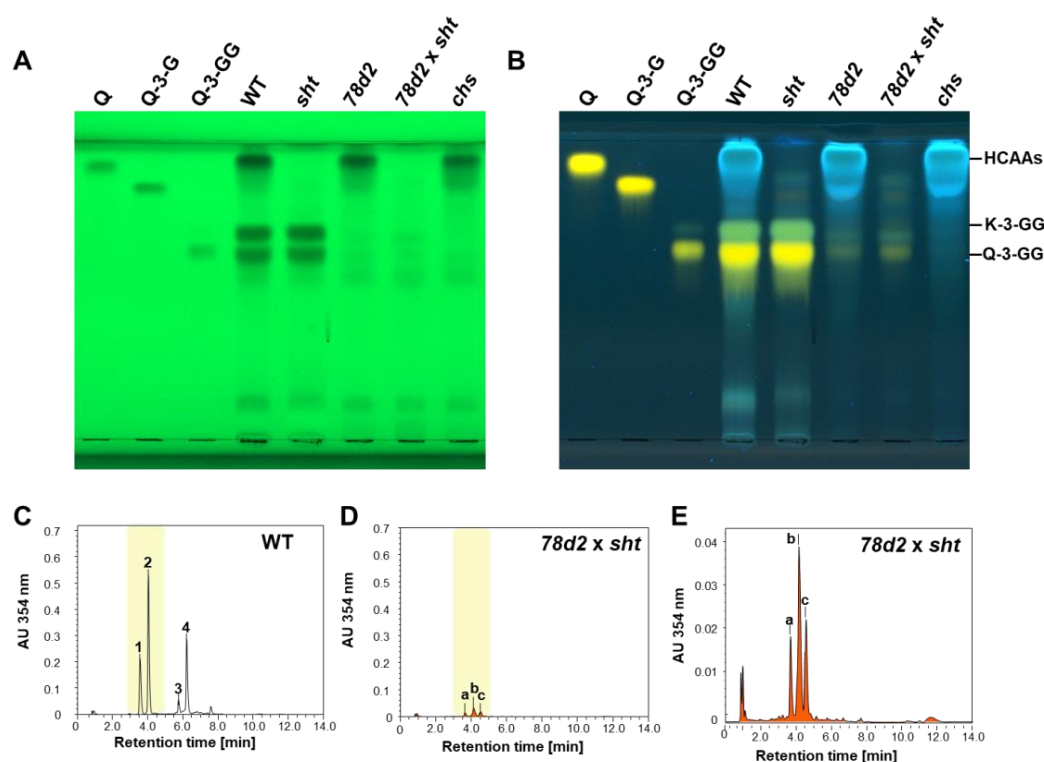


**Figure 3-17** Reduced phenylpropanoid levels of *78d2 x sht* pollen.

(A and B) Methanolic pollen extracts from wild-type (WT), the *78d2 x sht* (*78d2 x sht*) as well as the single mutants *78d2* (*78d2*) and *sht* (*sht*) and the *chs* mutant were analysed by HPTLC. The phenylpropanoid pattern was detected (A) before and (B) after DPBA staining illuminated at 254 nm and 366 nm, respectively. Thereby, the hydroxycinnamic acid amides (HCAAs) are blue and the flavonol sophorosides are coloured in green (kaempferol-3-*O*-sophoroside, K-3-GG) and yellow (quercetin-3-*O*-sophoroside, Q-3-GG). Standards: quercetin (Q), quercetin-3-*O*-glucoside (Q-3-G) and quercetin-3-*O*-sophoroside (Q-3-GG). (C, D and E) HPLC-MS analysis of the *78d2 x sht* pollen extract distinctly revealed the nearly absence of both phenylpropanoid classes as compared to the wild-type (WT). The flavonol diglucosides (1) quercetin-3-*O*-sophoroside (625.3 m/z) and (2) kaempferol-3-*O*-sophoroside (609.3 m/z) are highlighted in yellow. The HCAAs (3) with 720.4 m/z and (4) with 734.3 m/z are completely absent. (E) Scaled up chromatogram of the residual compounds on the *78d2 x sht* pollen coat preliminary identified as (a) an residual quercetin-3-*O*-sophoroside (625.3 m/z), (b) an isorhamnetin diglycoside (639.3 m/z) and (c) a putative isorhamnetin-pentose-hexose (607.3 m/z).

Flavonol sophorosides are present in the *sht* single mutant, whereas HCAAs are absent. The flavonol-3-*O*-glycosyltransferase knockout *78d2* exhibited a nearly complete reduction of both flavonol sophorosides, but the content of HCAAs was not reduced. The HPLC-MS analysis of *78d2 x sht* pollen extracts revealed only traces of flavonoid glycosides (Figures 3-17 D and E). 1 mg pollen material extracted in 90% (v/v) methanol was loaded on each lane. For HPLC-MS analysis and the quantification of flavonol sophoroside content (Table 3-4), the extracts were diluted and quantified by the standard curve based on quercetin-3-*O*-glucoside and kaempferol-3-*O*-glucoside (Appendix Figure 8-8). For wild-type, mean values of 523 pmol/mg (quercetin-3-*O*-sophoroside) and 1104 pmol/mg (kaempferol-3-*O*-sophoroside) were determined. The *78d2 x sht* mutant showed strongly reduced levels of 43 pmol/mg for quercetin-3-*O*-sophoroside. The kaempferol-3-*O*-sophoroside was not detectable at all in the mutant. Instead, peaks for isorhamnetin diglycoside (639.3 m/z) and a putative isorhamnetin-pentose-hexose (607.3 m/z) were identified from the mutant. Summarizing, the *78d2 x sht* double knockout line exhibited a nearly complete reduction of flavonol diglycosides as well as HCAAs on their pollen coat.

**Table 3-4** Quantification of flavonol-3-*O*-sophorosides on *78d2* x *sht* pollen. Quantities of quercetin- and kaempferol-3-*O*-sophoroside were quantified based on UV354nm-absorbance of quercetin- and kaempferol-3-*O*-glucoside. Presented are the mean values  $\pm$  standard deviation ( $n = 3$ ), n.d. means not detectable.

compound	wild-type [pmol/mg pollen]	<i>fst1</i> [pmol/mg pollen]
Quercetin-3- <i>O</i> -sophoroside	523 $\pm$ 48	43 $\pm$ 8
Kaempferol-3- <i>O</i> -sophoroside	1104 $\pm$ 152	n.d.

### 3.9.3 Morphological appearance of the *78d2* x *sht* mutant

The *78d2* x *sht* mutant plants exhibited a combination of the formerly described single mutant phenotypes (Yin et al., 2014; Grienenberger et al., 2009) when grown under greenhouse conditions.

The double mutant showed a dwarf-growth phenotype (Figure 3-18) in the green house as described before for the *78d2* T-DNA line (SALK\_049338C) (Yin et al., 2014). This dwarf phenotype of *78d2* likely appears due to the impact of the flavonoid glycosyltransferase on the polar auxin transport (Yin et al., 2014).

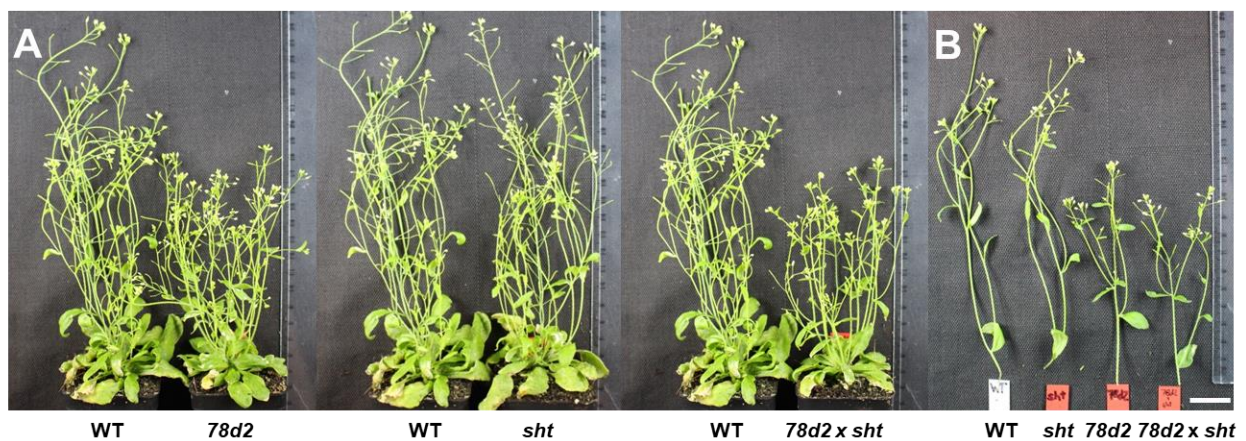


**Figure 3-18** Morphological appearance of *78d2* x *sht* in the green house.

(A) Comparison of the growth size of Arabidopsis wild-type (WT), the *78d2* x *sht* (*78d2* x *sht*) and the respective single mutant line *sht* (*sht*) and *78d2* (*78d2*). (B) Shoots of the wild-type and the individual mutant lines. Beside the clearly evident dwarf growth of the *78d2* x *sht* line caused by the *78d2* mutation (Yin et al., 2014), no morphological changes were obvious concerning shoot branching, leaf size or siliques. Arabidopsis plants were pictured after 25 days of growth. Bar = 2 cm.

The *78d2* x *sht* pollen colour was pale yellow, like that of the *sht* mutant (Figure 3-19). In contrast, the flavonoid deficient *78d2* mutant pollen exhibited an ochre colour similar to the wild-type pollen. Interestingly, this observation is in line with data of Grienenberger et al. (2009) who noticed changed autofluorescence of *sht* knockout pollen. This illustrates that the flavonols itself have surprisingly no visual impact on the pollen colour in Arabidopsis. The yellow pollen colouration is due to the absence of HCAs on the pollen coat. Manifestation of other typical pollen phenotypes like glossy, sticky or square forms according to the categories of Dobritsa et al. (2011) were not obviously changed in *78d2* x *sht* pollen grains. An alternated branching or less mature siliques were not observed. Shorter stamen filaments as described for the *myb99* mutant (Battat et al., 2019) were not observed.



**Figure 3-19** Colouration of wild-type, *78d2 x sht*, *sht*, and *78d2* mutant pollen.

Wild-type pollen (WT) has an ochre colour whereas the *78d2 x sht* (*78d2 x sht*) and the *sht* mutant pollen (*sht*) are pale yellow. The flavonoid deficient *78d2* mutant pollen (*78d2*) is coloured as the wild-type. Bar = 2 cm.

### 3.9.4 *78d2 x sht* pollen development revealed no ultrastructural variances

In contrast to the characterized *fst1* transporter mutant, the *78d2 x sht* line contains two null mutations of genes which are essential for the flavonol-3-*O*-sophoroside and HCAA biosynthesis (3.9.2). A complete lack of these compounds which are synthesised and stored in the tapetum could lead to structural changes helpful to identify their location within the tapetal cell. Direct spatial visualization of metabolites would otherwise just be possible by MS-imaging which did not work (data not shown).

Cross sections of anthers from wild-type and the *78d2 x sht* line were subjected to TEM microscopy to detect putative ultrastructural changes. Additionally, young inflorescences were stained with toluidine blue and analysed by light microscopy. The toluidine blue staining showed no obvious morphological changes between wild-type and *78d2 x sht* mutant plants (Figures 3-20 A and E). The majority of *78d2 x sht* microspores were comparable to wild-type concerning pollen grain number, size, and shape. Slight abnormalities of the pollen structure including pollen wall irregularities and depressions as recently discussed for the *sht* mutant (Grienenberger et al., 2009; Elejalde-Palmett et al., 2015) were not identified.

TEM microscopy revealed no structural changes within the *78d2 x sht* tapetum (Figures 3-20 B and F). The tapetum appeared intact and functional during the early microgametogenesis. Tapetosomes of wild-type as well as *78d2 x sht* were closely distributed to the fine ER-extensions and possessed dense, punctate structures identified as vesicles. No obvious changes of the tapetosomal structures were observed. Besides, no visible structural alterations of the ER, where the UGT79B6 (3.9.1) might be located and flavonoid biosynthesis takes place (Nakayama et al, 2019), were noted. The vacuole pattern and the number of orbicules of the anther wall were also unchanged. Asynchronous divided generative and vegetative cells and the intact tricellular pollen indicate a normal microgametogenesis (Figures 3-20 C, D, F, and G). Despite both phenylpropanoids are absent in the double mutant, the tryphine appeared unchanged compared to wild-type (Figures 3-20 D and F).



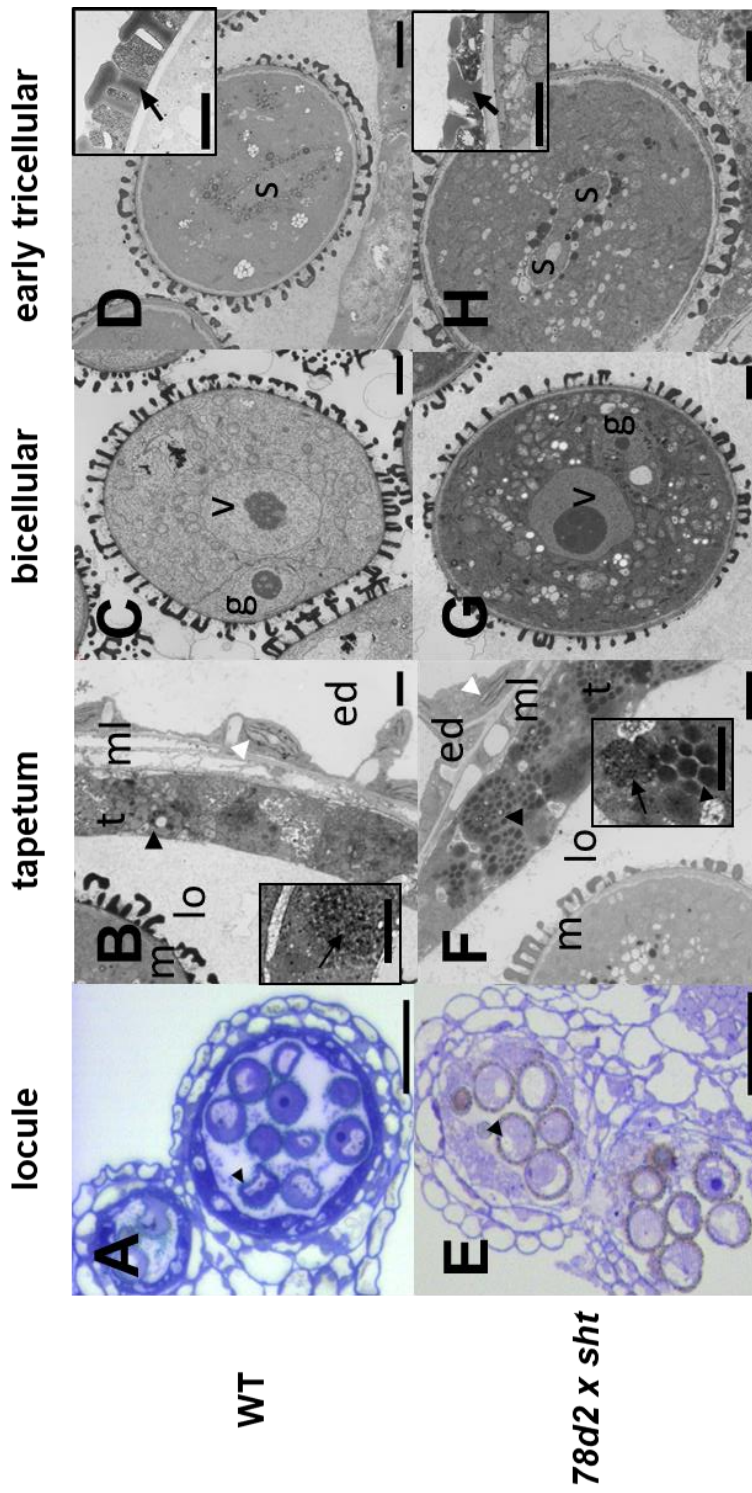


**Figure 3-20** Pollen development of the *78d2 x sht* mutant.

Microspore development of wild-type (**A to D**) and *78d2 x sht* mutant (**E to H**) visualized by light microscopy (**A** and **E**) and TEM (**B**, **C**, **D**, **F**, **G** and **H**). Pollen and tapetal cells exhibited no morphological anomalies. (**A** and **E**) Pollen sacs during early microgametogenesis stained by toluidine blue are normally developed. Microspores are indicated by an arrow head. Bars = 100  $\mu$ m. (**B** and **F**) The microspores (**m**) inside the locular space (**lo**) are coated by the anther wall formed by the tapetal cell layer (**t**), the middle layer (**ml**), the endothecium (**ed**) and the epidermis (not pictured). Tapetal eliaoplasts and chloroplasts of the anther wall are marked by a black and white arrow head, respectively. Bars = 2  $\mu$ m. The Inserts in **B** and **F** indicate tapetosomes (arrow) and an eliaoplast (arrowhead). Bars = 2  $\mu$ m. (**C** and **G**) Bicellular pollen before the second mitosis with clearly unequal divided generative (**g**) and central vegetative (**v**) cell. Bars = 2  $\mu$ m. (**D** and **H**) Early tricellular pollen grains after the second mitosis appear normally. The generative sperm cells (**s**) are indicated. The deposition of the tryphine inside the pollen coat is still incomplete for both lines at this stage. Bars = 2  $\mu$ m. Inserts in (**D**) and (**H**) show baculae (arrows) filled with the tryphine. Bars = 1  $\mu$ m

### 3.9.5 Preliminary assays with *78d2 x sht* mutant pollen

The 'phenylpropanoid-free' *78d2 x sht* pollen coat might be associated with defects in plant fertility as discussed decades ago (Martin-Tanguy, 1985). However, *in vitro* pollen tube germination rates of 44% for the *78d2 x sht* mutant were comparable to wild-type with 46% (Figure 3-21 A). Morphological differences in pollen tube length or shape were not detected between wild-type and double mutant. This result is consistent with data of the *fst1* line which has reduced levels of flavonoids (3.6) and a previous study by Grienenberger et al. (2009) that mentioned no altered pollen fertility by the *sht* mutation in *Arabidopsis*.

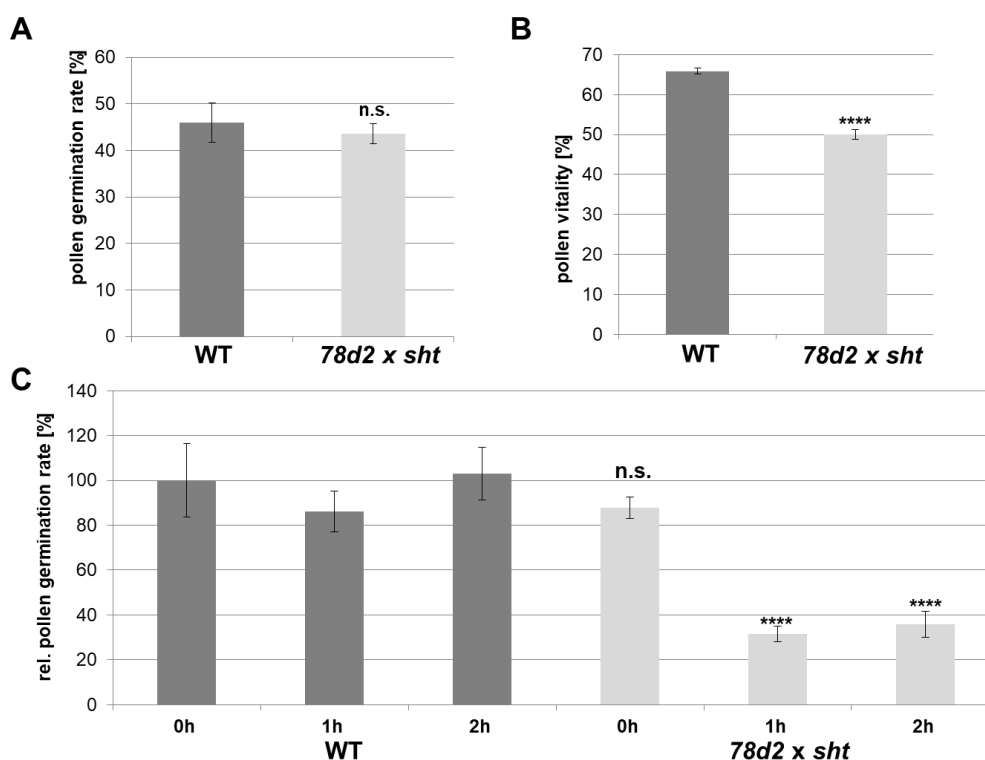


**Figure 3-21** Classical pollen assays of wild-type and *78d2 x sht* mutant pollen.

(A) Relative *in vitro* pollen tube germination rate of wild-type (WT) and *78d2 x sht* double mutant pollen (*78d2 x sht*). Pollen tube formation was examined after 8 hours. At least 300 pollen grains were counted per trial. Three independent experiments were performed ( $n = 3$ ). (B) Relative pollen viability of wild-type and *78d2 x sht* pollen grains analysed by FDA-staining. Four replicates were analysed and 600 pollen grains were counted per trial ( $n = 4$ ). (C) Relative pollen germination with UV-treatment for zero, one and two hours. Percentage of pollen germination is presented and wild-type set to 100%. Four independent trials ( $n = 4$ ) were measured for wild-type and six independent trials were determined for the *78d2 x sht* mutant. At least 200 pollen grains were counted per trial. Shown are the relative mean values  $\pm$  standard errors. Significance analysis was performed by *students t*-test comparing wild-type with *78d2 x sht* (in C per time point) (\*\*\*\* indicates  $p$ -value  $< 0.0001$  and n.s. means no significance).

Pollen viability of the *78d2 x sht* double knockout line was further analysed by a standard FDA staining method. In this assay, relative pollen viability of the wild-type amounted to about 65.8% and *78d2 x sht* about 50% viable pollen (Figure 3-21 B). The data were validated in four independent trials. The 15% higher abortion compared to wild-type indicates compromised pollen viability for the *78d2 x sht* line. Interestingly, these results agree well to the reported reduction of pollen viability to

approximately 20% for the *myb99* Arabidopsis mutant line by Battat et al. (2019). This mutant line showed also absent flavonol-3-*O*-sophorosides and HCAAs levels in stamen extracts.

The *fst1* line did not show any effect upon increased UV-radiation (3.6). Similar UV-light experiments were performed with *78d2* x *sht* pollen (Figure 3-21 C). Thereby, the ability of the *78d2* x *sht* pollen to germinate *in vitro* was strongly decreased to only 30% after one hour radiation as compared to wild-type which was completely unaffected by this treatment. Interestingly, no further reduction of *78d2* x *sht* pollen germination was observed after two hours of UV-light stress.

The result implied that specifically HCAAs have a crucial role as UV-protectants. It could be validated in future UV-radiation pollen germination assays, including the parental single mutant lines, *78d2* and *sht*.

## 4 Discussion

### 4.1 Transport of pollen-specific flavonol glycosides in *Arabidopsis*

#### 4.1.1 Identification of a tapetal flavonoid glycoside transporter

While flavonoids are almost 'classical', secondary metabolites in plants concerning their well-studied biosynthesis and the huge number of examples of their diverse biological roles, there are still uncertainties about transport processes of these compounds (Zhao, 2015). The aim of this work was to isolate and characterize a specific transporter related to the tapetal-derived flavonol-3-*O*-sophorosides in the model plant *A. thaliana*.

The initial focus was set on ABC- and MATE-transporters which are considered as canonical transporters of secondary metabolites. For these approaches, putative candidate genes which are specifically expressed in anthers and/ or predicted to be co-expressed with the *UGT79B6* were selected and T-DNA insertion lines were tested for chemotypes (3.3.2).

Although many examples were reported on the impact of ABC transporters in the formation of the exine and tryphine (Quilichini et al., 2014a; Choi et al., 2014) or their capability in the transport of flavonoids (Goodman et al., 2004; Banasiak et al., 2013; Behrens et al., 2019), any identification and correlation to pollen coat phenylpropanoids was not achieved. The candidate mutants *abcg17* and *abcg18* exhibited no effect on flavonoid accumulation on the pollen surface. This lack of experimental proofs supported the idea of ABC subfamily G members being transporters of more lipophilic compounds (Landgraf et al., 2014; Yadav et al., 2014).

Knockout lines of the MATE candidate genes that were chosen based on suggestions of Thompson et al. (2010b) and Wang, L. et al. (2016) who reported their clustering in a group of flavonoid transporters, showed as well no detectable changes in the flavonoid levels. Even the most obvious anther-specific *DTX34* (*At4g00350*) which is highly co-expressed with the *UGT79B6* (*At5g54010*) was not confirmed by our data. There is a possibility that some of these 'zero effect' transporters could be involved in intracellular transport processes due to the high redundancy of transporters in plants which could mask metabolic alterations. Especially, for members of the MATE-family like *DTX1* a broad substrate spectrum has been reported (Li et al., 2002). A loss of function of an intracellular transporter would not be mandatory accompanied by a reduction of the target compounds. For such intracellular transporters, the conformation of their transport activity would be up to now primarily depend on a functional driven screen in a heterologous expression system.

The MATE transporter *TT12* (*At3g59030*) was tested using two independent knockout lines which are confirmed by the SALK Institute. This approach was initiated by reports about the role of *TT12* in the transport of flavonoids in tapetum cells (Hsieh and Huang, 2007; Zhao, 2015). *TT12* was originally characterized as vacuolar antiporter of cyanidin-3-*O*-glucose involved in proanthocyanidin-accumulation in the seed coat (Debeaujon et al., 2001; Marinova et al., 2007). Thereby, it was also evaluated by Marinova et al. (2007) that no flavonol glycosides as well as aglycones and flavan-3-ol dimers were transported by *TT12*. These findings are inconsistent with the work of Hsieh and Huang (2007). They

reported that TT12 acts in the flavonoid transport into ER-derived tapetosomes together with TT19 (*At5g17220*) and that homozygous knockout lines (*tt4*, *tt12* and *tt19*) show reduced flavonoid levels on pollen. The latter observation could not be verified in this thesis for the tested homozygous *tt12-1*, *tt12-2* and *tt19-8* knockout lines. Additionally, no anther-specific transcription of the *TT12* gene could be verified by qRT-PCR analysis (3.4.1). These findings led to the exclusion of the TT12 as putative tapetal flavonol glycoside transporter candidate. Notably, the *tt19-8* knockout showed also no effect on the flavonoid accumulation on the pollen surface. It implies that the tapetal flavonol-3-*O*-sophorosides are not escorted or require GST proteins. This may be in opposite to the positive charged anthocyanins which are probably 'escorted' by GST proteins in different plant species (Mueller et al., 2000; Sun et al., 2012). Either a GST-mediated transport is less essential for flavonol glycosides or GST-aided flavonoid transport is limited to intracellular and vacuolar transport. Interestingly, the work of Sun et al. (2012) suggests that TT19 is not essential for transport of flavonol glycosides compared to anthocyanins resulting in a higher expression of the flavonol synthase accompanied by 36% higher flavonoid levels in the *tt19* mutant, but not to their reduction as in case of the carried anthocyanins.

Only when the focus was extended to candidates of the NPF-family, one promising candidate was found. Members of the NPF2-subfamily were already shown to be required for the transport of plant secondary metabolites (Nour-Eldin et al., 2012; Payne et al., 2017). It was therefore hypothesized that a member of the NPF2-subfamily might also function as flavonol glycoside transporter. Only two members of the NPF-family, *NPF2.8* (*At5g28470*) and *NPF7.1* (*At5g19640*) were predicted by the BAR eFP browser to be anther-specific expressed. Although both candidates were not highly ranked to *UGT79B6* by the web-based co-expression analysis tools, ATTED-II (<http://atted.jp/>) and Genevestigator (<https://genevestigator.com/gv/>), they were at least temporally expressed in the same flower stages 6-8 and 9-11 like *UGT79B6* (BAR eFP browser (<http://bar.utoronto.ca/>) and TRAVA (<http://travadb.org/>)). Interestingly, this stage-specific transcription coincides with the expression of *ABCG9* (*At4g27420*) and *ABCG31* (*At2g29940*) which translocate sterol glycosides as constituents of the pollenkit (Choi et al., 2014). The biosynthetic enzymes SHT (*At2g19070*) and TSM1 (*At1g67990*) which are essential for the formation of the pollenkit-specific HCAAs are also shown to be specifically expressed in stage 9-11 suggesting this time point as essential for the soluble tryphine formation in Arabidopsis. Surprisingly, *ABCG26* (*At3g13220*) which is required for deposition of polyketide precursors of the exine, is apparently highly transcribed in the later stages 12-14 (Quilichini et al., 2014a).

#### 4.1.2 FST1-depending transport of flavonol sophorosides

Pollen grains of the *npf2.8* mutant revealed a 90% reduction of quercetin-3-*O*- and kaempferol-3-*O*-sophoroside (3.3.2). Therefore, the candidate *NPF2.8* (*At5g28470*) was subsequently termed FLAVONOID SOPHOROSIDE TRANSPORTER1 (FST1) according to its proposed physiological function. This result was based on the LC-MS analysis of methanolic *fst1* pollen extracts and the complete complementation of the *fst1* chemotype by expressing of the *FST1* wild-type gene (3.4.4). The results provide evidence that the tapetum-derived flavonoids are exported to the pollen surface by a FST1-depending mechanism. This assumption corresponds with the demonstrated subcellular localization of the transporter to the plasmalemma (3.4.5) and the anther-specific expression of its encoding gene within the tapetum (3.4.3) where the flavonol sophoroside formation is situated (3.3.1). The unchanged levels of



these specialized metabolites in whole *fst1* anthers (Table 3-2) compared to wild-type, suggests that their biosynthesis is not affected by suppression of *FST1*.

#### 4.1.3 Regulatory aspects of flavonol-3-O-sophoroside biosynthesis

The *in silico* analysis of *cis*-regulatory motifs within the putative *UGT79B6* and *FST1* promoter regions revealed the presence of identical flavonoid- and phenylpropanoid-associated elements (3.4.2). Conspicuously, many predicted DNA binding sites for MYB family transcription factors were found which implicate a MYB transcription factor controlled *FST1* expression. This correlates well with recent reports on the impact of MYB factors on flavonoid metabolism (Akagi et al., 2009; Fornalé et al., 2014). Especially, MYB transcription factors of the R2R3 class were reported to be involved in tapetum development like AtMYB103 (Higginson et al., 2003). It was previously shown that the accumulation of flavonol-3-O-sophorosides in *Arabidopsis* is independent of the R2R3-MYB transcription factors MYB11, MYB12, and MYB111 (Stracke et al., 2010). Recently, Battat et al. (2019) reported that a regulatory triad of MYB99, MYB24, and MYB21 controls exclusively the production of tapetum diglycosylated flavonols and HCAAs. As a result, they demonstrated that the *UGT79B6* promoter is activated by MYB99 or MYB24 by promoter activation experiments. Besides, it was found that *myb99*, *myb24*, and *myb21* lines were deficient in at least 14 different HCAAs in young anthers (Battat et al., 2019). The MYB2 binding motif MYB1AT was predicted in both promoters (3.4.2). Promoter binding site mutation assays as well as transcription factor overexpression and suppression could be used as demonstrated for the tapetal A9 promoter (Verma and Burma, 2017) to reveal detailed regulatory aspects of the flavonol-3-O-sophoroside biosynthesis.

*Cis*-regulatory elements for members of the R2-R3 MYB transcription factor gene family suggest a jasmonate regulated *FST1* and *UGT79B6* expression. Furthermore, the presence of gibberellin related *cis*-regulatory elements correlates with the central role of both hormones in anthers and pollen (Singh et al., 2002; Cheng et al., 2009).

## 4.2 Unsolved HCAA transport to the tryphine

The profile of the LC-MS-analysed methanolic pollen extracts exhibited no altered levels of HCAAs indicating that *FST1* is not involved in the transport of these conjugates. Interestingly, all tested ABC- and MATE-candidates also showed no impact on the phenolamides. But the MATE-candidates were pre-selected based on *in silico* prediction as putative flavonoid transporters according to Thompson et al. (2010b) and Wang, L. et al. (2016). Noteworthy, the defence related coumaroylagmatine on *Arabidopsis* leaves is exported by the MATE transporter DTX18 (*At3g23550*) (Dobritsch et al., 2016). The MATE-transporter DTX17 (*At1g73700*) that shares 42% amino acid sequence identity to DTX18 could be a putative candidate. *DTX17* clusters close to *DTX18* in phylogenetic analysis and is notated to be anther-specific transcribed during the flower stages 9-11 (TRAVA).

Another possible transport of the semi-polar HCAAs to the pollen coat could be fulfilled by lipid transfer proteins (LTPs). LTPs are small secretory proteins in plants defining lipid-binding structures and are assumed to be involved in lipid exocytosis. In the tapetal cells, type-III LTPs are abundant and are exported via the ER-*trans*-Golgi-network through the locule to the exine (Huang et al., 2013). This

suggested route via the ER-*trans*-Golgi-network could be in accordance with the ER-membrane association of CYP enzymes involved in phenylpropanoid biosynthesis (Jørgensen et al., 2005; Ralston and Yu, 2006; Nakayama et al., 2019). Indeed, CYP98A8 (*At1g74540*) and CYP98A9 (*At1g74550*) which participate in the HCAA-biosynthesis (Matsuno et al., 2009) are strongly suggested by SUBA (<https://suba.live/>) to be ER-localized. In Arabidopsis, all three type-III LTPs (*At5g07230*, *At5g52160*, *At5g62080*) as well as the type-IX LTPs *At3g07450* and *At3g52130* are annotated by ATTED-II (<http://atted.jp/>) to be closely co-expressed with ACOS5 (*At1g62940*), CYP704B1 (*At1g69500*) and CYP98A9 (*At1g74550*) which are key enzymes of sporopollenin formation and spermidine metabolic processing, respectively (Matsuno et al., 2009; Lallemand et al., 2013; Wang et al., 2018). This putative functional association and their indicated anther-specific expression during the stages 9-11, 12-14, and 15-18 (TRAVA, <http://travadb.org/>) make them promising candidates. Indeed, Wang, B. et al. (2016) demonstrated that a lipid transfer protein (AaLTP3) indeed enhanced the transport of (dihydro-) artemisinic acid in *N. benthamiana* leaves, suggesting that specific LTPs are capable to transfer lipophilic, specialized metabolites. Comprehensive reverse genetics using available LTP SALK-lines and subcellular co-localization studies of biosynthetic and decorating enzymes in the HCAA-biosynthesis may contribute to proof this assumption.

Regarding polyamines which are precursors in HCAA biosynthesis, controlled transport by the *L*-amino acid transporter family is discussed in plants (Fujita and Shinozaki, 2014). Therefore, the putative polyamine uptake transporter (PUT) PUT3 (*At5g05630*) which is spermidine-induced (Sagor et al., 2016) and PUT4 (*At3g13620*) should be analysed. Notably, they are also specifically expressed in anthers during stages 9-11, 12-14, and 15-18 (TRAVA, <http://travadb.org/>). Interestingly, a choline transporter (*At5g17830*) might also be involved in the transport of polyamines. The *At5g17830* gene is anther-specific transcribed during the flower stages 12-14 and 15-18 (TRAVA, <http://travadb.org/>). Furthermore, *At5g17830* is annotated to be co-expressed with the spermidine disinapolyacyltransferase (SDT, *At2g23510*) contributing to HCAA production in tapetal cells and several other organs (Fellenberg and Vogt, 2015).

### 4.3 The NPF-candidates in the current literature

#### 4.3.1 NPF-transporters and specialized metabolites

Once the specific transport activity towards glucosinolates emerged in literature (Nour-Eldin et al., 2012; Jørgensen et al., 2017), the NPF-family became more closely associated to specific glucosinolate transport. Therefore, both selected NPF-candidates were initially not favoured as putative flavonoid transporter candidates. However, the transport activity of FST1 towards flavonol glycosides revealed an until now unknown substrate specificity of the NPF2-subfamily to flavonoids. In addition, it confirmed the earlier assumption that the NRT/PTR-family encodes long-sought transporters of specialized metabolites (Nour-Eldin and Halkier, 2013). In *A. thaliana* the NPF2-subfamily consists of fourteen members that show a wide range of tissue and developmental specificity (Léran et al., 2014; Niño-González et al., 2019). Inside this heterogeneous subfamily, substrate-specificities include nitrate, glucosinolates, indole alkaloids and diverse phytohormones as gibberellins and jasmonates (Nour-Eldin et al., 2012; Payne et al., 2017; Niño-González et al., 2019). Since the increased numbers of NRT1/PTR

family members in plant genomes were proven, it was speculated that these low-affinity nitrate transporters could be involved in other specialized transport processes (Tsay et al., 2007; Nour-Eldin and Halkier, 2013). Up to now 365 NPF2-members have been identified in different plant species (Léran et al., 2014).

There are no examples in the literature which would advise transporters of the NPF-family as flavonoid transporters. Up to now, there is only one report about a member of the high-affinity nitrate transporter family, NRT2.7 (*At5g14570*). NRT2.7 which may affect the proanthocyanin accumulation in Arabidopsis seeds and shows a transparent testa phenotype which resembles the *tt10* mutant accumulating more soluble proanthocyanins (David et al., 2014). Compared to reduced levels of biflavonoids, the amounts of flavonol glycosides were not affected in the *nrt2.7* mutant. The role of this vacuolar high-affinity nitrate transporter in proanthocyanin accumulation is still unclear (David et al., 2014; Zhao, 2015). It is just assumed that the *nrt2.7*-mutation could interfere with the pH-stability, tonoplast stabilisation or other hitherto-unknown mechanisms. These could directly or indirectly impact the transport activities of TT12 and AHA10 (*At1g17260*), an H<sup>+</sup>-ATPase (David et al., 2014).

#### 4.3.2 FST1 is neither a glucosinolate transporter nor a nitrogen exporter

FST1 (NPF2.8) was recently examined using the *Xenopus laevis* oocyte expression system to translocate indole as well as aliphatic glucosinolates (Jørgensen et al., 2017) (Figure 4.1 A). Although FST1 (NPF2.8) shows just a sequence identity of about 38%, it clusters close to the glucosinolate transporters GTR1 (NPF2.10) and GTR2 (NPF2.11) (Nour-Eldin et al., 2012; Jørgensen et al., 2017). Even though no pollen- or anther-specific glucosinolates are described for Arabidopsis, it has been reported that pollen from the *Brassica* rapeseed and high glucosinolate Indian mustard may contain significant amounts of predominantly aliphatic glucosinolates, although they contribute less than 10% to the fresh weight compared to seeds (Dungey et al., 1988). These compounds act as ovipositioning and feeding stimulants for several specialist insects like the cabbage butterfly (*Pieris rapae*) and the pollen beetle (*Meligethes aeneus*) whose larvae predominantly feed on pollen (Traynier and Truscott, 1991; Giamoustaris and Mithen, 1995). However, a significant glucosinolate transport activity for FST1 (NPF2.8) was not measurable (Figure 4.1 A). This supports the assumption that the physiological function of the strict anther-specific FST1 (NPF2.8) differs from the glucosinolate transporter subgroup. For a complete verification, the levels of pollen-specific glucosinolates between Arabidopsis wild-type and the *fst1* mutant should be experimentally verified.

In parallel, Babst et al. (2019) published a report on the second NPF-candidate NPF7.1 (*At5g19640*), apparently required for normal nitrogen cycling under low nitrogen conditions. Besides, the *fst1* knockout line SALK\_027288C was also tested in this work by <sup>13</sup>N-export assays from leaves. Thereby, the *fst1* mutant exhibited no alteration in the nitrogen export in leaves (Figure 4.1. B), and was excluded as putative leaf nitrogen exporter.

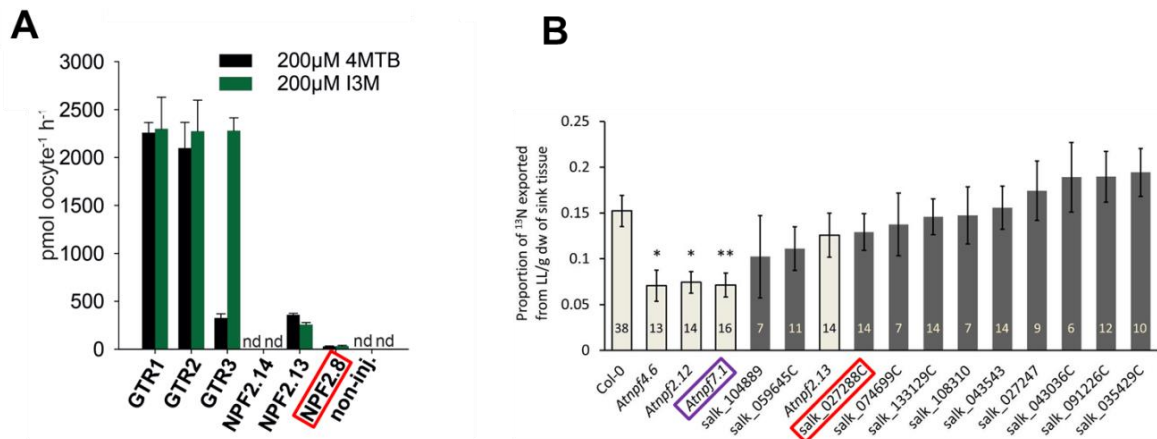


**Figure 4-1** The candidate FST1 (NPF2.8) in the current literature.

(A) Transport activity of the NPF2-subfamily members including glucosinolate transporters (GTR1, GTR2, GTR3) and FST1 (NPF2.8, red-framed) measured in the presents of methylthiobutyl glucosinolate (4MTB) and indol-3-ylmethylglucosinolate (I3M) in *Xenopus* oocytes. Proportions of glucosinolates accumulated within the oocytes were measured by LC-MS. 3 x 5 oocytes were used for each candidate gene. Bars indicate  $\pm$  standard derivation (n = 3, experiment was performed twice, n.d. means not detectable) (from Jørgensen et al., 2017). (B) <sup>13</sup>N-export in leaves of wild-type and different T-DNA insertion lines, including the *fst*- and *npf7.1* knockout lines SALK\_027288C (red-framed) and SALK\_138950C (purple-framed) under low N availability. Bars present amounts of assimilated <sup>13</sup>N applied as <sup>13</sup>NH<sub>3</sub> exported from loaded leaves to the sink tissues. Values were normalized by sink tissue mass. Means  $\pm$  SE (n indicated in the bars) (\*P<0.05; P<0.01) (from Babst et al., 2019).

The parallel investigations by Jørgensen et al. (2017) and Babst et al. (2019) demonstrated that FST1 (*At5g28470*) was not functionally classified up to date. Neither glucosinolate transport nor the earlier supposed role in general nitrogen transport could be verified, although residual low-affinity nitrate transport activity is considered as a common feature within the NPF-family (Nour-Eldin and Halkier, 2013; Niño-González et al., 2019).

## 4.4 Putative transport mechanism

### 4.4.1 Initial aspects about the origin of substrate specificity

The *in planta* FST1 characterization approach was completed by microbial uptake assays (3.7). For this the transporter protein was heterologous expressed in *E. coli* which has been well-established as a routinely used system for functional characterization (Haferkamp and Linka, 2012). Even larger proteins of the complex structured ABC-transporter superfamily could be expressed and characterized in this prokaryotic system (Lee et al., 2008).

The transport assays demonstrated a promiscuous substrate specificity of FST1 (3.7), it can be assumed that the flavonoid glycoside pattern of the pollen grains results from the specificity of the UGT79B6 (Yonekura-Sakakibara et al., 2014). After determination of the position specificity of the sugars, substrate specificity towards the flavonoid aglycone remains to be examined. Such studies would also be interesting with respect to the origin and evolution of the substrate specificity within the NPF-family (Jørgensen et al., 2017; Corratgé-Faillie and Lacombe, 2017).

The tapetum-specific expression of *FST1* and its minor co-expression with biosynthetic genes of the flavonoid and tryphine biosynthesis indicate that the transporter evolved independently of the

flavonoid or HCAA biosynthesis. Jørgensen et al. (2017) discussed that the development of new substrate specificities can arise from multifunctional, ancestral transporters of chemically similar or more ancient substrates by gene duplication. The authors concluded that the specificity for glucosinolates within the NPF-family evolved from earlier cyanogenic glucoside transporters through a promiscuous transporter that was capable to accept both types of substrate. It is assumed that after glucosinolate biosynthesis was established, individual NPF-members have become more specialized towards specific glucosinolates through subfunctionalization (Jørgensen et al., 2017). This is sustained by phylogenetic reconstruction analysis of the NPF-transporter family in algae, plants and animals (von Wittgenstein et al., 2014). Only a small number of 18 NPF-members exist in the moss *Physcomitrella* and even less in green algae while in land plants an extremely broad diversification occurs accompanied by neo-functionalization (Nour-Eldin and Halkier, 2013; von Wittgenstein et al., 2014). Despite the broad functional diversification, the NPF-transporter family is monophyletic (von Wittgenstein et al., 2014). The number of well-studied transporters and species is too small to convincingly answer the question about the origin of substrate specificity. In the case of the ubiquitous flavonoids a starting of a detailed classification would be to take a closer look at could functional orthologous of *FST1* genes. In this case, plant species should be chosen which have evolved special metabolic branches or exhibit unusual pollen-specific flavonoids. It is known that several *Populus* species accumulate pollen-specific anthocyanins in high amounts (Alcalde-Eon et al., 2016). Other suitable model plants and their special flavonoid group could be legumes, like *Medicago truncatula* (isoflavonoids) and monocots like *Zea mays* (3-deoxyanthocyanins) (Winkel-Shirley, 2001). For in-depth comprehensive substrate specificity studies, *FST1* orthologous from non-leguminous plants from the Rutaceae, Cannabaceae or Solanaceae which are also isoflavonoid producer could be further investigated. Close *FST1* orthologous from *Medicago truncatula*, *Zea mays*, several Solanaceae and *Citrus clementia* (Rutaceae) were already identified by the phylogenetic analysis which exhibit high protein sequence identities of 50% to 60%.

A detailed functional investigation will certainly elucidate the hidden mechanisms of pleiotropic transporters. Members of the NPF-family as well as ABC transporters show a scarcely understood multi-specificity towards chemically unrelated substrates (Corratgé-Faillie and Lacombe, 2017; Lefèvre and Boutry, 2018). Whereby, it was demonstrated for some NPF-members that the original nitrate transporter activity is not competing with their novel-assigned substrate specificity for abscisic acid (Kanno et al., 2013). Especially, former neglected transporter families which have been generally considered to be limited to the primary metabolite transport have revealed an unexpected multiple substrate specificity. Besides the NPF-family, the sugar-selective SWEET transporters AtSWEET13 and AtSWEET14 were examined to act also as gibberellin transporters (Kanno et al., 2016). Further examples for such a neo-functionalization (Nour-Eldin and Halkier, 2013) of primary metabolite transporters have also been reported for the purine uptake permease (PUP) family. In this case, the NUP1 (nicotine uptake permease 1) demonstrated to be a high-specific importer of nicotine in tobacco roots (Hildreth et al., 2011). More recently, it was reported that another member of the PUP-family is capable to translocate benzylisoquinoline alkaloids and pathway precursors from opium poppy alkaloids (Dastmalchi et al., 2019). These transporters belong to a new composed superfamily of secondary

transporters which is distinct from the other recognized multidrug transporter superfamilies termed as drug metabolite transporter (DMT) superfamily (Jack et al., 2001).

#### 4.4.2 Conserved motifs

An *in silico* analysis of the FST1 and other NPF-family members also revealed insights into the presence of conserved motifs and sustained first thoughts about the putative transport mechanism. A representative protein alignment is also given in the Appendix (Figure 8-13). FST1 showed a low protein sequence identity of about 27% to the dual-affinity nitrate transporter NPF6.3 (NRT1.1) (Sun and Zheng, 2015). NPF6.3 (NRT1.1) represents a well-studied basic member of the NPF-family and exhibits also significant sequence identity to mammalian and bacterial PTR transporters (Tsay et al., 1993; Parker and Newstead, 2014). Up to now, the NRT1.1 is the only member of the NRT/NPF superfamily that has been crystallized (Figure 4-2) (Parker and Newstead, 2014; Sun et al., 2014). The replacement of His356, which is essential for nitrate binding (Parker and Newstead, 2014), in FST1 and its homologues, sustained a physiological function of FST1 other than nitrate transport (Appendix Figure 8-13). His356 is also not conserved within the glucosinolate transporters NPF2.10 (GTR1) and NPF2.11 (GTR2) (Appendix Figure 8-13).

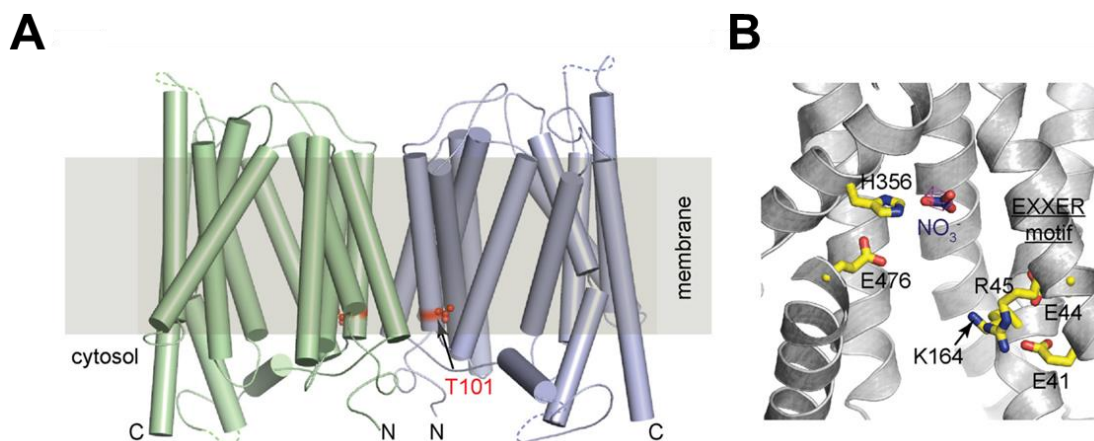


**Figure 4-2** Crystal structure of NPF6.3 (NRT1.1).

(A) The NPF6.3 dimer shown as cylinder representation, the Thr101 phosphorylation sites are red-indicated. (B) Amino acid residues of NPF6.3 required for substrate binding and proton coupling. Nitrate and the side chains of His356, Glu476, Lys164 and the EXXER-motif are shown as sticks. (Figures adopted from Sun and Zheng, 2015).

Apart from this difference, other critical amino acids are conserved even between distant members. This is obvious for a relevant phosphorylation site: FST1 has a threonine at position 91 corresponding to Thr101 (Appendix Figure 8-13), which is reported as phosphorylation site located in a loop between the third and the fourth transmembrane region in NPF6.3 (NRT1.1) (Sun and Zheng, 2015). The phosphorylation status of Thr101 determines the nitrate affinity of the dual-affinity nitrate transporter NPF6.3 (NRT1.1). Phosphorylation-mimicking studies demonstrated that a non-phosphorylated-mimicking Thr101Ala resulted in low-affinity, whereas a phosphorylated-mimicking Thr101Asp resulted in high-affinity nitrate transport activity (Liu and Tsay, 2003). Furthermore, fluorescence resonance energy transfer assays revealed that the de-/phosphorylation status of NPF6.3 (NRT1.1) determines the formation of a dimer (Thr101Ala, de-phosphorylated) or a monomer (Thr101Asp, phosphorylated) (Sun and Zheng, 2015). This site is also conserved in NPF2.10 (GTR1) and NPF2.11 (GTR2) at the

positions 135 and 117, respectively. The consensus phosphorylation site could be maintained as general post-transcriptional regulation point throughout the NPF-family. In Arabidopsis, 36 NPF-members exhibit this consensus sequence (Liu and Tsay, 2003).

Membrane transport activities by pumps, channels and transporters are generally regulated by protein phosphorylation, but little is known about the detailed mechanisms by which phosphorylation controls transporter activity (Liu and Tsay, 2003; Blakely and Bauman, 2000; Büttner 2010; Stolarczyk et al., 2011). Recently, it was shown that the de-phosphorylation of the corresponding Thr135 in the NPF2.10 (GTR1) besides dimerization, determines its plasma membrane localisation (Ishimaru et al., 2017). But in contrast to the modified nitrate affinity in NPF6.3 (NRT1.1), it was also demonstrated that the phosphorylation status of Thr135 has no significant effect on the glucosinolate transport activity of NPF2.10 (GTR1). Ishimaru et al. (2017) identified no significantly differed  $K_m$ -values between the NPF2.10 wild-type variant and Thr135Ala and Thr135Asp mutants. Whereas, the transport activity towards gibberellic acid which is transported in addition by NPF2.10 (Saito et al., 2015) showed modified  $K_m$ -values from 1 mM (wild-type) and higher (Thr135Ala) to extremely low levels (non-detectable) for the Thr135Asp (monomeric, phosphorylated-mimicking) mutated variant (Ishimaru et al., 2017). Although the corresponding Thr91 in FST1 was not identified by the PhosPhat4.0 server as a phosphorylation site, FST1 mutated versions may be produced to reveal effects of dimerization and possible substrate affinity. Additionally, Jørgensen et al. (2015) tested Ser52 and Ser635 which were also assumed as possible phosphorylation sites in NPF2.10 (GTR1), but no differences in the NPF2.10 glucosinolate transport activity were measured by corresponding phosphorylation-mimicking-assays in *Xenopus* oocytes. In contrast to the Thr101, the consensus serine residues 52 and 635 are not conserved in FST1.

The comparison of the FST1 protein sequence with GTR1/2 and FST1 orthologues revealed that the EXXEK-motif (Jørgensen et al., 2015) is also present in the FST1 candidate and its orthologues (Figure 3-14). The EXXEK-motif appears to be highly conserved within the NPF-family (Jørgensen et al., 2015). It is located in the first transmembrane region and appears essential in proton-coupling. The motif was demonstrated by site-directed mutagenesis and *Xenopus* oocyte transporter assays to be crucial for the glucosinolate transport activity of NPF2.11 (Jørgensen et al., 2015). Thereby, it was shown that the glutamate residues and the lysine are crucial for the  $H^+$  co-transport. The ability of NPF2.11 to over-accumulate glucosinolates was lost if non-charged residues XX were changed to positive- or negative charged residues. Therefore, it was hypothesized that charged X-residues disturb the proton-coupling mechanism mediated by the glutamate and lysine residues (Jørgensen et al., 2015). Site-directed mutagenesis combined with  $^{14}C$ -quercetin-3-*O*-sophoroside uptake assays could not confirm these findings in the case of FST1 (3.7). Although the FST1 subgroup contains the EXXEK-motif, the two mutated FST1 variants Glu31Ala and Phe33Asp had surprisingly no significant effect on transport activity. Whether other FST1 subgroup-specific motifs replace the functional EXXEK-motif require additional tests.

#### 4.4.3 Putative relationship between pH and flavonoid transport

These findings also imply that the transport mechanism of FST1 differs from NPF2.11 which works as  $H^+$ /glucosinolate symporter (Nour-Eldin et al., 2012; Jørgensen et al., 2015). This assumption is

further supported by the relatively low protein sequence identity between FST1 and NPF2.11 of only 38%. NPF2.11 acts as an importer which is driven by the proton gradient from the apoplast (pH 5.5) to the cytosol (pH 7.4) (Jørgensen et al., 2015). In contrast, the plasma membrane localized FST1 may act as flavonol glycoside exporter to the locule space. Furthermore, regarding the physiological environment, the electrochemical gradient is assumed to be conversely orientated. In contrast to the cytosol with a pH of 7.5 (Kader and Lindberg, 2010), the anther locule drastically changes during development of the male gametophytes. From the early microsporogenesis at pH 4.8 it rises later to pH 5.2 during meiosis in garlic (Winiarczyk et al., 2012). In the case of petunia, the locule pH value *in vivo* decreases from pH 6.8 to 7 during the meiosis to pH 5.9 and rises to pH 6.2 (Izhar and Frankel, 1971). These drastic changes of the pH are accompanied by increased callase activity which is critical for microspore release from the tetrad stage and finally for male fertility (Izhar and Frankel, 1971; Winiarczyk et al., 2012). The concomitant proton gradients are generally generated by a plasma membrane H<sup>+</sup>-ATPase as in the case of the ATPase AHA10 (TT13) that is required for the accumulation of proanthocyanins in the outer seed envelop and presumably affects TT12 transport activity (Baxter et al., 2005). This example illustrates the sensitive interplay between proton gradient and transport of specialized metabolites.

In the case of the tapetum, the plasma membrane H<sup>+</sup>-ATPases AHA6 (*At2g07560*) and AHA9 (*At1g80660*) are specifically expressed in anthers (Houlné and Boutry, 1994). Unfortunately, the physiological conditions of the Arabidopsis anther locule and the intracellular pH value of the slowly degenerating tapetal cells during the late microgametogenesis when the tryphine is formed are unknown. The scenario in Arabidopsis anthers might yet be similar to petunia and garlic.

It was shown that Arabidopsis mutants of the intracellular male gametophyte impaired anthers (MIA), P-five type ATPases reveal a tetrad-pollen (*quartet*) phenotype due to failed microspore relation and acidification of the locule, respectively (Jakobsen et al., 2005). Interestingly, transcription of the MATE transporter *DTX34* (*At4g00350*) is decreased in MIA insertion mutant lines suggesting a putative role of this former candidate in the vesicular ER-Golgi transport, whereas transcription of *AHA6* and *AHA9* is increased in MIA insertion lines (Jakobsen et al., 2005).

So far, the transport activity of the NPF-family is depending on proton electrochemical gradients across the membrane (Tsay et al., 2007). Most NPF-members identified in plants are H<sup>+</sup>/substrate symporters utilizing the inwardly directed proton gradient to promote substrate uptake (Nour-Eldin et al, 2012; Li et al., 2017; Jørgensen et al., 2017). But as mentioned above, it appears unlikely that FST1 could easily function as H<sup>+</sup>/flavonoid-symporter working against a presumable steep locule H<sup>+</sup>-proton gradient. From literature it is known that some NPF-family members act as antiporters against an extracellular H<sup>+</sup>-proton gradient. The NPF7.3 (*At1g32450*) has been reported as proton-coupled H<sup>+</sup>/K<sup>+</sup> antiporter loading K<sup>+</sup> from root parenchyma cells into the xylem (Li et al., 2017). In this case, the xylem sap exhibits also an acidic pH value of 5.5 to 6.5 that promotes K<sup>+</sup>-release out of the parenchyma cells, whereas an external pH about 7.4 dramatically reduced K<sup>+</sup>-efflux tested by *Xenopus* oocyte assays (Li et al., 2017). In opposite to FST1 and most of the NPF-members, NPF7.3 contains uncharged residues (QGLAT) instead of the EXXEK motif mentioned above. Conversely, the glycine residue 209 which is not



conserved in FST1 and its orthologues is essential for the NPF7.3 antiporter activity. This has been considered as a hint for an alternative proton-coupling mechanism in NPF7.3 by Li et al. (2017). This also corroborates the remarks of Jørgensen et al. (2017) who proposed that the evolution of new substrate specificities in coupled secondary transporters is connected to changes in the electrogenic properties of the transport mechanism. It is imaginable that minor changes in the substrate binding loop could be sufficient to change transport mechanism or specificity. The latter has already been discussed by Parker and Newstead (2014) who also showed based on the crystal structure of NPF6.3 (NRT1.1) that minor changes inside the substrate binding side of NPF6.3 (NRT1.1) are sufficient to switch from peptide to nitrate transport activity. Therefore, replacement of the large, aromatic residues Phe28 and Tyr29 required for the recognition of peptides by smaller, apolar residues in NPF6.3 creates the space for nitrate binding (Parker and Newstead, 2014). Furthermore, switches from antiporter to symporter transport mechanism between closely related transporter proteins are reported in the literature for nucleotide transporters (NTTs). For example, the diatom ATP/ADP-transporter NTT1 shares high sequence similarity to plastid NTTs that are so far ATP/ADP-antiporters, but, NTT1 acts intriguingly as H<sup>+</sup>/adenine-symporter (Ast et al., 2009). To elucidate the FST1 transport mechanism, classical H<sup>+</sup>-uncoupler transporter uptake assays in the presence of the protonophore carbonyl cyanide *m*-chlorophenyl hydrazone (CCCP) were subsequently performed in *E. coli* at two different CCCP concentrations in cooperation with Dr. Ilka Haferkamp (Figure 4-3).

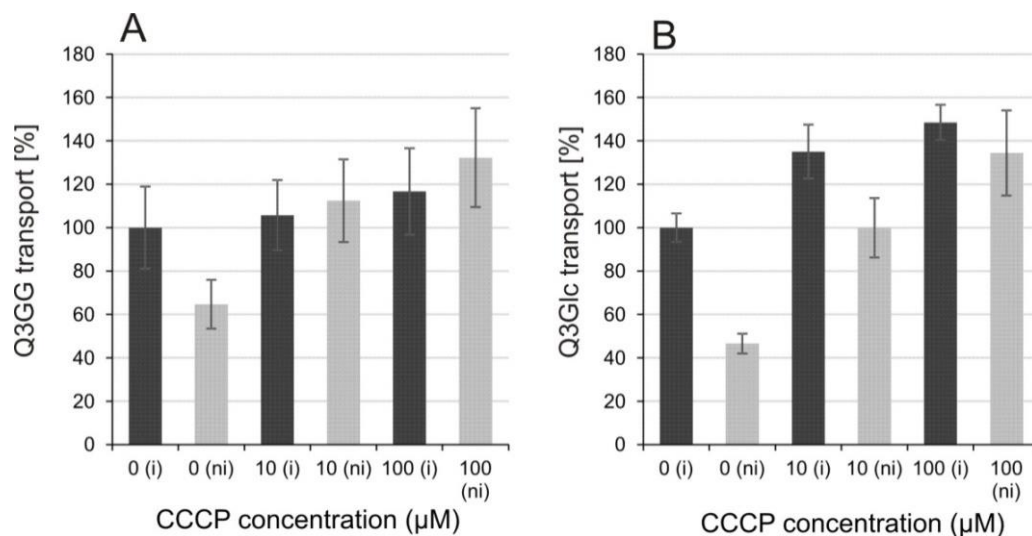


**Figure 4-3** *In vitro* transport of flavonol glycosides in presence of CCCP.

Uptake of quercetin-3-*O*-sophoroside (QGG) (A) or quercetin-3-*O*-glucoside (Q3Glc) (B) into induced (i) Rosetta II cells expressing FST1 (black bars) was compared with the uptake into non-induced cells (ni; grey bars). Transport medium contained 10 μM <sup>14</sup>C-labelled substrate and the given concentration of the protonophore *m*-chlorophenylhydrazone (CCCP). Transport was allowed for 10 min. Label of the cells expressing FST1 without supplement (0, black bar) was set to 100% and the remaining rates were normalized according to this value. (Figure modified from Grunewald et al. (2020) and with friendly permission of Dr. Ilka Haferkamp).

But so far, the results were inconclusive. No decrease of transport activity as expected in case of an H<sup>+</sup>/flavonol-3-*O*-glycoside symport mechanism was observed. Instead, transport of flavonol-3-*O*-glycosides slightly increased in induced as well as non-induced cells. The FST1 mechanism, therefore, could be proton independent or tentatively indicate an antiport. In general, an increase of transport

activity in presence of CCCP is an indicator of an antiporter mechanism as in the case of the diatom NTT2 transporter (Ast et al., 2009).

The FST1-mediated flavonoid transport might also be H<sup>+</sup>-independent and only driven by the substrate gradient. During the switch of substrate specificity from cyanogenic glucosides to glucosinolates, a hypothetical promiscuous transporter may have shown a non-electronic transport of cyanogenic glucosides. In opposite to this ancestor, later but also some evolutionary earlier members were all demonstrated to utilize proton-driven transport (Jørgensen et al., 2017). In conclusion, it is possible that a tapetal flavonol-glycoside-specific NPF-transporter could have evolved using a non-electronic transport mechanism. In contrast to positive charged anthocyanins, flavonol glycosides are uncharged at the physiological conditions.

FST1 may therefore act as a simple facilitator which is independent from any H<sup>+</sup>-proton gradient. It is imaginable that the gradient of the transferred flavonol glycosides from the cytosol to the anther locule is sufficient to drive the transport. At the short period of the intense tapetal biosynthesis of soluble phenylpropanoids during microgametogenesis with high expression levels of corresponding genes in the phenylpropanoid biosynthetic pathways (Fellenberg et al., 2008; Grienberger et al., 2009; Yonekura-Sakakibara et al., 2014), a steep product gradient between tapetum cells and locule fluid is certainly generated. In addition, in the locules the transported flavonol-3-*O*-sophorosides are permanently unloaded at the pollen surface, whereby the equilibrium of the transport would actually be shifted to the locule space. Therefore, the concentration of locule-solved substrates is presumably constantly lower than inside the tapetum cells where the metabolites are synthesised. If a slightly acid pH-value of the locule fluid stabilizes transferred flavonol glycosides and promotes their deposition on the outer pollen wall remains to be established.

## 4.5 New insights in the tapetal biosynthesis of flavonol glycosides

Recent reports revealed that assembly of sporopollenin and the heterogeneous tryphine including the flavonoid transport is a controlled process (Pacini and Hesse, 2005; Hsieh and Huang, 2007; Quilichini et al., 2010; Quilichini et al., 2014a; Choi et al., 2014). The current image of flavonoid transport within the tapetal cells and to the pollen grains through the locule fluid predominantly includes the tapetosomes as specialized, tapetum-specific, ER-derived organelles (Wu et al., 1997; Hsieh and Huang, 2007; Li et al., 2012). The GFP-based subcellular localization of the FST1 and UGT79B6 as well as TEM imaging of the flavonoid deficient mutants offer further insights about the sites of flavonoid biosynthesis and transport (Figure 4-4).

In contrast to other sporopollenin mutants (Yang et al., 2007; Kim et al., 2010; Choi et al. 2014; Quilichini et al., 2014b), no ultrastructural changes of the tapetum, the microgametes or the tryphine were observed by TEM for the *fst1* and the *78d2 x sht* double knockout mutant (3.5 and 3.9.4). The organelle structures of the ER and their derived tapetosomes appeared intact and of the same size and number in both mutant lines. Morphological changes within the tapetum seem to be unlikely due to the fact that the flavonoid biosynthesis itself is not affected. Remarkably, also in the case of the *chs* mutant, which is completely devoid of flavonoids, no morphological alterations of the cytosol or the tapetosomes are apparent (Hsieh and Huang, 2007).

No alterations of vesicles abundance and smaller orbicules inside the locule fluid were observed in our present study. Interestingly, TEM studies from maize showed that in late tapetum stages elaioplast and tapetosomes were absent suggesting the existence of an alternative transport route (Li et al., 2012). The universal presence of FST1 orthologues in the phylogenetic analysis supports the idea of a conserved tapetosom-independent transport mechanism, since tapetosomes have been considered as exclusive for Brassicaceae. These findings suggest that these special organelles may not directly be required for tapetal flavonoid storage and transport to the pollen surface. This is further supported by the fact that FST1 which appeared as essential flavonoid glycoside exporter is plasma membrane located in subcellular localization assays in epidermal leaf cells of *N. benthamiana* and FST1-GFP complementation lines. Furthermore, all tested FST1-GFP lines were able to complement the wild-type levels of flavonol-3-*O*-sophorosides univocally indicating the plasma membrane as functional site of the transporter (3.4.6).

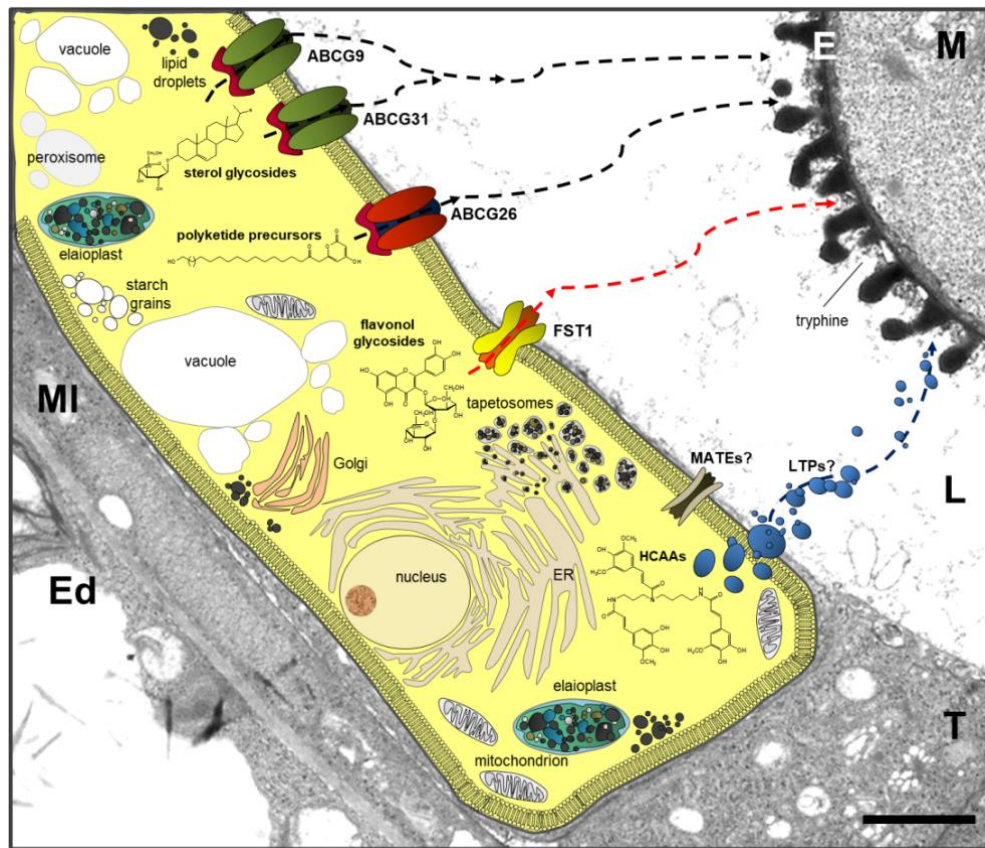


**Figure 4-4** Currently identified transporters involved in Arabidopsis pollen coat formation.

Schematically drawn tapetal cell imbedded in a TEM image (Figure 3-11 F, Bar = 2  $\mu$ m) of the anther wall (according to Grunewald et al., 2020). Indicated are the endothecium (Ed), the middle layer (MI), and the tapetum (T) enclosing the locule space (L) which contains the male microgametophyte (M) covered by the exine (E). Three transporter-mediated pathways involved in the formation of the outer pollen wall, are shown. ABCG9 and ABCG31 are required for transport of sterol glycosides (Choi et al., 2014). ABCG26 is required for the deposition of polyketide precursors for sporopollenin formation (Quilichini et al., 2014a). FST1 is required for flavonol sophoroside deposition for tryphine formation (red indicated). ER-derived tapetosomes may contribute to the flavonoid metabolism (Hsieh and Huang, 2007). The role of MATE transporters as well as the transport mechanism of the HCAAs are still unknown. The putative contribution of lipid transfer proteins (LTPs) or vesicle-mediated transport (blue indicated) is speculative. (Cartoon modified from Grunewald et al., 2020).

The ER-association of the terminal glycosyltransferase UGT79B6 (3.9.1) is special and controversial. In general, plant glycosyltransferases are soluble enzymes considered to be free in the cytosol (Li et al., 2015; Sun et al., 2016; Demurtas et al., 2019). The UGT79B6 orthologue UGT79B31 from *P. hybrida* was previously shown to be a cytosolic protein (Knoch et al., 2018), despite earlier suggestions of a (pollen-) membrane association (Vogt and Taylor, 1995). The GFP-based subcellular localization assays of the UGT79B6-GFP by CLSM suggest an association of the glycosyltransferase to the cytosolic site of the ER, although *in silico* predictions revealed no putative post-translational modification sites by which a covalent membrane association could be realized like for example S-acylation.

An ER-localization would be in line with the presumed association of the flavonoid biosynthesis at the cytosolic site of the ER (Burbulis and Winkel-Shirley, 1999; Dastmalchi et al., 2016; Nakayama et al., 2019) which may be also valid for the tapetum (Hsieh and Hunag, 2007; Li et al., 2012). Contemporary studies provide support for the assumption that the ER acts as general branching point for several pathways of the secondary metabolism (Jørgensen et al., 2005; Demurtas et al., 2018; Nakayama

et al., 2019) with cytochrome P450 enzymes as anchors for the formation of a dynamic metabolon while most of the other enzymes are proposed to be soluble (Ralston and Yu, 2006; Nakayama et al., 2019). In *Arabidopsis*, in contrast to Fabales, Poales and Lamiales, the chalcone synthase is the central core for a mutually *in planta* exclusive protein-protein interactions with FLS1 and DFR (Crosby et al., 2011; Nakayama et al., 2019). The CHS-mediated interactions can differ due to organ-, organelle- and temporary-specific expression (Nakayama et al., 2019) but also substrate profile which would be consistent with the idea of a unique, tapetum-specific flavonoid metabolon. The presence of a tapetal flavonoid metabolon appears also consistent with the knowledge of recent findings about a comparable ER-associated metabolon of sporopollenin biosynthetic enzymes in the tapetum (Lallemand et al., 2013).

Immuno-gold-labelling of UGT79B6 would enable the indirect, sub-localization of this special glycosyltransferase directly inside the tapetum with the benefits of high-resolution electron microscopy. Due to the strong expression observed by the promoter-GFP reporter assays, a sufficient UGT79B6 signal intensity could be expected. A promoter-UGT79B6:UGT79B6-*mCherry* construct which could be stable transformed in the background of a suitable *Arabidopsis* ER-reporter lines (ER-gk CS16251 (GFP), ER-yk CS16252 (YFP)) as provided by Nelson et al. (2007). Transient expression of UGT79B6-GFP in *N. benthamiana* leaves and (sub-) organelle isolation by ultracentrifugation combined with immunoblot analysis and verification of the enzymatic activity could also shed light on the subcellular localization. Comparable approaches, including pull-down assays were performed by Lallemand et al. (2013) to verify the ER-localization of sporopollenin biosynthetic enzymes in *Arabidopsis* anthers.

## 4.6 Physiological aspects of pollen-specific flavonol glycosides

### 4.6.1 Flavonol glycosides and pollen tube germination

Classical *in vitro* studies of the pollen tube germination rate of *fst1* and *78d2 x sht* mutant pollen revealed no convincing significant changes in comparison to the wild-type (3.6 and 3.9.5). These results were not unexpected. In *Arabidopsis* is still an apparent lack of knowledge about the functional role of flavonoids on the pollen coat in contrast to other plant species (Ylstra et al., 1996; Burbulis et al., 1996; Fellenberg and Vogt, 2015). In maize and the Solanaceae it is well-known that these specialized metabolites are essential for plant fecundity and those corresponding flavonoid-deficient *chs* mutant lines are drastically deficient in pollen germination (Mo et al., 1992; Ylstra et al., 1992; Pollak et al., 1995; Schijlen et al., 2007). Flavonoid deficient mutants in petunia and maize are reversible conditional male fertile; their mutants are self-infertile but still functional in outcrosses, when specific flavonols are applied (Mo et al., 1992; Pollak et al., 1995). Whereby, in maize *chs* mutant pollen is able of *in vitro* and *in vivo* pollen tube formation, the pollen tube aborts before fertilization of the ovaries (Pollak et al., 1995). Further, silencing of the chalcone synthase in tomato also causes male sterility and is accompanied by reduced fruit set with parthenocarpic fruits (Schijlen et al., 2007). Moreover, the highly conserved  $\beta$ -1  $\rightarrow$ 2-glycosyl-linkage of the flavonol-3-*O*-sophorosides and their high amounts on the pollen of diverse plant species implicate an evolutionary conserved physiological function *in planta* (Ceska and Styles, 1984; Markham and Campos, 1996; Ferreres et al., 1989). Conversely, *Arabidopsis chs* mutants have no obvious effects on male fertility (Ylstra et al., 1996; Burbulis et al., 1996). The *fst1*, *78d2*,

and *78d2 x sht* mutant lines exhibited no significant restriction of plant reproduction in the greenhouse. If this exception in the case of *Arabidopsis* could be related to the dry Brassicaceae stigma type which differs from the wet Solanaceae stigma, and if this phenomenon is also applicable for other Brassicales, is still unstudied. It is discussed that in the *chs* *Arabidopsis* mutant the lack of flavonoids could be compensated by brassinosteroids which also promote pollen tube formation and control male fertility in plants (Ylstra et al., 1995; Ye et al., 2010). While sinapate esters were reported to act as pollen germination inhibitors suggesting the presence of a complex system of positive and negative pollen tube elongation factors (Kim et al., 1996). Altogether, the rapid pollen tube germination response to specific flavonols applied in just nanomolar concentrations (Mo et al., 1992) correlates to their discussed signalling function in plants (an excellent review about this topic was published by Taylor and Grotewold (2005)). The work of Kim et al. (1996) clearly suggested that on *Arabidopsis* pollen the lack/presence of flavonols (quercetin) or sinapate esters results in just qualitative alterations of the pollen tube elongation and has just minor effects on the germination rate instead of drastically loss-of-functions as reported for Solanaceae (Mo et al., 1992; Ylstra et al., 1992). Noteworthy, these kinds of qualitative changes were measured by Kim et al. (1996) for *chs* pollen which is, in opposite to the *fst1* pollen, completely devoid of pollen flavonoids. It should be pointed out that the *fst1* pollen still contains 10% of the flavonol-3-*O*-sophorosides of the wild-type level which could be still sufficient for its physiological function. But in *Arabidopsis* (Kim et al., 1996), as well as in petunia and tobacco the flavonol aglycones are demonstrated to be the biological active compounds (Mo et al., 1992; Ylstra et al., 1992). Vogt et al. (1995) demonstrated that rapid pollen tube formation in *P. hybrida* is just inducible by non-modified flavonols exposing free 3-OH and 7-OH positions. It can be assumed that, the glycosylation provides the required solubility and protection of the aglycone against oxidation in the locule fluid. The glycosylation gives the flavonols additionally an amphipathic character. Interestingly, Kim et al. (1996) also observed that *Arabidopsis* wild-type pollen showed the slowest pollen tube growth rate in *chs* pistils, suggesting that the action of flavonols is also dependent on the pistil rather than only limited to the pollen.

#### 4.6.2 UV-stress and pollen flavonoids

Due to the limited effects in *Arabidopsis*, the question arises, if 'sophorosylated' flavonols fulfil additional biological roles besides pollen tube formation? According to their biological function flavonoids are generally considered as protectants against UV-light in literature (Dixon and Paiva, 1995; Agati and Tattini, 2010). Notwithstanding, mainly UV-stress inducible anthocyanins are reported to function as UV-protectants (Yamasaki et al., 1996; Acquaviva et al., 2003). This suggestion is supported by the findings of the *in silico* analysis of the specific *cis*-regulatory motifs (3.4.2). Within the promoter sequences of the *FST1* and the *UGT79B6* the light responsive *cis*-regulatory element IBOXCORE was highly frequent and a high presence of MYB *cis*-regulatory elements which are also discussed in literature to regulate phenylpropanoid biosynthesis in response to UV-stress (Hemm et al., 2001).

The flavonol-3-*O*-sophorosides show two absorbance maxima about 250-260 nm and about 350 nm (Appendix Figure 8-10 A and B) consistent with the maxima of most flavonoid glycosides (Tsimogiannis et al., 2007). UV-stress before pollen germination assays with *fst1* pollen revealed no alterations between *fst1* mutant line and wild-type. Somewhat surprising, this finding contrasts with earlier

reports which strongly suggested an increased susceptibility of pollen germination in flavonoid deficient mutant lines (*chs*, *tt12*, *tt19*) (Hsieh and Huang, 2007). This disparity could be explained by the differential experimental set up (UV-stress before versus during germination) and the residual 10% of flavonol glycosides on *fst1* pollen. Further, the second large group of tryphine phenylpropanoids, the HCAAs which exhibit also an even higher absorbance maximum in the UV-B range (Fellenberg and Vogt, 2015) were unchanged. Interestingly, the absorbance band of the two major HCAA compounds in *Arabidopsis* show a maximum about 315 nm - 325 nm (Appendix Figure 8-10 C and D) which exactly fits in the gap between the flavonoid absorbance maxima. This underlines the idea that both tryphine phenylpropanoids are protective against UV-light. To test this assumed photoprotective role a double knockout line between the well-studied UGT78D2 (*At5g17050*) and the key enzyme of the HCAA biosynthesis, the SHT (*At2g19070*) was crossed (3.9.2). HPLC-MS analysis of methanolic extracts of harvested pollen from the resulting *78d2 x sht* mutant line confirmed that just traces of flavonoids are left and the HCAAs are completely missing. UV-stress pollen germination assays of the *78d2 x sht* pollen where both phenylpropanoids are completely absent revealed a clear reduction of the relative pollen tube germination rate of about over 60% after 2 hours. These findings support the suggestion that both phenylpropanoid classes have an additive effect. For further proof, it will be indispensable to test the single mutant lines *78d2* and *sht* in future UV-stress experiments. In addition, the pollen viability rate without UV-stress of the *78d2 x sht* double knockout line was significantly lower than the wild-type. Interestingly, these results agree well to the reported reduction of pollen viability about 20% for the *myb99* *Arabidopsis* mutant line which shows absent flavonol-3-*O*-sophoroside and HCAAs levels in stamen by Battat et al. (2019). Nevertheless, further experimental approaches with pollen from all mutants *78d2 x sht*, *chs*, *78d2*, *sht* and *fst1* will be helpful to verify the relevance of UV-stress response of these pollen-specific phenylpropanoids. Furthermore, other abiotic kinds of stress like water/drought stress (Choi et al., 2014) could be tested.

#### 4.6.3 Heat stress and pollen flavonoids

Flavonoids are also discussed in the current literature as associated to heat-stress during the male gametophyte development. So, it was shown that pollen viability and pollen tube germination and elongation is drastically decreased in a flavonoid deficient tomato mutant line under heat-stress resulting in reduced seed set (Muhlemann et al., 2018). Interestingly, a *chs* null allele mutant in purple morning glory (*Ipomoea purpurea*) is also reported to be self-fertile as the *Arabidopsis chs* mutant but shows conditional infertility under heat stress (Coberly and Rausher, 2003). Furthermore, it has been shown that flavonoids are also heat-inducible, so a kaempferol di-hexose significantly increases 16.7 times on mature pollen in tomato under heat-stress conditions (Paupière et al., 2017). All these findings support the assumption of an additional physiological function of these specialized metabolites in general pollen and plant fitness. The male gametophyte is generally reported to be highly vulnerable to heat-stress and its derived effects like ROS accumulation and carbohydrate starvation, especially, during its earlier developmental stages (Müller and Rieu, 2016; Begcy et al., 2019). There, flavonols are suggested to have a protective role under heat stress conditions due to their antioxidative properties (Müller and Rieu, 2016; Muhlemann et al., 2018). Especially, the tapetum itself has been pointed out as highly vulnerable point for plant fecundity and male fertility (Parish et al., 2012). Several reports

indicate that male fertility is dramatically sensitive to heat-stress, particular in crop plants including rice, barley, and wheat at temperatures as of 30 °C which is consequently accompanied by tapetum-malfunction (Parish et al., 2012). In rice tapetum cells, heat-stress cause ultrastructural changes in mitochondria and in the ER (Ku et al., 2003). Conversely to these structural changes in rice, no abnormalities of the mitochondria or the ER are detected by the TEM imaging of *fst1* and *78d2 x sht* anther cross sections (3.5 and 3.9.4). But these plants were grown at moderate 24 °C (day) / 19 °C (night) conditions in a climatic green house. Pollen and tapetum accumulate about twenty times more mitochondria than vegetative cells and have a fast respiration rate during development and pollen tube growth by which a dramatic increase of reactive oxygen species can be assumed under heat-stress conditions (Müller and Rieu, 2016). Evidence for this protective role has shown that the ROS-producing complex I and cytochrome c are indeed targets of flavonoids by which hydrogen peroxide production in mitochondria is prevented (Lagoa et al., 2011). In the light of agricultural production and often discussed global warming (Müller and Rieu, 2016), it will be important to understand this fertility-protection by flavonoids concerning the dramatic temperature-sensitivity of pollen (Paupière et al., 2014).

#### **4.6.4 Are pollen-specific flavonoid glycosides involved in biotic interactions?**

In the current literature additional physiological functions of pollen-associated flavonoids and their specific modification are hypothesised concerning biotic interactions. One suggestion is a mechanism for the limitation of cross pollination due to the species, sex, and family-specific found flavonoid glycoside patterns (Markham and Campos, 1996). A function as visual or flavourful attractant of pollinators is also thinkable like the 8-methoxy-kaempferol-3-*O*-sophoroside which was identified as yellow pigment on almond pollen (Ferrerres et al., 1989). Wilmsen et al. (2017) reported that the yellow quercetin is required as an initial visual stimulus for bumblebees. But the visual stimulus alone is not sufficient to trigger the full behavioural of the pollinator. Besides visual and olfactory also gustatory stimuli are required which could be provided by specific glycosylation patterns. It is known that the occurrence and specific linkage of glycosylation patterns determines the gustatory perception of natural compounds in humans (Esaki et al., 1994; Frydman et al., 2004). Similar mechanisms of gustatory perception are likely conserved in insects and other pollinators. The flavonol-3-*O*-sophoroside precursor quercetin-3-*O*-glucoside on the pollen surface of *Helianthus annuus* was reported as feeding stimuli of the corn root worm (*Diabrotica virgifera*) (Lin and Mullin, 1999). Likewise, some swallowtail butterflies are stimulated to lay eggs on Citrus leaves by quercetin-3-*O*-rutinoside, but are deterred by quercetin-3-*O*-(2- $\beta$ -D-xylopyranosylrutinoside) on the non-host plant *Orixa japonica* (Nishida et al., 1990). These examples provide support that specific-glycosylated flavonoids can act in a complex manner as gustatory stimuli in insects. The pollen from the phenylpropanoid deficient tryphine mutant line *78d2 x sht* as well as the individual mutants *78d2*, *sht*, *fst1* and the classical *chs* mutant present valuable tools which could be tested in prospective insect feeding assays to test their potential as putative stimuli to pollinators like honey bees or pests like the corn root worm. On the other hand, similar  $\beta$ -1  $\rightarrow$ 2-linked flavonol glycosides are not exclusively for insect pollinated angiosperms. Such flavonol glycosides are also present on pollen of wind-pollinated plants, monocots as well as dicots, suggesting an even wider conserved function not only limited to attraction.



## 4.7 Future aspects for applied research

The functional characterization of plant specialized metabolite transporters is essential not only for our understanding of physiological processes, but also for possible applications in agricultural crop breeding or biotechnology (Nour-Eldin and Halkier, 2013; Niño-González et al., 2019).

The expression of transporters has already successfully been used to improve plant stress tolerance illustrating their enormous potential for advanced breeding and genetic engineering. Recently, it was demonstrated that the overexpression of a cotton MATE transporter leads to increased drought, salt and cold stress tolerance in *Arabidopsis* (Lu et al., 2019). It was further reported that increased accumulation of glucosinolates in a *gtr1gtr2* *Arabidopsis* mutant improved plant defence against the pest *Myzus persicae* (Madsen et al., 2015). Such specific genetic silencing of NPF-transporters has also been successfully demonstrated by the 70% reduction of toxic glucosinolates in *Brassica* oilseeds (Nour-Eldin et al., 2017). The implementation of similar applied approaches by transporter engineering of FST1 orthologues that were preliminary identified in potato, tomato, and maize (3.8) could be feasible.

Flavonoids play determinant roles in modulation of plant tolerance to environmental stresses and are crucial for male-fertility and seed set in various crops (maize, tomato, tobacco) (Mo et al., 1992; Pollak et al., 1995; Schijlen et al., 2007; Muhlemann et al., 2018). Therefore, tapetum-specific flavonol-glycoside transporters in crop plants could be possible targets for the generation of desirable traits including male sterile cultivars, seed-less fruits, or improved thermo-tolerance during pollen development. Impaired self-pollination in flavonol-deficient crops could also be used to generate ideal female lines for hybrid seed production like the two-line system of environment-sensitive genetic male sterility (Chen and Liu, 2014). Thereby, male sterility is requested to generate high-yield hybrid crop varieties and to prevent unintended outbreeding and possible release of transgenes into the food chain (Konagaya et al., 2008; Chen and Liu, 2014). Furthermore, anther-specific promoters as identified in this study have also been tested as novel tools to generate genetically engineered male-sterile lines in various crops (Roque et al., 2007; Konagaya et al., 2008).

Regarding biotechnological flavonoid producing systems, engineered microbes cannot completely fulfil industrial requirements (Zha et al., 2019). Introduction of transporters in microbial systems could help to overcome limitations caused by product feedback inhibitions and toxicity effects; or facilitate product isolation from the growth medium resulting in higher product yields.

## 5 Summary

Flavonol sophorosides are well documented as soluble components of the pollenkit in diverse angiosperms since several decades. Their biosynthesis, regulation, and physiological function are an ongoing topic of research. The Intention of the present thesis was to investigate the transport of flavonol sophorosides from the tapetum to the pollen surface.

During the identification various putative candidate of the ABC-, MATE-, and NPF-transporter families were examined via screening of pollen extracts of their corresponding Arabidopsis knockout lines. Thereby, a knockout of the gene *At5g28470* encoding the transporter NPF2.8, resulted in a drastic reduction of flavonol-3-*O*-sophorosides in methanolic pollen extracts, whereas these were not reduced in extracts of whole *npf2.8* anthers. The second class of phenylpropanoids on pollen grains, the hydroxycinnamic acid amides (HCAAs) were unaffected. NPF2.8 thereupon was annotated as a tapetal flavonol glycoside transporter and termed FLAVONOL SOPHOROSIDE TRANSPORTER 1 (FST1). FST1 (*At5g28470*) was further characterized in terms of its cellular and physiological function. The reduced flavonol-3-*O*-sophoroside level of the *fst1* mutant was restored to wild-type level in complementation lines proving the role of FST1. qRT-PCR analysis and *promFST1:GFP* reporter localization studies indicated that *FST1* is specifically expressed in anthers, inside the tapetum. GFP-based localization studies showed that FST1 is localized in the plasma membrane, whereby, CLSM studies of *promFST1:FST1-GFP* lines confirmed the plasma membrane localization in tapetal cells. By means of the former characterized UGT79B6 and UGT78D2 <sup>14</sup>C-labelled flavonol-3-*O*-glycosides were produced as substrates for *in vitro* functional characterization studies. The transport of these radioactive labelled substrates in microbial uptake assays demonstrated that FST1 has flavonoid glycoside transporter activity.

To determine the physiological function of pollen-specific phenylpropanoids, a *78d2 x sht* double mutant was generated by crossing of two Arabidopsis lines which are deficient for two key enzymes of the flavonoid and HCAA biosynthesis. Pollen extracts of the *78d2 x sht* double mutant had no detectable HCAAs and just traces of flavonol glycosides. Whereas the *fst1* mutant did not show reduced pollen viability or pollen germination in UV-stress experiments, the *78d2 x sht* line exhibited reduced pollen viability and significant reduced pollen germination rate. Morphological changes within the tapetum and during the microgametogenesis were neither observed for the *fst1* nor for the *78d 2 x sht* line.

The discovery that a member of the nitrate/peptide transporter family is involved in flavonoid transport once more illustrates the enormous plasticity and diversity of evolutionary processes during the development of plant secondary metabolism originating from primary metabolism.

## 6 Zusammenfassung

Flavonolsophoroside sind als lösliche Komponenten des Pollenkitts in diversen Angiospermen seit einigen Jahrzehnten umfassend dokumentiert. Ihre Biosynthese, Regulation und physiologische Funktion sind Gegenstand aktueller Forschung. Die Aufgabe der vorliegenden Arbeit war es den Transport der Flavonolsophoroside vom Tapetum zur Pollenoberfläche zu untersuchen.

Im Rahmen der Identifizierung wurden mehrere mögliche Kandidaten aus den Familien der ABC-, MATE- und NPF-Transporter durch Screening von Pollenextrakten ihrer entsprechenden Arabidopsis *knockout*-Linien untersucht. Dabei zeigte sich, dass ein Ausschalten des Gens *At5g28470*, welches den Transporter NPF2.8 codiert, zu einer drastischen Reduktion der Flavonol-3-*O*-sophoroside in methanolischen Pollenextrakten führt, wobei diese in Extrakten ganzer *npf2.8*-Antheren nicht reduziert waren. Die zweite Klasse von Pollen spezifischen Phenylpropanoiden, die Hydroxyzimtsäureamide (HCAAs) war unverändert. *NPF2.8* wurde daraufhin charakterisiert als Tapetum Flavonolglykosid-Transporter und als FLAVONOL SOPHOROSIDE TRANSPORTER 1 (FST1) bezeichnet. FST1 (*At5g28470*) wurde in Hinsicht auf seine zelluläre und physiologische Funktion weiter untersucht. Das Niveau der reduzierten Flavonol-3-*O*-sophoroside der *fst1*-Mutante wurde in Komplementationslinien wieder auf das Niveau des Wildtyps zurückversetzt. Diese Versuche belegen FST1 als spezifischen Transporter. Über qRT-PCR-Analyse und *promFST1:GFP*-Reporter-Lokalisationsstudien wurde gezeigt, dass *FST1* Antheren-spezifisch, im Tapetum exprimiert wird. GFP-basierte Lokalisationsstudien zeigten, dass FST1 in der Plasmamembran lokalisiert ist, wobei CLSM-Studien mit *promFST1:FST1-GFP*-Linien auf die Lokalisation in der Plasmamembran von Tapetumzellen hinweisen. Mit Hilfe der zuvor charakterisierten UGT79B6 und UGT78D2 wurden <sup>14</sup>C-markierte Flavonol-3-*O*-glykoside als Substrate für die funktionelle *in vitro* Charakterisierung von FST1 hergestellt. Der Transport dieser markierten Substrate in mikrobiellen Aufnahmeversuchen zeigte, dass FST1 die Aktivität eines Flavonoidglykosid-Transporters besitzt.

Um darüber hinaus die physiologische Funktion Pollen-spezifischer Phenylpropanoide aufzuklären, wurde eine *78d2 x sht*-Doppelmutante durch Kreuzung zweier Arabidopsis Linien, welche defizient sind für die Schlüsselenzyme der Flavonoid- und HCAA-Biosynthese, generiert. Pollenextrakte der *78d2 x sht*-Doppelmutante enthielten keine nachweisbaren HCAAs und nur noch Spuren von Flavonoidglykosiden. Die *fst1*-Mutante zeigte weder bei klassischen Pollenassays noch UV-Stressversuchen eine deutlich veränderte Pollenvitalität oder -keimung. In Gegensatz dazu, wies die *78d2 x sht*-Linie eine Reduktion der Pollenvitalität und unter UV-Stress eine stark verminderte Pollenkeimungsrate auf. Morphologische Veränderungen innerhalb des Tapetums und während der Mikrogametogenese wurden weder für die *fst1*- noch die *78d2 x sht*-Linie beobachtet.

Die Erkenntnis das ein Transporter aus der Familie der Nitrat- und Peptid-Transporter im Flavonoid-Transport involviert ist, ist ein weiteres Beispiel für die Plastizität und Vielfältigkeit evolutiver Prozesse während der Entwicklung des pflanzlichen Sekundärmetabolismus aus potentiellen Vorläufern des Primärstoffwechsels.

## 7 References

- Abe, H., Urao, T., Ito, T., Seki, M., Shinozaki, K., and Yamaguchi-Shinozaki, K.** (2003) Arabidopsis AtMYC2 (bHLH) and AtMYB2 (MYB) function as transcriptional activators in abscisic acid signaling. *Plant Cell* 15: 63-78.
- Acquaviva, R., Russo, A., Galvano, F., Galvano, G., Barcellona, M.L., Volti, G.L., and Vanella, A.** (2003) Cyanidin and cyanidin 3-O-beta-D-glucoside as DNA cleavage protectors and antioxidants. *Cell Biol. Toxicol.* 19: 243-252.
- Agati, G., and Tattini, M.** (2010) Multiple functional roles of flavonoids in photoprotection. *New Phytol.* 186: 786-793.
- Akagi, T., Ikegami, A., Tsujimoto, T., Kobayashi, S., Sato, A., Kono, A., and Yonemori, K.** (2009) DkMyb4 is a MYB transcription factor involved in proanthocyanidin biosynthesis in persimmon fruit. *Plant Physiol.* 151: 2028-2045.
- Akbari, M., Nejadatari, T., Noori, M., Majd, A., and Cheregani, A.** (2017) Pollen grain flavonoid studies of four Iranian *Trifolium* (Leguminosae) taxa as future honey biomarkers. *Phytologia Balcanica*, 23: 17-22.
- Alcalde-Eon, C., García-Estévez, I., Rivas-Gonzalo, J.C., Rodríguez de la Cruz, D., and Escribano-Bailón, M.T.** (2016) Anthocyanins of the anthers as chemotaxonomic markers in the genus *Populus* L.. Differentiation between *Populus nigra*, *Populus alba* and *Populus tremula*. *Phytochemistry*. 128: 35-49.
- Alonso, J.M., Stepanova, A.N., Leisse, T.J., Kim, C.J., Chen, H., Shinn, P., Stevenson, D.K., Zimmerman, J., Barajas, P., Cheuk, R., Gadrinab, C., Heller, C., Jeske, A., Koesema, E., Meyers, C.C., Parker, H., Prednis, L., Ansari, Y., Choy, N., Deen, H., Geralt, M., Hazari, N., Hom, E., Karnes, M., Mulholland, C., Ndubaku, R., Schmidt, I., Guzman, P., Aguilar-Henonin, L., Schmid, M., Weigel, D., Carter, D.E., Marchand, T., Risseeuw, E., Brogden, D., Zeko, A., Crosby, W.L., Berry, C.C., and Ecker, J.R.** (2003) Genome-wide insertional mutagenesis of *Arabidopsis thaliana*. *Science* 301: 653–657.
- Altschul, S.F., Madden, T.L., Schäffer, A.A., Zhang, J., Zhang, Z., Miller, W., and Lipman, D.J.** (1997) Gapped BLAST and PSI-BLAST: a new generation of protein database search programs. *Nucleic Acids Res.* 25: 3389-3402.
- Amano, I., Kitajima, S., Suzuki, H., Koeduka, T., and Shitan, N.** (2018) Transcriptome analysis of *Petunia axillaris* flowers reveals genes involved in morphological differentiation and metabolite transport. *PLoS One* 13: e0198936.
- Ast, M., Gruber, A., Schmitz-Esser, S., Neuhaus, H.E., Kroth, P.G., Horn, M., and Haferkamp, I.** (2009) Diatom plastids depend on nucleotide import from the cytosol. *Proc. Natl. Acad. Sci.* 106: 3621-3626.
- Babst, B.A., Gao, F., Acosta-Gamboa, L.M., Karve, A., Schueller, M.J., and Lorence, A.** (2019) Three NPF genes in Arabidopsis are necessary for normal nitrogen cycling under low nitrogen stress. *Plant Physiol. Biochem.* 143: 1-10.
- Banasiak, J., Biała, W., Staszko, A., Swarczewicz, B., Kępczyńska, E., Figlerowicz, M., and Jasiński, M.** (2013) A *Medicago truncatula* ABC transporter belonging to subfamily G modulates the level of isoflavonoids. *J. Exp. Bot.* 64: 1005-1015.

- Baranowskij, N., Froberg, C., Prat, S., and Willmitzer, L.** (1994) A novel DNA binding protein with homology to Myb oncoproteins containing only one repeat can function as a transcriptional activator. *EMBO J.* 13: 5383-5392.
- Bate, N., and Twell, D.** (1998) Functional architecture of a late pollen promoter: pollen-specific transcription is developmentally regulated by multiple stage-specific and co-dependent activator elements. *Plant Mol. Biol.* 37: 859-869.
- Battat, M., Eitan, A. Rogachev, I., Hanhineva, K., Fernie, A., Tohge, T., Beekwilder, J., and Aharoni, A.** (2019) A MYB triad controls primary and phenylpropanoid metabolites for pollen coat patterning. *Plant Physiol.* 180: 87-108.
- Baxter, I.R., Young, J.C., Armstrong, G., Foster, N., Bogenschutz, N., Cordova, T., Peer, W.A., Hazen, S.P., Murphy, A.S., and Harper, J.F.** (2005) A plasma membrane H-ATPase is required for the formation of proanthocyanidins in the seed coat endothelium of *Arabidopsis thaliana*. *Proc. Natl. Acad. Sci.* 102: 2649-2654.
- Begcy, K., Nosenko, T., Zhou, L.Z., Fagner, L., Weckwerth, W., and Dresselhaus, T.** (2019) Male sterility in maize after transient heat stress during tetrad stage of pollen development. *Plant Physiol.* 181: 683-700.
- Begum, A.A., Leibovitch, S., Migner, P., and Zhang, F.** (2001) Specific flavonoids induced nod gene expression and pre-activated nod genes of *Rhizobium leguminosarum* increased pea (*Pisum sativum* L.) and lentil (*Lens culinaris* L.) nodulation in controlled growth chamber environments. *J. Exp. Bot.* 52: 1537-1543.
- Behrens, C.E., Smith, K.E., Iancu, C.V., Choe, J.-Y., and Dean, J.V.** (2019) Transport of anthocyanins and other flavonoids by the Arabidopsis ATP-binding cassette transporter AtABCC2. *Sci. Rep.* 9: 437.
- Birt, D.F., Hendrich, S., and Wang, W.** (2001) Dietary agents in cancer prevention: flavonoids and isoflavonoids. *Pharmacol. Ther.* 90: 157-177.
- Blackmore, S., Wortley, A.H., Skvarla, J.J., and Rowley, J.R.** (2007) Tansley Review: Pollen wall development in flowering plants. *New Phytol.* 174: 483-498.
- Blakely, R.D., and Bauman, A.L.** (2000) Biogenic amine transporters: regulation in flux. *Curr. Opin. Neurobiol.* 10: 328-336.
- Boachon, B., Lynch, J.H., Ray, S., Yuan, J., Caldo, K.M.P., Junker, R.R., Kessler, S.A., Morgan, J.A., and Dudareva, N.** (2019) Natural fumigation as a mechanism for volatile transport between flower organs. *Nat. Chem. Biol.* 15: 583-588.
- Bradford, M.M.** (1976) A rapid and sensitive method for the quantitation of microgram quantities of protein utilizing the principle of protein-dye binding. *Anal. Biochem.* 72: 248-254.
- Buer, C.S., Imin, N., and Djordjevic, M.A.** (2010) Flavonoids: New roles for old molecules. *J. Integ. Plant. Biol.* 52: 98-111.
- Büttner, M.** (2010) The Arabidopsis sugar transporter (AtSTP) family: An update. *Plant Biol. (Stuttg.)* 12(1): 35-41.
- Burbulis, I.E., Iacobucci, M., and Shirley, B.W.** (1996). A null mutation in the first enzyme of flavonoid biosynthesis does not affect male fertility in Arabidopsis. *Plant Cell* 8: 1013-1025.
- Burbulis, I.E., and Winkel-Shirley, B.** (1999) Interactions among enzymes of the Arabidopsis flavonoid biosynthetic pathway. *Proc. Natl. Acad. Sci.* 96: 12929-12934.

- Card, S.D., Pearson, M.N., and Clover, G.R.G.** (2007) Plant pathogens transmitted by pollen. *Australian Plant Pathology* 36: 455–461.
- Ceska, O., and Styles, E.D.** (1984) Flavonoids from *Zea mays* pollen. *Phytochemistry* 23:1822-1823.
- Cheng H., Song, S., Xiao, L., Soo, H.M., Cheng, Z., Xie, D., and Peng, J.** (2009) Gibberellin acts through jasmonate to control the expression of *MYB21*, *MYB24*, and *MYB57* to promote stamen filament growth in *Arabidopsis*. *PLoS Genet.* 5: e1000440.
- Chen, L., and Liu, Y.G.** (2014) Male sterility and fertility restoration in crops. *Annu. Rev. Plant Biol.* 65: 579-606.
- Choi, H., Ohyama, K., Kim, Y.Y., Jin, J.Y., Lee, S.B., Yamaoka, Y., Muranaka, T., Suh, M.C., Fujioka, S., and Lee, Y.** (2014) The role of *Arabidopsis* ABCG9 and ABCG31 ATP binding cassette transporters in pollen fitness and the deposition of steryl glycosides on the pollen coat. *Plant Cell* 26: 310-324.
- Clought, S.J., and Bent, A.** (1998) Floral dip: a simplified method for *Agrobacterium*-mediated transformation of *Arabidopsis thaliana*. *Plant J.* 16: 735-743.
- Coberly, L.C., and Rausher, M.D.** (2003) Analysis of a chalcone synthase mutant in *Ipomoea purpurea* reveals a novel function for flavonoids: amelioration of heat stress. *Mol. Ecol.* 12: 1113-1124.
- Corratgé-Faillie, C., and Lacombe, B.** (2017) Substrate (un)specificity of *Arabidopsis* NRT1/PTR family (NPF) proteins. *J. Exp. Bot.* 68: 3107-3113.
- Crosby, K.C., Pietraszewska-Bogiel, A., Gadella, T.W., and Winkel, B.S.** (2011) Förster resonance energy transfer demonstrates a flavonoid metabolon in living plant cells that displays competitive interactions between enzymes. *FEBS Lett.* 585: 2193-2198.
- Dastmalchi, M., Bernards, M.A., and Dhaubhadel, S.** (2016) Twin anchors of the soybean isoflavonoid metabolon: evidence for tethering of the complex to the endoplasmic reticulum by IFS and C4H. *Plant J.* 85: 689-706.
- Dastmalchi, M., Chang, L., Cheng, R., Yu, L., Cheng, X., Hagel, J.M., and Facchini, P.J.** (2019) Purine permease-type benzylisoquinoline alkaloid transporters in opium poppy. *Plant Physiol.* 183: 916-933.
- David, L.C., Dechorgnat, J., Berquin, P., Routboul, J.M., Debeaujon, I., Daniel-Vedele, F., and Ferrario-Méry, S.** (2014) Proanthocyanidin oxidation of *Arabidopsis* seeds is altered in mutant of the high-affinity nitrate transporter NRT2.7. *J. Exp. Bot.* 65: 885-893.
- Debeaujon, I., Peeters, A.J.M., Léon-Klosterziel, K.M., and Koornneef, M.** (2001) The *TRANSPARENT TESTA12* gene of *Arabidopsis* encodes a multidrug secondary transporter-like protein required for flavonoid sequestration in vacuoles of the seed coat endothelium. *Plant Cell* 13: 853-871.
- Del Río, J.A., Fuster, M.D., Gómez, P., Porras, I., García-Lidon, A., and Ortuño, A.** (2004) *Citrus limon*: A source of flavonoids of pharmaceutical interest. *Food Chemistry* 84: 457-461.
- Demurtas, O.C., de Brito Francisco, R., Diretto, G., Ferrante, P., Frusciante, S., Pietrella, M., Aprea, G., Borghi, L., Feeney, M., Frigerio, L., Coricello, A., Costa, G., Alcaro, S., Martinoia, E., and Giuliano, G.** (2019) ABCC transporters mediate the vacuolar accumulation of crocins in saffron stigmas. *Plant Cell* 31: 2789-2804.
- Demurtas, O.C., Frusciante, S., Ferrante, P., Diretto, G., Azad, N.H., Pietrella, M., Aprea, G., Taddei, A.R., Romano, E., Mi, J., Al-Babili, S., Frigerio, L., and Giuliano, G.** (2018) Candidate enzymes for saffron crocin biosynthesis are localized in multiple cellular compartments. *Plant Physiol.* 177: 990–1006.

- Dixon, R.A., and Paiva, N.L.** (1995) Stress-induced phenylpropanoid metabolism. *Plant Cell* 7: 1085-1097.
- Dixon, R.A., and Strack, D.** (2003) Phytochemistry meets genome analysis, and beyond. *Phytochemistry* 62: 815-816.
- Dobritsa, A.A., Geanconteri, A., Shrestha, J., Carlson, A., Kooyers, N., Coerper, D., Urbanczyk-Wochniak, E., Bench, B.J., Sumner, L.W., Swanson, R., and Preuss, D.** (2011) Large-scale genetic screen in *Arabidopsis* to identify genes involved in pollen exine production. *Plant Physiol.* 157: 2947-2970.
- Dobritzsch, M., Lübken, T., Eschen-Lippold, L., Gorzolka, K., Blum, E., Matern, A., Marillonnet, S., Böttcher, C., Dräger, B.C., and Rosahl, S.** (2016) MATE Transporter-dependent export of hydroxycinnamic acid amides. *Plant Cell* 28: 583-596.
- Dungey, S.G., Sang, J.P., Rothnie, N.E., Palmer, M.V., Burke, D.G., Knox, R.B., Williams, E.G., Hilliard, E.P., and Salisbury, P.A.** (1988) Glucosinolates in the pollen of rapeseed and Indian mustard. *Phytochemistry*. 27: 815-817.
- Edelheit, O., Hanukoglu, A., and Hanukoglu, I.** (2009) Simple and efficient site-directed mutagenesis using two single-primer reactions in parallel to generate mutants for protein structure-function studies. *BMC Biotechnology* 9:61.
- Edreva, A., Velikova, V., Tsoney, T., Dagnon, S., Gürel, A., Aktaş, L., and Gesheva, E.** (2008) Stress-protective role of secondary metabolites: diversity of functions and mechanisms. *Gen. Appl. Plant Physiology* 34: 67-78.
- Elejalde-Palmett, C., Dugé de Bernonville, T., Glevarec, G., Pichon, O., Papon, N., Courdavault, V., St-Pierre, B., Giglioli-Guivarc'h, N., Lanoue, A., and Besseau, S.** (2015) Characterization of a spermidine hydroxycinnamoyltransferase in *Malus domestica* highlights the evolutionary conservation of trihydroxycinnamoyl spermidines in pollen coat of core Eudicotyledons. *J. Exp. Bot.* 22: 7271-7285.
- Engler, C., Youles, M., Gruetzner, R., Ehnert, T.-M., Werner, S., Jones, J.D.G., Patron, N.J., and Marillonnet, S.** (2014) A Golden Gate modular cloning toolbox for plants. *ACS Synth. Biol.* 3: 839-843.
- Esaki, S., Nishiyama, K., Sugiyama, N., Nakajima, R., Takao, Y., and Kamiya, S.** (1994) Preparation and taste of certain glycosides of flavanones and dihydrochalcones. *Biosci. Biotechnol. Biochem.* 58: 1479-1485.
- Fellenberg, C., Böttcher, C., and Vogt, T.** (2009) Phenylpropanoid polyamine conjugate biosynthesis in *Arabidopsis thaliana* flower buds. *Phytochemistry* 70:1392-1400.
- Fellenberg, C., Milkowski, C., Hause, B., Lange, P.-R., Böttcher, C., Schmidt, J., and Vogt, T.** (2008) Tapetum specific location of a cation-dependent *O*-methyltransferase in *A. thaliana*. *Plant J.* 56: 132-145.
- Fellenberg, C., van Ohlen, M., Handrick, V., and Vogt, T.** (2012b) The role of CCoAOMT1 and COMT1 in *Arabidopsis* anthers. *Planta* 236: 51-61.
- Fellenberg, C., and Vogt, T.** (2015) Evolutionarily conserved phenylpropanoid pattern on angiosperm pollen. *Trends Plant Sci.* 20: 212-218.
- Fellenberg, C., Ziegler, J., Handrick, V., and Vogt, T.** (2012a) Polyamine homeostasis in wild type and phenolamide deficient *Arabidopsis thaliana* stamens. *Front. Plant Sci.* 3: 180.

- Ferreres, F., Tomás-Barberán, F.A., Tomás-Lorente, F., Nieto, J.L., Rumbero, A., and Olías, J.M.** (1989) 8-Methoxykaempferol 3-sophoroside, a yellow pigment from almond pollen. *Phytochemistry* 28: 1901-1903.
- Fornalé, S., Lopez, E., Salazar-Henao, J.E., Fernández-Nohales, P., Rigau, J., and Caparros-Ruiz, D.** (2014) AtMYB7, a new player in the regulation of UV-sunscreens in *Arabidopsis thaliana*. *Plant Cell Physiol.* 55: 507-516.
- Francisco, R.M., Regalado, A., Ageorges A., Burla, B., Bassin B., Eisenach, C., Zarrouk, O., Vialet, S., Marlin T., Chaves, M.M., Martinoia, E., and Nagya, R.** (2013) ABCC1, an ATP binding cassette protein from grape berry, transports anthocyanidin 3-*O*-glucosides. *Plant Cell* 25: 1840–1854.
- Frank, S., Keck, M., Sagasser, M., Niehaus, K., Weisshaar, B., and Stracke, R.** (2011) Two differentially expressed MATE factor genes from apple complement the *Arabidopsis* transparent testa12 mutant. *Plant Biol. (Stuttg).* 13: 42-50.
- Freudenberg, K., Knauber, H., and Cramer, F.** (1951) Die Übereinstimmung der Sophorose mit 2-[ $\beta$ -Glucosido]-glucose. *Chemische Berichte* 84: 144-146.
- Frydman, A., Weisshaus, O., Bar-Peled, M., Huhman, D.V., Sumner, L.W., Marin, F.R., Lewinsohn, E., Fluhr, R., Gressel, J., and Eyal, Y.** (2004) Citrus fruit bitter flavors: isolation and functional characterization of the gene *Cm1,2RhaT* encoding a 1,2 rhamnosyltransferase, a key enzyme in the biosynthesis of the bitter flavonoids of citrus. *Plant J.* 40: 88-100.
- Fu, X., Shi, P., He, Q., Shen, Q., Tang, Y., Pan, Q., Ma, Y., Yan, T., Chen, M., Hao, X., Liu, P., Li, L., Wang, Y., Sun, X., and Tang, K.** (2017) AaPDR3, a PDR transporter 3, is involved in sesquiterpene  $\beta$ -Caryophyllene transport in *Artemisia annua*. *Front Plant Sci.* 8:723.
- Fujita, M., and Shinozaki, K.** (2014) Identification of polyamine transporters in plants: Paraquat transport provides crucial clues. *Plant Cell Physiol.* 55: 855-861.
- Giamoustaris, A., and Mithen, R.** (1995) The effect of modifying the glucosinolate content of oilseed rape (*Brassica napus ssp. oleifera*) on its interaction with specialist and generalist pests. *Annals of Applied Biology* 126: 347–363.
- Goiris, K., Muylaert, K., Voorspoels, S., Noten, B., De Paepe, D., E Baart, G.J., and De Cooman, L.** (2014) Detection of flavonoids in microalgae from different evolutionary lineages. *J. Phycol.* 50: 483-492.
- Gomez, C., Terrier, N., Torregrosa, L., Vialet, S., Fournier-Level, A., Verrièrs C., Souquet, J.M., Mazauric, J.P., Klein, M., Cheynier, V., and Ageorges, A.** (2009) Grapevine MATE-type proteins act as vacuolar H<sup>+</sup>-dependent acylated anthocyanin transporters. *Plant Physiol.* 150: 402-415.
- Goodman, C.D., Casati, P., and Walbot, V.** (2004) A multidrug resistance-associated protein involved in anthocyanin transport in *Zea mays*. *Plant Cell* 16: 1812–1826.
- Goto, T., and Kondo, T.** (1991) Structure and molecular stacking of anthocyanins: flower color variation. *Angew. Chem.* 30: 17-33.
- Grace, M.L., Chandrasekharan, M.B., Hall, T.C., and Crowe, A.J.** (2004) Sequence and spacing of TATA box elements are critical for accurate initiation from the beta-phaseolin promoter. *J. Biol. Chem.* 279: 8102-8110.
- Grienenberger, E., Besseau, S., Geoffroy, P., Debayle, D., Heintz, D., Lapierre, C., Pollet, B., Heitz, T., and Legrand, M.** (2009) A BAHD acyltransferase is expressed in the tapetum of *Arabidopsis* anthers and is involved in the synthesis of hydroxycinnamoyl spermidines. *Plant J.* 58: 246-259.



- Grotewold, E., Drummond, B.J., Bowen, B., and Peterson, T.** (1994) The *myb*-homologous *P* gene controls phlobaphene pigmentation in maize floral organs by directly activating a flavonoid biosynthetic gene subset. *Cell* 76: 543-553.
- Grunewald, S., Marillonnet, S., Hause, G., Haferkamp, I., Neuhaus, H.E., Veß, A., Hollemann, T., and Vogt, T.** (2020) The tapetal major facilitator NPF2.8 is required for accumulation of flavonol glycosides on the pollen surface in *Arabidopsis thaliana*. *Plant Cell* 32: 1727-1748.
- Haferkamp, I., and Linka, N.** (2012) Functional expression and characterisation of membrane transport proteins. *Plant Biology* 14: 675-690.
- Hamilton, D.A., Schwarz, Y.H., and Mascarenhas, J.P.** (1998) A monocot pollen-specific promoter contains separable pollen-specific and quantitative elements. *Plant Mol. Biol.* 38: 663–669.
- Harborne, J.B.** (1963) Flavonoid sophorosides. *Experientia* 19: 7–8.
- Harborne, J.B., and Baxter, H.** (1999) *The Handbook of Natural Flavonoids*, Vol. 1. John Wiley & Sons, Chichester, UK, pp. VII-XIII.
- Hartmann, U., Sagasser, M., Mehrrens, F., Stracke, R., and Weisshaar, B.** (2005) Differential combinatorial interactions of *cis*-acting elements recognized by R2R3-MYB, BZIP, and BHLH factors control light-responsive and tissue-specific activation of phenylpropanoid biosynthesis genes. *Plant Mol. Biol.* 57: 155–171.
- Hemm, M.R., Herrmann, K.M., and Chapple, C.** (2001) AtMYB4: A transcription factor general in the battle against UV. *Trends Plant Sci.* 6: 135-136.
- Hempel, F., Stenzel, I., Heilmann, M., Krishnamoorthy, P., Menzel, W., Golbik, R., Helm, S., Dobritsch, D., Baginsky, S., Lee, J., Hoehenwarter, W., and Heilmann, I.** (2017) MAPKs influence pollen tube growth by controlling the formation of phosphatidylinositol 4,5-bisphosphate in an apical plasma membrane domain. *Plant Cell* 29: 3030-3050.
- Heslop-Harrison, J., and Heslop-Harrison, Y.** (1970) Evaluation of pollen viability by enzymatically induced fluorescence; intracellular hydrolysis of fluorescein diacetate. *Stain Technol.* 45: 115-120.
- Higginson, T., Li, S.F., and Parish, R.W.** (2003) AtMYB103 regulates tapetum and trichome development in *Arabidopsis thaliana*. *Plant J.* 35: 177-192.
- Higo, K., Ugawa, Y., Iwamoto, M., and Korenaga, T.** (1999) Plant *cis*-acting regulatory DNA elements (PLACE) database: 1999. *Nucleic Acids Res.* 27: 297-300.
- Hildreth, S.B., Gehman E.A., Yang, H., Lu, R.-H., Ritesh, K.C., Harich, K.C., Yu, S., Lin, J., Sandoe, J.L., Okumoto, S., Murphy, A.S., and Gelesko, J.G.** (2011) Tobacco nicotine uptake permease (NUP1) affects alkaloid metabolism. *Proc. Natl. Acad. Sci.* 108: 18179–18184.
- Hoballah, M.E., Stuurman, J., Turlings, T.C.J., Guerin, P.M., Connétable, S., and Kuhlemeier, C.** (2005) The composition and timing of flower odour emission by wild *Petunia axillaris* coincide with the antennal perception and nocturnal activity of the pollinator *Manduca sexta*. *Planta* 222: 141-150.
- Hooper, C.M., Castleden, I.R., Tanz, S.K., Aryamanesh, N., and Millar, H.H.** (2017) SUBA4: the interactive data analysis center for Arabidopsis subcellular protein locations *Nucleic Acid Res.* 45: D1064–D1074.
- Houlné, G., and Boutry, M.** (1994) Identification of an *Arabidopsis thaliana* gene encoding a plasma membrane H(+)-ATPase whose expression is restricted to anther tissue. *Plant J.* 5: 311-317.

- Hsieh, K., and Huang, A.H.** (2005) Lipid-rich tapetosomes in *Brassica* tapetum are composed of oleosin-coated oil droplets and vesicles, both assembled in and then detached from the endoplasmic reticulum. *Plant J.* 43: 889-899.
- Hsieh, K., and Huang, A.H.** (2007) Tapetosomes in *Brassica* tapetum accumulate endoplasmic reticulum-derived flavonoids and alkanes for delivery to the pollen surface. *Plant Cell* 19: 582-596.
- Huang, M.D., Cheng, T.L.L., and Huang, A.H.C.** (2013) Abundant type III lipid transfer proteins in *Arabidopsis* tapetum are secreted to the locule and become a constituent of the pollen exine. *Plant Physiol.* 163: 1218-1229.
- Ichino, T., Fuji, K., Ueda, H., Takahashi, H., Koumoto, Y., Takagi, J., Tamura, K., Sasaki, R., Aoki, K., Shimada, T., and Hara-Nishimura, I.** (2014) GFS9/TT9 contributes to intracellular membrane trafficking and flavonoid accumulation in *Arabidopsis thaliana*. *Plant J.* 80: 410-423.
- Ischebeck, T., Stenzel, I., and Heilmann, I.** (2008) Type B phosphatidylinositol-4-phosphate 5-kinase mediate *Arabidopsis* and *Nicotiana tabacum* pollen tube growth by regulating apical pectin secretion. *Plant Cell* 20: 3312-3330.
- Ishimaru, Y., Oikawa, T., Suzuki, T., Takeishi, S., Matsuura, H., Takahashi, K., Hamamoto, S., Uozumi, N., Shimizu, T., Seo, M., Ohta, H., and Ueda, M.** (2017) GTR1 is a jasmonic acid and jasmonoyl-L-isoleucine transporter in *Arabidopsis thaliana*. *Biosci. Biotechnol. Biochem.* 81: 249–55.
- Ismail, N., and Alam, M.** (2001) A novel cytotoxic flavonoid glycoside from *Physalis angulata*. *Fitoterapia* 72: 676-679.
- Izhar, S., and Frankel, R.** (1971) Mechanism of male sterility in *Petunia*: The relationship between pH, callase activity in the anthers, and the breakdown of the microsporogenesis. *Theor. Appl. Genet.* 41: 104-108.
- Jack, D.L., Yang, N.M., and Saier, M.H.** (2001) The drug/metabolite transporter superfamily. *Eur. J. Biochem.* 268: 3620-3639.
- Jakobsen, M.K., Poulsen, L.R., Schulz, A., Fleurat-Lessard, P., Møller, A., Husted, S., Schiøtt, M., Amtmann, A., and Palmgren, M.G.** (2005) Pollen development and fertilization in *Arabidopsis* is dependent on the *MALE GAMETOGENESIS IMPAIRED ANthers* gene encoding a type V P-type ATPase. *Genes Dev.* 19: 2757-2769.
- Jasiński, M., Stukkens, Y., Degand, H., Purnelle, B., Marchand-Brynaert, J., and Boutry, M.** (2001) A plant plasma membrane ATP binding cassette-type transporter is involved in antifungal terpenoid secretion. *Plant Cell* 13: 1095-1108.
- Jessen, D., Olbrich, A., Knüfer, J., Krüger, A., Hoppert, M., Polle, A., and Fulda, M.** (2011) Combined activity of *LACS1* and *LACS4* is required for proper pollen coat formation in *Arabidopsis*. *Plant J.* 68: 715-726.
- Jin, Y.S.** (2019) Recent advances in natural antifungal flavonoids and their derivatives. *Bioorg. Med. Chem. Lett.* 29: 126589.
- Johnson-Brousseau, S.A., and McCormick, S.** (2004) A compendium of methods useful for characterization *Arabidopsis* pollen mutants and gametophytically-expressed genes. *Plant J.* 39: 761-775.
- Jørgensen, K., Rasmussen, A.V., Morant, M., Nielsen, A.H., Bjarnholt, N., Zagrobelny, M., Bak, S., and Møller, B.L.** (2005) Metabolon formation and metabolic channeling in the biosynthesis of plant natural products. *Curr. Opin. Plant Biol.* 8: 280-291.

- Jørgensen, M.E., Olsen, C.E., Geiger, D., Mirza, O., Halkier B.A., and Nour-Eldin, H.H.** (2015) A functional EXXEK motif is essential for proton coupling and active glucosinolate transport by NPF2.11. *Plant Cell Physiol.* 56: 2340-2350.
- Jørgensen, M.E., Xu, D., Crocoll, C., Ernst, H.A., Ramírez, D., Motawia, M.S., Olsen, C.E., Nour-Eldin, H.H., and Halkier, B.A.** (2017) Origin and evolution of transporter substrate-specificity within the NPF family. *eLife* 6: e19466.
- Kader, M.S., and Lindberg, S.** (2010) Cytosolic calcium and pH signalling in plants under salinity stress. *Plant Signal. Behav.* 5: 233-238.
- Kang, J., Park, J., Choi, H., Burla, B., Kretschmar, T., Lee, Y., and Martinoia, E.** (2011) Plant ABC transporters. *Arabidopsis Book*. 2011: e0153.
- Kanno, Y., Kamiya, Y., and Seo, M.** (2013) Nitrate does not compete with abscisic acid as a substrate of AtNPF4.6/NRT1.2/AIT1 in *Arabidopsis*. *Plant Signal. Behav.* 8: e26624.
- Kanno, Y., Oikawa, T., Chiba, Y., Ishimaru, Y., Shimizu, T., Sano, N., Koshihara, T., Kamiya, Y., Ueda, M., and Seo, M.** (2016) AtSWEET13 and AtSWEET14 regulate gibberellin-mediated physiological processes. *Nat Commun.* 26: 13245.
- Kim, S.S., Grienenberger, E., Lallemand, B., Colpitts, C.C., Kim, S.Y., de Azevedo Souza, C., Geoffroy, P., Heintz, D., Krahn, D., Kaiser, M., Kombrink, E., Heitz, T., D.Y. Suh, Legrand, M., and Douglas, C.J.** (2010) *LAP6/POLYKETIDE SYNTHASE A* and *LAP5/POLYKETIDE SYNTHASE B* encode hydroxy-alkyl  $\alpha$ -pyrone synthases required for pollen development and sporopollenin biosynthesis in *Arabidopsis thaliana*. *Plant Cell* 22: 4045-4066.
- Kim, T.H., Ku, S.-K., Lee, I.-C., and Bae, J.-S.** (2012) Anti-inflammatory effects of kaempferol-3-O-sophoroside in human endothelial cells. *Inflamm. Res.* 61: 217-224.
- Kim, Y.S., Song, K.S., and Cheong, H.S.** (1996) Effects of flavonoids on pollen tube growth in *Arabidopsis thaliana*. *J. Plant Biol.* 39: 273-278.
- Kitamura, S., Shikazono, N., and Tanaka, A.** (2004) TRANSPARENT TESTA 19 is involved in the accumulation of both anthocyanins and proanthocyanins in *Arabidopsis*. *Plant J.* 37: 104-114.
- Kitamura, S., Matsuda, F., Tohge, T., Yonekura-Sakakibara, K., Yamazaki, M., Saito, K., and Narumi, I.** (2010) Metabolic profiling and cytological analysis of proanthocyanidins in immature seeds of *Arabidopsis thaliana* flavonoid accumulation mutants. *Plant J.* 62: 549-559.
- Kitamura, S., Oono, Y., and Narumi, I.** (2016) *Arabidopsis pab1*, a mutant with reduced anthocyanins in immature seeds from banyuls, harbors a mutation in the MATE transporter FFT. *Plant Mol. Biol.* 90: 7-18.
- Klahre, U., Gurba, A., Herman, K., Saxenhofer, M., Bossolini, E., Guerin, P.M., and Kuhlemeier, C.** (2011) Pollinator choice in *Petunia* depends on two major genetic Loci for floral scent production. *Curr. Biol.* 21: 730-739.
- Klepikova, A.V., Kasianov, A.S., Gerasimov, E.S., Logacheva, M.D., and Penin, A.A.** (2016) A high resolution map of the *Arabidopsis thaliana* developmental transcriptome based on RNA-seq profiling. *Plant J.* 88: 1058-1070.
- Knoch, E., Sugawara, S., Mori, T., Nkabayashi, R., Saito, K., and Yonekura-Sakakibara, K.** (2018) UGT79B31 is responsible for the final modification step of pollen specific flavonoid biosynthesis in *Petunia hybrida*. *Planta* 247: 779-790.

- Konagaya, K., Ando, S., Kamachi, S., Tsuda, M., and Tabei, Y.** (2008) Efficient production of genetically engineered, male-sterile *Arabidopsis thaliana* using anther-specific promoters and genes derived from *Brassica oleracea* and *B. rapa*. *Plant Cell Rep.* 27: 1741-1754.
- Kovinich, N., Kayanja, G., Chanoca, A., Riedl, K., Otegui, M.S., and Grotewold, E.** (2014) Not all anthocyanins are born equal: distinct patterns induced by stress in *Arabidopsis*. *Planta* 240: 931-940.
- Ku, S., Yoon, H., Suh, S.H., and Chung, Y.-Y.** (2003) Male-sterility of thermo sensitive genic male-sterile rice is associated with premature programmed cell death of the tapetum. *Planta* 217: 559–565.
- Laemmli, U.K.** (1970) Cleavage of structural proteins during the assembly of the head of bacteriophage T4. *Nature* 227: 680-685.
- Lagoa, R., Graziani, I., Lopez-Sanchez, C., Garcia-Martinez, V., and Gutierrez Merino, C.** (2011) Complex I and cytochrome *c* are molecular targets of flavonoids that inhibit hydrogen peroxide production by mitochondria. *Biochim. Biophys. Acta* 1807: 1562–1572.
- Lallemand, B., Erhardt, M., Heitz, T., and Legrand, M.** (2013). Sporopollenin biosynthetic enzymes interact and constitute a metabolon localized to the endoplasmic reticulum of tapetum cells. *Plant Physiol.* 162: 616-625.
- Landgraf, R., Smolka, U., Altman, S., Eschen-Lippold, L., Senning, M., Sonnewald, S., Weigel, B., Frolova, N., Strehmel, N., Hause, G., Scheel, D., Böttcher, C., and Rosahl, S.** (2014) The ABC transporter ABCG1 is required for suberin formation in potato tuber periderm. *Plant Cell* 26: 3403-3415.
- Larsen, B., Xu, D., Halkier, B.A., and Nour-Eldin, H.H.** (2017) Advances in methods for identification and characterization of plant transporter function. *J. Exp. Bot.* 68: 4045-40456.
- Lee, M., Choi, Y. Burla, B., Kim, Y.Y., Jeon, B., Maeshima, M., Yoo, J.Y., Martinoia, E., and Lee, Y.** (2008) The ABC transporter AtABC14 is a malate importer and modulates stomatal response to CO<sub>2</sub>. *Nat. Cell Biol.* 10: 1217-1223.
- Lefèvre, F., and Boutry, M.** (2018) Towards identification of the substrates for ATP-binding cassette transporters. *Plant Physiol.* 178: 18-39.
- Leopoldini, M., Russo, N., and Toscano, M.** (2011) The molecular basis of working mechanism of natural polyphenolic antioxidants. *Food Chemistry* 125: 288-306.
- Léran, S., Varala, K., Boyer, J.C., Chiurazzi, M., Crawford, N., Daniel-Vedele, F., David, L., Dickstein, R., Fernandez, E., Forde, B., Gassmann, W., Geiger, D., Gojon, A., Gong, J.-M., Halkier, B.A., Harris, J.M., Hedrich, R., Limami, A.M., Rentsch, D., Seo, M., Tsay, Y.-F., Zhang, M., Coruzzi, G., and Lacombe, B.** (2014) A unified nomenclature of NITRATE TRANSPORTER1/PEPTIDE TRANSPORTER family members in plants. *Trends Plant Sci.* 19: 5-9.
- Li, H., Rachel, M.H., Michael, X.Z., and Zhenbiao, Y.** (1999) Control of pollen tube tip growth by a rop GTPase-dependent pathway that leads to tip-localized calcium influx. *Plant Cell* 11: 1731-1742.
- Li, H., Yu, M., Du, X.-Q., Wang, Z.-F., Wu, W.-H., Quintero, F.J., Jin, X.-H., Li, H.-D., and Wang, Y.** (2017) NRT1.5/NPF7.3 functions as a proton-coupled H<sup>+</sup>/K<sup>+</sup> antiporter for K<sup>+</sup> loading into the xylem in *Arabidopsis*. *Plant Cell* 29: 2016-2026.
- Li, J.-Y., Fu, Y.L., Pike, S.M., Bao, J., Tian, W., Zhang, Y., Chen, C.-Z., Zhang, Y., Li, H.-M., Huang, J., Li, L.G., Schroeder, J.I., Gassmann, W., and Gong, J.-M.** (2010) The *Arabidopsis* nitrate transporter NRT1.8 functions in nitrate removal from the xylem sap and mediates cadmium tolerance. *Plant Cell* 22: 1633-1646.

- Li, L., He, Z., Pandey, G.K., Tsuchiya, T., and Luan, S.** (2002) Functional cloning and characterization of a plant efflux carrier for multidrug and heavy metal detoxification. *J. Biol. Chem.* 277: 5360-5368.
- Li, W., Zhang, F., Chang, Y., Zhao, T., Schranz, M.E., and Wang, G.** (2015) Nicotinate *O*-glucosylation is an evolutionarily metabolic trait important for seed germination under stress conditions in *Arabidopsis thaliana*. *Plant Cell* 27: 1907–1924.
- Li, Y., Suen, D.F., Huang, C.-Y., Kung, S.-Y., and Huang, A.H.C.** (2012) The maize tapetum employs diverse mechanisms to synthesize and store proteins and flavonoids and transfer them to the pollen surface. *Plant Physiol.* 158: 1548-1561.
- Lim, E.-K.** (2005) Plant glycosyltransferases: their potential as novel biocatalysts. *Chem. Eur. J.* 11: 5486-5494.
- Lim, E.-K., Ashford, D.A., Hou, B., Jackson, R.G., and Bowles, D.J.** (2004). *Arabidopsis* glycosyltransferases as biocatalysts in fermentation for regioselective synthesis of diverse quercetin glucosides. *Biotechnol. Bioeng.* 87: 623–631.
- Lin, S., and Mullin, C.A.** (1999) Lipid, polyamide, and flavonol phagostimulants for adult western corn rootworm from sunflower (*Helianthus annuus* L.) pollen. *J. Agric. Food Chem.* 47: 1223-1229.
- Liu, K.-H., and Tsay, Y.-F.** (2003) Switching between the two action modes of the dual-affinity nitrate transporter CHL1 by phosphorylation. *EMBO J.* 22: 1005-1013.
- Logemann, E., Parniske, M., and Hahlbrock, K.** (1995) Modes of expression and common structural features of the complete phenylalanine ammonia-lyase gene family in parsley. *Proc. Natl. Acad. Sci.* 92: 5905-5909.
- Lu, P., Magwanga, R.O., Kirungu, J.N., Hu, Y., Dong, Q., Cai, X., Zhou, Z., Wang, X., Zhang, Z., Hou, Y., Wang, K., and Liu, F.** (2019) Overexpression of cotton a *DTX/MATE* gene enhances drought, salt, and cold stress tolerance in transgenic *Arabidopsis*. *Front. Plant Sci.* 10: 299.
- Lüscher, B., and Eisenman, R.N.** (1990) New light on Myc and Myb. Part II. Myb. *Genes Dev.* 4: 2235-2241.
- Madsen, S.R., Kunert, G., Reichelt, M., Gershenson, J., and Halkier, B.A.** (2015) Feeding on leaves of the glucosinolate transporter mutant *gtr1gtr2* reduces fitness of *Myzus persicae*. *J. Chem. Ecol.* 41: 975-984.
- Maher, P., Akaishi, T., and Abe, K.** (2006) Flavonoid fisetin promotes ERK-dependent long-term potentiation and enhances memory. *Proc. Natl. Acad. Sci.* 103: 16568-16573.
- Markham, K.R., and Campos, M.** (1996) 7- and 8-*O*-methylherbacetin-3-*O*-sophorosides from bee pollens and some structure/activity observations. *Phytochemistry* 43: 763-767.
- Markham, K.R., and Porter, L.J.** (1969) Flavonoids in the green algae (chlorophyta). *Phytochemistry* 9: 1777-1781.
- Marinova, K., Pourcel, K., Weder, B., Schwarz, M., Barron, D., Routaboul, J.M., Debeaujon, I., and Klein, M.** (2007) The *Arabidopsis* MATE transporter TT12 acts as a vacuolar flavonoid/H<sup>+</sup>-antiporter active in proanthocyanidin-accumulating cells of the seed coat. *Plant Cell* 19: 2023-2038.
- Martinoia, E., Maeshima, M., and Neuhaus, H.E.** (2007) Vacuolar transporters and their essential role in plant metabolism. *J. Exp. Bot.* 58: 83-102.
- Martin-Tanguy, J.** (1985) The occurrence and possible function of hydroxycinnamoyl acid amides in plants. *Plant Growth Regul.* 3: 381–399.

- Matsuno, M., Compagnon, V., Schoch, G.A., Schmitt, M., Debayle, D., Bassard, J.E., Pollet, B. Hehn, A., Heintz, D., Ullmann, P., Lapierre, C., Bernier, F., Ehltng, J., and Werck-Reichhart, D.** (2009) Evolution of a novel phenolic pathway for pollen development. *Science* 325: 1688-1692.
- Mayfield, J.A., and Preuss, D.** (2000) Rapid initiation of Arabidopsis pollination requires the oleosin-domain protein GRP17. *Nat. Cell Biol.* 2: 128-130.
- Meurer, B., Wray, V., Wiermann, R., and Strack, D.** (1988) Hydroxycinnamic acid-spermidine amides from pollen of *Alnus glutinosa*, *Betula verrucosa* and *Pterocarya fraxinifolia*. *Phytochemistry* 27: 839–843.
- Miyahara, T., Sakiyama, R., Ozeki, Y., and Sasaki, N.** (2013) Acyl-glucoside-dependent glucosyltransferase catalyzes the final step of anthocyanin formation in Arabidopsis. *J. Plant Physiol.* 170: 619–624.
- Mo, Y., Nagel, C., and Taylor, L.P.** (1992) Biochemical complementation of chalcone synthase mutants defines a role for flavonols in functional pollen. *Proc. Natl. Acad. Sci.* 89: 7213-7217.
- Mueller, L.A., Goodman, C.D., Silady, R.A., and Walbot, V.** (2000) AN9, a Petunia glutathione S-transferase required for anthocyanin sequestration, is a flavonoid-binding protein. *Plant Physiol.* 123: 1561-1570.
- Müller, F., and Rieu, I.** (2016) Acclimation to high temperature during pollen development. *Plant Reprod.* 29: 107–118.
- Muhlemann, J.K., Younts, T.L.B., and Muday, G.K.** (2018) Flavonols control pollen tube growth and integrity by regulating ROS homeostasis during high-temperature stress. *Proc. Natl. Acad. Sci.* 115: E11188-E11197.
- Muriga, M., Charzynska, M., Rougier, M., and Cresti, M.** (1991) Secretory tapetum of *Brassica oleracea* L.: polarity and ultrastructural features. *Sex. Plant Reprod.* 4: 28-35.
- Murphy, D.J.** (2006) The extracellular pollen coat in members of the Brassicaceae: composition, biosynthesis, and functions in pollination. *Protoplasma.* 228: 31-39.
- Nakayama, T., Takahashi, S., and Waki, T.** (2019) Formation of flavonoid metabolons: functional significance of protein-protein interactions and impact on flavonoid chemodiversity. *Front. Plant Sci.* 10: 1-12.
- Napoli, C.A., Fahy, D., Wang, H.Y., and Taylor, L.P.** (1999) White anther: A petunia mutant that abolishes pollen flavonol accumulation, induces male sterility, and is complemented by a chalcone synthase transgene. *Plant Physiol.* 120: 615-622.
- Nebenführ, A., Gallagher, L.A., Dunahay, T.G., Frohlick, J.A., Mazurkiewicz, A.M., Meehl, J.B., and Staehelin, L.A.** (1999) Stop-and-go movements of plant Golgi stacks are mediated by the actomyosin system. *Plant Physiol.* 121: 1127-1142.
- Nelson, B.K., Cai, X., and Nebenführ, A.** (2007) A multicolored set of *in vivo* organelle markers for colocalization studies in Arabidopsis and other plants. *Plant J.* 51: 1126-1136.
- Niño-González, M., Novo-Uzal, E., Richardson, D.M., Barros, P.M., and Duque, P.** (2019) More transporters, more substrates: The Arabidopsis major facilitator superfamily revisited. *Mol. Plant* 12: 1182-1202.
- Nishida, R., Ohsugi, T., Fukami, H., and Nakajima, S.** (1990) Oviposition deterrent of a *Rutaceae*-feeding swallowtail butterfly, *Papilio xuthus*, from a non-host rutaceous plant, *Orixa japonica*. *Agric. Biol. Chem.* 54: 1265-1270.

- Nour-Eldin, H.H., Andersen, T.G., Burow, M., Madsen, S.R., Jørgensen, M.E., Olsen, C.E., Dreyer, I., Hedrich, R., Geiger, D., and Halkier, B.A.** (2012) NRT/PTR transporters are essential for translocation of glucosinolate defence compounds to seeds. *Nature* 488: 531-534.
- Nour-Eldin, H.H., and Halkier, B.A.** (2013) The emerging field of transport engineering of plant specialized metabolites. *Curr. Opin. Biotechnol.* 24: 263-270.
- Nour-Eldin, H.H., Madsen, S.R., Engelen, S., Jørgensen, M.E., Olsen, C.E., Andersen, J.S., Seynnaeve, D., Verhoye, T., Fulawka, R., Denolf, P., and Halkier, B.A.** (2017) Reduction of antinutritional glucosinolates in *Brassica* oilseeds by mutation of genes encoding transporters. *Nat. Biotechnol.* 35: 377-382.
- Novy, R., Drott, D., Yaeger, K., and Mierendorf, R.** (2001) Overcoming the codon bias of *E. coli* for enhanced protein expression. *inNOVations* 12: 1-3.
- Obayashi, T., Aoki, Y., Tadaka, S., Kagaya, Y., and Kinoshia, K.** (2018) ATTED-II in 2018: A Plant Co-expression Database Based on Investigation of Statistical Property of the Mutual Rank Index. *Plant Cell Physiol.* 59: e3.
- Ogawa, M., Hanada, A., Yamauchi, Y., Kuwahara, A., Kamiya, Y., and Yamaguchi, S.** (2003) Gibberellin biosynthesis and response during Arabidopsis seed germination. *Plant Cell* 15: 1591-1604.
- Okamoto, M., Vidmar, J.J., and Glass, A.D.** (2003) Regulation of NRT1 and NRT2 gene families of *Arabidopsis thaliana*: responses to nitrate provision. *Plant Cell Physiol.* 44: 304-317.
- Omote, H., Hiasa, M., Matsumoto, T., Otsuka, M., and Moriyama, Y.** (2006) The MATE proteins as fundamental transporters of metabolic and xenobiotic organic cations. *Trends Pharmacol. Sci.* 27: 587-593.
- Ortuño, A., Báidez, A., Gómez, P., Arcas, M.C., Porras, I., García-Lidón, A., and Del Rio, J.A.** (2006) *Citrus paradisi* and *Citrus sinensis* flavonoids: Their influence in the defence mechanism against *Penicillium digitatum*. *Food Chemistry* 98: 351-358.
- Osmani, S.A., Bak, S., and Møller, B.L.** (2009) Substrate specificity of plant UDP-dependent glycosyltransferases predicted from crystal structures and homology modeling. *Phytochemistry* 70: 325-347.
- Owen, H.A., and Makaroff, C.A.** (1995) Ultrastructure of microsporogenesis and microgametogenesis in *Arabidopsis thaliana* (L.) Heynh. ecotype Wassilewskija (Brassicaceae). *Protoplasma* 185: 7–21.
- Pacini, E., Franchi, G.G., and Hesse, M.** (1985) The tapetum: its form, function and possible phylogeny in *Embryophyta*. *Plant Syst. Evol.* 149: 155–185.
- Pacini, E., and Hesse, M.** (2005) Pollenkitt – Its composition, forms, and function. *Flora* 200: 399-315.
- Palanichamy, S., and Nagarajan, S.** (1990) Analgesic activity of *Cassia alata* leaf extract and kaempferol 3-O-sophoroside. *J. Ethnopharmacol.* 29: 73-78.
- Pao, S.S., Paulsen, I.T., and Saier, M.H.** (1998) Major facilitator superfamily. *Microbiol. Mol. Biol. Rev.* 62: 1-34.
- Parish, R.W., Phan, H.A., Iacuone, S., and Li, S.F.** (2012) Tapetal development and abiotic stress: A centre of vulnerability. *Functional Plant Biology* 39: 553-559.
- Parker, J.L., and Newstead, S.** (2014) Molecular basis of nitrate uptake by the plant nitrate transporter NRT1.1. *Nature* 507: 68-72.

- Patil, S.S., Prashant, R., Kadoo, N.Y., Upadhyay, A., and Gupta, V.S.** (2019) Global study of MFS superfamily transporters in *Arabidopsis* and grapes reveals their functional diversity in plants. *Plant Gene* 18: 100179.
- Paul, W., Hodge, R., Smartt, S., Draper, J., and Scott, R.** (1992) The isolation and characterisation of the tapetum-specific *Arabidopsis thaliana* A9 gene. *Plant Mol. Biol.* 19: 611–622.
- Paupière, M.J., Müller, F., Li, H., Rieu, I., Tikunov, Y.M., Visser, R.G.F., and Bovy, A.G.** (2017) Untargeted metabolomics analysis of tomato pollen development and heat stress response. *Plant Reprod.* 30: 81-94.
- Payne, R.M., Xu, D., Foureau, E., Carqueijeiro, M.I.S.T., Oudin, A., Dugé de Bernonville, T., Novak, V., Burow, M., Olsen, C.-E., Jones, D.M., Tatsis, E.C., Pendle, A., Halkier, B.A., Geu-Flores, F., Courdavault, V., Nour-Eldin, H.H., and O'Connor, S.** (2017) An NPF transporter exports a central monoterpene alkaloid intermediate from the vacuole. *Nat. Plants* 3: 16208.
- Pierman, B., Toussaint, F., Bertin, A., Lévy, D., Smargiasso, N., De Pauw, E., and Boutry, M.** (2017) Activity of the purified plant ABC transporter NtPDR1 is stimulated by diterpenes and sesquiterpenes involved in constitutive and induced defences. *J. Biol. Chem.* 292: 19491-19502.
- Piffanelli, P., Ross, J.H.E., and Murphy, D.J.** (1998) Biogenesis and function of the lipidic structures of pollen grains. *Sex. Plant Reprod.* 11: 65-80.
- Planchais, S., Perennes, C., Glab, N., Mironov, V., Inzé, D., and Bergounioux, C.** (2002) Characterization of *cis*-acting element involved in cell cycle phase-independent activation of *Arabidopsis thaliana*; *CycB1*; 1 transcription and identification of putative regulatory proteins. *Plant Mol. Biol.* 50: 109–125.
- Plaza, M., Pozzo, T., Liu, J., Gulshan Ara, K.Z., Turner, C., and Nordberg Karlsson, E.** (2014) Substituent effects on *in vitro* antioxidizing properties, stability, and solubility in flavonoids. *J. Agric. Food Chem.* 62: 3321-3333.
- Pollak, P.E., Hansen, K., Astwood, J.D., and Taylor, L.P.** (1995) Conditional male fertility in maize. *Sex. Plant Reprod.* 8: 231–241.
- Pratviel-Sosa, F., and Percheron, F.** (1972) Les sophorosides de flavonols de quelques pollens. *Phytochemistry* 11: 1809-1813.
- Quilichini, T.D., Douglas, C.J., and Samuels, A.L.** (2014b) New views on tapetum ultrastructure and pollen exine development in *Arabidopsis thaliana*. *Ann. Bot.* 114: 1189-1201.
- Quilichini, T.D., Friedmann, M.C., Samuels, A.L., and Douglas, C.J.** (2010) ATP-binding cassette transporter G26 is required for male fertility and pollen exine formation in *Arabidopsis*. *Plant Physiol.* 154: 678-690.
- Quilichini, T.D., Samuels, A.L., and Douglas, C.J.** (2014a) ABCG26-mediated polyketide trafficking and hydroxycinnamoyl spermidines contribute to pollen wall exine formation in *Arabidopsis*. *Plant Cell* 26: 4483-4496.
- Rabaté, M.M.J., and Dussy, J.** (1938) Etude biochimique des fruits de *Sophora japonica* L. II. – Sur la présence de rutósido et de *Sophora* flavonolósido dans les fruits verts de *Sophora japonica*. *Bull. Soc. Chim. biol.* 20: 459-467.
- Ralston, L., and Yu, O.** (2006) Metabolons involving plant cytochrome P450s. *Phytochem. Rev.* 5: 459.
- Rogers, H.J., Bate, N., Combe, J., Sullivan, J., Sweetman, J., Swan, C., Lonsdale, D.M., and Twell, D.** (2001) Functional analysis of *cis*-regulatory elements within the promoter of the tobacco late pollen gene *g10*. *Plant Mol. Biol.* 45: 577-585.



- Roque, E., Gómez, M.D., Ellul, P., Wallbraun, M., Madueño, F., Beltrán, J.-P., and Cañas, L.A.** (2007) The *PsEND1* promoter: A novel tool to produce genetically engineered male-sterile plants by early anther ablation. *Plant Cell Rep.* 26: 313-325.
- Sagor, G.H., Berberich, T., Kojima, S., Niitsu, M., and Kusano, T.** (2016) Spermine modulates the expression of two probable polyamine transporter genes and determines growth responses to cadaverine in Arabidopsis. *Plant Cell Rep.* 35: 1247-1257.
- Saito, H., Oikawa, T., Hamamoto, S., Ishimaru, Y., Kanamori-Sato, M., Sasaki-Sekimoto, Y., Utsumi, T., Chen, J., Kanno, Y., Masuda, S., Kamiya, Y., Seo, M., Uozumi, N., Ueda, M., and Ohta, H.** (2015) The jasmonate-responsive GTR1 transporter is required for gibberellin mediated stamen development in Arabidopsis. *Nat. Commun.* 6: 6095-7005.
- Sasaki, N., Nishizaki, Y., Ozeki, Y., and Miyahara, T.** (2014) The role of acyl-glucose in anthocyanin modifications. *Molecules* 19: 18747-18766.
- Saslowky, D., and Winkel-Shirley, B.** (2001) Localization of flavonoid enzymes in Arabidopsis roots. *Plant J.* 27: 37-48.
- Schijlen, E.G., de Vos, C.H., Martens, S., Jonker, H.H., Rosin, F.M., Molthoff, J.W., Tikunov, Y.M., Angenent, G.C., van Tunen, A.J., and Bovy, A.G.** (2007) RNA interference silencing of chalcone synthase, the first step in the flavonoid biosynthesis pathway, leads to parthenocarpic tomato fruits. *Plant Physiol.* 144: 1520-1530.
- Schwacke, R., Schneider, A., Van Der Graaff, E., Fischer, K., Catoni, E., Desimine, M., Frommer, W.B., Flügge, U.I., and Kunze, R.** (2003) ARAMEMNON, a Novel Database for Arabidopsis integral membrane proteins. *Plant Physiol.* 131:16-26.
- Scott, R.J.** (1994) Pollen exine – the sporopollenin enigma and the physics of pattern. In: Scott, R.J., Stead, M.A. (eds.) *Molecular and cellular aspects of plant reproduction*. Cambridge University Press, Cambridge pp. 49-81.
- Serrano, M., Wang, B., Aryal, B., Garcion, C., Abou-Mansour, E., Heck, S., Geisler, M., Mauch, F., Nawrath, C., and Métraux, J.P.** (2013) Export of salicylic acid from the chloroplast requires the multidrug and toxin extrusion-like transporter EDS5. *Plant Physiol.* 162: 1815-1821.
- Shitan, N., Bazin, I., Dan, K., Obata, K., Kigawa, K., Ueda, K., Sato, F., Forestier, C., and Yazaki, K.** (2003) Involvement of CjMDR1, a plant multidrug-resistance-type ATP-binding cassette protein, in alkaloid transport in *Coptis japonica*. *Proc. Natl. Acad. Sci.* 100: 751-756.
- Shitan, N., Morita, M., and Yazaki, K.** (2009) Identification of a nicotine transporter in leaf vacuoles of *Nicotiana tabacum*. *Plant Signal. Behav.* 4: 530-532.
- Shoji, T.** (2014). ATP-binding cassette and multidrug and toxic compound extrusion transporters in plants. *International Review of Cell and Molecular Biology*, 303–346.
- Shoji, T., Inai, K., Yazaki, Y., Sato, Y., Takase, H., Shitan, N., Yazaki, K., Goto, Y., Toyooka, K., Matsuoka, K., and Hashimoto, T.** (2009) Multidrug and toxic compound extrusion-type transporters implicated in vacuolar sequestration of nicotine in tobacco roots. *Plant Physiol.* 149: 708-718.
- Singh, D.P., Jermakow, A.M., and Swain, S.M.** (2002) Gibberellins are required for seed development and pollen tube growth in Arabidopsis. *Plant Cell* 14: 3133-3147.
- Solano, R., Nieto, C., Avila, J., Cañas, L., Diaz, I., and Paz-Ares, J.** (1995) Dual DNA binding specificity of a petal epidermis-specific MYB transcription factor (MYB.Ph3) from *Petunia hybrida*. *EMBO J.* 14: 1773-1784.

- Spurr, A.R.** (1969) A low-viscosity epoxy resin embedding medium for electron microscopy. *J. Ultrastruct. Res.* 26: 31-43.
- Stolarczyk, E.I., Reiling, C.J., and Paumi, C.M.** (2011) Regulation of ABC transporter function via phosphorylation by protein kinases. *Curr. Pharm. Biotechnol.* 12: 621-635.
- Stracke, R., Jahns, O., Keck, M., Tohge, T., Niehaus, K., Fernie, A.R., and Weisshaar, B.** (2010) Analysis of PRODUCTION OF FLAVONOL GLYCOSIDES-dependent flavonol glycoside accumulation in *Arabidopsis thaliana* plants reveals MYB11-, MYB12- and MYB111-independent flavonol glycoside accumulation. *New Phytol.* 188: 985-1000.
- Sun, J., Bankston, J.R., Payandeh, J., Hinds, T.R., Zagotta, W.N., and Zheng, N.** (2014) Crystal structure of the plant dual affinity nitrate transporter NRT1.1. *Nature* 507: 73-77.
- Sun, J., and Zheng, N.** (2015) Molecular Mechanism underlying the plant NRT1.1 dual-affinity nitrate transporter. *Front. Physiol.* 6: 386.
- Sun, W., Liang, L., Meng, X., Li, Y., Gao, F., Liu, X., Wang, S., Gao, X., and Wang, L.** (2016) Biochemical and molecular characterization of a flavonoid 3-O-glycosyltransferase responsible for anthocyanins and flavonols biosynthesis in *Freesia hybrida*. *Front. Plant Sci.* 31: 410.
- Sun, Y., Li, H., and Huang, J.R.** (2012) Arabidopsis TT19 functions as a carrier to transport anthocyanin from the cytosol to tonoplasts. *Mol. Plant* 5: 387-400.
- Takanashi, K., Shitan, N., and Yazaki, K.** (2014) The multidrug and toxic compound extrusion (MATE) family in plants. *Plant Biotechnology* 31: 1-14.
- Tal, I., Zhang, Y., Jørgenson, M.E., Pisanti, O., Barbosa, I.C.R., Zourelidou, M., Regnault, T., Crocoll, C., Olson, C.E., Weinstein, R., Schwechheimer, C., Halkier, B.A., Nour-Eldin, H.H., Estelle, M., and Shani, E.** (2016) The Arabidopsis NPF3 protein is a GA transporter. *Nat. Commun.* 7: 11486-11497.
- Tanaka, Y., Sasaki, N., and Ohmiya, A.** (2008) Biosynthesis of plant pigments: anthocyanins, betalains and carotenoids. *Plant J.* 54: 733-749.
- Tatsuzawa, F., Saito, N., Toki, K., Shinoda, A., Shigihara, A., and Honda, T.** (2010) Acylated cyanidin 3-sophoroside-5-glucosides from the purple roots of red radish (*Raphanus sativus* L.) 'Benikanmi'. *J. Japan. Soc. Hort. Sci.* 79: 103-107.
- Taylor, L.P., and Grotewold, E.** (2005) Flavonoids as developmental regulators. *Curr. Opin. Plant Biol.* 8: 317-323.
- Teakle, G.R., Manfield, I.W., Graham, J.F., and Gilmartin, P.M.** (2002) *Arabidopsis thaliana* GATA factors: Organisation, expression and DNA-binding characteristics. *Plant Mol. Biol.* 50: 43-57.
- Terzaghi, W.B., and Cashmore, A.R.** (1995) Light-regulated transcription. *Annu. Rev. Plant Physiol. Plant Mol. Biol.* 46: 445-474.
- Thompson, E.P., Davis, J.M., and Glover, B.J.** (2010b) Identifying the transporters of different flavonoids in plants. *Plant Signal. Behav.* 5: 860-863.
- Thompson, E.P., Wilkins, C., Demidchik, V., Davis, J.M., and Glover, B.J.** (2010a) An Arabidopsis flavonoid transporter is required for anther dehiscence and pollen development. *J. Exp. Bot.* 61: 439-451.
- Tissier, A.** (2018) Plant secretory structures: more than just reaction bags. *Curr. Opin. Biotechnol.* 49: 73-79.

- Tissier, A., Morgan, J.A., and Dudareva, N.** (2017) Plant volatiles: going 'in' but not 'out' of trichome cavities. *Trends Plant Sci.* 22: 930-938.
- Tohge, T., Watanabe, M., Hoefgen, R., and Fernie, A.R.** (2013) The evolution of phenylpropanoid metabolism in the green lineage. *Crit. Rev. Biochem. Mol. Biol.* 48: 123-152.
- Tomás-Barberán, F.A., Tomás-Lorente, F., Ferreres, F., and Garcia-Viguera, C.** (1989) Flavonoids as biochemical markers of the plant origin of bee pollen. *J. Sci. Food Agric.* 47: 337-340.
- Trapero, A., Ahrazem, O., Rubio-Moraga, A., Jimeno, M.L., Gómez, M.D., and Gómez-Gómez, L.** (2012) Characterization of a glucosyltransferase enzyme involved in the formation of kaempferol and quercetin sophorosides in *Crocus sativus*. *Plant Physiol.* 159: 1335-1354.
- Traynier, R.M., and Truscott, R.J.** (1991) Potent natural egg-laying stimulant for cabbage butterfly *Pieris rapae*. *J. Chem. Ecol.* 17: 1371-1380.
- Tsay, Y.-F., Chiu, C.C., Tsai, C.B., Ho, C.H., and Hsu, P.K.** (2007) Nitrate and peptide transporters. *FEBS Lett.* 581: 2290-2300.
- Tsay, Y.-F., Schroeder, J.I., Feldmann, K.A., and Crawford, N.M.** (1993) The herbicide sensitivity gene CHL1 of *Arabidopsis* encodes a nitrate-inducible nitrate transporter. *Cell* 72:705-713.
- Tsimogiannis, D., Samiotaki, M., Panayotou, G., and Oreopoulou, V.** (2007) Characterization of flavonoid subgroups and hydroxyl substitution by HPLC-MS/MS. *Molecules.* 12: 593-606.
- Twell, D., Park, S.K., and Lalanne, E.** (1998) Asymmetric division and cell-fate determination in developing pollen. *Trends Plant Sci.* 3: 305-310.
- van der Meer, I.M., Stam, M.E., van Tunen, A.J., Mol, J.N., and Stuitje, A.R.** (1992) Antisense inhibition of flavonoid biosynthesis in petunia anthers results in male sterility. *Plant Cell* 4: 253-262.
- Verma, N., and Burma, P.K.** (2017) Regulation of tapetum-specific A9 promotor by transcription factors AtMYB80, AtMYB1 and AtMYB4 in *Arabidopsis thaliana* and *Nicotiana tabacum*. *Plant J.* 92: 481-494.
- Verrier, P.J., Bird, D., Burla, B., Dassa, E., Forestier, C., Geisler, M., Klein, M., Kolukisaoglu, U., Lee, Y., Martinoia, E., Murphy, A., Rea, P.A., Samuels, L., Schulz, B., Spalding, E.J., Yazaki, K., and Theodoulou, F.L.** (2008) Plant ABC proteins – a unified nomenclature and updated inventory. *Trends Plant Sci.* 13: 151-159.
- Vogt, T.** (2010) Phenylpropanoid biosynthesis. *Mol. Plant.* 3: 2-20.
- Vogt, T., and Jones, P.** (2000) Glycosyltransferases in plant natural product synthesis: characterization of a supergene family. *Trends Plant Sci.* 5: 380-386.
- Vogt, T., and Taylor, L.P.** (1995) Flavonol 3-O-glycosyltransferases associated with *Petunia* pollen produce gametophyte-specific flavonol diglycosides. *Plant Physiol.* 108: 903-911.
- Vogt, T., Wollenweber, E., and Taylor, L.P.** (1995) The structural requirements of flavonols that induce pollen germination of conditionally male fertile *Petunia*. *Phytochemistry* 38: 589-592.
- von Wittgenstein, N.J., Le, C.H., Hawkins, B.J., and Ehling, J.** (2014) Evolutionary classification of nitrate, ammonia, and peptide transporters in land plants. *BMC Evol. Biol.* 14: 11.
- Wagner, H., Horhammer, L., Dirscherl, R., Farkas, L., and Ndgra`di, M.** (1968) Über die Synthese von Quercetin-3-glykosiden. *Chem. Ber.* 101: 1186-1189.

- Walczak, H.A., and Dean, J.V.** (2000) Vacuolar transport of the glutathione conjugate of *trans*-cinnamic acid. *Phytochemistry* 53: 441-446.
- Wang, B., Kashkooli, A.B., Sallets, A., Ting, H.M., de Ruijter, N.C.A., Olofsson, L., Brodelius, P., Pottier, M., Boutry, M., Bouwmeester, H., and van der Krol, A.R.** (2016) Transient production of artemisinin in *Nicotiana benthamiana* is boosted by a specific lipid transfer protein from *A. annua*. 38: 159-169.
- Wang, K., Guo, Z.L., Zhou, W.T., Zhang, C., Zhang, Z.Y., Lou, Y., Xiong, S.X., Yao, X.Z., Fan, J.J., Zhu, J., and Yang, Z.N.** (2018) The regulation of sporopollenin biosynthesis genes for rapid pollen wall formation. *Plant Physiol.* 178: 282-294.
- Wang, L., Bei, X., Gao, J., Li, Y., Yan, Y., and Hu, Y.** (2016) The similar and different evolutionary trends of MATE family occurred between rice and *Arabidopsis thaliana*. *BMC Plant Biol.* 16: 207.
- Welchen, E., and Gonzalez, D.H.** (2005) Differential expression of the Arabidopsis cytochrome c genes *Cytc-1* and *Cytc-2*. Evidence for the involvement of TCP-domain protein-binding elements in anther- and meristem-specific expression of the *Cytc-1* gene. *Plant Physiol.* 139: 88-100.
- Weng, J.-K., Philippe, R.N., and Noel, J.P.** (2012) The rise of chemodiversity in plants. *Science* 336: 1667-1670.
- Wiermann, R., and Vieth, K.** (1983) Outer pollen wall, an important accumulation site for flavonoids. *Protoplasma* 118: 230-233.
- Williams, C.A., and Grayer, R.J.** (2004) Anthocyanins and other flavonoids. *Nat. Product Rep.* 21: 539-573.
- Wilmsen, S., Gottlieb, R., Junker, R.R., and Lunau, K.** (2017) Bumblebees require visual pollen stimuli to initiate and multimodal stimuli to complete a full behavioral sequence in close-range flower orientation. *Ecol. Evol.* 7: 1384-1393.
- Winkel-Shirley, B.** (2001) Flavonoid biosynthesis. A colorful model for genetics, biochemistry, cell biology, and biotechnology. *Plant Physiol.* 126: 485-493.
- Winiarczyk, K., Jaroszuk-Ściśeł, J., and Kupisz, K.** (2012) Characterization of callase ( $\beta$ -1,3-D-glucanase) activity during microsporogenesis in the sterile anthers of *Allium sativum* L. and the fertile anthers of *A. atropurpureum*. *Sex. Plant Reprod.* 25: 123-131.
- Wu, S.S., Platt, K.A., Ratnayake, C., Wang, T.W., Ting, J.T., and Huang, A.H.** (1997) Isolation and characterization of neutral-lipid-containing organelles and globuli-filled plastids from *Brassica napus* tapetum. *Proc. Natl. Acad. Sci.* 94: 12711-12716.
- Yadav, V., Molina, I., Ranathunge, K., Castillo, I.Q., Rothstein, S.J., and Reed, J.W.** (2014) ABCG Transporters are required for suberin and pollen wall extracellular barriers in Arabidopsis. *Plant Cell* 26: 3569-3588.
- Yamasaki, H., Uefuji, H., and Sakihama, Y.** (1996) Bleaching of the red anthocyanin induced by superoxide radical. *Arch. Biochem. Biophys.* 332: 183-186.
- Yang, C., Vizcay-Barrena, G., Conner, K., and Wilson, Z.A.** (2007) MALE STERILITY1 is required for tapetal development and pollen wall biosynthesis. *Plant Cell* 19: 3530-3548.
- Yang, S., Jiang, Y., Xu, L., Shiratake, K., Luo, Z., and Zhang, Q.** (2016) Molecular cloning and functional characterization of *DkMATE1* involved in proanthocyanidin precursor transport in persimmon (*Diospyros kaki* Thunb.) fruit. *Plant Physiol. Biochem.* 108: 241-250.

- Yazaki, K.** (2005) Transporters of secondary metabolites. *Curr. Opin. Plant Biol.* 8: 301-307.
- Ye, Q., Zhu, W., Li, L., Zang, S., Yin, Y., Ma, H., and Wang, X.** (2010) Brassinosteroids control male fertility regulating the expression of key genes involved in Arabidopsis anther and pollen development. *Proc. Natl. Acad. Sci.* 107: 6100-6105.
- Yin, R., Han, K., Heller, W., Albert, A., Dobrev, P.I., Zažímalová, E., and Schöffner, A.R.** (2014) Kaempferol 3-*O*-rhamnoside-7-*O*-rhamnoside is an endogenous flavonol inhibitor of polar auxin transport in Arabidopsis shoots. *New Phytol.* 201: 466-75.
- Yin, R., Messner, B., Faus-Kessler, T., Hoffmann, T., Schwab, W., Hajirezaei, M.-R., von Saint Paul, V., Heller, W., and Schöffner, A.R.** (2012) Feedback inhibition of the general phenylpropanoid and flavonol biosynthetic pathways upon a compromised flavonol-3-*O*-glycosylation. *J. Exp. Bot.* 63: 2465-2478.
- Ylstra, B., Muskens, M., and van Tunen, A.J.** (1996) Flavonols are not essential for fertilization in *Arabidopsis thaliana*. *Plant Mol. Biol.* 32: 1155-1158.
- Ylstra, B., Touraev, A., Brinkmann, A.O., Heberle-Bors, E., and van Tunen, A.J.** (1995) Steroid hormones stimulate germination and tube growth of *in vitro* matured tobacco pollen. *Plant Physiol.* 107: 639-643.
- Ylstra, B., Touraev, A., Moreno, R.M.B., Stöger, E., van Tunen, A.J., Vicente, O., Mol, J.N.M., and Heberle-Bors, E.** (1992) Flavonols stimulate development, germination, and tube growth of tobacco pollen. *Plant Physiol.* 100: 902-907.
- Yonekura-Sakakibara, K., Higashi, Y., and Nakabayashi, R.** (2019) The origin and evolution of plant flavonoid metabolism. *Front. Plant Sci.* 10: 943.
- Yonekura-Sakakibara, K., Nakabayashi, R., Sugawara, S., Tohge, T., Ito T., Koyanagi, M., Kitajima, M., Takayama, H., and Saito, K.** (2014) A flavonoid 3-*O*-glucoside:2''-*O*-glucosyltransferase responsible for terminal modification of pollen-specific flavonols in *Arabidopsis thaliana*. *Plant J.* 79: 769-782.
- Yoo, S., Cho, Y., and Sheen, J.** (2007) Arabidopsis mesophyll protoplasts: A versatile cell system for transient gene expression analysis. *Nature Protoc.* 2: 1565-1572.
- Zha, J., Wu, X., Gong, G., and Koffas, M.A.G.** (2019) Pathway enzyme engineering for flavonoid production in recombinant microbes. *Metab. Eng. Commun.* 9: e00104.
- Zhang, H., Zhao, F.G., Tang, R.J., Yu, Y., Song, J., Wang, Y., Li, L., and Luan, S.** (2017) Two tonoplast MATE proteins function as turgor-regulating chloride channels in Arabidopsis. *Proc. Natl. Acad. Sci.* 114: E2036-E2045.
- Zhao, J.** (2015) Flavonoid transport mechanisms: How to go, and with whom. *Trends Plant Sci.* 20: 576-585.
- Zhao, J., Huhman, D., Shadle, G., He, X.Z., Sumner, L.W., Tang, Y., and Dixon, R.A.** (2011) MATE2 mediates vacuolar sequestration of flavonoid glycosides and glycoside malonates in *Medicago truncatula*. *Plant Cell* 23: 1536-1555.
- Zhu, Q., Ordiz, M.I., Dabi, T., Beachy, R.N., and Lamb, C.** (2002) Rice TATA binding protein interacts functionally with transcription factor IIB and the RF2a bZIP transcriptional activator in an enhanced plant *in vitro* transcription system. *Plant Cell* 14: 795-803.
- Zimmermann, P., Hirsch-Hoffmann, M., Hennig, L., and Gruissem, W.** (2004) GENEVESTIGATOR. Arabidopsis microarray database and analysis toolbox. *Plant Physiol.* 136: 2621-2632.

## 8 Appendix

**Table 8-1** Overview of the examined T-DNA insertion lines obtained from NASC. Shown are the Arabidopsis accession numbers, the term for the candidates, the individual SALK numbers, the tested genotypes, and the verification of the predicted knockout by RT-PCR. The confirmed *chs* deficient line N85 is a point mutation and additionally included into the list.

accession	term	T-DNA line	genotype	knockout verified
<i>At4g00350</i>	<i>dtx34-1</i>	SAIL-535_H04C1	homozygous	confirmed knockout
<i>At4g00350</i>	<i>dtx34-2</i>	SALK_203507C	homozygous	confirmed knockout
<i>At3g26590</i>	<i>dtx29</i>	SALK_119274C	homozygous	confirmed knockout
<i>At5g65380</i>	<i>dtx27</i>	SALK_124549C	homozygous	confirmed knockout
<i>At1g47530</i>	<i>dtx33</i>	SALK131275C	homozygous	confirmed knockout
<i>At1g11670</i>	<i>dtx36</i>	SALK_025900C	homozygous	confirmed knockout
<i>At3g59030</i>	<i>tt12-1</i>	W10067	not tested	confirmed knockout. ( <i>tt</i> -phenotype)
<i>At3g59030</i>	<i>tt12-2</i>	GK797D03	homozygous	confirmed knockout. ( <i>tt</i> -phenotype)
<i>At5g17220</i>	<i>tt19-8</i>	SALK_105779C	homozygous	confirmed by NASC ( <i>tt</i> -phenotype)
<i>At5g17220</i>	68448	SALK_068448.42.40	heterozygous	wild-type
<i>At3g55110</i>	<i>abcg18</i>	SALK_100187C	homozygous	confirmed knockout
<i>At3g55100</i>	<i>abcg17</i>	SALKseq_119869.4	homozygous	confirmed knockout
<i>At3g60160</i>	<i>abcc9</i>	SALK_087700C	homozygous	wild-type
<i>At5g28470</i>	<i>fst1</i>	SALK_027288C	homozygous	confirmed knockout
<i>At5g28470</i>	113184C	SALK_113184C	homozygous	knockabout
<i>At5g19470</i>	<i>npf7.1</i>	SALK_138950C	homozygous	confirmed knockout by NASC
<i>At5g17050</i>	<i>78d2</i>	SALK_049338C	homozygous	confirmed knockout
<i>At2g19070</i>	<i>sht</i>	SALK_055511C	homozygous	confirmed knockout
<i>At5g13930</i>	<i>chs (tt4)</i>	N85 (point mutation)	homozygous	confirmed knockout ( <i>tt</i> -phenotype)

**Table 8-2** Primers used for conformation of the T-DNA-insertion lines.

candidate	genotyping primer	RT-PCR primer
<i>dtx34-1</i>	LP 5'-TGAAGGAGTTGTGGAGGTGAC-3' RP 5'-ACGAAGATGCTTGTGAAGGAG-3'	fw 5'-ATGGAGATCCCGGTTTCGAGA-3' rw 5'-ATTTCTCATATCCAGTCCCC-3'
<i>dtx34-2</i>	LP 5'-GTTCTTGGCTTATCCTCCTCG-3' RP 5'-TATATAAGCCACCGGTGCTT-3'	fw 5'-ATGGAGATCCCGGTTTCGAGA-3' rw 5'-ATTTCTCATATCCAGTCCCC-3'
<i>dtx29</i>	LP 5'-TTCAACGTGGAAACCAAAAAG-3' RP 5'-GCATAACAGCAGAAGCCAAAAG-3'	fw 5'-ATGGCAAAGACAAAGATATAACG-3' rw 5'-CCTCCCCATTCTCTTATCC-3'
<i>dtx27</i>	LP 5'-TTGTTTTATTGCAAATCCACG-3' RP 5'-TTGGGTATTAGGTGACTGCG-3'	fw 5'-ATGAGGGGAGGTGATGGA-3' rw 5'-TACGAGCACTTGCTTTCTG-3'
<i>dtx33</i>	LP 5'-TTATGTTTTGGGGTTCACAGC-3' RP 5'-TTTGGCTTAGCAACAACCATC-3'	fw 5'-ATGGGAAAGGATAAGACTTTG-3' rw 5'-TCACTCCTGCGCCGT-3'
<i>dtx36</i>	LP 5'-CAGAAGCTGACTTCAGGATGG-3' RP 5'-CAGGGTCTTAAGAAGTCCGG-3'	fw 5'-ATGGGTTCGGAAGCGACCA-3' rw 5'-TTATTGCTTAAGAAGCGGAGATGT-3'

(Table 8-2 continued)

<b>candidate</b>	<b>genotyping primer</b>	<b>RT-PCR primer</b>
<i>tt12-1</i>	not genotyped not genotyped	fw 5'-ATGAGCTCCACAGAGACATACG-3' rw 5'-TTAAACACCTGCGTTAGCCATC-3'
<i>tt12-2</i>	LP 5'-TGCTTCCAAATGGATCATTTTC-3' RP 5'-CAGTGTGGGAGTCAAAGCTTC-3'	fw 5'-ATGAGCTCCACAGAGACATACG-3' rw 5'-TTAAACACCTGCGTTAGCCATC-3'
<i>tt19-8</i>	LP 5'-TCAAAAGTGGTTGTTGGGAAG-3' RP 5'-TATCCGAAATCTCTCCACC-3'	fw 5'-CTATATGGACAGGTAACAGCAGC-3' rw 5'-GTGACCAGCCAGCACCATAAG-3'
<i>tt19</i>	LP 5'-CACCACATGTTCTACCCAACC-3' RP 5'-CTAATTCAGTGACCAGCCAGC-3'	fw 5'-CTATATGGACAGGTAACAGCAGC-3' rw 5'-GTGACCAGCCAGCACCATAAG-3'
<i>abcg18</i>	LP 5'-AGAAGAGACCCCAAGCTAACG-3' RP 5'-TCACAGAGTTCGCACTTGATG-3'	fw 5'-GATGAAGGACATCGTGGAG-3' rw 5'-CATGTAACATCATGACATTC-3'
<i>abcg17</i>	LP 5'-CTTACCGCCATAAGAAAAGGG-3' RP 5'-GATGGCTTACCCGCTTTTATC-3'	fw 5'-ATGCTGCAAAGAGACGCCGTGATC-3' rw 5'-TCACGCCCTCTTATTCTTGCTCC-3'
<i>abcc9</i>	LP 5'-GAGATCAATGAAGGAGCTCCC-3' RP 5'-CGACTTGACTGGTCTTCTTGC-3'	fw 5'-ATGTTCAAGCCCTTGGTTTCGC-3' rw 5'-CAAGTGCTGAGAGGAGATCAGGT-3'
<i>fst1</i>	LP 5'-TGGCCTCAATGAGCTTAATTG-3' RP 5'-TAGATTAGGCCACCGTTAGG-3'	fw 5'-ATGGACGTGCAATCTTCATCAC-3' rw 5'-TTAGTGCCTTTTTGTTTTAGTGG-3'
<i>fst1</i>	LP 5'-GTGGTAGCCTCGAGACTGTTG-3' RP 5'-AGGCTAAAACCTTTGGCAACC-3'	fw 5'-ATGGACGTGCAATCTTCATCAC-3' rw 5'-TTAGTGCCTTTTTGTTTTAGTGG-3'
<i>78d2</i>	LP 5'-CTCTTCGTTATTTCTCCGG-3' RP 5'-TCAAACCCATCTTCGTGAAG-3'	fw 5'-ATGACCAAACCCTCCGAC-3' rw 5'-TCAAATAATGTTTACAACGC-3'
<i>sht</i>	LP 5'-TAAAAGGCCACAAATTACCC-3' RP 5'-GACGCTAAGGCTTATTCCACC-3'	fw 5'-CACTATAGTACCGGCCGAAC-3' rw 5'-TTCTTGAAGGCCTCCATGTG-3'
<b>Left border primers of the T-DNA insertion</b>		
<b>term</b>	<b>sequence</b>	
LBa1 for SALK-lines	5'-TGGTTCACGTAGTGGGCCATCG-3'	
LBb1.3 for SALK-lines	5'-ATTTTGCCGATTTTCGGAAC-3'	
LB3 for SAIL-lines	5'-TAGCATCTGAATTTTATAACCAATCTCGATACAC-3'	
<b>RT-PCR primer for the positiv control</b>		
<b>acession</b>	<b>term</b>	<b>sequence</b>
<i>At5g54160 (COMT1)</i>	COMT1_For COMT1_Rev	5'-GGACTGACCCTAGATTCAAC-3' 5'-CCTTGAAGCCTGATGCTTTG-3'
<i>At5g54010 (UGT79B6)</i>	UGT79B6_For UGT79B6_Rev	5'-ATGGGGTCAAAGTTTCATG-3' 5'-TCATTCAAGATTTATATTTGGAC-3'

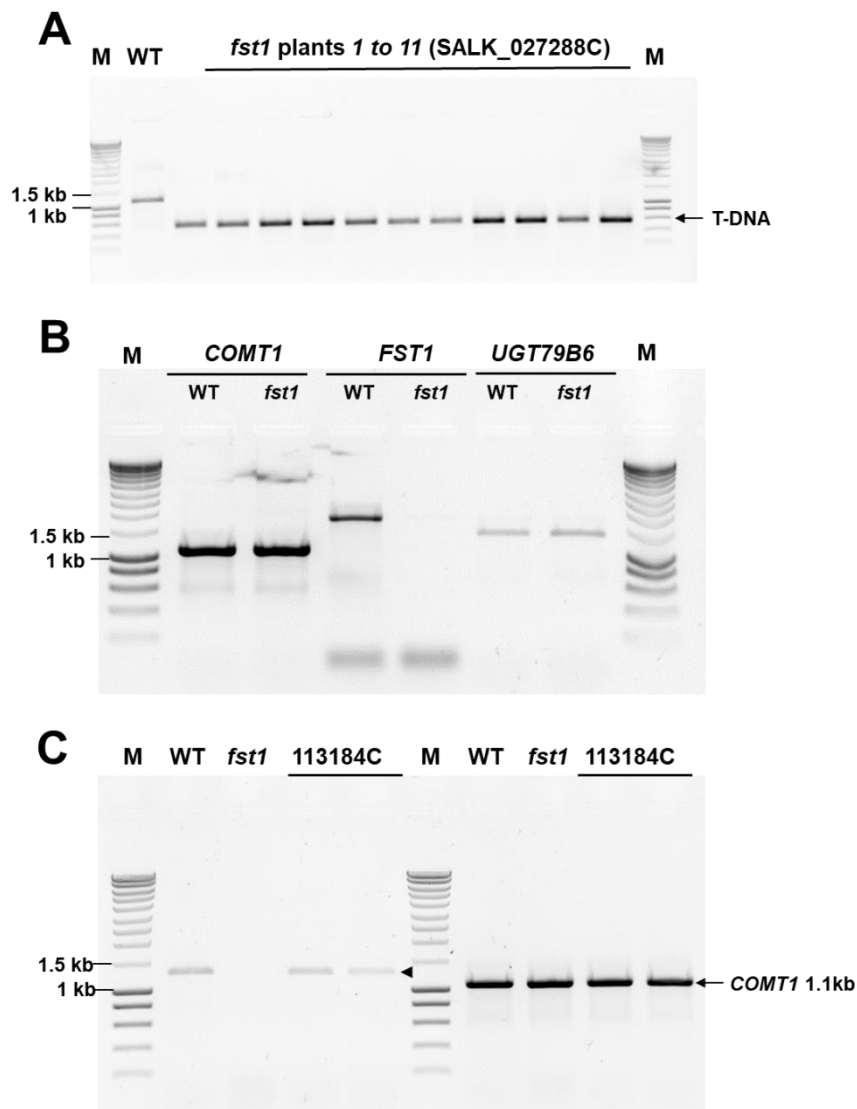


**Figure 8-1** Verification of the *fst1* knockout line.

(A) To confirm the correct T-DNA insertion in the SALK\_027288C line a PCR was performed with genomic DNA as template and the corresponding *At5g28470* genotyping primers LP, RP, and LBa1 (Table 8-2). The wild-type control (WT) had the calculated product length about 1.17 kb (without T-DNA insertion). In the case of the tested *fst1* plants (*fst1*) no product was detected. Only a smaller product (about 600 bp) specific for the T-DNA insertion was amplified. (B) Full-length-specific primers were used to confirm the *fst1* knockout by RT-PCR using cDNA from young buds of the *fst1* mutant line and wild-type as template. In the case of the *fst1* cDNA no product was amplified. Estimated product length of *FST1* is 1680 bp. To verify that transcript formation of specific, terminal glycosyltransferase *UGT79B6* (Yonekura-Sakakibara et al., 2014) is not affected in the mutant, its full-length product of the (1362 bp) is also shown. (C) Verification of transcripts in the second independent T-DNA insertion line of *At5g28470* (SALK\_113184C) compared to wild-type and the first *fst1* line (SALK\_027288C). For this second T-DNA line, a PCR product (indicated by an arrowhead) was amplified from cDNA of the line Salk\_113184C but not from SALK\_027288C. For this analysis, a different set of primers was used for amplification generating a product length of 1295 bp. The line Salk\_113184C therefore, can be termed as a 'knockabout' line. As control for the quality of the cDNA used in both RT-PCRs an additional PCR was performed with full-length primers specific for the caffeate *O*-methyltransferase 1 (*COMT1*, 1092 bp, Fellenberg et al, 2012b).



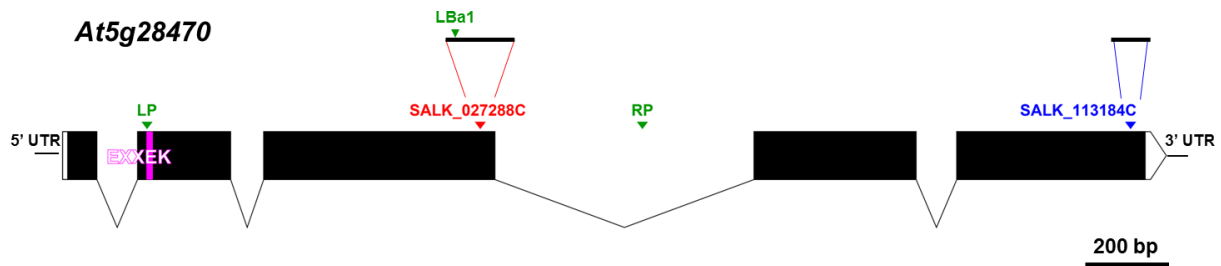


**Figure 8-2** Scheme of the *At5g28470* allele encoding FST1.

Shown are the length and the location of the T-DNA insertion from the *fst1* knockout line SALK\_027288C (red) (163 bp) and the knock about line SALK\_113184C (blue) (99 bp). The nucleotide sequence encoding for the EXXEK motif (purple) and parts of the untranslated regions (5' UTR/ 3' UTR) are indicated. Additionally, the binding sites of the used genotyping primers of the *fst1* mutant line (SALK\_027288C) are marked (LP, left primer; RP, right primer; LBa1 left border primer of the T-DNA). The scale bar represents 200 bp. (Drawn with Exon-Intron Graphic Maker, <http://wormweb.org/exonintron>).

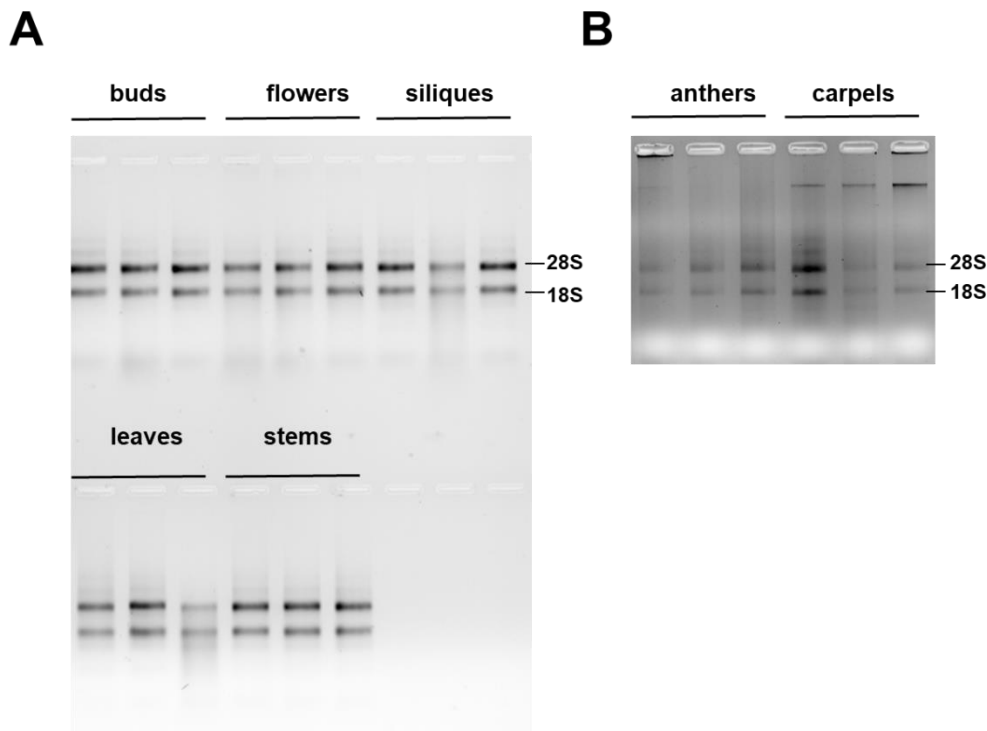


**Figure 8-3** Quality of isolated plant RNA preparations.

Clearly visible 28S and 18S RNA signals of the isolated RNA prove their integrity. RNA was extracted from *Arabidopsis* buds, open flowers, siliques, leaves and stem shown in (A) (500 ng RNA was loaded). (B) Because of the low sample amounts just 120 ng RNA was loaded in the case of anthers and carpels. In the case of the carpels residual impurities of genomic DNA were visible which were later removed by additional DNase I digestion.

GAA TTC **T** **ATG** GGC TCG AAA TTT CAT GCC TTT ATG TTC CCC TGG TTC GGA TTT GGC CAC ATG ACA GCA TTT CTT  
 CAT CTG GCG AAC AAA CTG GCG GAG AAA GAT CAC AAA ATT ACC TTC CTG TTA CCG AAG AAA GCG CGG AAA CAG  
 TTG GAG TCA CTG AAC CTC TTT CCG GAT TGT ATC GTG TTC CAA ACG CTC ACC ATT CCA TCA GTT GAC GGA CTG  
 CCT GAT GGT GCT GAA ACG ACT TCC GAT ATT CCG ATC TCC CTC GGT TCG TTT CTG GCC AGT GCG ATG GAT CGT  
 ACG CGC ATT CAA GTT AAG GAA GCT GTC TCT GTA GGC AAA CCG GAT CTG ATC TTC TTC GAC TTC GCG CAT TGG  
 ATT CCG GAA ATT GCA CGC GAA TAT GGT GTC AAA AGC GTG AAC TTC ATT ACG ATT AGT GCA GCG TGT GTA GCC  
 ATT TCG TTC GTT CCC GGT CGT AGC CAA GAC GAT CTG GGT TCA ACT CCT CCA GGC TAT CCG AGC AGT AAA GTG  
 TTA CTC CGT GGG CAT GAA ACC AAT AGC CTG TCC TTC CTT AGC TAT CCC TTT GGA GAT GGT ACC AGC TTT TAC  
 GAA CGC ATT ATG ATC GGT CTG AAG AAT TGC GAT GTG ATC TCT ATC CGT ACA TGC CAG GAA ATG GAA GGC AAA  
 TTT TGC GAC TTT ATC GAG AAT CAG TTT CAG CGC AAA GTG CTG TTA ACC GGC CCA ATG TTG CCG GAA CCG GAC  
 AAT AGC AAA CCG TTA GAA GAT CAG TGG CGC CAA TGG TTG TCT AAG TTT GAT CCT GGG AGC GTG ATT TAC TGT  
 GCC CTT GGG AGT CAG ATC ATT CTG GAG AAG GAC CAG TTC CAG GAA TTG TGC CTT GGT ATG GAG TTA ACC GGG  
 TTG CCG TTT CTG GTC GCA GTG AAA CCA CCG AAA GGC AGC TCA ACG ATC CAG GAA GCG CTG CCG AAA GGC TTT  
 GAG GAA CGC GTA AAA GCC CGT GGT GTG GTC TGG GGC GGT TGG GTT CAA CAA CCT CTG ATT CTG GCA CAC CCA  
 AGC ATT GGT TGC TTT GTC TCG CAC TGT GGT TTC GGC TCT ATG TGG GAA GCT CTG GTT AAC GAC TGC CAG ATC  
 GTG TTC ATT CCG CAT CTG GGC GAA CAG ATT CTG AAC ACC CGC CTG ATG TCC GAA GAG CTG AAA GTA TCG GTG  
 GAA GTA AAA CGC GAA GAG ACT GGC TGG TTT TCC AAG GAA TCG TTA TCA GGC GCC GTT CGT TCC GTT ATG GAT  
 CGG GAT AGT GAA CTC GGC AAT TGG GCT CGT CGC AAT CAC GTT AAG TGG AAA GAA TCT CTG CTT CGC CAT GGA  
 CTG ATG AGT GGG TAC CTG AAC AAA TTT GTC GAA GCG TTG GAG AAA CTG GTG CAG AAC ATC AAC CTG GAG **TAA**  
AAG CTT

**Figure 8-4** *UGT79B6* codon-optimized sequence for *E. coli*.

The coding nucleotide sequence of the *At5g54010* was adapted to the codon usage in *E. coli* and synthesized by MWG Eurofins. The coding sequence contains 1362 bp (bold letters) and is flanked by the EcoRI and HindIII restriction sites (underlined twice) used for cloning into the petDuet-1 expression vector. A thymine (highlighted in red) as additional base was inserted for cloning in the correct reading frame. The start codon (green) and the stop codon (purple) are marked.

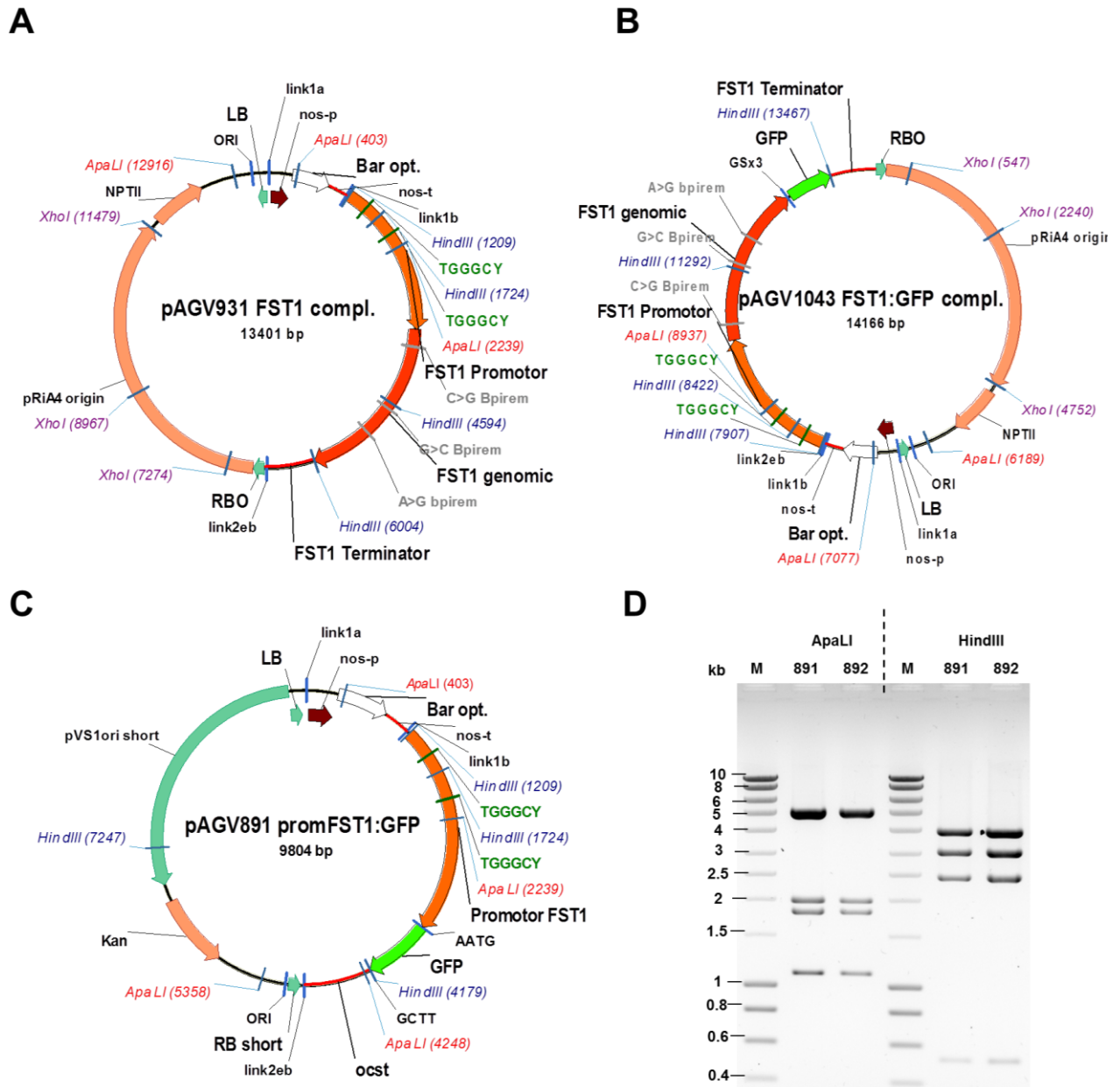


**Figure 8-5** Golden Gate constructs for *in planta* approaches.

Shown are the binary vectors **(A)** pAGV993 and **(B)** pAGV1043 for the complementation experiment which encode the FST1 transporter without and with GFP reporter fusion (green highlighted), respectively. **(C)** The FST1 promoter GFP-reporter shuttle vector whose promoter activity was promising for the generation of functional complementation lines. Inscribed are the single modular cloned elements: the FST1 promoter (2245 bp), the genomic FST1 sequence (2550 bp) and the FST1 terminator (719 bp). The sites of the consensus sequence TGGGCY of the anther-specific *cis*-regulatory element SITEIIATCYTC are marked in green. Further indicated are: the removed *Bsa*I and *Bpi*I restriction sites (grey) and the *Apa*LI, *Hind*III and *Xho*I endonuclease sites for the final restriction analyses. **(D)** Representative restriction analysis of the construct pAGV891 exhibited the correct restriction patterns (*Apa*LI restriction: 4.8 kb, 2 kb, 1.8 kb and 1.1 kb and *Hind*III restriction: 3.7 kb, 3 kb, 2.45 kb and 515 bp). Thereby, a correct molecular assembly of the Golden Gate construct was confirmed. Termination: RB (right T-DNA border), LB (left T-DNA border), nos-p (noptaline synthase promoter), nos-t (noptaline synthase terminator), ocs-t (octopine synthase terminator), Bar opt. (optimized Bar-gene), Kan (kanamycin resistance marker gene), ORI (pucOri required for amplification in *E. coli*), pVS1 ori (origin of replication suitable for amplification in *Agrobacteria*)

**Table 8-3** Golden Gate cloning primers. The coloured recognition sites of *Bsal* (GGTCTC(N)<sub>1</sub>, blue) and *Bpil* (GAA-GAC(N)<sub>2</sub>, red) were used for cloning into level -1 (*Bsal*) and level 0 (*Bpil*), respectively. The four base overhangs ACAT and ACAA (orange) were used for cloning into the universal level -1 vector pAGM1311. The green highlighted base pairs are used for insertion into level 0 vectors (pICH41295 / pAGM1287 / pICH41276).

term	sequence
<b><i>FST1</i> promotor</b>	
promfst1	5'-TTGGTCTCAACATGGAGAACATTTTACGTAGAAGAGGAGGCG-3'
promfst2	5'-TTGGTCTCAACAACAGCTCATCACAAGAAAAACAAAAGTGAAGCAG-3'
promfst3	5'-TTGGTCTCAACATGCTGTCAAACCTCCCTTCCCTCCCAG-3'
promfst4	5'-TTGGTCTCAACAATAGGGGTAGGGGAACTTTGGTGAAGGG-3'
promfst5	5'-TTGGTCTCAACATCCTATACCACAAATGCTTGGGCTATTGTAC-3'
promfst6	5'-TTGGTCTCAACAACATTTTTGTCTTTGGTTGAGAGGAAATGAAAAATGC-3'
<b><i>FST1</i> full genomic sequence</b>	
FST7	5'-TTGGTCTCAACATAATGGACGTCGAATCTTCATCACCATCG-3'
FST8	5'-TTGGTCTCAACACACCACCAAGATTATATTTTGTTCATGAG-3'
FST9	5'-TTGGTCTCAGTGTCTTGGTGAACGTCATCAACATATGG-3'
FST10	5'-TTGGTCTCAACAAGAGCTATATAAGAGTCTCTATTGATTAATAAGAAATCCAGC-3'
FST11	5'-TTGGTCTCAACATGCTCTTCATACAACCTTAGACATAACACTAATGC-3'
FST12	5'-TTGGTCTCACCTCGTTAACTCGTTCCGATTTCGTTACG-3'
FST13	5'-TTGGTCTCAGAGGACGGTAACGCGAAGTACAAATGGAG-3'
FST14	5'-TTGGTCTCAACAAGCTTAGTGTCTTTTTGTTTTCAGTGGCATACTTG-3'
<b><i>FST1</i> terminator</b>	
termfst15	5'-TTGGTCTCAACATGCTTAGATGTTTAGATAAGACTTCAGAGAGG-3'
termfst16	5'-TTGGTCTCAACAAGCGTTAAGGAACTGAACCGTTCCACG-3'
<b><i>FST1</i> subcellular localization</b>	
subcfst1	5'-TTGGTCTCAACATAATGGACGTCGAATCTTCATCACCATCG-3'
subcfst2	5'-TTGGTCTCAACACACCACCAAGATTATATTTTGTTCATGAG-3'
subcfst3	5'-TTGGTCTCAGTGTCTTGGTGAACGTCATCAACATATGG-3'
subcfst4	5'-TTGGTCTCAACAACCTCGTTAACTCGTTCCGATTTCGTTACG-3'
subcfst5	5'-TTGGTCTCAACATGAGGACGGTAACGCGAAGTACAAATGGAG-3'
subcfst6	5'-TTGGTCTCAACAACGAACCGTGTCTTTTTGTTTTCAGTGGC-3'
<b><i>UGT79B6</i> subcellular localization</b>	
subc79b1	5'-TTGGTCTCAACATAATGGGGTCAAAGTTTCATGCTTTTATG-3'
subc79b2	5'-TTGGTCTCAACAACCTTGAGTTCCTCGCTCATC-3'
subc79b3	5'-TTGGTCTCAACATGGTTTCGGTAGAGGTGAAAAGAGAGG-3'
subc79b4	5'-TTGGTCTCAACAACGAACCTCAAGATTTATATTTGGACTAGTTTCTCC-3'
<b><i>UGT79B6</i> promotor</b>	
prom79b1	5'-TTGAAGACAAGGAGACAGATCCGAGTGTATGTTATTATACTTGTGATG-3' AGTGTGGGCTTAGTCTACATATTGATTGTGTACTIONGG-3'
prom79b2	5'-TTGAAGACAACATTATGTTCTTCGGGGAAAATAAAAATAAATATGTTCC-3'
<b><i>TSM1</i> promotor</b>	
promTSM1	5'-TTGAAGACAAGGAGTCAAAAGACTACTTGAAGAGTAC-3'
promTSM1	5'-TTGAAGACAACATTCTCTCTTGTCTCGATCGTG-3'
<b><i>SHT</i> promotor</b>	
promSHT1	5'-TTGAAGACAA GGAG TATAGTGACTCGTATGTGTGAGAG-3'
promSHT2	5'-TTGAAGACAACATTACACAAACCCCTTCTTTTTCTCTTC-3'

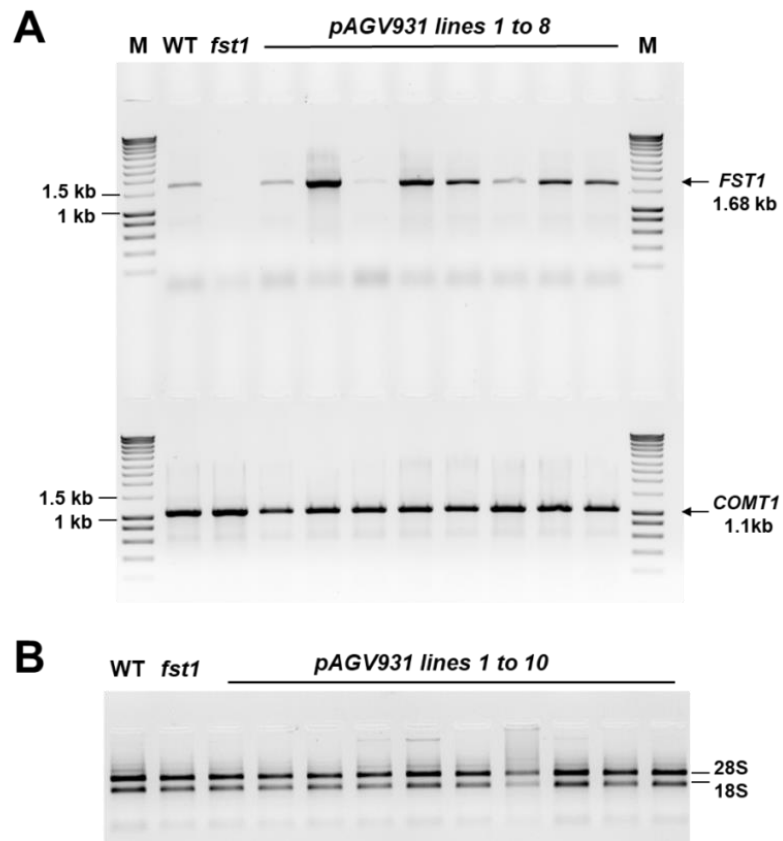


**Figure 8-6** Control of the individual pAGV931 complementation lines.

**(A)** Expression of the pAGV931 complementation construct in the *fst1* mutant was verified by RT-PCR. As template cDNA from young buds of individual pAGV931 lines from the T1-generation (pAGV931 1 to 8) were used and compared to wild-type (WT) and *fst1* mutant (*fst1*). As quality control of the used cDNA second PCR was performed with full-length primers specific for the caffeine *O*-methyltransferase 1 (*COMT1*, 1092 bp). **(B)** Isolated RNA from wild-type, *fst1* line and pAGV931 lines showed no degradation. The typical 28 S and 18 S rRNA bands are clearly visible indicating a high integrity.

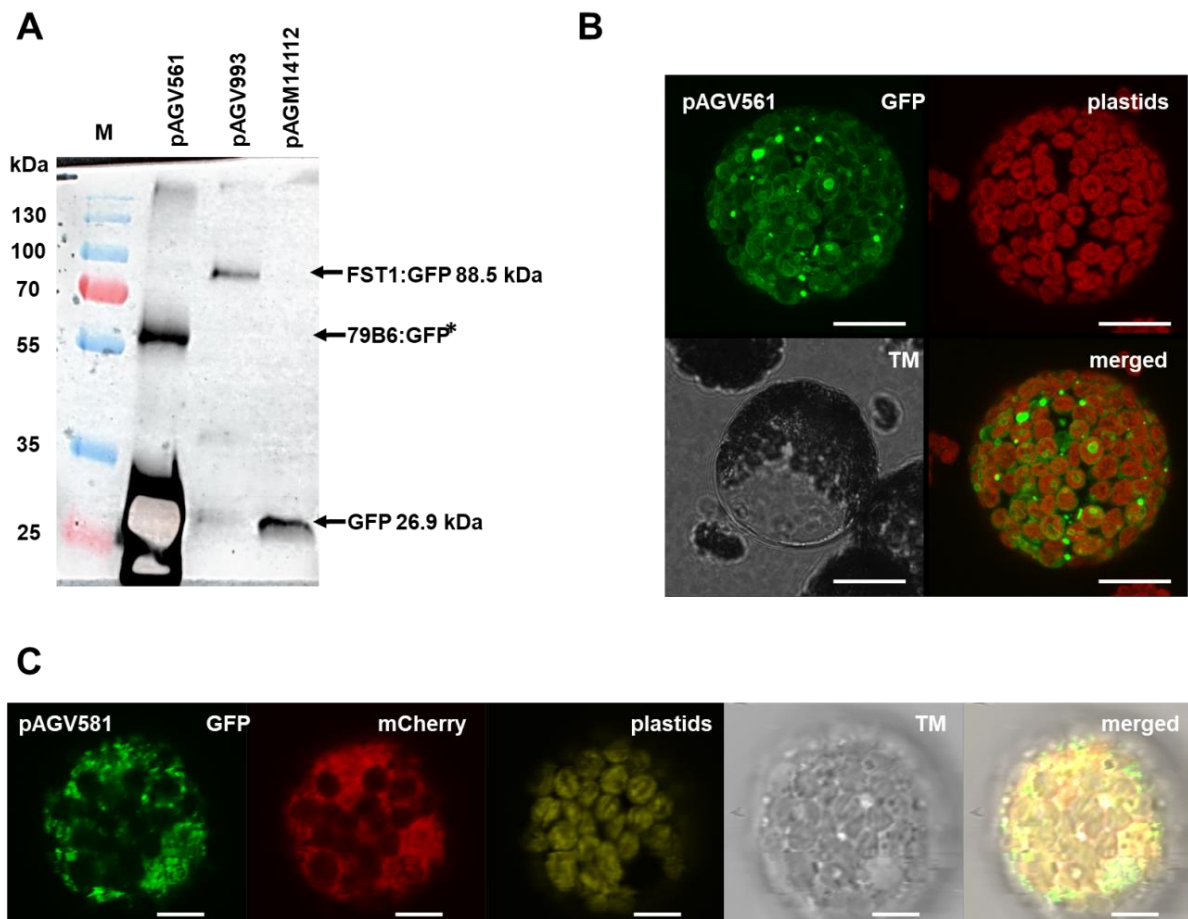


**Figure 8-7** Additional controls for the subcellular localization studies.

**(A)** Immuno blot detection of the transiently expressed fusion proteins 79B6-GFP (pAGV561) and FST1-GFP (pAGV993) as well as the GFP control (pAGM14112) in crude extracts from *N. benthamiana* leaf discs. The calculated molecular mass is indicated. \*In the case of the UGT79B6-GFP fusion protein with an calculated molecular size of 77.7 kDa a lower protein band was detected over 55 kDa accompanied by strong signals lower than 35 kDa, indicating degeneration of the fusion protein. **(B)** Confocal fluorescence image of *A. thaliana* protoplast expressing pAGV561 encoding *prom35S:UGT79B6-GFP* (with friendly permission of Dr. Ilka Haferkamp, TU Kaiserslautern). Bar = 10  $\mu$ m. **(C)** Confocal fluorescence image of the N-terminal GFP-tagged UGT79B6 reporter protein encoded by the pAGV581 Golden Gate construct, transiently co-expressed with free mCherry in a *N. benthamiana* protoplast. Bar = 10  $\mu$ m. Imaged are the GFP-channel (GFP), a channel for the mCherry fluorescence (mCherry), the autofluorescence of chlorophyll A (plastids, yellow coloured), the transmission image (TM) and the merged image (merge).

**Table 8-4** Solvent gradients for HPLC-analysis. Solvent A is 0.1% (v/v) formic acid and solvent B is acetonitril. All HPLC-gradients were used at the same flow rate (0.6 ml min<sup>-1</sup>).

<b>program</b>	MS_5cm_QDA_Transp354nm_14min	
<b>time [min]</b>	<b>A (v/v) [%]</b>	<b>B (v/v) [%]</b>
	90	10
8	55	45
8.5	20	80
9	20	80
9.1	90	10
14	90	10
<b>program</b>	MS_25cm_C8_Flavonoide_26min	
<b>time [min]</b>	<b>A (v/v) [%]</b>	<b>B (v/v) [%]</b>
	90	10
20	50	50
20.5	20	80
21	20	80
21.2	90	10
26	90	10
<b>program</b>	MS_Qshell_QDA_5cm_12min_79B6	
<b>time [min]</b>	<b>A (v/v) [%]</b>	<b>B (v/v) [%]</b>
	95	5
8	65	35
8.5	10	90
8.9	10	90
9	95	5
12	95	5
<b>program</b>	MS_QDA_5cm_12min_78D2_V287A	
<b>time [min]</b>	<b>A (v/v) [%]</b>	<b>B (v/v) [%]</b>
	90	10
8	45	55
8.2	10	90
8.7	10	90
8.8	90	10
12	90	10

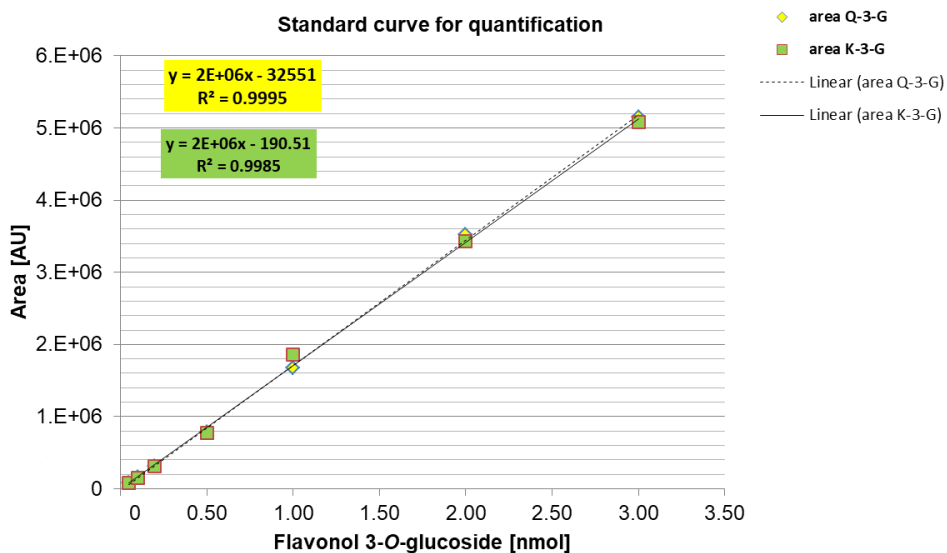


**Figure 8-8** Calibration curve for quantification of flavonol glycosides.

To determine the amounts of the flavonol glycosides of interest different concentrations from 5  $\mu\text{M}$  to 300  $\mu\text{M}$  of quercetin-3-glucoside (Q-3-G) and kaempferol-3-*O*-glucoside (K-3-G) were used. The correlation is linear with reliable correlation coefficients (*R*-value about 0.998). The abscissa indicates the added amount of flavonol-3-*O*-glucoside in pmol. The ordinate shows the peak area in absorption units (AU). Absorption was recorded at 354 nm. Formulas of the calibration curves are given (Q-3-G, yellow), (K-3-G, green).

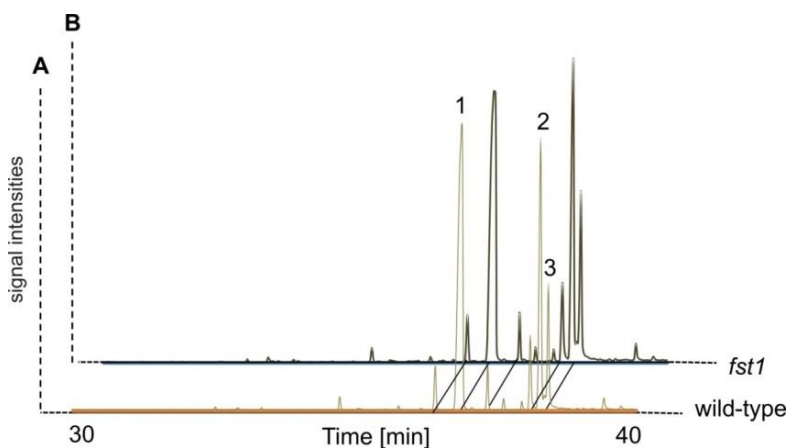


**Figure 8-9** GC-MS analysis of Arabidopsis pollen hexane extracts.

No differences in the metabolite profiles between (A) wild-type and (B) *fst1* mutant pollen hexane extracts are evident. For preparation 10 mg freshly collected pollen were extracted with 500  $\mu\text{l}$  hexane, ultra-sonicated, centrifuged and 1  $\mu\text{l}$  supernatant was analysed by GC-MS. Three major peaks were identified by using the NIST-GC-MS library: nonacosane (peak 1, RT 36.91 min), nonacosanone (peak 2, RT 38.3 min) and octacosanol (peak 3, 38.44 min). The measurement was performed three times with independent biological samples of wild-type and *fst1* mutant pollen ( $n = 3$ ). (Figure with friendly permission from Dr. Thomas Vogt).



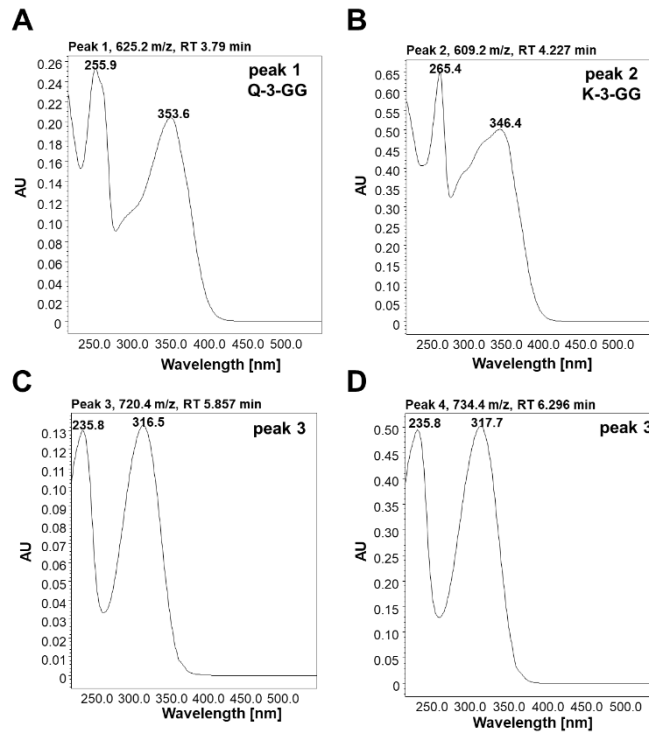


**Figure 8-10 UV-/Vis-absorbance spectra from the HPLC-MS profiles.**

Shown are the absorbance spectra of the peaks 1 and 2 which were identified as the flavonol glycosides (A) quercetin-3-*O*-sophoroside (Q-3-GG) and (B) kaempferol-3-*O*-sophoroside (K-3-GG) in comparison to the peaks 3 and 4 of two major phenolamides (C and D). The retention time and the *m/z* ([*M-H*]<sup>-</sup> in the case of flavonoids and [*M+H*]<sup>+</sup> in the case of hydroxycinnamic acids) are indicated.

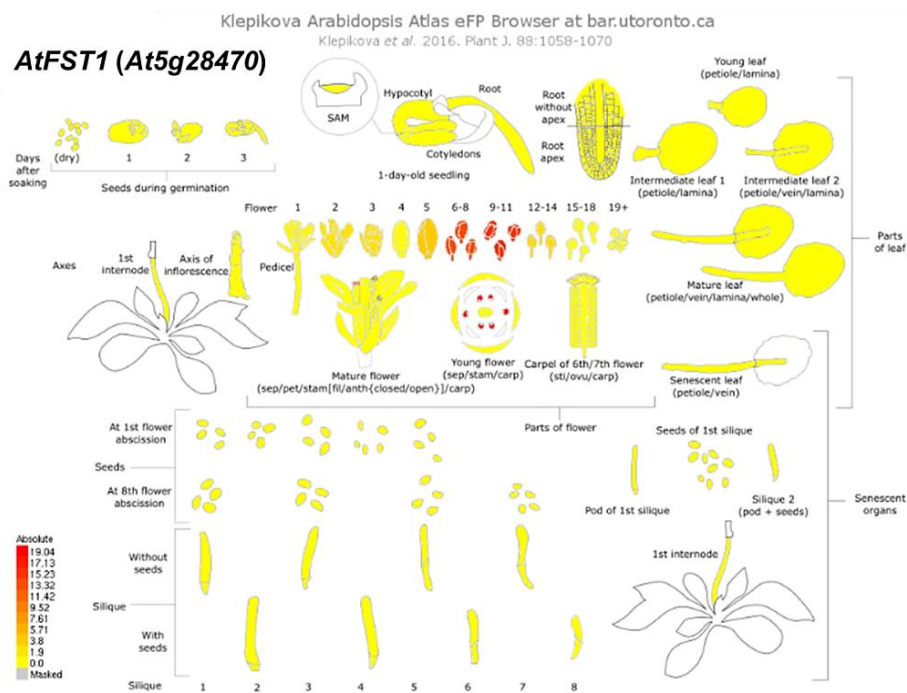


**Figure 8-11 FST1 expression by the Arabidopsis eFP browser.**

FST1 (*At5g28470*) is predicted to be specifically expressed in anthers during early flower stages. Expression values of FST1 were obtained from the public microarray database BAR Arabidopsis eFP browser (<http://bar.utoronto.ca/efp/cgi-bin/efpWeb.cgi>).

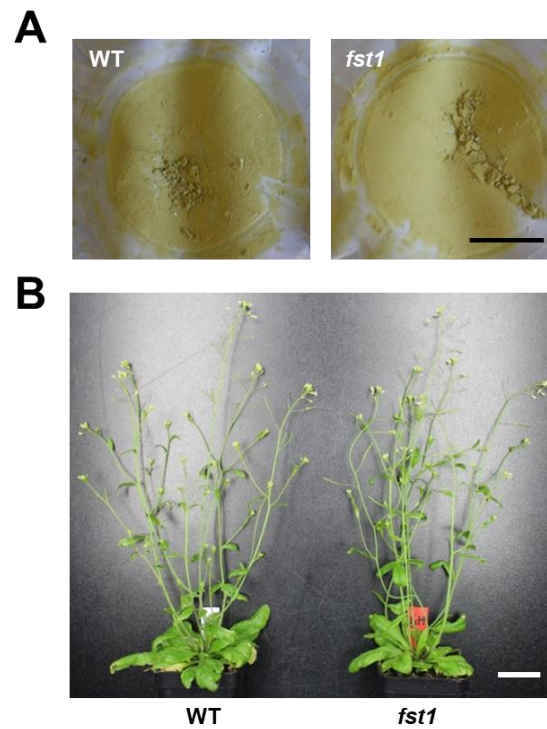


**Figure 8-12** Appearance of the *fst1* mutant line.

**(A)** Arabidopsis pollen grains highly purified by the vacuum cleaner method. Arabidopsis pollen grains from wild-type (WT) and the *fst1* mutant line (*fst1*) exhibited the same ochre colouration. Bar = 2 cm **(B)** No obvious phenotype was observed for the *fst1* line as compared to the wild-type. Bar = 2 cm.

NRT1.1	-----MSLPETKSDIL-----LD	14
GTR1	MKSRVILNHRDRRDKNHNNNTNHYTQVDTMERKPLEVEPSTTTN-----TD	48
GTR2	-----MERKPLELESTDNHQNPSSAVYGGSVTAVD	30
FST1	-----MDVESSPSSH-----	11
	<b>EXXEK-motif</b>	
NRT1.1	AWDFQGRPADRSKTGGWASAAMILCTE <b>EAVER</b> LTTLGI GVNLVYTLTGMHLGNATAANTV	74
GTR1	VVDSFEEEQRKIVYRGWKVMPFII <b>GNETFEK</b> LGIIGTLSNLLVYLT SVFNLKSYTAATII	108
GTR2	SVEEDVQNKVVYRGWKVMPFII <b>GNETFEK</b> LGIIGTLSNLLVYLTAVFNLKSITAATII	90
FST1	-----ALIKKEKGGWRAIKYII <b>ANESFEK</b> LASMSLIGNLSVYLMTKYNLGGVFLVNV	64
	<b>Thr101</b>	
NRT1.1	TNFLGTSFMLCLLGGFIADTFLGRYLT <b>IAIFAAIQ</b> ATGVSILTSTIIPGLRPPRCNPPT	134
GTR1	NAFSGTINFGTFIAAFLCDTYFGRYK <b>LSVAVIAC</b> FLGSFVILLTAAIPSLHPVACGNKI	168
GTR2	NAFSGTINFGTFVAAFLCDTYFGRYK <b>LSVAVIAC</b> FLGSFVILLTAAVPQLHPAACGTAA	150
FST1	NIWFGSCNILLTAGAFVSDAYLGRFW <b>LLLSIAS</b> FI GMGIFALTAALPSLRPDACIDPS	124
NRT1.1	SSHC-EQASGIQLTVLYLALYLTALGTGGVKASVSGFGSDQFDETEPKERSKMTYFFNRF	193
GTR1	S--C-EGPSVGQILFLLMGLGFLVVGAGGIRPCNLAFGADQFNPKSESGKKGINSFFNWF	225
GTR2	DSIC-NGPSGGQIAFLLMGLGFLVVGAGGIRPCNLAFGADQFNPKSESGKRGIDSFFNWF	209
FST1	N--CSNQPAKWQLGVLFSGLGLLAIGAGGVRPCNIAFGADQFDTSTKKGKAHLETFNWF	182
NRT1.1	FFCINVGSLAVTVLVYVQDDVGRKWGYGICAFIVLALS VFLAGTNRYR FKKLIGSPMT	253
GTR1	FFTFTFAQIIISLTAVVYIQSNVSWTIGLIIPVALMFLACVIF FAGDRLYVVKV KASGSPLA	285
GTR2	FFTFTFAQILSLTLVVYVQSNVSWTIGLTIIPAVLMFLACLIFFAGDKLYVKIKASGSPLA	269
FST1	YFSFTVALVIALTGVVYIQTNISWVIGFVIPTACLALSITTFVIGQHTYICAKAEGSVFA	242
NRT1.1	QVAIVIVAAWRNRRKLELPADP-SYLYDVDDIIAAEGSMKKGQKL-PHTEQFRSLDKAAIR	311
GTR1	GIARVIAAAIKKRGLKPVKQPPVNLVNH---IPSNYA---NTTL-KYTDQFRFLDKAAIM	338
GTR2	GIAQVI AVAIKKRGLKPAKQPWLNLYN---YPPKYA---NSKL-KYTDQFRFLDKAAIL	322
FST1	DIVKVVIAACKRRKVKPGSD--ITFYIG---PSNDGS---PTTLVRDKHRLRFFDKASIV	294
	<b>His356</b>	
NRT1.1	DQEAGVTS--NVFNKWTLSLTLDVEEVKQIVRMLPIWATCILFWTV <b>HAQL</b> TTLSVAQSET	369
GTR1	TPEEKLNSDGTASDPWKLCTLQQVEEVKQIVRVPIWFASTIYYL <b>AT</b> IQTMYPVFQALQ	398
GTR2	TPEDKLQPDGKPADPWKLCTMQQVEEVKQIVRVLPWFASSIYYL <b>TT</b> IQMTPPVFQALQ	382
FST1	TNPNELNEDGNAKYKWLCSVQQVKNLKCVTALPVVWVTGIACFIL <b>TD</b> QQNIYGILQAMQ	354
NRT1.1	LDRSIGS--FEIPASMAVFYVGGLLLTAVYDRVAIRLCKKLFNYPHGLRPLQRIGLGL	427
GTR1	SDRRLGSGGFRI PAATYVVFLMTGMTVFIIFYDRVLVPSLRRVTGLETGISLLQRIGAGF	458
GTR2	SDRRLGSGGFVI PAATYVVFLMTGMTVFIIFYDRVLVPTMRRITGLDTGITLLQRIGTGI	442
FST1	MDKTFGPHNFQVPAGWMNLVSMITLAIWISLYECVIIPIVKQITGRKKRLTLKHRI--EI	412
NRT1.1	FFGSMAMAVAALVELKRLRTAHAGPTVKTLP-----LGFYLLIPQYLIVGIGEALIIY	480
GTR1	TFAIMSLLVSGFIEERR-RNFALTKPTLGMAPRTGEISSMSALWLI PQLTLAGIAEAFAA	517
GTR2	FFATASLVVAGFVEERR-RTFALTKPTLGMAPRKGEISSMSAMWLI PQLSLAGVAEAFAA	501
FST1	VMGIICMIVAGFQEKKR-RASALKNGSF-VSP-----VSIVMLLPQFALAGLTEAFSA	463
NRT1.1	TGQLDFFLRECPKMGKGMSTGLLLSTLALGFFFSSVLVTIVEKFTGK--AHPWIAD-DLN	537
GTR1	IGQMEFYKQFPENMKS FAGSIFYVGAGVSSYLASFLISTVHRTTAHSPSGNWLAE-DLN	576
GTR2	IGQMEFYKQFPENMRS FAGSIFYVGGVSSYLGSFLIATVHRTTQNSSGGNWLAE-DLN	560
FST1	VALMEFLTVRMPEHMRVAGAIFFLSSSIASYICTLLINVIDAVTRKE-GKSWLGDKDLN	522
NRT1.1	KGRLYNFYWLVAVLVALNFLIFLVFSKWYVYKEKRLAEVGIELDDDEPSIPMGH-----	590
GTR1	KAKLDYFYFMLTGLMVVNMAFYLLMARWYRYKGGNDEDITEIETNEEETKQQQLQDKNSV	636
GTR2	KGRLDLFYFMIAGILAVNFAYFLVMSRWYRYKGS-DEVTTYETNENIKQQD--KNVA	616
FST1	KNRLENYFFIIAGIQVANLLYFRLFASRYATENKK-----GH-----	559

**Figure 8-13** Protein sequence alignment of NPF-family members.

Protein sequences of NRT1.1 (NPF6.3), GTR1 (NPF2.10), GTR2 (NPF2.11), and FST1 (NPF2.8) were aligned using the Clustal multiple sequence alignment tool MUSCLE (3.8) from the European Bioinformatics Institute (EMBL-EBI) (<https://www.ebi.ac.uk/Tools/msa/muscle/>). Indicated are the EXXEK-motif (red, black-filled) (Jørgensen et al., 2015), the putative phosphorylation site Thr101 of NRT1.1 (purple-highlighted) (Liu and Tsay, 2003; Sun and Zheng, 2015), and the His356 of NRT1.1 (blue-highlighted) which is discussed to be essential for nitrate binding (Parker and Newstead, 2014).



## Lebenslauf

### Persönliche Angaben:

Name: Stephan Grunewald  
 Geburtsdatum: 10.05.1989  
 Geburtsort: Berlin

### Berufliche Praxis:

**08.2015 – 10.2019**

#### **Wissenschaftlicher Mitarbeiter**

Doktorand am Leibniz Institut für Pflanzenbiochemie (IPB)

**10.2014 – 07.2015**

#### **Wissenschaftliche Hilfskraft**

IPB, Abt. Stoffwechsel- u. Zellbiologie (SZB)

### Ausbildung:

**10.2012 –10.2014**

**Masterstudium** Biochemie an der Martin-Luther-Universität Halle-Wittenberg (MLU)  
 Abschluss als *Master of Science*, Note: 1,5  
 Thema der Masterarbeit: „Biosynthese der Flavonolsophoroside in *Arabidopsis thaliana* Antheren“ am IPB, Abt. SZB, AG Phenylpropanstoffwechsel, Dr. Thomas Vogt, Note: 1,1

**10.2008 –11.2012**

**Bachelorstudium** Biochemie an der MLU  
 Abschluss als *Bachelor of Science*, Note: 2,4  
 Thema der Bachelorarbeit: „Untersuchung eines Genes für eine Terpensynthese aus *Solanum tuberosum* L.“ am IPB, Abt. Stress- u. Entwicklungsbiologie, AG Induzierte Pathogenabwehr, Prof. Dr. Sabine Rosahl, Note: 1,6

**2001 – 2008**

**Abitur**, Europaschule Gymnasium Stephaneum, Aschersleben, Note: 1,7

## List of publications

**Grunewald, S., Marillonnet, S., Hause, G., Haferkamp, I., Neuhaus, H.E., Veß, A., Hollemann, T., and Vogt, T.** (2020) The tapetal major facilitator NPF2.8 is required for accumulation of flavonol glycosides on the pollen surface of *Arabidopsis thaliana*. *Plant Cell* 32: 1727-1748.

**Schubert, R., Grunewald, S., von Sivers, L. and Hause, B.** (2019) Effects of Jasmonate on ethylene function during the development of tomato stamens. *Plants* 8: E277.

## **Danksagung**

An dieser Stelle möchte ich mich bei Allen bedanken, die mich bei der Anfertigung dieser Arbeit sowie im Laboralltag unterstützt haben.

An erster Stelle möchte ich mich bei **Dr. Thomas Vogt** bedanken, dass ich nach meiner Masterarbeit die Möglichkeit bekommen habe, die Thematik der Pollen-spezifischen Flavonolsophorose von einer ganz anderen Perspektive - der des Metabolit-Transports - zu erforschen. Ebenfalls danke ich ihm für die stetige Unterstützung und den fachlichen Austausch.

Daneben möchte ich mich bei **Prof. Dr. Alain Tissier** bedanken für die Möglichkeit innerhalb der Abteilung Stoffwechsel- und Zellbiologie zu arbeiten und die Vertrags-Verlängerung am Ende meiner Arbeit ohne die ich die Komplementationsexperimente nicht mehr hätte beenden können.

Weiterhin bedanke ich mich bei **Prof. Dr. Ingo Heilmann** und **Prof. Dr. Enrico Martinoia** dafür, dass sie sich bereit erklärt haben meine Arbeit zu begutachten.

Bei **Prof. Dr. Bettina Hause** und **Hagen Stellmach** möchte ich mich auf diese Weise herzlich bedanken für die Unterstützung bei der Fluoreszenzmikroskopie und das Sie mir bei Fragen am LSM780 immer sofort mit viel Interesse geholfen haben.

**Dr. Gerd Hause** vom Biozentrum danke ich für die wunderbaren Elektronenmikroskopie-Aufnahmen unserer Antheren- und Pollenquerschnitte und die damit verbundene Möglichkeit „einmal den Zellen bei der Arbeit zuzusehen“. Hierbei möchte ich mich auch bei **Simone Frass** für die Präparation der ultrafeinen TEM-Schnitte und die Toluidinblau-Färbung bedanken.

Bei **Dr. Ilka Haferkamp** bedanke ich mich auch noch einmal herzlich, dass ich bei Ihr unterkommen konnte und den einwöchigen „Crashkurs“ bei ihr an der TU Kaiserslautern für unsere radioaktiven Uptake-Assays und die Durchführung der CCCP-Transporterassays.

Des Weiteren möchte ich auch **Prof. Dr. Thomas Hollemann** und **Dr. Astrid Veß** vom Institut für Physiologische Chemie der MLU danken für ihre Mithilfe bei den Vorarbeiten für die *Xenopus* Oocyten Versuche für mögliche zukünftige Projekte.

Bei **Dr. Sylvestre Marillonnet** möchte ich mich besonders bedanken, dass er mir das Golden Gate Cloning beigebracht hat und für die interessanten kleinen Pausen, in denen er mit mir über Anthocyane gesprochen hat oder wir zusammen Flavonolsynthase-defiziente *N. benthamiana* Mutanten bestäubt haben.

**Dr. Lennart Eschen-Lippold** möchte ich danken für den Austausch über das 'Westernblotten' von Membranproteinen.

**Prof. Dr. Bernhard Westermann** und **Angela Schaks** danke ich für die Synthese des Azaleatins und auch **Dr. Wolfgang Brandt** für das Modeling der UGTs, auch wenn diese Nebenprojekte nicht mehr in die Arbeit eingeflossen sind.

Ein kleines Dankeschön auch an **Frank Lange** und **Andrea Piskol** für die Hilfe der Beschaffung insbesondere älterer Literaturquellen wie Kim et al., 1996 und Rabaté and Dussy, 1938.

Ein großes Dankeschön möchte ich den **Gärtnern am IPB** aussprechen, insbesondere **Petra Jansen**, **Sabine Voigt** und **Phillip Plato** für die Vorbereitung all der bestellten 96iger Multitöpfe sowie die Anzucht und Pflege meiner Arabidopsis Linien im GWH. Petra, ich weiß, Ihr werdet meine „Großbestellungen“ und den ungewöhnlichen Anblick von mir beim Pollensammeln mit dem Staubsauger vermischen.

Ein besonderes Dankeschön möchte ich an **Kerstin Manke** richten, die mir immer eine freundliche Gesellschaft und Hilfe in unserem kleinen Labor, A118 war. In diesen Zusammenhang möchte ich mich natürlich auch bei **Ramona Grützner** herzlich bedanken, für Plasmide, kompetente Agros und LB-Platten (im Tausch gegen weiße Schokolade und Minions<sup>^</sup>), dass sie mir die praktischen Grundlagen zur Agrotransformation beigebracht hat und ihre erfrischend witzig-ironischen Bemerkungen. Vielen Dank auch, dass Ihr beiden mich oft mitgenommen habt zu den Sushi-All-you-can-eat-Büffets.

Ich möchte mich auch bei meiner Bachelorstudentin **Christine Wagner** für ihre fleißige Unterstützung bei unseren Arbeiten an den TT12-Transporter bedanken.

Daneben möchte ich aber auch all den Doktoranden und Mitstreitern herzlich danken, die mir während meiner Zeit am IPB gute Freunde waren und die alltägliche Routine im Labor immer ein bisschen bunter gemacht haben mit Teepausen, Kinobesuchen, freundlichen Gesprächen auf Deutsch oder Englisch, Kochen, gemeinsamen Mittagspausen in der Mensa, Kickern, den Austragen von Tischtennis-`Duellen` bzw. die Hilfe beim Organisieren unserer beiden IPB-Tischtennisturniere oder mit mir das Pharmaziepraktikum betreut haben: **Christine H.**, **Tina**, **Alfredo**, **Micha**, **Kathleen**, **Irene**, **Stephanie**, **Khanza**, **Caro**, **Chris**, **Anja**, **Chandan**, **Nick**, **Kira** und meine `Lieblings-Tischtennis-Kontrahenten` - **Haider**, **Markus**, **Heena**, **Manuel**, **Pradeep** und **Mukesh**.

Besonders möchte ich **Ramona** danken, für unser gemeinsames, kleines Paper, das wir `nebenbei-gemacht` haben und besonderst dafür dass wir im Gegenüber immer einen Freund zum Reden und Zuhören gefunden haben. Außerdem danke ich **Heena** und **Ramona** für die Möglichkeit, das ich auch mal `kreativ` mit unserer Wissenschaft umgehen konnte beim Basteln an all den Doktorandenhüten.

Daneben möchte ich auch die Gustav Klimt und die Nolde/Marc/Macke Ausstellung in der Moritzburg nicht vergessen. Oder das Tiere Skizzieren im Zoo, den Radierkurs von **Regina**, den „Abendakt“ an der Burg und **Prof. Thomas Rug**, der mir die Möglichkeit gegeben hat an der Jahresausstellung der Burg Giebichenstein teilzunehmen.

Abschließend möchte ich ganz besonders meinen **Eltern** danken, dass sie mich (und meinen Bruder) immer unterstützt und mein Studium ermöglicht haben.

## ***Eidesstattliche Erklärung***

Hiermit erkläre ich, dass ich mich mit der vorliegenden Arbeit erstmals um die Erlangung des Doktorgrades *Doctore rerum naturalium (Dr. rer. nat.)* bewerbe. Die vorliegende wissenschaftliche Arbeit wurde an keiner anderen Fakultät oder Universität zur Begutachtung eingereicht. Weiterhin erkläre ich, dass ich keine anderen als die von mir aufgeführten Quellen und Hilfsmittel benutzt habe und die wissenschaftliche Arbeit selbstständig und ohne fremde Hilfe angefertigt habe. Von mir benutzte wörtlich oder inhaltlich entnommene Stellen habe ich als solche kenntlich gemacht. Die eingereichte schriftliche Fassung der Arbeit entspricht der auf dem elektronischen Speichermedium. Basierend auf den Ergebnissen der vorliegenden Arbeit wurde aus Prioritätsgründen bereits veröffentlicht:

**Grunewald, S., Marillonnet, S., Hause, G., Haferkamp, I., Neuhaus, H.E., Veß, A., Hollemann, T., and Vogt, T.** (2020) The tapetal major facilitator NPF2.8 is required for accumulation of flavonol glycosides on the pollen surface in *Arabidopsis thaliana*. *Plant Cell* 32: 1727-1748.

Halle (Saale), 16.07.2020